A COMPREHENSIVE SEISMIC RESPONSE AND SLOPE STABILITY ANALYSIS FRAMEWORK FOR EVALUATING THE STABILITY OF HYDRAULIC-FILL DAMS

by

SAYANTAN CHAKRABORTY

Presented to the Faculty of the Graduate School of

The University of Texas at Arlington

in Partial Fulfillment of the Requirements

for the Degree of

DOCTOR OF PHILOSOPHY

THE UNIVERSITY OF TEXAS AT ARLINGTON

August 2018

Acknowledgements

I would like to extend my sincere gratitude to my advisor, Dr. Anand J. Puppala, for his constant help, support, and guidance. It was an honor to get an opportunity to work under the supervision of Dr. Puppala and be a part of his research group. I would also like to thank the committee members, Dr. Laureano R. Hoyos, Dr. Xinbao Yu and Dr. Pranesh B. Aswath for their guidance and support.

The help, support and advice of Dr. Tejo V. Bheemasetti, Dr. Aritra Banerjee, and Dr. Jasaswee T. Das, at different stages of this research work, is highly appreciated. Their valuable suggestions and continuous guidance enabled me to complete this research work. I would also like to thank my friends and co-workers at UT Arlington, Dr. Aravind Pedarla, Dr. Raju Acharya, Dr. Tom Taylor, Dr. Ujwal K. Patil, Dr. Santiago Caballero, Dr. Minh Hai, Mr. Ali Shafikhani, Mr. Shi He, Ms. Anu George, Ms. Leila Mosadegh, Ms. Rinu Samuel, Mr. Puneet Bhaskar, Mr. Burak Boluk, Mr. Sarat Congress, Mr. Ashrafuzzaman Khan, Mr. Manikanta Saladhi, and Mr. Nripojyoti Biswas. I am also grateful to Mr. Louie Verreault, Ms. Dorota Koterba and Mr. Jason Gehrig of Tarrant Regional Water District, Fort Worth, Texas for their valuable advice and insightful comments.

Lastly, I would like to thank my parents, brother, and sister-in-law, for their continuous support and blessings.

July 17, 2018

Abstract

A COMPREHENSIVE SEISMIC RESPONSE AND SLOPE STABILITY ANALYSIS FRAMEWORK FOR EVALUATING THE STABILITY OF HYDRAULIC-FILL DAMS

Sayantan Chakraborty

The University of Texas at Arlington, 2018

Supervising Professor: Dr. Anand J. Puppala

The stability and serviceability of earthen embankment structures such as dams and levees are extremely crucial to avoid the catastrophic consequences of the failure of these structures. Such man-made geo-structures are usually stable under normal working conditions; however, the stability and subsequent functionality may be affected during earthquake events. Hence, the evaluation of seismic response and structural stability of earthen dams is an important facet in the field of geotechnical earthquake engineering. Dams and levees built in earthquake-prone regions are usually designed to withstand expected seismic events, and in-depth time-history-based dynamic analyses are typically performed to assess the behavior of these structures during earthquakes. However, earthen dams located in regions of newly declared induced-seismicity, like Texas, may not have been specifically designed to withstand these dynamic excitations. Hence, it is imperative to evaluate the performance of dams and levees located in such zones of induced seismicity.

In this study, the stability of the Eagle Mountain dam, an 85-year-old hydraulic-fill dam, located in Fort Worth, Texas, is evaluated. Historical evidence concerning the poor performance of hydraulic-fill dams around the world during earthquake events further necessitates the assessment of seismic stability of the Eagle Mountain dam. Moreover, there is an inherent variability associated with the material properties along the body of the dam due to the hydraulic-fill method of construction that is not often captured in the traditional method of analysis. In this research, a framework is developed to study the seismic response and stability of hydraulic-fill dams incorporating the effect of material variability and induced seismicity. Three-dimensional models of the dam, depicting the variations in different shear strength properties, were developed by interpolating the in-situ test results using geostatistics-based kriging analysis. These models along with additional available bore log information were used to assign the material properties to the finite-element models of the dam.

In the absence of earthquake time-history data recorded at the dam site, a new natural-frequency-based approach was devised to select the acceleration-time data required for the analysis. A novel method was also developed to determine the strain-dependent natural frequency of the earthen embankment structures. To comprehensively characterize the performance of the dam in the event of probable earthquakes, a broad spectrum of earthquake data having varying peak accelerations and frequency contents were selected. Extensive stability analyses,

including static, pseudo-static, Newmark deformation, and dynamic analyses, were performed to identify the critical sections of the dam. A reliability-based pseudo-static analysis and a sensitivity analysis were also performed to gauge the effect of uncertainty associated with the estimation of the strength parameters and small strain shear modulus of subsurface layers, respectively.

Results indicate that the dam is safe under static conditions and during earthquakes with peak ground accelerations (PGA) of 0.02g, similar to what the dam has already experienced in the past. Moreover, the dam is expected to be safe during earthquakes with PGA less than 0.09g, provided that the predominant frequency of the earthquake is not close to the natural frequency of the dam. Some parts of the upstream shell and foundation sand layers, especially near the toe of the dam, may liquefy. However, flow liquefaction of the foundation sand layers is not expected to happen. The middle portion of the dam, from stations 14.5 to 27, were found to be the most critical, based on the results of the pseudo-static and dynamic analyses.

Keywords: Hydraulic-fill dam, seismic response, SASW, slope stability, liquefaction, natural frequency, reliability analysis.

Table of Contents

List of Figures

List of Tables

Chapter 1: Introduction

1.1 Overview

Earthen dams and levees are crucially important structures whose stability is of paramount importance to geotechnical engineers (Chowdhury et al. 2009; FEMA 2017; Seed et al. 1978). These water-retaining structures are designed to withstand the hydrostatic pressure of the impounded water and are usually stable under normal working conditions. However, during seismic events, the induced forces may affect the structure and have a detrimental effect on its stability and serviceability (Chatterjee and Choudhury 2014; Choudhury et al. 2007; Fell et al. 2005; Hack et al. 2007; Meehan and Vahedifard 2013; Seed and Martin 1966; Seed 1981). Thus, seismic response and stability analysis are performed for different probable earthquake scenarios to evaluate the stability of the structure and determine the conditions which may hamper its integrity and serviceability (Tezcan et al. 2001). Such stability analysis can facilitate engineers to determine the possible reasons of failure of a dam, modify the design requirements in case of building a new dam or take proactive remedial measures to ensure the stability of an existing dam (Babu et al. 2007; Mejia et al. 2005).

Slope stability analysis is one of the oldest types of geotechnical engineering problems (Duncan et al. 2014). The stability analysis techniques evolved over the years from the simple hand-calculation-based ordinary method of

slices and analysis using design charts (Baker 2003; Taylor 1937) to limit equilibrium method and numerical approaches using commercially available software packages (Duncan 1996; Jibson 2011; Steward et al. 2011). With the advent of computers, the tedious hand-calculation-based problems can be easily solved using these software packages (Duncan 1996). Numerical approaches such as finite element and finite difference methods enable engineers to perform wide spectrum of stability analyses on earthen embankment structures, with varying geometric configurations, material properties, incorporate the effect of seepage of water, include different seismic loading conditions and account for the associated increase in pore water pressure during earthquakes (Chopra 1967; Clough and Chopra 1966; Jibson 2011; Yu et al. 1998).

Numerical modelling using advanced constitutive models can perform coupled non-linear analysis, which incorporates the effect of increase in excess pore water pressure and associated deformations during the earthquake, resulting in changes in material properties at the time of shaking (Elia et al. 2011; Prevost et al. 1985; Xia et al. 2010; Yiagos and Prevost 1991). Although these types of analyses can capture the actual behavior of the geomaterials during an earthquake event, it requires sophisticated constitutive models and high quality field and laboratory test data for model calibration (Aydingun and Adalier 2003; Montgomery et al. 2014); both of which are seldom available in the case of real projects (Cascone and Rampello 2003; Elia et al. 2011; Jibson 2011). Hence limit equilibrium analysis

and pseudo-static approach still remain as the preferred analysis tools among the practicing engineers, at least for preliminary analysis (Cheng et al. 2007; Choudhury et al. 2007; USSD 2007).

Commercially available software packages have made it easy to perform the slope stability analysis for practicing engineers. However, the efficacy of the analyses results depends on the accuracy with which the numerical model portrays the actual field conditions (Cascone and Rampello 2003). The external geometric configuration of the dam can be modelled with acceptable accuracy in the software using the as-built drawings of the dam, or data obtained from simple surveying and levelling techniques, or with the aid of advanced techniques such as LiDAR scans or aerial photography using UAVs (Shafikhani 2018; Shafikhani et al. 2017, 2018). However, the principal challenge in numerical modelling lies in defining the material properties of the dam and incorporating the effect of heterogeneity and changes in the material property at different sections of the dam. The embankment structure is often idealized as a zoned structure with the respective representative material properties assigned to the individual zones (Babu et al. 2007; Boulanger and Montgomery 2016; Pelecanos 2013; Tezcan et al. 2001). The accuracy of a subsequent analysis result may be questionable since this crude approximation in assigning averaged values of different material properties, at different segments of a dam section, may not portray the actual field conditions.

The most important properties used for seismic slope stability analysis includes the small strain shear modulus, damping ratio and strength parameters such as the cohesion intercept, friction angle and the undrained shear strength (Cascone and Rampello 2003; Hack et al. 2007). These parameters are not intrinsic properties of a geomaterial, rather they are dependent on the conditions which a soil layer experiences under field conditions (Holtz and Kovacs 1981; Kramer 1996). The behavior of a soil and the material properties which it exhibits is highly dependent on the stress state of the soil layer. Hence assuming uniform material property throughout the core or the shell of the dam, near the crest as well as at deeper layers close to the foundation, does not represent the field condition and may lead to an erroneous result in a stability analysis. Extensive laboratory and in-situ test results along with advanced interpolation techniques are thus required to capture the variation in material properties along the dam and accurately model the scenario using a commercially available software.

The extent of material variability along different sections of the dam depends on the construction method employed to build the dam. Unlike homogeneous dams or zoned earthen dams, the degree of material variability is significantly high in case of tailing dams and hydraulic-fill dams (Boulanger and Montgomery 2016; Popescu et al. 1997). Hence assuming similar material properties over different zones of the dam may lead to a high margin of error while analyzing a hydraulic-fill dam. In-situ tests conducted along the dam can provide

important information on the extent of variation in different material properties. Additional laboratory tests on undisturbed samples, collected from different locations of the dam, can furnish important complementary information in addition to those obtained from in-situ tests (Babu et al. 2007). Although the accuracy of the analysis results increases with the availability of high-quality test data, it is practically impossible to perform a high number of field tests due to budget constraints (Chakraborty et al. 2017a). The material properties at other locations of the dam, where the test results are unavailable, is either assumed to be same as that of the nearest section or are obtained by interpolating the data from the adjacent sections, where test results are available. Hence it is expected that enhancing the quality of the interpolation technique can be useful in improving the efficacy of the analysis.

The values of different material properties obtained from in-situ tests depend on the correlations used to interpret the test results and the accuracy of the laboratory tests on undisturbed samples rely on the exactness of the conditions used to simulate the actual field stress state (Chaney et al. 1996; Suits et al. 2005). A significant amount of engineering judgement, based on prior experience, is thus required in such cases and a considerable degree of uncertainty is always associated with estimating the material properties (Babu and Srivastava 2010; Boulanger and Montgomery 2016; Duncan 2000; Griffiths et al. 2010; Wolff 1996; Xiong and Huang 2017; Zhenyu et al. 2015). A reliability-based analysis or a sensitivity

analysis can provide important information on the impact of erroneous estimation of different material properties and the effect of the associated uncertainties in these properties (Babu et al. 2007; Baecher and Christian 2005; Garevski et al. 2013; Liang et al. 1999; Yegian et al. 1991). Besides estimating the material properties, earthquake time-history data depicting the variation of acceleration with the time of earthquake is also required for performing a seismic slope stability analysis (Cascone and Rampello 2003; Cetin et al. 2005).

The earthquake time-history data is readily available for earthen dams located in earthquake-prone regions, which has a history of previous earthquakes. In case of dams located in new, induced seismicity zones, previous earthquake data is rarely available. However, it is imperative to check the stability of the earthen dams under probable seismic events and take proactive measures to avoid any catastrophic consequences. Selecting an earthquake time-history data becomes a challenging task in such cases and a rational approach is required in deciding the time-history data to be used for performing a Newmark deformation analysis or a time-history-based dynamic analysis. All earthquake excitations don't affect an earthen dam to the same extent (Crespellani et al. 1998; Tezcan et al. 2001). The response of a structure to a seismic excitation depends on its natural frequency, which is primarily dependent on the geometric configuration and the material properties of the dam (Hack et al. 2007). The vibration is amplified, due to strong resonance conditions, when the predominant frequency of the seismic excitation is

close to the natural frequency of the structure (Chakraborty et al. 2019b; Parish et al. 2009; Zhu and Zhou 2010). Thus earthquake time-history data of two different earthquakes, having the same peak acceleration and duration of excitation, will have different effects on the response and stability of the structure, if the predominant frequencies are widely different.

In this study, the seismic response and stability analysis of the eighty-five years old Eagle Mountain (EM) dam in North Texas is performed. The dam is located on the West Fork Trinity River in Tarrant County, Texas, USA. The construction of this 26m high and 1463m long dam started in January, 1930 and was completed in October, 1932 (TRWD 2016). The dam was partially built by wetting and rolling the soil and partly by the hydraulic-fill method of construction. Series of laboratory and field test results were available along the crest, slopes and downstream toe of the dam from previous ground investigation studies conducted at the dam site. Piezocone penetration tests with pore pressure measurements (CPTu), spectral analysis of surface waves (SASW) tests and laboratory test results suggested a high degree of material variability along the length of the dam, owing to the hydraulic-fill method of construction. A framework is established as a result of this study to perform seismic stability evaluation of highly heterogeneous hydraulic-fill dams located in new, induced-seismicity zones.

1.2 Motivation

Even a decade ago, Texas was not considered to be a high seismicity zone. There were no significant earthquake excitations which may cause alarming consequences on dams and levees located in Texas. However, in 2016, United States Geological Society (USGS) declared Oklahoma-Kansas, the Raton Basin, North Texas, North Arkansas, and New Madrid to be high seismic hazard zone due to a rapid increase in the number of M3+ earthquakes (Figure 1-1) because of induced seismicity (USGS 2016). This necessitates taking proactive measures to study the stability of old earthen dams which may not have been specifically designed and built to withstand these new, induced earthquake excitations. The study was performed on the 85 years old Eagle Mountain dam located in North Texas, which is owned and operated by Tarrant Regional Water District (TRWD). The Eagle Mountain Dam is a hydraulic-fill dam, which has a great extent of variability in material properties due to the hydraulic-fill method of construction. Hydraulic-fill dams around the world have a history of unsatisfactory performance in withstanding seismic events (Heinz 1976; Küpper 1991; Mejia et al. 2005; Seed 1981). Hence it was necessary to evaluate the stability of the dam under different earthquake conditions and determine the probable problematic sections of the dam, which may be detrimental to the stability and serviceability of the structure during seismic events.

The purpose of this research study is to develop a comprehensive framework to perform seismic response and stability analysis of a highly heterogeneous hydraulic-fill dam, incorporating the effect of material variability and induced seismicity. Most of the methods developed as a part of this study and the findings of the research will be of interest to researchers and are expected to be especially useful to practicing engineers.

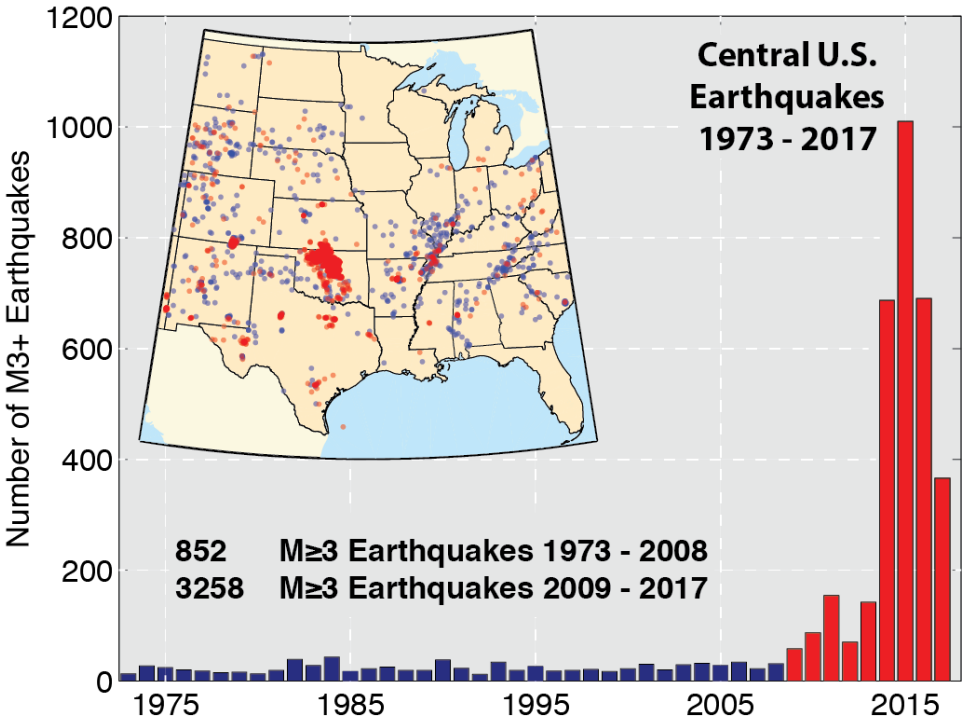

Figure 1-1: Number of M3+ earthquakes in central USA

(Source: https://earthquake.usgs.gov/research/induced/overview.php)

1.3 Research objective

The objective of the dissertation study is to develop a framework for performing a seismic response and stability analysis of hydraulic-fill dams located in newly-declared induced-seismicity zones and evaluate the performance of such dams during probable seismic events. The research also focuses on addressing several issues usually faced while performing a seismic response and stability analysis.

A typical stability analysis begins with the determination of different material properties of the dam, which are used as input parameters for the analysis. These properties are determined from a limited number of in-situ tests or laboratory tests on extracted soil samples. The strength parameters are usually obtained from in-situ tests (CPT or SPT correlations) or by performing laboratory tests (triaxial or direct shear tests) on soil samples. However, it is practically impossible to extract soil samples at each and every location of the dam. Hence interpolation techniques are used to assess the material properties at different locations of the dam where test results are not available. As a part of this project, three-dimensional visualization models of the dam were generated using geostatistics-based kriging analysis. These models are then used to assign material properties for analyzing the stability of different sections of the dam.

Besides obtaining the strength parameters, stiffness properties such as small strain shear modulus are of paramount importance for performing seismic response

and stability analysis. Small strain shear modulus is often determined by spectral analysis of surface waves (SASW) test, a non-intrusive and non-destructive test based on dispersive nature of Rayleigh waves. However, performing a SASW test on the field requires several numbers of trials to obtain acceptable test data, based on 'coherence', which is a measure of the quality of a particular test. It is hence necessary to develop a method to improve the efficiency of the SASW test and obtain high-quality data.

The analysis results and the inferences drawn from these results solely depend on the accuracy of the estimated strength and stiffness properties. The estimated values of a given material property in-turn depend on the testing technique and on the type of correlations used for interpreting the CPT or SPT test data. Moreover, the analysis is at times performed with assumed material properties assessed by the engineer, solely based on his/her experience. All these circumstances, in addition to the inherent heterogeneity of the dam materials, can lead to inaccurate analysis result. It is thus necessary to study the effect of erroneous estimation of different material properties on the analysis using sensitivity analysis and reliability-based analysis.

Real earthquake time-history data is required to perform the seismic response and stability analysis of an earthen dam, which was however not available for the EM dam site. Hence a natural-frequency-based approach is required to select

the earthquake time-history data. The existing methods used to determine the natural frequency of an earthen embankment structure can be used to determine the natural frequency at low strain levels. However, during real earthquake events, the body of the dam experiences different strain levels, which is associated with changes in shear modulus and damping ratio. Determining the natural frequency at low strain levels cannot portray the behavior of a dam during real earthquake conditions. Hence a method is required to determine the strain-dependent natural frequency of an earthen embankment structure, incorporating the effect of non-linear behavior of the material.

1.4 Organization

The dissertation consists of seven chapters.

Chapter 1 contains the introduction, an overview of the topic, motivation and need for the study, and the objectives of the research.

Chapter 2 summarizes the salient information gathered from the literature reviewed. This chapter provides an overview of different types of earthen dams, especially hydraulic-fill dams. The construction procedure of hydraulic-fill dams is also elucidated. Methods for determination of small strain shear modulus and the associated uncertainty is discussed. Finally, the natural frequency determination methods and the existing methods for performing the static and seismic stability analysis is presented.

Chapter 3 presents the developed analysis framework and the methodology of the research.

Chapter 4 describes the method developed to improve the quality and repeatability of the SASW test and presents the shear wave velocity profiles at different sections of the Eagle Mountain dam. These shear wave velocity profiles will be later used in Chapters 5 and 6 for determination of natural frequency of the dam and evaluating the stability of its slopes during seismic events, respectively.

Chapter 5 explains the novel method developed to determine the strain-dependent natural frequency of earthen embankment structures such as dams and levees. The variation of natural frequency along the length of the dam is presented in this chapter. The estimated natural frequencies, presented in this chapter, will be used in Chapter 6 to select the earthquake time-history data, used for performing seismic slope stability analyses.

Chapter 6 presents the results of a comprehensive seismic slope stability analysis performed for EM dam, incorporating the effect material variability. The critical sections of the dam are also identified based on the static, pseudo-static, Newmark deformation analysis and earthquake time-history-based dynamic analysis. The results of the reliability-based pseudo-static analysis and the expected performance level of the different sections of the dam, under probable earthquake conditions, are also presented.

Chapter 7 enunciates the importance of an additional sensitivity analysis to comprehend the impact of uncertainty associated with the estimation of small strain shear modulus, of different layers of an earthen embankment structure, on its seismic response and stability analysis.

Chapter 8 summarizes the findings of the study, applications of the developed framework and scope for future studies.

Chapter 2: Literature Review

2.1 Earthen dams

Dams are important engineered infrastructure which offers a wide range of social, economic and environmental benefits and is essential for the development of any nation (Tortajada 2015). These mega-structures provide flood control, water storage for irrigation purposes, electricity generation, recreational sites and navigation by inland water transportation (FEMA 2018). Dams are primarily classified into concrete dams and earthen dams, based on the material used for construction (Caballero 2017; Pelecanos 2013). A brief overview of earthen dams is provided in this section, with emphasis on the construction techniques of hydraulic-fill dams.

Earthen dams are made up of geomaterials, which are designed and constructed in different ways based on the function it serves, materials available from borrows, quarries or mining wastes, and suitability for a particular site. Earthen embankment dams can be classified into three major categories: homogeneous earth-fill dams, zoned earth or rock-fill dams and upstream membrane dams (National Research Council 1983; MacGregor et al. 2014; Pelecanos 2013).

As the name suggests, homogeneous earth-fill dams are primarily made up of the same type of soil having similar material properties. Whereas a zoned earthen

dam has different zones made up of earth or rock-fill, and each zone serves a specific role towards the stability and serviceability of the structure (MacGregor et al. 2014).

Homogeneous earth-fill dams are probably the simplest and oldest design type and are rarely used in practice for large dams. These dams were built in ancient times when advanced technology and construction tools were unavailable (Pelecanos 2013). Figure 2-1 and Figure 2-2 presents typical schematic diagrams of different earth-fill dams, rock-fill and concrete-faced membrane dams. The function of the different zones marked in these figures is described in Table 2-1.

A zoned earth-fill dam consists of a zone of fine-grained soil which primarily controls seepage of water through the dam, and the earth-rockfill zone provides lateral support and stability (Fell et al. 2005). The filter drains controls erosion caused by seepage of water and facilitates in the dissipation of the excess pore water pressure. The grout curtain also plays an important role in reducing seepage and enhancing the stability of the structure.

Figure 2-3 shows some of the earlier construction techniques of embankment dams which are currently not followed in practice. One of these methods of construction is hydraulic-filling the dam embankment by transporting the soil as a suspension in water and depositing the slurry along the outside edges of the embankment. This method of construction was widely followed in the late

19th century and the early 20th century in Russia, Canada and the United States (Küpper 1991). Although the hydraulic-fill method of construction is not continued any longer in the USA, there are several hydraulic-fill structures which are still in service. The following section describes the hydraulic-fill method of construction and presents the history of the performance of some hydraulic-fill dams around the world, during seismic events.

Table 2-1: Description and function of different zones of embankment dams (after Fell at al. 2005)

Zone	*Description*	*Function*
1	Earthfill ("core")	Controls seepage through the dam
2A	Fine filter (or filter drain)	(a) Controls erosion of Zone 1 by seepage water, (b) Controls erosion of the dam foundation (where used as horizontal drain), (c) Controls buildup of pore pressure in downstream face when used as vertical drain
2B	Coarse filter (or filter drain)	(a) Controls erosion of Zone 2A into rockfill, (b) Discharge seepage water collected in vertical or horizontal drain
2C	(i) Upstream filter (ii) Filter under rip rap	Controls erosion of Zone 1 into rockfill upstream of dam core Controls erosion of Zone 1 through rip rap
2D	Fine cushion layer	Provides uniform support for concrete face; limit leakage in the event of the concrete face cracking or joints opening
2E	Coarse cushion layer	Provides uniform layer support for concrete face. Prevents erosion of Zone 2D into rockfill in the event of leakage in the face
1–3	Earth-rockfill	Provides stability and has some ability to control erosion
3A	Rockfill	Provides stability, commonly free draining to allow discharge of seepage through and under the dam. Prevents erosion of Zone 2B into coarse rockfill
3B	Coarse rockfill	Provides stability, commonly free draining to allow discharge of seepage through and under the dam
4	Rip rap	Controls erosion of the upstream face by wave action, and may be used to control erosion of the downstream toe from backwater flows from spillways

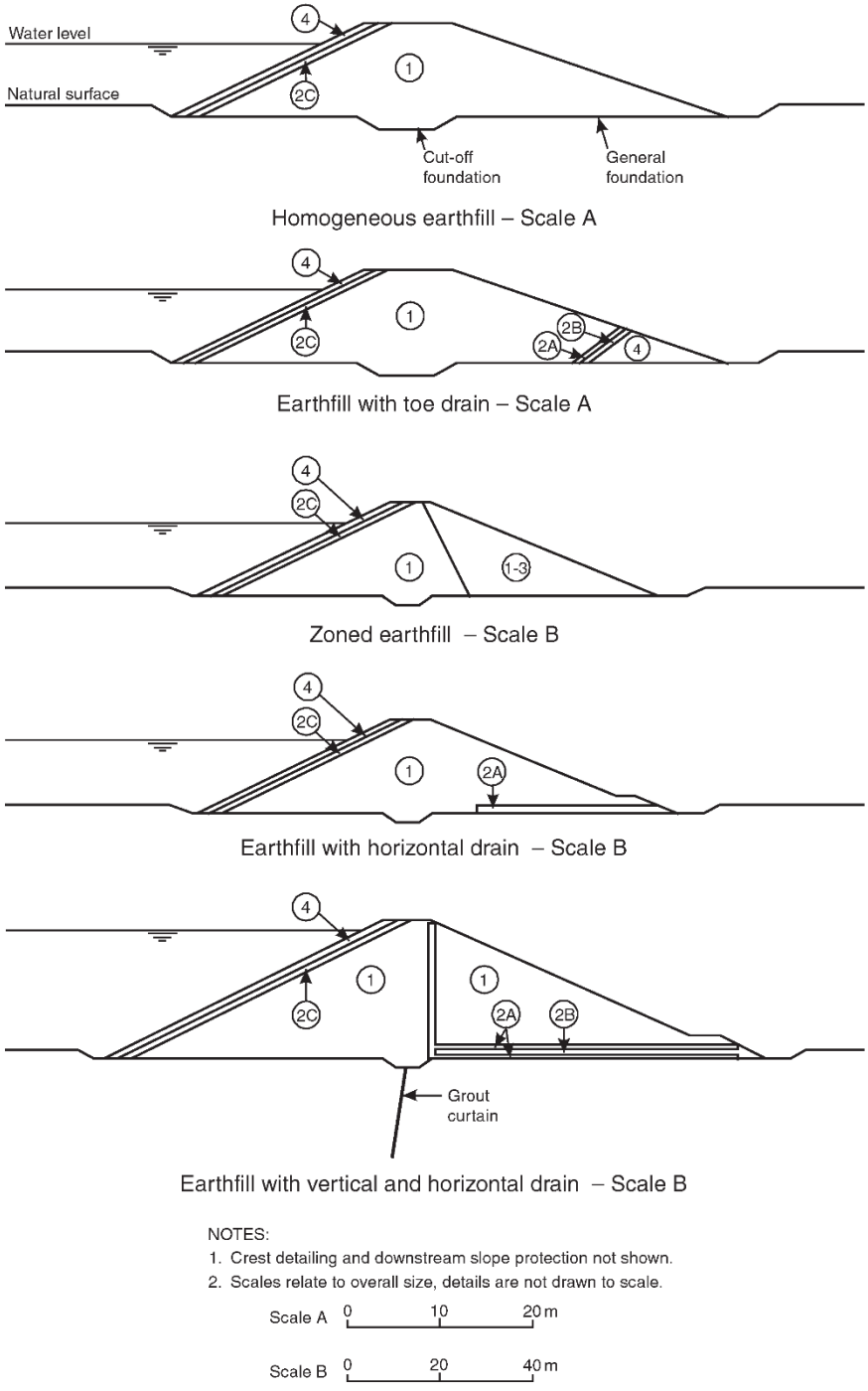

Figure 2-1: Typical cross-sections of earth-fill dams
(after Fell at al. 2005)

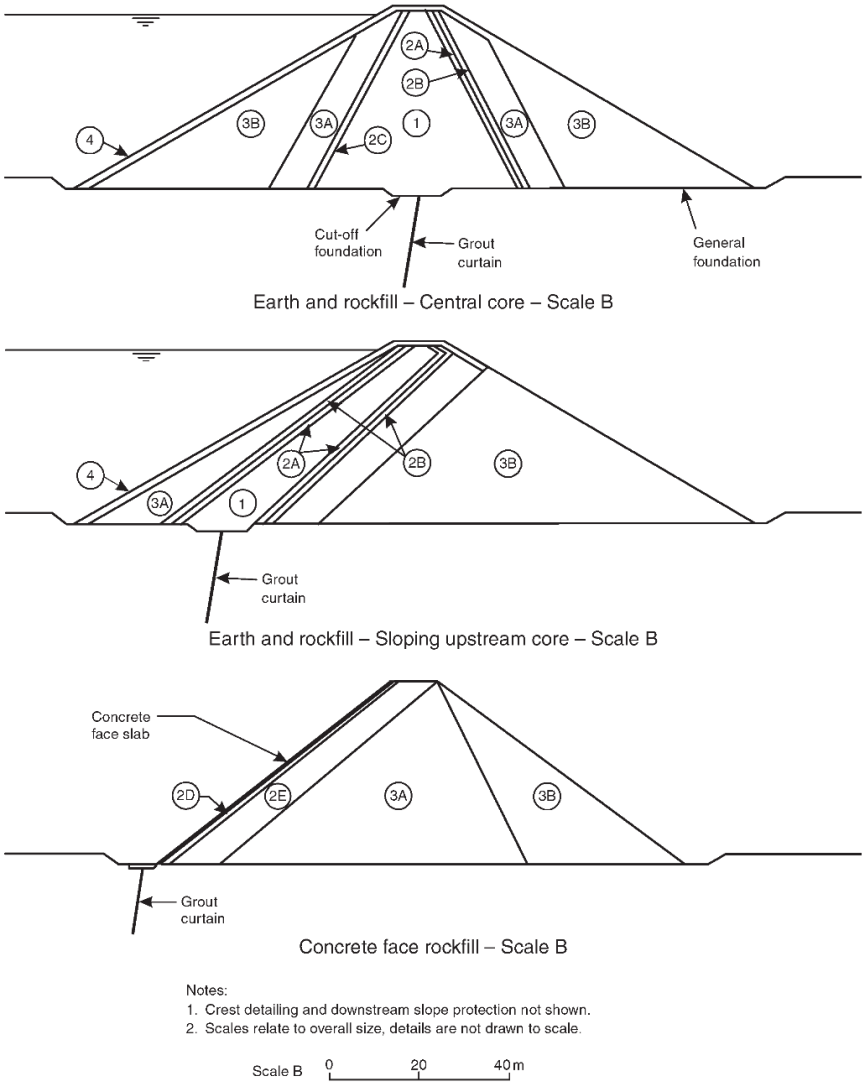

Figure 2-2: Typical cross-sections of earth-fill, rock-fill and concrete face dams (after Fell at al. 2005)

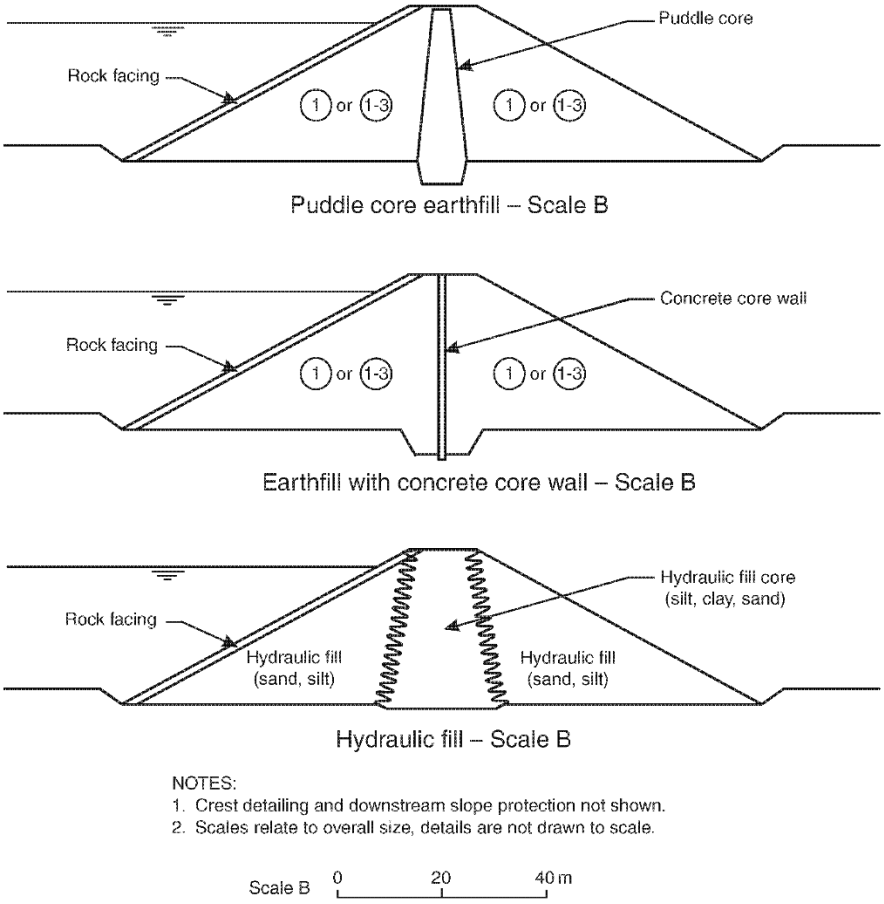

Figure 2-3: Typical cross-sections of some earlier types of dam (after Fell at al. 2005)

2.2 Hydraulic-fill dam

2.2.1 Construction process

Hydraulic-fill method of construction was a widely used technique, for building earthen dams in Canada, USA and Russia (Küpper 1991; Melent'ev 1980; Vick 1996; Wiltshire 2002), in the late 19th century and the early 20th century (Valenzuela 2015, 2016). In those days, sophisticated construction tools and techniques were

not available and hence hydraulic-fill method was a viable option for constructing embankments with the borrow area close to the site. In the ‘true’ hydraulic method of construction, the borrow soil was excavated using shovels, draglines, dredges and hydraulic monitors, mixed with water and transported as a suspension through flumes, and discharged along the outer edges of the embankment through single point discharge or multiple spigots (Figure 2-4) (Heinz 1976; Küpper 1991; Vick 1996; Wiltshire 2002). The semi-hydraulic-fill method was used at sites where water supply was not favorable for transporting the borrow soil. In such cases, the soil was hauled to the site by some other suitable means, mixed with water and placed in the embankment similar to the ‘true’ hydraulic-fill method (Heinz 1976). The outer edges were built at first to form a deposition basin in the middle, where the core of the dam would eventually be formed (Figure 2-4 and 2-5). The outer edges of the embankment acted as starter dykes which contained the deposited slurry and allowed free drainage of the excess water.

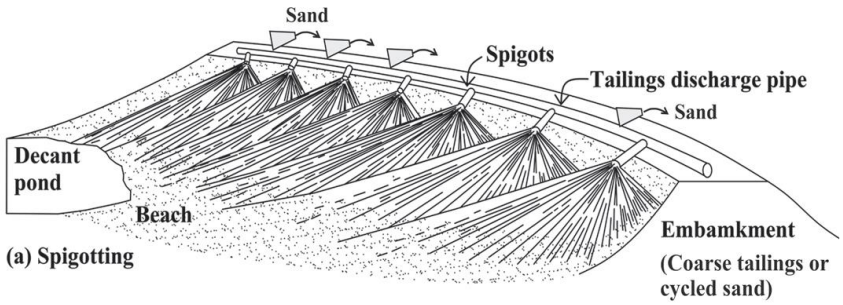

Figure 2-4: Discharge of slurry through spigots in hydraulic-fill construction (after Valenzuela, 2016)

After the slurry was discharged from the flumes, the ingredient soil particles settled down due to gravity based on the grain size. The coarse-grained particles got deposited at first, close to the point of discharge and formed the shell of the dam (Figure 2-5 and Figure 2-6). Whereas, the fine-grained clay particles were held in suspension for the longest time and got deposited near the center of the embankment to form the water-tight core (Vick 1996). The silts formed the transition zone between the clayey core and sandy shell of the embankment dam. The deposited soils were not rolled and compacted, rather the embankment got compacted gradually due to gravity as the excess water drained through the permeable shell.

The rate of construction was an important decisive factor while constructing a hydraulic-fill dam. There had been several incidents where the dam failed during the time of construction due to improper drainage and build-up of excess pore water pressure (Küpper 1991). In March 1918, the Calaveras Dam in California had faced a similar fate during construction, when the still-fluid clay core spilt out through the upstream face into the reservoir (Jansen 2012). Although many hydraulic-fill dams around the world have performed satisfactorily during its design life, there have been several events where the hydraulic-fill dams have failed during seismic events (Heinz 1976; Küpper 1991; Morgenstern and Küpper 1988; Seed 1981; Valenzuela 2016; Vick 1996).

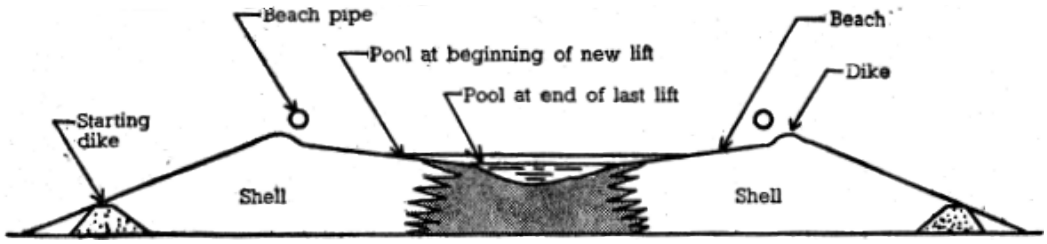

Figure 2-5: Formation of shell and core of a hydraulic-fill dam
(Source: http://community.dur.ac.uk/~des0www4/cal/dams/cons/conss4.htm)

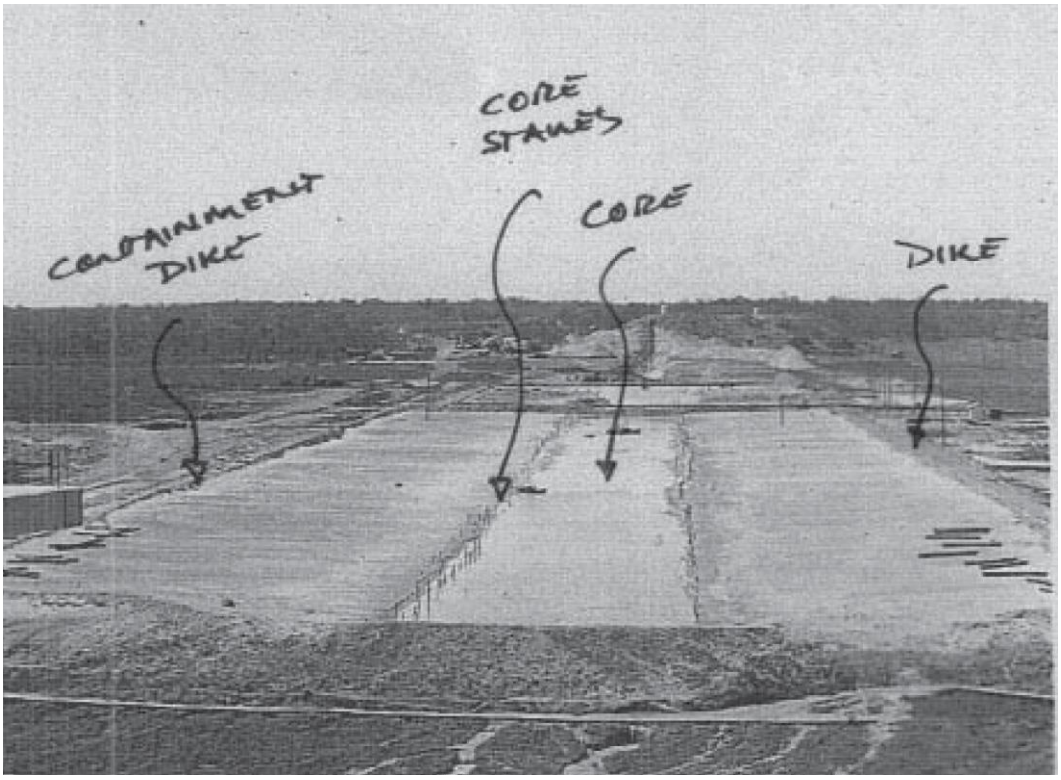

Figure 2-6: Eagle Mountain dam in Texas built by hydraulic-fill method with the aid of starter dykes
(Courtesy TRWD)

2.2.2 Earthquake resilience of hydraulic-fill dams

There have been several incidents in the past when these hydraulic-fill dams failed during earthquakes (Heinz 1976; Seed 1979, 1981). Several hydraulic-fill dams, including the El Cobre dams in Chile, which is one of the most earthquake-prone countries in the world, failed due to the March 1965 earthquake (Dobry and Alvarez 1967). The Mochikoshi tailing dam in Japan failed due to liquefaction during the Izu-Ohshima-Kinkai earthquake in 1978 (Ishihara 1984). Some hydraulic-fill dams also failed following the March 1985 earthquake in Chile (Troncoso 1988). However, there have been instances when hydraulic-fill dams were even able to withstand strong ground motions, without any catastrophic failures (Ambraseys 1960a). Dashishe dam in China is one such example which did not experience a catastrophic failure during the M 7.8 Tangshang earthquake in 1975 (Küpper 1991). The dam was located 15km and 40km from the epicenters of the two main shocks and was able to bear the earthquake with some cracks, sand boils and water sprouts.

One of the most studied cases of failure of hydraulic-fill dam is that of the lower and upper San Fernando Dam in California, USA, which incurred extensive damage due to the M 6.6 earthquake of February, 1971 (Castro et al. 1985, 1992; Gu et al. 1993; Heinz 1976; Seed 1979, 1981; Seed et al. 1975a; b, 1978). The upstream shell of the lower San Fernando Dam, which was constructed by the hydraulic-fill method, suffered a sliding failure and was followed by a subsequent collapse of the core and top 9m (30ft) of the downstream slope (Seed 1979; Seed

et al. 1975a). The Upper San Fernando Dam also incurred some damages, although it was not as catastrophic as that of the lower dam. The upper dam had moved 1.5 to 2m (5 to 7ft) towards the downstream side, due to the earthquake (Seed 1979, 1981). Extensive field tests, laboratory tests and research studies were performed on these dams to comprehend the behavior of hydraulic-fill earthen dams during earthquakes and re-assess the efficacy of the analysis methods, which were then used in practice (Seed 1979, 1981).

Before the San Fernando earthquake of 1971, engineers mostly assumed earthen dams to be inherently stable to earthquake loading. Pseudo-static method of analysis, which approximates the earthquake loading in terms of a constant horizontal body force on the slip surface, was the most common method of assessing the seismic stability of the slopes. Five years before the 1971 earthquake, a reputed agency performed pseudo-static analysis on the lower San Fernando Dam and declared it to be stable (Seed 1979). Pseudo-static analysis with a seismic coefficient of 0.15 (i.e. an additional constant horizontal force of 0.15 times the weight of the slip surface) resulted in a factor of safety of 1.3 for the lower dam and between 2 to 2.5 for the upper dam (Figure 2-7 and 2-8) (Seed 1979). Although pseudo-static analysis suggested that both the dams were stable to seismic loading conditions, in reality, the dams were extensively affected by the 1971 San Fernando earthquake. Extensive research identified liquefaction of sand layers to be the primary reason behind the observed failures.

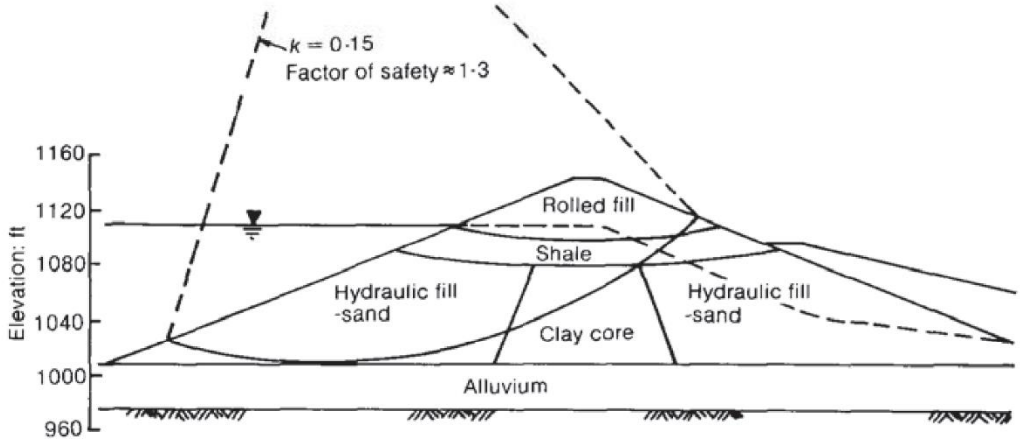

Figure 2-7: Factor of safety for pseudo-static analysis of lower San Fernando dam (after Seed 1979)

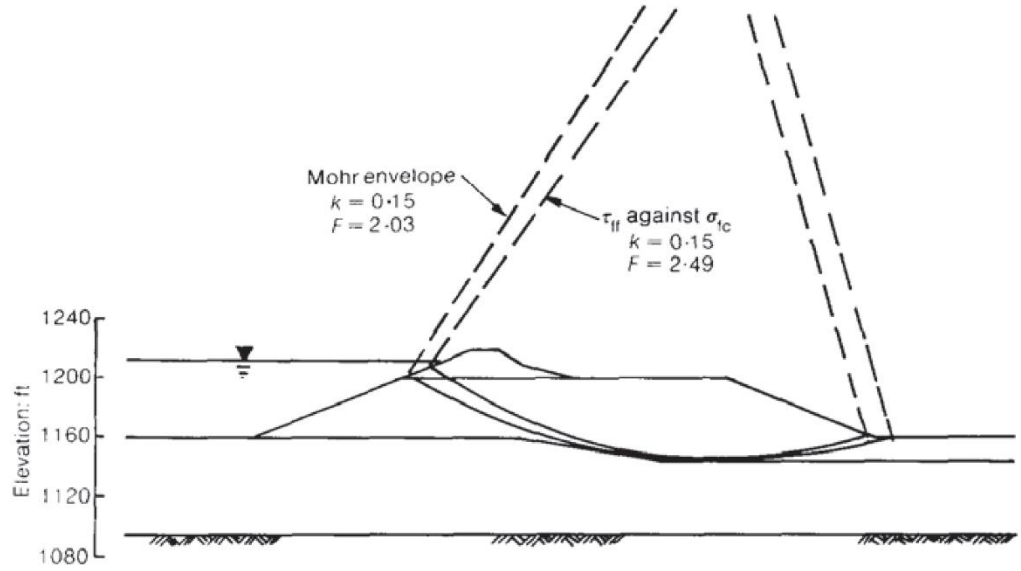

Figure 2-8: Factor of safety for pseudo-static analysis of upper San Fernando dam (after Seed 1979)

Results from dynamic finite element analysis, performed with material properties determined from laboratory and field tests, suggested that extensive

zones of the upstream shell and some portions of the downstream shell liquefied (marked in black in Figure 2-9). The dam did not fail during the earthquake shaking, hence it was inferred that inertia forces were not the reason behind the failure of the dam (Seed 1979). The pore pressure parameter (r_u = change in pore water pressure/ initial effective confining pressure) reached unity in the portion of the dam marked with black in Figure 2-9, and hence the corresponding shear strength dropped to zero due to liquefaction (Figure 2-10).

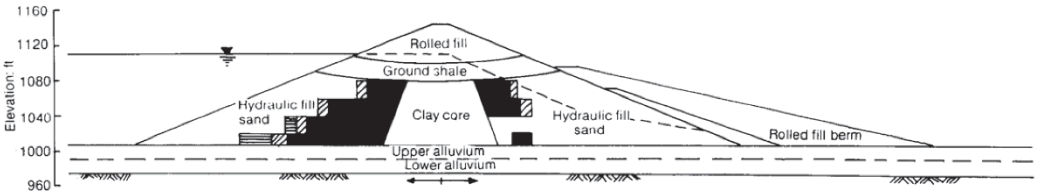

Figure 2-9: Zones of failure due to liquefaction in lower San Fernando dam (after Seed 1979)

The dense sand near the toe of the dam showed dilative behavior during shearing and the undrained strength was estimated to be 3,600psf (170kPa). Stability analysis with these parameters suggested a static factor of safety of 1.4, and hence the dam did not fail during the earthquake shaking (Figure 2-10).

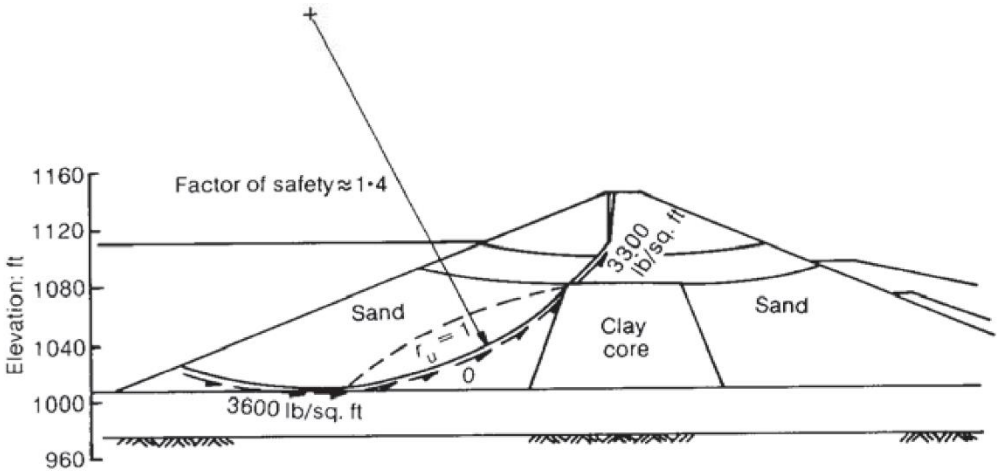

Figure 2-10: Post-earthquake factor of safety of lower San Fernando Dam (after Seed 1979)

However, after the shaking seized, the excess pore water pressure got redistributed and moved towards the zone which showed dilative behavior during shaking. This post-earthquake redistribution of pore water pressure resulted in an increase in pore water pressure near the upstream toe (Seed 1979, 1981). A subsequent post-earthquake drained analysis suggested a decrease in shear strength, as shown in Figure 2-11. The computed factor of safety after redistribution of pore water pressure dropped to 0.8, which supports the sliding failure of the upstream shell of the dam.

The shell of the dam provides support and stability to the inner core and hence the sliding failure of the shell resulted in instability of the core (Figure 2-12). A stability analysis with representative strength properties showed a factor of safety of 1.03, which supports the observed failure of the core and 30ft of the upstream

slope (Figure 2-13). It was inferred that the pseudo-static analysis should not be used to evaluate the stability of an earthen structure where there are chances of significant strength loss (>15%) and development of excess pore water pressure (Seed 1979).

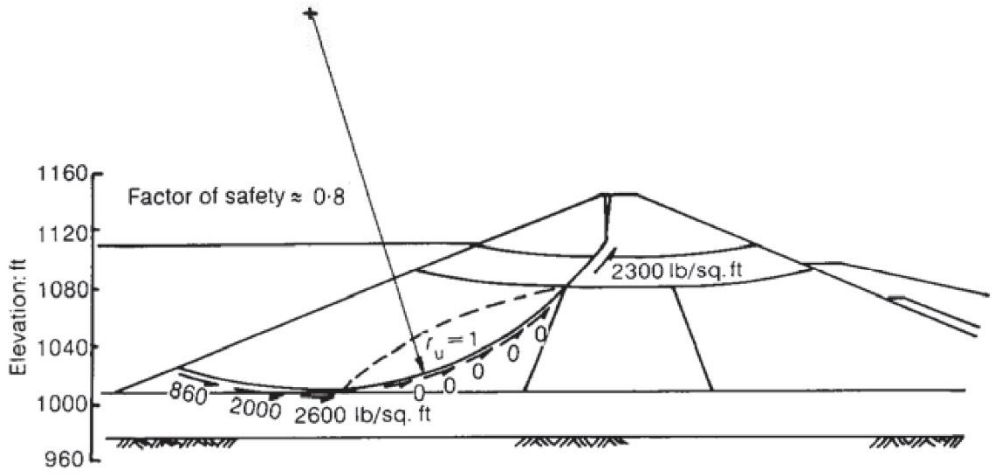

Figure 2-11: Factor of safety of lower San Fernando Dam short term after earthquake
(after Seed 1979)

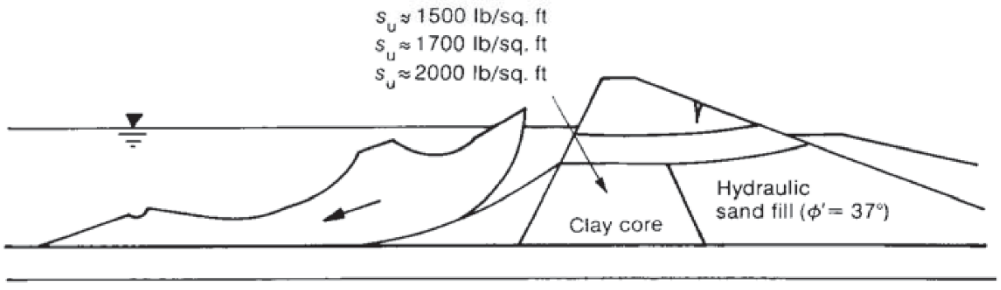

Figure 2-12: Failure of upstream shell of lower San Fernando
(after Seed 1979)

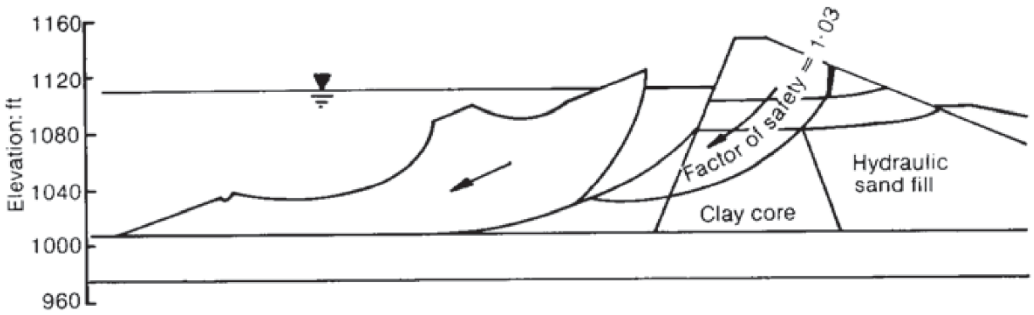

Figure 2-13: Progressive failure of core and downstream slope of lower San Fernando Dam
(after Seed 1979)

A step-by-step guide was provided by Seed (1979) to analyze similar dams. The steps involve (a) determining the geometry and material properties of the dam; (b) selecting appropriate earthquake time-history data; (c) evaluating the initial static stress condition of the dam before the earthquake, using numerical methods, such as finite element analysis; (d) determining dynamic properties of soil such as small strain shear modulus and damping ratio, along with their variations at different strain levels; (e) computing earthquake induced stresses in the dam using a suitable software; (f) performing laboratory tests on representative soil samples under similar initial and earthquake-induced stress conditions and determine the excess pore water pressure and associated permanent strains and (g) using the obtained laboratory results to assess the stability slopes during seismic events using dynamic finite element analysis and estimate the deformation incurred due to seismic loading.

The analysis performed by engineers on the stability of existing structures are mere speculations on the probable behavior of the structure. Unfortunately, engineers and researchers are able to validate the theories and reasons behind the failure of a structure, only when a structure fails (Seed 1979). However, the efficacy of the analysis results depends on the accuracy with which the material properties are estimated and the exactness with which the probable behavior of the geo-materials is predicted.

The following section presents the material properties required to perform a dynamic analysis. Special emphasis is provided to the shear modulus determination techniques and the variability in the estimated G_{max} values since it is the most important parameter which governs the seismic response of earthen dams. Spectral analysis of surface waves (SASW) was used to determine the shear wave velocity profile of the dam by conducting tests along the crest of the EM dam. Hence the SASW test principle, testing procedure, and the analysis steps were reviewed and are discussed in detail.

2.3 Material properties for dynamic analysis

2.3.1 Small strain shear modulus (G_{max})

Shear wave velocity (V_s) and small strain shear modulus (G_{max}) are important fundamental soil properties, which are widely used in geotechnical engineering problems related to dynamic loading conditions (Chaney et al. 1996; Kayen et al.

2013; Mayne and Rix 1995). These parameters are used for estimating the response of earthen structures such as dams and levees subjected to earthquake loading conditions, assess the stability of slopes and evaluate soil liquefaction potential (Gazetas 1981; Kayen et al. 2013; Piao et al. 2006; Raptakis and Makra 2015). The maximum shear modulus (G_{max}) corresponds to the shear modulus of the soil at strain level less than 0.001% (Mayne and Rix 1995; Robertson et al. 1986b; Stokoe et al. 1991). Maximum shear modulus is related to the shear wave velocity as shown in equation 2.1. Shear wave velocity can be estimated by different methods, such as laboratory tests on undisturbed soil samples, in-situ tests or by using empirical or semi-empirical correlation equations.

$$G_{max} = \rho . V_s^{\,2} \ , \tag{2.1}$$

where ρ is the bulk density of the soil

2.3.1.1 Shear modulus determination methods

Laboratory tests include bender element tests or resonant column tests on undisturbed soil samples, performed under similar confining pressure conditions as expected in the field (Chaney et al. 1996; Suits et al. 2005; Youn et al. 2008). However, sample disturbances and incorrect estimation of the stress state of the soil under in-situ condition may lead to erroneous estimation of G_{max}, with a difference of 100% or more as compared to field test results (Anderson et al. 1978; Hryciw 1990). However, the best method to estimate these parameters is to conduct in-situ

tests with minimum soil disturbance (Hryciw 1990; Mayne and Rix 1995). Thus, the tests conducted under field conditions are expected to provide a better estimate of the G_{max} values. The in-situ tests include invasive methods such as cross-hole test, down-hole test, suspension logging test, or seismic cone penetration test (SCPT) (Hryciw 1990; Mayne and Rix 1995; Moss 2008; Robertson et al. 1986b); and non-invasive techniques such as spectral analysis of surface waves (SASW), multichannel analysis of surface waves (MASW), frequency-wavenumber method (f-k method), spatial auto correlation, refraction microtremor (ReMi), seismic reflection/refraction test or microtremor array measurements (MAM) (Hiltunen and Woods 1988; Marosi and Hiltunen 2004; Moss 2008; Stokoe et al. 1991).

Under certain circumstances, such as economic constraints or unavailability of specialized equipment, G_{max} is estimated using semi-empirical or empirical correlations (Mayne and Rix 1995). Semi-empirical correlations relate G_{max} to mean effective stress, void ratio, relative density, plasticity index, over consolidation ratio, and other factors which influence the shear wave velocity of soil (Hryciw 1990; Kramer 1996; Robertson et al. 1995; Seed and Idriss 1970; Seed et al. 1986). The values of V_s or G_{max} can also be estimated from empirical correlations with standard penetration tests (SPT), cone penetration tests (CPT), dilatometer test (DMT), pressuremeter test (PMT) or Becker penetration test (BPT) (Ahmed 2016; Akin et al. 2011; Hryciw 1990; Kramer 1996; Robertson and Cabal 2015; Rollins et al. 1998). A vast database of V_s (or G_{max}) values for different types

of soil from around the globe and their corresponding test results (SPT, CPT, BPT, DMT, PMT, etc.) were used by researchers to perform regression analysis and obtain these correlations. The choice of a particular method for determining the subsurface shear wave velocity profile depends on several factors including the type and importance of the project, associated cost and budget, and expertise and experience of engineers.

2.3.1.2 Variability in estimated G_{max} values

There are various methods for estimation of G_{max}, however, a significant difference is observed in the results obtained by these methods. Several researchers have studied the intra-method and inter-method variability in estimated G_{max} values. The inherent variability and heterogeneity of subsurface soil layers, the fundamental difference in the philosophy behind different testing methods, and the difference in interpretation of results by individuals primarily lead to the variability in the estimated G_{max} values obtained from different methods (Moss 2008). Moreover, the extent of the difference in estimated V_s varies with depth and complexity of subsurface soil profile (Marosi and Hiltunen 2004; Moss 2008; Raptakis and Makra 2015). Robertson et al. (1986) reported that V_s obtained from CPT downhole tests was consistently higher than those obtained from the crosshole tests by a margin of 20%, leading to a deviation of about 40% in the estimated G_{max} values. The average error in G_{max} obtained using empirical correlations with Dilatometer test was found to be around 23% (Hryciw 1990). A study by Mayne and Rix (1995) showed that

V_s obtained from CPT correlations deviated from those obtained using SASW test; with an error margin upto 50%. The difference in the V_s profile was found to decrease with prior knowledge about the void ratio profile of the site. However, such an information is seldom available beforehand for any projects.

Correlation equations used to obtain shear wave velocity from equivalent N_{60} from Becker penetration test was reported to vary within a margin of ± 30% of that obtained from field tests (Rollins et al. 1998). The deviation was found to be as high as ± 50% in some cases. The intra-method variability for SASW tests was reported to have a coefficient of variation of 5-6%, while those for downhole tests and SCPT varied from 1 to 3% (Moss 2008). The study by Moss (2008) also provides an excellent compilation of inter-method variability (using various invasive and non-invasive field testing techniques) in the estimated V_s, reported by several researchers. A maximum difference of 60% was reported for shear wave velocity obtained using two different techniques (Asten and Boore 2005). Other studies have stated that the margin of error in estimating shear wave velocity may vary from -30% up to +110% (Ahmed 2016; Raptakis and Makra 2015).

The aforementioned in-situ tests are mostly conducted on the crest of the dam; hence simplifying assumptions have to be made regarding the G_{max} of the shell of the dam. The dam is often idealized to consist of horizontal layers, and the material is assigned with the G_{max} values obtained from in-situ tests conducted on

the dam crest (Pelecanos 2013). In some cases, the shell of the dam is considered to have uniform G_{max} properties (Cetin et al. 2005; Parish et al. 2009), whereas some analyses assume G_{max} to increase as a function of effective mean stress (Tsiatas and Gazetas 1982).

The existing literature hence provides some insight on the possibility of erroneous estimation (both underestimation and overestimation) of V_s using different methods available. Although the extent of deviation of the estimated V_s may depend on the testing technique or correlations used and vary from one site to another, it is evident from the available literature that a significant uncertainty remains in the estimation of shear wave velocity profile and small strain shear modulus. Since the shear wave velocity and small strain shear modulus are important parameters in seismic response analysis and seismic slope stability analysis of earthen structures like dams and levees, it is expected that error in the estimation of G_{max} will affect the behavior of the structure to dynamic loading.

The shear wave velocity profiles (and G_{max} values) at the dam site were determined using SASW test. Hence extensive literature was reviewed to understand the testing principle and procedure. The following section presents an overview of the SASW testing technique and the problems faced while performing a SASW field test.

2.3.1.3 G_{max} determination using Spectral Analysis of Surface Waves

Small strain shear modulus G_{max} with strain level less than 0.001% (Addo and Robertson 1992; Aouad et al. 1993; Hiltunen and Woods 1988; Joh 1996; Nazarian and Stokoe II 1983; Nazarian and Stokoe 1985; Sanchez-Salinero et al. 1986; Stokoe et al. 1991) is an important parameter used in geotechnical engineering problems, especially while dealing with dynamic loading conditions. G_{max} values of subsurface layers are required for pavement design and pavement condition monitoring, liquefaction and dynamic stability studies of slopes subjected to earthquake loading, landslide investigation and characterization of a geotechnical site based on stiffness properties (Joh 1996; Stokoe et al. 1991). As mentioned in the previous section, several field tests like the crosshole test, downhole test, seismic cone penetration test or laboratory tests like the resonant column or bender element tests are conducted to determine G_{max}.

The above-mentioned field tests are intrusive in nature (Stokoe et al. 1991) and the laboratory test requires undisturbed samples to perform the test. In most cases, it is difficult to get perfectly undisturbed samples, simulate in-situ conditions and perform the test in the laboratory. Under such circumstances, a non-destructive testing technique like Spectral Analysis of Surface Waves (SASW) is a feasible option for determining the subsurface stiffness profile. In order to obtain the subsurface shear wave velocity profile at the dam site, it was necessary to conduct

SASW tests. Hence the theory, working principle and steps involved to obtain the shear wave velocity profile using SASW test were reviewed.

SASW test principle: SASW is a non-intrusive and non-destructive testing technique widely used to determine the in-situ shear wave velocity and small strain shear modulus of subsurface layers. Although the final aim of the test is to determine the shear wave velocity profile of a given site, Rayleigh waves are used to indirectly calculate the shear wave velocity (Al-Hunaidi 1993; Heisey et al. 1982) because of the following reasons: (a) $2/3^{rd}$ of the impact energy of a vertically oscillating impact source emanates as Rayleigh waves and (b) Rayleigh wave energy varies as $1/\sqrt{r}$ when compared with shear wave energy which varies as $1/r^2$ (r is the distance from the impact source)(Miller and Pursey 1955) . Hence at a given distance away from the impact source location, most of the energy received by geophones will be in the form of Rayleigh waves. The testing philosophy is based on the dispersive nature of Rayleigh waves (surface wave) (Addo and Robertson 1992; Al-Hunaidi 1993; Kumar and Hazra 2014; Kumar and Rakaraddi 2013; Nazarian and Stokoe II 1983; Nazarian and Stokoe 1985; Stokoe et al. 1991). Unlike a homogeneous medium, surface waves of different wavelengths travel with different velocities in a heterogeneous medium. Hence the SASW test can acquire information of a wide range of frequency/wavelength with a single impact of hammer on the ground surface.

Steps for V_S determination using SASW: The test involves three major tasks: (a) field test, (b) obtaining dispersion curve from field tests and (c) inversion analysis to determine the shear wave velocity profile (Joh 1996; Kumar and Rakaraddi 2013). A brief overview of the major tasks performed for SASW testing is provided in the following section. A detailed description of the theoretical aspects can be found elsewhere (Heisey et al. 1982; Nazarian and Stokoe II 1983; Nazarian and Stokoe 1985; Stokoe et al. 1991).

Field test: The first and most important task for SASW testing is to conduct the test at the site of interest and obtain acceptable representative subsurface information. Theoretically, only one geophone spacing should be sufficient to get information for all the subsurface layers. But from practical considerations, the test needs to be performed with different geophone spacing in order to get information about different layers located at different depths from the ground surface (Al-Hunaidi 1993; Stokoe et al. 1991). A test with shorter geophone spacing usually gives information about the near-surface layers whereas a higher geophone spacing is required to get the shear wave velocity of deeper layers. Usually, the distance between geophones is doubled after each test to provide enough overlap zone in the dispersion curves obtained from the respective tests conducted at different spacings (Joh 1996; Nazarian and Stokoe II 1983; Nazarian and Stokoe 1985; Stokoe et al. 1991). For a given geophone spacing "D", the impact source is placed at a distance of at least D/2 from the nearest geophone. The type of hammer required to generate

the Rayleigh waves depends not only on the site characteristics but also on the geophone spacing.

Although different types of impact source like hand-held hammer, sledgehammer, dropped weights, vertical drop hammer, excavator shovels, SPT hammers has been used for SASW testing, the most commonly used type of impact source used are hand-held hammers of varying weights (Addo and Robertson 1992; Al-Hunaidi 1993; Hiltunen and Woods 1988; Mancuso and Vinale 1993; Nazarian and Stokoe II 1983; Nazarian and Stokoe 1985; Stokoe et al. 1991). The type of hammer to be used for a test is site-dependent. A particular impact source type suitable for a given site may not be suitable for a different site.

The quality and acceptability of a test are judged based on the coherence and wrapped phase information obtained at the time of the test. A coherence close to 1 implies a low noise signal, which is desirable for the acceptability of the test (Heisey et al. 1982; Joh 1996; Kumar and Hazra 2014; Kumar and Rakaraddi 2013; Nazarian and Stokoe II 1983; Nazarian and Stokoe 1985; Stokoe et al. 1991). In other words, a coherence close to 1 suggests that most of the waves received by the geophone nearest to the impact source were also received by the furthest geophone. For most field tests, a coherence of at least 0.95 is desired in order to obtain representative shear wave velocity profile of a given site. For a given geophone spacing, the same test is repeated four to five times in order to reduce the effect of background noise by averaging the data in the frequency domain (Al-Hunaidi 1993;

Heisey et al. 1982). For the next higher geophone spacing, the spacing is doubled following common geophone midpoint geometry (Mancuso and Vinale 1993; Nazarian and Stokoe 1985; Stokoe et al. 1991). After conducting the field tests with different geophone spacing, the next step is to obtain the dispersion curve.

Dispersion curve from field test: A dispersion curve shows the variation of phase velocity of the generated set of Rayleigh waves with the respective wavelengths. Since not much information can be extracted from the data obtained in the time domain, the analysis is performed in the frequency domain after performing a Fourier Transform on the time domain data (Heisey et al. 1982). The following set of equations are used to obtain the dispersion curve.

- $t(f) = \emptyset(f)/(360\ X\ f)$ (2.2)
- $V_R(f) = \ D/t(f)$ (2.3)
- $L_R(f) = V_R(f)/f$ (2.4)

The frequency content of the signal "*f*" is obtained from Fourier transform of the signal and the phase $\emptyset(f)$ is determined after unwrapping the phase data obtained from the field test. The frequency and wrapped phase data which has a coherence > 0.95 is used for further analysis, after masking the region with unacceptable coherence (Heisey et al. 1982; Joh 1996). Even if the coherence is close to 1 for the initial low-frequency region, the wavelength data used for analysis is restricted to 3D (Al-Hunaidi 1993; Heisey et al. 1982; Nazarian and Stokoe 1985; Stokoe et al.

1991). For a given geophone spacing D, the phase velocity $V_R(f)$ and wavelength $L_R(f)$ is determined for any given frequency using equations 2.2 to 2.4.

Inversion analysis: The dispersion curve for all the different geophone spacing is combined to obtain the global dispersion curve. The number of layers, layer thickness, density, Poisson's ratio and shear wave velocity are initially assumed for performing the inversion analysis using a software (Addo and Robertson 1992; Al-Hunaidi 1993; Joh 1996; Nazarian and Stokoe II 1983; Nazarian and Stokoe 1985; Stokoe et al. 1991). A suitable software is used to determine the theoretically calculated dispersion curve from the input data and compare with the field dispersion curve. The layer thickness, shear wave velocity and Poisson's ratio are modified subsequently after each iteration so that the theoretical and field dispersion curve almost matches with an RMS error value less than 10 (Chakraborty et al. 2019b).

Although the SASW test apparently seems simple, the biggest challenge faced during field test is to decide the type of impact source required and obtain a coherence close to 1 for the frequency range of interest. Several repetitions are often required to acquire an acceptable test and a significant amount of human judgment is involved in accepting or rejecting a particular test result. Shear modulus is the most important parameter in a seismic response and stability analysis of an earthen

structure; hence, it is of utmost importance to ensure the accuracy of the estimated shear modulus values.

Besides shear modulus, damping (or damping ratio of soil) is another important input parameter required for a dynamic analysis. The following section presents an overview of damping and the different laboratory and in-situ methods to obtain damping ratio.

2.3.2 Damping

Cyclically loaded soil mass systems or soil bodies subjected to earthquake vibration loses energy, primarily in terms of heat, due to damping (Richart et al. 1970). The ratio of the amount of energy lost in one cycle of oscillation as compared to the maximum stored elastic energy is defined as the specific damping capacity (Ashmawy et al. 1995). In geotechnical engineering problems dealing with dynamic loading conditions, the damping is often represented as 'damping ratio', a term ideally applicable for a single degree of freedom (SDOF) system.

The damping ratio is defined as the ratio of coefficient of damping to the critical damping of a system (Richart et al. 1970). The critical damping of a system represents the amount of damping required to stop the body exactly after one complete oscillation, when the vibrating body returns to its original position. A system is considered to be overdamped if the damping is higher than critical and as underdamped if the damping is lower than critical.

The damping in soil layers can be determined using laboratory or in-situ tests. Laboratory tests include performing resonant column, cyclic triaxial and torsional shear tests on soil samples (Ashmawy et al. 1995; Lentini and Castelli 2017). The damping can be obtained from free-vibration of an initially disturbed sample in a resonant column test and recording the decay of amplitude (logarithmic decrement) (Richart et al. 1970). The damping ratio can also be obtained from resonant column test data using the "half-power method" on the response of the soil (magnification) recorded by varying the input frequencies (Kramer 1996; Wu 2015). The area under hysteresis curve (Figure 2-14) is used to calculate the hysteretic damping ratio in case of cyclic triaxial and torsional simple shear (Ashmawy et al. 1995; Teachavorasinskun et al. 1991).

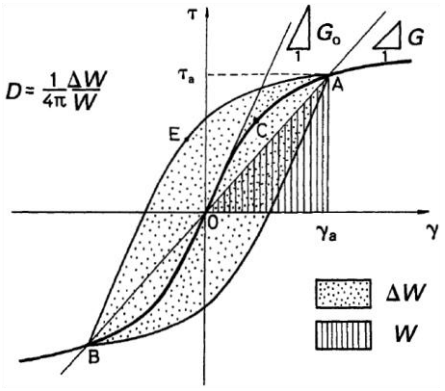

Figure 2-14: Shear stress-strain relationship and hysteresis loop
(after Ishihara 1996)

In-situ tests include back calculating damping ratio of different soil layers to match the response recorded by accelerographs due to forced vibration tests

(Abdel-Ghaffar and Scott 1979a, 1981; Cantieni 2001; Jafari and Davoodi 2006). Usually, the damping ratio for natural soils ranges between 0.5-5% (Kallioglou et al. 2008; Vucetic and Dobry 1991). The damping ratio is also specified in terms of viscous damping or Rayleigh damping (Figure 2-15), which unlike hysteretic damping, is a frequency-dependent damping (Amorosi et al. 2008; Gazetas 1987; Parish et al. 2009; Song and Su 2017; Woodward and Griffiths 1996). The Rayleigh damping is composed of a linear combination of a mass term and a stiffness term and needs to be calibrated to provide the required damping within a range of frequencies of interest (Hall 2006).

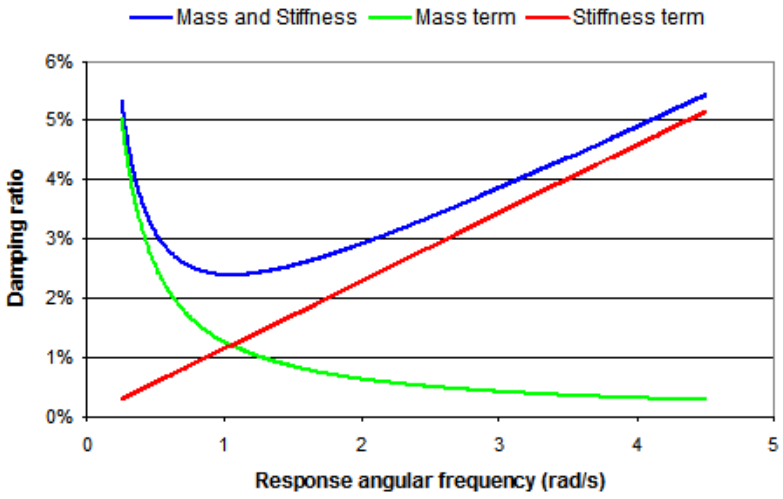

Figure 2-15: Mass and stiffness term in Rayleigh damping

(Source:https://www.orcina.com/SoftwareProducts/OrcaFlex/Documentation/Help/Content/html/RayleighDamping,Guidance.htm)

The next section presents an overview of the different existing methods to perform seismic response analysis of earthen dams along with their advantages and

disadvantages. The techniques for determining the natural frequency of earthen embankment structures and the limitations of the methods in determining the strain-dependent natural frequency is also elucidated.

2.4 Seismic response of earthen dams

Dams are some of the most important engineered structures which plays an important role in flood control, water storage, irrigation, electricity generation, recreational facilities and towards the betterment of a nation (FEMA, 2016). Despite the efforts of engineers to incorporate different possible modes of failure in design consideration of these structures, there have been several instances in different parts of the world, where dams have incurred catastrophic failures. Such events not only affect the economy of the country but also the lives of thousands. Over the period of time, improvement in technology, increased knowledge and understanding on the behavior of dams have enhanced the confidence on the performance of these mega-structures. However, a lot remains unexplored about these large inhomogeneous structures. Unlike concrete dams, earthen dams are highly heterogeneous in nature, with materials existing in multiple phases, exhibiting non-linear and anisotropic behavior (Yiagos and Prevost 1991). Hence, engineers and researchers are in a continuous strive to understand more about the behavior of these structures, especially under adverse conditions like floods or earthquakes.

Earthen dams or levees, which are otherwise stable under normal conditions may be susceptible to failure when subjected to seismic excitations. The behavior of an earthen dam is a complex phenomenon which has been studied since the late 19th century. All earthquakes do not affect an earthen dam to the same extent. Broadly speaking, the response of an earthen dam to seismic excitation primarily depends on its geometry, material properties and canyon geometry (Gazetas 1987; Mejia and Seed 1983; Woodward and Griffiths 1993). However, there are several other case-specific factors which affect the behavior of a particular dam. A resonance condition may occur if the predominant frequency of an earthquake excitation is close to the natural frequency of the structure, resulting in amplified vibration (Dakoulas and Gazetas 1985; Gazetas 1987; Parish et al. 2009; Wood 1973; Zhu and Zhou 2010). Thus researchers and engineers try to estimate the response and induced forces on the structure during seismic events, and estimate the natural frequencies, mode shapes and modal participation factors for different modes of vibration.

2.4.1 Seismic response analysis methods

The response of a dam, when subjected to earthquake shaking, is usually simulated using a dynamic finite element or finite difference based software packages. The seismic excitation is propagated from the base of the foundation, where the excitation is applied, to the crest of the dam. The most important parameters which govern this process of propagation of seismic excitation are the shear modulus and

the damping ratio of the soil layers present in the body of the dam. The unit weight of the soil layers is also an important parameter since the earthquake-induced inertia force depends on the mass of the system, which in turn depends on the assigned unit weight of the soil layers. The shaking type analysis can be performed assuming the soil layers to be linear elastic or by incorporating the non-linear stress-strain behavior of the geomaterials.

2.4.1.1 Linear elastic analysis

The linear elastic type of analysis is the simplest type of analysis in which the soil is assumed to exhibit linear elastic behavior (Krahn 2004a). This implies that the shear modulus of the soil layers remains constant, irrespective of the strain level attained during the shaking analysis. The linear elastic type analysis is usually not performed for analyzing actual problems since the shear modulus of different soil types decreases with increase in strain levels (Rathje and Bray 2000). The linear elastic analysis may, however, be used to analyze the effect of very low-intensity earthquakes, where the strain levels induced during shaking is not significant to cause non-linear behavior in the soil system (Chopra and Chakrabarti 1973).

The linear analysis doesn't account for the reduction in shear modulus and increase in damping ratio with the increase in strain experienced by the soil when the dam is subjected to seismic loading conditions (Krahn 2004a). The non-linear

behavior of soil is incorporated in the analysis using the iterative equivalent linear or non-linear method (Gazetas 1987; Idriss 1973; Prevost et al. 1985).

2.4.1.2 Equivalent linear analysis

The equivalent linear analysis tries to capture the non-linear stress-strain behavior of the soil by performing an iterative analysis (Gazetas 1987; Jibson 2011). The variation of shear modulus and damping ratio with strain depends primarily on the mean effective confining pressure, plasticity index and type of soil (Ishibashi and Zhang 1993; Seed and Idriss 1970; Seed et al. 1986; Vucetic and Dobry 1991). The analysis starts with the G_{max} values assigned by the user, for the respective soil layers, and the software performs the shaking analysis to determine the maximum shear strain at every Gauss numerical integration points (Krahn 2004a). At the end of the first iteration, the shear modulus corresponding to the calculated maximum shear strain induced, is assigned to the respective soil layers following the shear modulus-degradation curves provided by the user, for the different soil layers (Figure 2-16). Successive iteration continues until there is a parity between the shear modulus assumed for that iteration and the strain levels induced (Seed et al. 1986). For each individual iteration, the shear modulus of the different soil layers are held constant and the shear modulus values are modified at the start of the next iteration. The equivalent-linear method of analysis is effectively a linear-elastic method of analysis and cannot capture the actual behavior of the soil layers during seismic shaking (Seed et al. 1986). Nonetheless, this method has been found to

provide acceptable results for almost all practical purposes, other than for very strong seismic excitations (Rathje and Bray 2000).

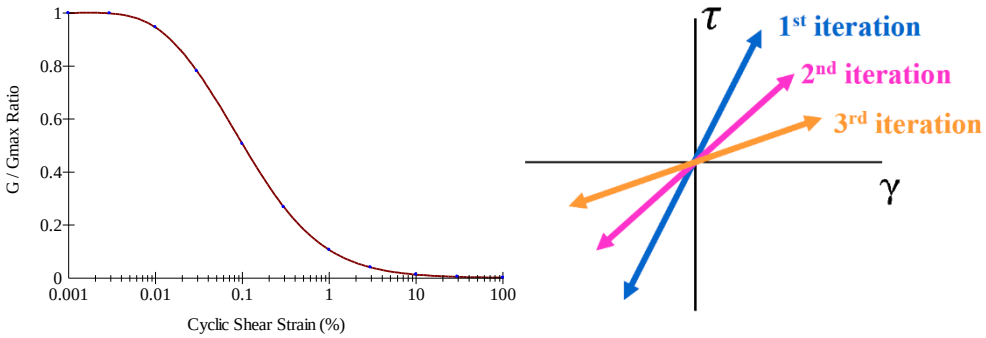

(a) (b)

Figure 2-16: (a) Typical modulus degradation curve and (b) change in shear modulus with each iteration
(after Krahn 2004a)

2.4.1.3 Non-linear analysis

In the fully non-linear analysis, the changes in pore water pressure and strain are computed at every time-step of the earthquake loading and the subsequent changes in shear modulus is also computed at every time-step (Abouseeda and Dakoulas 1998; Krahn 2004a; Prevost et al. 1985). Hence the non-linear analysis is expected to capture the actual behavior of the soil layers during shaking. However, suitable pore-pressure models along with non-linear constitutive relations are required to compute the increase in pore water pressure and associated changes in shear modulus due to different strain levels induced at every time-step of the earthquake (Beaty and Byrne 1998; Boulanger and Ziotopoulou 2015; Martin et al. 1975).

These models need to be calibrated based on extensive laboratory tests on undisturbed samples collected from the site (Boulanger and Montgomery 2016).

All the commercially available software which can perform non-linear analysis work on the same basic principle, although, the input parameters vary based on the constitutive models used by the software to analyze the problem. However, due to the lack of undisturbed samples extracted from the shell portion of the Eagle Mountain dam, it was not possible to calibrate the models and perform a fully non-linear analysis. Using advanced constitutive models with assumed values of different input parameters does not guarantee the authenticity of the obtained result. Many studies have found that the simple equivalent linear method converges well and predicts real problems satisfactorily (Abdel-Ghaffar and Scott 1979b; Mejia and Seed 1983; Prevost et al. 1985; Rathje and Bray 2000); it is thus widely used in practice and was adopted in this research study.

2.4.2 Natural frequency determination methods

The natural frequencies of earthen dams can be determined by simple analytical methods like shear beam model or numerical methods using finite element or finite difference methods. The natural frequency can also be determined from field tests by studying the response of the structure to ambient and forced vibration tests (Cetin et al. 2005; Chopra 1967; Clough and Chopra 1966; Gazetas 1987; Ishizaki and Hatakeyama 1962; Mononobe et al. 1936; Okamoto 1984; Okamoto et al. 1969). However, all these methods are applicable for determining the natural

frequency corresponding to low strain levels. A brief overview of the different methods is presented in this section.

2.4.2.1 Analytical method: The shear beam method

In the shear beam method, the dam is considered as a beam having "variable wedge-shaped cross-section", as shown in Figure 2-17 (Ambraseys 1960b; Ike 2008; Okamoto 1984). The displacement of any point on a horizontal section is assumed to be same and uniform (Okamoto 1984) and the dam is assumed to vibrate in pure shear. The shear beam approach was first introduced by Mononobe et al. (1936) as simple 1D shear beam method, where the length of the wedge was significantly longer than its height. Whereas in narrower canyons, where the ratio of the length to the height of the dam was comparatively less, the response was studied using two-dimensional shear beam model (Ambraseys 1960b; Hatanaka 1955). Ambraseys (1960b) developed theoretical expressions for deflection and shear stress developed in a shear wedge and calculated the frequencies for first six modes of vibration for different truncation ratios for 1D and 2D cases.

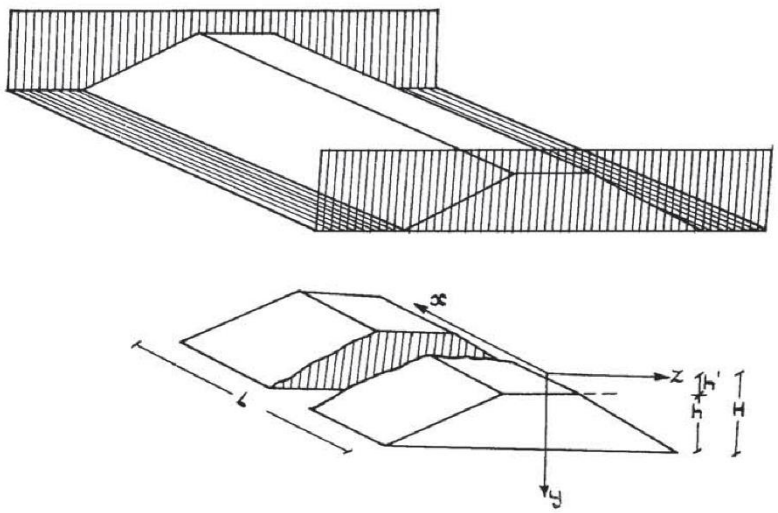

Figure 2-17: Geometry of dam for shear beam method
(after Ambraseys 1960b)

Okamoto et al. (1969) presented the data available from eight seismometers distributed on the crest, mid-slope of downstream side and at both sides of the bank of 37m high Sannokai Dam and interpreted the dynamic properties of the material using the 1D shear beam. Abdel-Ghaffar and Scott (Abdel-Ghaffar and Scott 1979a; b, 1981) estimated the natural frequency, shear wave velocity, modal participation and dynamic material properties of Santa Felicia Dam. The parameters were computed from data available for two earthquakes (obtained from accelerometers installed at the site), and from forced vibration tests and compared the results with that obtained from shear beam method. The above-mentioned studies were performed assuming the dam to be homogeneous in nature with uniform shear modulus throughout the section of the dam. The variation of shear modulus with depth (from the crest of the dam) was first incorporated in the shear beam analysis by Dr. George Gazetas (Gazetas 1981).

Static finite element studies and laboratory data suggested that shear modulus increased as $2/3^{rd}$ power of depth from the crest. Gazetas (1981) developed a shear beam model incorporating the increase in shear modulus with depth. The model was evaluated by comparing modal displacement shapes, peak accelerations and seismic coefficient for a number of real dams subjected to different earthquakes. A comparative study was conducted on five earthen dams of various cross sections using shear beam model and plane strain finite element analysis by Tsiatas and Gazetas (Tsiatas and Gazetas 1982). Results suggested that shear beam model predicted natural frequencies and modal shapes close to that obtained by plane strain finite element method (within 10% deviation) for the first mode of vibration. The deviation in result was found to increase for higher modes due to bending-type movement associated with the vertical component of deformation.

A generalized non-homogeneous shear beam model was presented by Dakoulas and Gazetas (1985) to incorporate the effect of inhomogeneity and variation of shear modulus with depth. Closed form solutions were developed for natural frequency, mode shapes and modal participation factors for different degrees of non-homogeneity (represented as inhomogeneity factor, m). The results obtained using the generalized shear beam model were found to be consistent with the data available from five dams subjected to four different earthquakes. Although the shear beam model predicted results close to that obtained from some actual data available from dams subjected to earthquakes, there are some limitations of this

model which makes seismic response analysis with finite element method more accurate and realistic.

2.4.2.2 Numerical methods: Using finite element or finite difference methods

Clough and Chopra (Chopra 1967; Clough and Chopra 1966) were the first to use 2D plane strain finite element analysis to study the dynamic response of a dam made of linearly elastic, homogeneous and isotropic material. The natural frequencies were obtained by Eigen value analysis (Chopra 1967; Woodward and Griffiths 1993). The shear beam model assumes that an earthen embankment structure subjected to earthquake excitation exhibits pure shear behavior. However, finite element analysis showed that only the first mode of vibration exhibited pure shear behavior, whereas all the higher modes involved flexure type deformation with vertical movement (Chopra 1967; Clough and Chopra 1966; Gasparini and Sun 1982; Gazetas 1987). Unlike the assumptions made in the shear beam analysis, the displacement under the first mode of vibration was found to be significantly different at the face and at the centerline of the dam.

Ishizaki and Hatakeyama (1962) first represented 2D dynamic plane strain problem by finite difference discretization. They concluded that the shear beam representation of vibration of the dam is “imperfect” since the vibration of the dam surface and body consist of both horizontal and vertical motion. Moreover, the distribution of displacement and shear stress on a horizontal plane was found to be

significantly different from the uniform distribution assumed in the shear beam approach.

Plane strain finite element analysis or finite difference method can incorporate the effect of unequal side slopes, arbitrary geometric configurations and material non-homogeneity. Zones with different material properties and seismic excitation with both horizontal and vertical component of earthquake motion (Chopra 1967; Gazetas 1987; Yiagos and Prevost 1991) can be dealt with using numerical methods. Such analyses are thus expected to portray the actual behavior of the dam in a more realistic way than the shear beam approximation. However, the non-linear behavior of soil needs to be accounted for in the analysis (Clough and Chopra 1966). A brief overview on the evolution of seismic response analysis techniques has been presented here, however, the reader may refer to other literature (Gazetas 1987; Okamoto 1984; Pelecanos 2013) for a detailed study.

2.4.2.3 Field testing methods: Ambient and forced vibration tests

The seismic response of an earthen dam can also be studied, based on the data recorded during earthquake events by accelerographs/seismographs that are placed in different locations of the dam (Figure 2-18) (Okamoto et al. 1969; Abdel-Ghaffar & Scott 1979a; Abdel-Ghaffar & Scott 1979b; Cetin et al. 2005; Pelecanos et al. 2015; Yang et al. 2017), or by conducting ambient vibration or forced vibration tests (Abdel-Ghaffar and Koh 1981; Abdel-Ghaffar and Scott 1981; Castro et al.

1998; Jafari and Davoodi 2006). Accelerograph data is not usually available for dams that are located in newly identified regions of induced seismicity, and in such cases, ambient vibration or forced vibration tests may be utilised as an alternative approach. Ambient vibration test uses natural sources of excitation such as wind, low-intensity tectonic movements, microtremors, water release from reservoirs, and other sources of vibration (Abdel-Ghaffar and Koh 1981; Jafari and Davoodi 2006; Trifunac 1972).

In the forced vibration test, excitations are induced along the upstream-downstream directions, by rotating eccentric-mass vibration generators that are attached to the crest of the dam (Figure 2-19) (Abdel-Ghaffar and Scott 1981; Abdel-Ghaffar et al. 1980; Gauron et al. 2018; Gazetas 1987; Jafari and Davoodi 2006; Keightley 1966). The acceleration induced at the crest and at different locations of the side slopes are recorded, and the data is analysed to determine the natural frequency and mode shapes of the structure (Abdel-Ghaffar and Scott 1981; Petrovski et al. 1974). The forced vibration tests require sophisticated instruments for performing the tests and collecting the data, which might not be feasible for all projects. Similar analyses can also be performed using the response data recorded during actual earthquakes (Cetin et al. 2005). However, such data are not usually available for dams located in newly declared, induced seismicity regions.

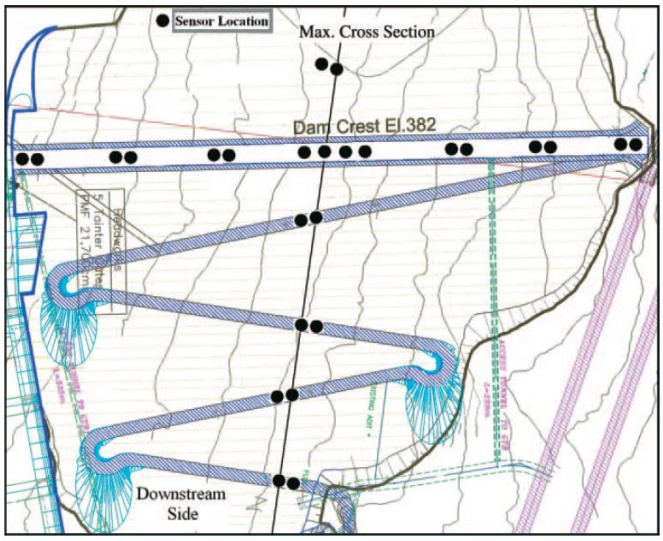

Figure 2-18: Location of sensors for ambient vibration test on Masjed Soleiman Dam
(after Jafari and Davoodi 2006)

Figure 2-19: Vibration generators used for forced vibration tests on Masjed Soleiman Dam
(after Jafari and Davoodi 2006)

2.5 Slope stability analysis

Evaluating the stability of slopes of earthen embankment structures, such as dams and levees is one of the oldest types of geotechnical engineering problems (Duncan et al. 2014). The stability of these engineered infrastructures is of paramount importance since the failure of such structures can have catastrophic consequences (Caballero et al. 2016). In earlier days, earthen dams were considered to be inherently stable to seismic disturbances (Seed 1981). However, after the extensive damage to Lower San Fernando Dam and substantial sliding movement of Upper San Fernando dam during San Fernando Earthquake of 1971, engineers and researchers realized the importance of studying the stability of dams under seismic loading conditions (Seed 1981). These massive structures which are otherwise stable under normal conditions may become unstable during earthquake events (Chatterjee and Choudhury 2014). The most important decision which an engineer needs to take while performing a stability analysis is to decide the suitable strength parameters which are expected to capture the behavior of the structure under a certain loading condition.

2.5.1 Strength parameters for slope stability analysis

Commercially available software packages have made it extremely easy for engineers to perform the slope stability analysis (Duncan 1996; Krahn 2003). Complex geometric conditions, regions with different material properties, various loading conditions and other complex scenarios can be easily solved with the use

of these software packages. However, the validity of the analysis results depends on the exactness with which the problem scenario is defined. The software can easily calculate the stresses state present due to gravity loading condition or perform a shaking analysis to determine the earthquake-induced stresses based on the unit weight, Poisson's ratio and shear modulus provided for different layers of the soil and depending on the specified boundary conditions. However, the most important input parameters of a slope stability analysis, which determines the resisting strength along a slip surface, are the shear strength parameters. Hence, it is critical to decide and select the suitable shear strength parameter for analysis.

Even though shear strength is a function of effective stress for any type of soil, it is often not possible to determine the increase in pore water pressure in a clayey type of soil (Duncan 1996; Duncan et al. 2014). In such cases, total stress analysis or undrained analysis is performed to estimate the available shear strength. A type of soil can be assumed to exhibit drained or undrained behavior depending on the rate of loading and the rate of dissipation of excess pore water pressure. Non-dimensional time factor T is often used to decide if a soil type can be assumed to exhibit drained or undrained behavior (Duncan 1996). If T is greater than 3, the soil is found suitable for effective stress analysis; whereas T less than 0.01 can be considered to exhibit undrained behavior. However, if a particular soil type has $0.01 < T < 3$, it can exhibit either type of behavior and both effective and total stress analysis is usually performed.

The shear strength parameters are usually obtained by performing triaxial or direct shear tests on soil samples in the laboratory (USACE 2003; USSD 2007). Existing correlations with in-situ test results, such as CPT or SPT are also widely used to obtain the shear strength parameters (Robertson and Cabal 2015). The shear strength parameters include (a) effective cohesion intercept and effective friction angle, used in effective stress analysis; (b) total cohesion intercept and total friction angle, used in total stress analysis; and (c) undrained cohesion, used in undrained analysis. The strength parameters used in effective stress analysis can be obtained by performing laboratory tests such as Consolidated Drained (CD) triaxial test or Consolidated Undrained (CU) triaxial test with pore pressure measurements or by performing a direct shear test at a very slow rate of shearing, to allow dissipation of excess pore water pressure generated during shearing (Banerjee and Puppala 2015; Banerjee et al. 2018b). Suitable CPT or SPT correlations can also be used to determine effective friction angle.

The total cohesion intercept and total angle of internal friction, which are required for total stress analysis, is usually obtained from Consolidated Undrained (CU) triaxial test or by performing a direct shear test at a high rate of shearing. However, the total friction angle is usually not obtained from CPT or SPT correlations, since the available correlations are valid for determining effective friction angle. Undrained cohesion can be obtained from Unconsolidated

Undrained (UU) triaxial test, or Unconfined Compressive Strength (UCS), or by using available correlation equations from in-situ tests.

The effective stress analysis parameters obtained from CD test is suitable for performing a stability analysis of an old earthen dam. The term 'old' is a subjective term and denotes the condition in which the excess pore water pressure generated at the time of construction or loading has dissipated and the current pore water pressure condition can be obtained from steady state seepage analysis (USACE 2003; USBR 2011; USSD 2007; Wiltshire 2002). Stability analysis of such a dam can be performed by assigning effective friction and cohesion intercepts for both the sand and clay layers.

The total stress analysis parameters obtained from CU test is suitable for performing the stability analysis of an 'old' earthen dam, subjected to an earthquake excitations. In such a scenario, similar to the previous case, it can be assumed that the excess pore water pressure generated during construction and initial loading phase have dissipated and the pore water pressure before the earthquake excitation can be determined using steady state seepage analysis. However, during earthquake excitation, it can be reasonably assumed that the excess pore water pressure cannot dissipate in case of either sand shell or clay core. Hence total stress analysis with total strength parameters can be used for both the sand and clay layers, if excess pore water pressure cannot be estimated accurately (Duncan 1996). However, if the

excess pore water pressure in the different soil types can be estimated using suitable constitutive models, effective stress analysis with effective strength parameters should be performed.

A recently constructed dam, subjected to earthquake loading conditions soon after the construction, can be considered as a scenario suitable for undrained analysis. Undrained cohesive strength is assigned to saturated clay layers since the soil did not get sufficient time to dissipate the excess pore water pressure, generated during construction. Furthermore, an additional seismic load was imposed on the structure, leading to the generation of excess pore water pressure.

Undrained shear strength is usually not assigned to sand layers unless the sand layer is susceptible to flow liquefaction or cyclic mobility. In such cases, the associated liquefaction induced deformation is large, and the shear strength is governed by undrained steady state shear strength. This topic is explained in detail in Section 2.7.

The strength parameters obtained are not intrinsic properties of the soil, rather are manifestations of the behavior of the soil subjected to a certain loading condition (Holtz and Kovacs 1981). The shear strength of a soil sample primarily depends on the extent of deformation experienced, the degree of compaction compared to the confining pressure and the past loading conditions.

The peak strength corresponds to the maximum strength mobilized at low strain levels. With further shearing, the fully softened strength is mobilized when the soil reaches the critical state, which is associated with deformations without any further change in volume (Fell et al. 2005). Further shearing the sample is associated with soil particle rearrangement and the minimum shear strength, known as the residual strength, is mobilized. For a normally consolidated clay and a loose sand, the peak, fully softened and residual shear strength are nearly similar. Whereas, overconsolidated clay and dense sand exhibit a significantly higher peak strength as compared to the residual strength (Patil et al. 2018).

Engineers often face a dilemma regarding the use the peak strength or the residual strength parameters while performing the slope stability analysis (Leshchinsky 2001). The rationale behind the use of peak or residual strength parameter lies in the type of problem and the associated deformation or strain levels expected at the different locations along a slip surface. The limit equilibrium method of analysis assumes the soil to behave as a ductile material and the magnitudes of the strain along the slip surface are not known (Duncan 1996). Hence at the end of an analysis, it is not possible to determine the specific locations where peak strength has been mobilized and the regions which may have experienced higher deformations associated with the residual strength. If the shear strength drops beyond the peak strength (strain-softening), extra unbalanced stresses may be transferred to the adjacent soil mass, leading to progressive failure of the soil

(Chowdhury et al. 2009; Law and Lumb 1978; USACE 2003). In such a scenario, a reliable approach to performing the stability analysis is to assign residual shear strengths throughout the system. However, such an analysis may be highly conservative and may lead to over-design while designing a new structure (Leshchinsky 2001).

The use of peak or residual strength for the analysis is also decided based on the factor of safety results obtained by using the peak shear strength parameters and performing a stability analysis using a finite element or finite difference based software (Krahn 2003). If the factor of safety is quite high throughout the slip surface, the use of peak shear strength parameters can be considered suitable for the problem. It can be reasonably assumed that a structure having a high factor of safety against sliding will have low associated deformation and hence peak shear strength may be used for the analysis (Jibson 2011; USBR 2011). However, if the factor of safety is close to one, there may be several regions along the slip surface which may have experienced high deformations and hence the residual shear strength should be used for analysis and the factor of safety should be re-calculated. In case of seismic slope stability analysis, residual strength parameters are used in the analysis if the associated deformation is high, and the factor of safety is close to 1 due to the earthquake-induced forces and generation of excess pore water pressure (Marcuson et al. 1990).

2.5.2 Static slope stability analysis methods

The static slope stability analysis methods primarily include the use of design charts, limit equilibrium method and numerical methods using finite element or finite difference based software packages. The different analysis methods with their relative advantages and disadvantages are discussed in this section.

2.5.2.1 Design charts

Slope stability analysis design charts were first introduced by Taylor. These charts are applicable for total stress analysis in simple homogeneous soil conditions (Abramson et al. 2001; Baker 2003; Taylor 1937). Engineers at times use the charts for non-homogeneous soils by using an equivalent homogeneous soil property, based on their engineering judgement and experience (Abramson et al. 2001). These stability charts are easy to use and can provide a preliminary approximate estimate of the factor of safety before performing the detailed analysis using a commercially available software (Baker et al. 2006; Bishop and Morgenstern 1960; Duncan 1996).

2.5.2.2 Limit equilibrium method

Limit equilibrium method is one of the most popular methods of stability analysis, which is widely accepted and used by the geotechnical engineering fraternity. In this method of analysis, the slip surface, whose stability is being evaluated, is divided into multiple slices, and the normal stress acting at the base of each slice is

determined to obtain the mobilized shear strength (Abramson et al. 2001; Krahn 2003). The factor of safety of the slip surface is then obtained by calculating the ratio of the resisting strength of the slip surface to the driving stresses which tries to de-stabilize the slope (Duncan et al. 2014). The slope stability analysis using the method of slices is a statically indeterminate problem and hence different assumptions are made regarding the inter-slice forces (Table 2-2) (Abramson et al. 2001; Cheng et al. 2007; Krahn 2003, 2004a; Morgenstern and Price 1965). The various methods available to perform a limit equilibrium analysis varies from one another based on the assumptions which are made regarding the inter-slice forces and depending on the condition of statics it satisfies (Table 2-3), i.e. force equilibrium or moment equilibrium, or both (Abramson et al. 2001; Krahn 2003, 2004b).

The general limit equilibrium formulation incorporates the key elements of the methods listed in Table 2-2 and Table 2-3. Two equations, one satisfying the force equilibrium and the other satisfying moment equilibrium, are individually used to evaluate the factors of safety over a wide range of inter-slice force conditions (Figure 2-20) (Fredlund and Krahn 1977; Fredlund et al. 1981; Krahn 2003, 2004b; Lam and Fredlund 1993). The inter-slice force is determined using equation 2.5.

$$X = E \lambda f(x) \quad (2.5)$$

where, X is the inter-slice shear force, E is the inter-slice normal force, f(x) is a function and λ is a percentage of the function f(x) (Figure 2-21).

Table 2-2: Inter-slice forces used in different methods of limit equilibrium analysis
(after Krahn 2004)

Method	Interslice Normal (E)	Interslice Shear (X)	Inclination of X/E Resultant, and X-E Relationship
Ordinary or Fellenius	No	No	No interslice forces
Bishop's Simplified	Yes	No	Horizontal
Janbu's Simplified	Yes	No	Horizontal
Spencer	Yes	Yes	Constant
Morgenstern-Price	Yes	Yes	Variable; user function
Corps of Engineers – 1	Yes	Yes	Inclination of a line from crest to toe
Corps of Engineers – 2	Yes	Yes	Inclination of ground surface at top of slice
Lowe-Karafiath	Yes	Yes	Average of ground surface and slice base inclination
Janbu Generalized	Yes	Yes	Applied line of thrust and moment equilibrium of slice
Sarma – vertical slices	Yes	Yes	$X = C + E \tan \phi$

Table 2-3: Conditions of statics satisfied in different methods of limit equilibrium analysis
(after Krahn 2004)

Method	Moment Equilibrium	Force Equilibrium
Ordinary or Fellenius	Yes	No
Bishop's Simplified	Yes	No
Janbu's Simplified	No	Yes
Spencer	Yes	Yes
Morgenstern-Price	Yes	Yes
Corps of Engineers – 1	No	Yes
Corps of Engineers – 2	No	Yes
Lowe-Karafiath	No	Yes
Janbu Generalized	Yes (by slice)	Yes
Sarma – vertical slices	Yes	Yes

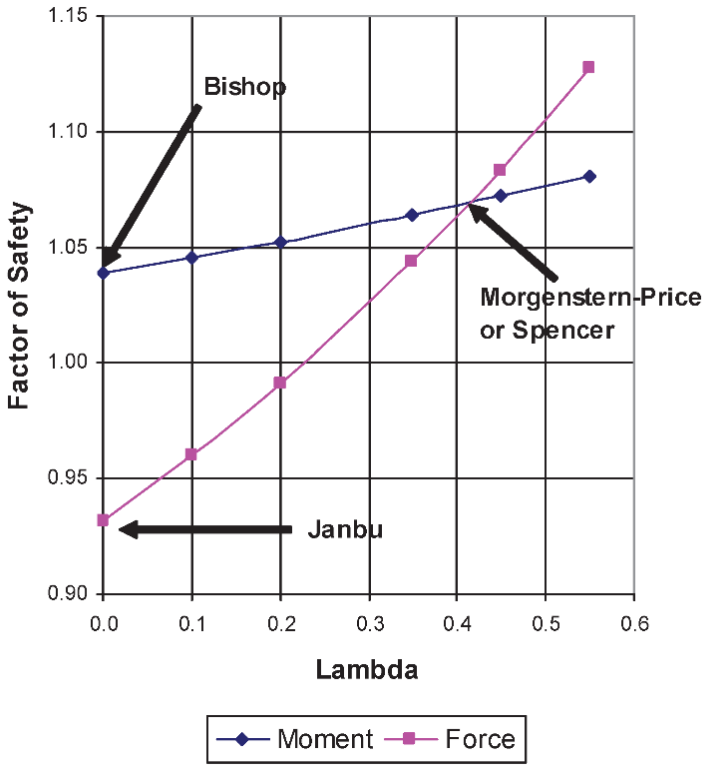

Figure 2-20: GLE plot showing variation of factor of safety versus lambda (after Krahn 2004)

The half sine function (or the clipped sine and the trapezoidal function) commonly used in the Morgenstern Price method tries to mimic the expected variation in the inter-slice force along the slip surface (Figure 2-21). The first and the last slice, from where the slip surface starts at the crest and ends at the toe, is assigned a low value of inter-slice shear force (Krahn 2004b). Whereas, the inter-slice force is expected to be maximum in the middle of the slip surface (Fan et al. 1986), hence justifying the half-sine shape of the inter-slice force function.

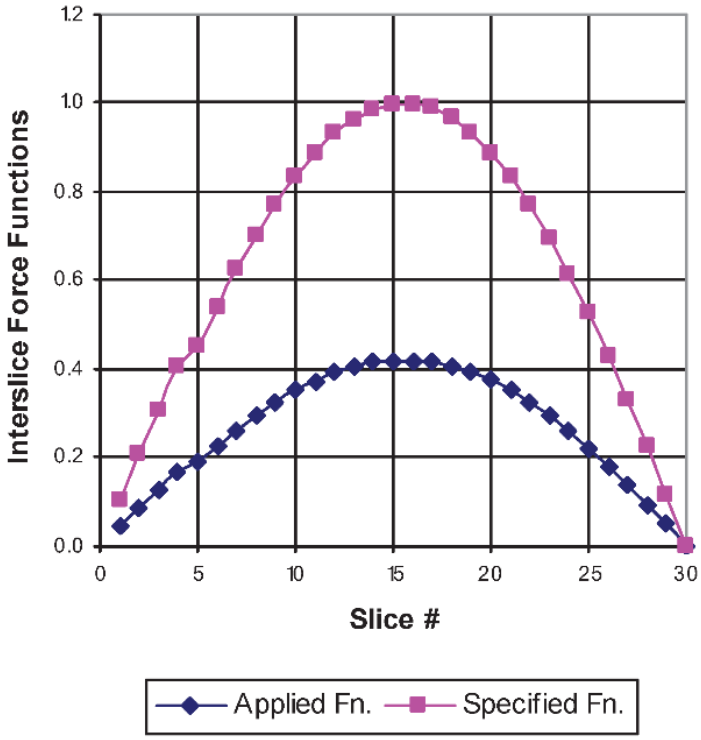

Figure 2-21: Half sine inter-slice force function
(after Krahn 2004)

Unlike the half-sine function used in Morgenstern-Price method, a constant function is used for Spencer's method (Duncan et al. 2014; Fan et al. 1986; Fredlund et al. 1981; Morgenstern and Price 1965; Spencer 1967). The value of lambda (λ), which scales the function f(x) to satisfy both force and moment equilibrium, is used for the Morgenstern-Price or Spencer method of analysis (Figure 2-20 and Figure 2-21). Researchers had observed that the choice of inter-slice force function does not have a significant impact on the computed factor of safety results (Abramson et al. 2001; Duncan 1996; Duncan et al. 2014; Fan et al.

1986) and hence any suitable inter-slice function may be selected without making significant mistakes in an analysis.

Determining the factor of safety by performing calculations by hand-calculators is a tedious task due to the iterative steps involved. With the aid of computer software packages, these complex problems can be easily solved for embankment slopes having different geometric configurations, varying material properties and complicated loading conditions. Since computer software packages are readily available in almost all design firms and research institutes, a suitable method which satisfies both moment and force equilibrium should be selected, instead of a using a method which satisfies either force equilibrium or moment equilibrium (Duncan 1996).

Although methods like Morgenstern-Price or Spencer's satisfies, both moment and force equilibrium, the normal stresses calculated at the base of each slice is not necessarily the same as that exists in reality (Krahn 2003, 2004b). A comparison of stresses calculated by performing a numerical analysis using a finite element based software can clearly show the difference. Moreover, an inherent assumption of a single constant factor of safety value, for all the slices, is made in the limit equilibrium method of slope stability analysis and hence the variation of factor of safety along the slip surface or the presence of weak layers cannot be identified (Duncan 1996; Krahn 2003, 2004b; Wright et al. 1973). The limit

equilibrium method simply provides a numerical value of factor of safety and does not provide any information of the deformation incurred by the slip surface (Duncan 1996; Krahn 2007). In such cases, numerical methods such as finite element analysis can provide better information regarding the stability and serviceability of the slope, as compared to the limit equilibrium method. Nonetheless, limit equilibrium method remains as one of the most widely used slope stability analysis methods among practicing engineers (Cheng et al. 2007; Duncan 1996; Griffiths and Lane 1999; Jibson 2011; Krahn 2003; Law and Lumb 1978).

2.5.2.3 Use of numerical methods in slope stability analysis

The two major shortcomings of the limit equilibrium method of analysis are (a) the constant value of factor of safety of an entire slip surface and (b) absence of information regarding the strain and deformation experienced by the slip surface and hence does not satisfy the displacement compatibility (Krahn 2003, 2007). The inclusion of finite element calculated stresses in the limit equilibrium method of analysis satisfies strain compatibility as well as the conditions of statics. Since no assumptions are required regarding the location and values of inter-slice forces, the obtained normal stresses are close to that expected to exist in the field (Griffiths and Lane 1999; Krahn 2004b; Seed 1981). Moreover, the variation of the factor of safety along the slip surface is easily determined based on the stresses and available shear strength along the slip surface (Krahn 2004b; Wright et al. 1973). Finite

element method can also be useful in determining the additional stresses induced due to the propagation of seismic excitation from the foundation to crest of an earthen structure during earthquake loading conditions (Chopra 1967; Clough and Chopra 1966; Jibson 2011; Krahn 2004a). These stresses can be included in the stability analysis to study the variation of the factor of safety with the time of the earthquake and compute the associated deformations. Suitable constitutive models such as the linear elastic, multilinear elastic, hyperbolic elastic, elastoplastic, elastoviscoplastic or such other stress-strain relationships are required to model different soil types and compute the deformation incurred due to different loading conditions (Duncan 1996).

A comparatively new approach to determine the factor of safety of a slope is the strength reduction method (SRM) (Griffiths and Lane 1999; Liu et al. 2015; Matsui and San 1992). The cohesion and friction angle is iteratively reduced in this method and the deformation is computed at different locations of the slope using numerical methods (Dawson et al. 2000). At a certain point, the reduced strength parameters cause the slope to fail uncontrollably, which is depicted by a state of non-convergence (Krahn 2007; Nian et al. 2011; Yingren and Shangyi 2004). The number by which the strength parameters needs to be divided to reach this state of non-convergence is denoted as the factor of safety (Krahn 2007; Matsui and San 1992). No slip surface is defined in this method, rather the deformed mesh of the structure, obtained by reducing the shear strength parameters, provides the location

of the failure and the associated values of deformation (Cheng et al. 2007; Griffiths and Lane 1999; Liu et al. 2015).

The SRM doesn't require the trial and error search of the critical slip surface, as followed in limit equilibrium analysis (Cheng et al. 2007). The failure pattern and probable location of the critical surface can be easily identified from the deformed mesh (Nian et al. 2011). However, the solution time is very high for the SRM and a well-defined critical surface, which most engineers are habituated to look at, is not obtained in the SRM (Cheng et al. 2007). Moreover, the SRM requires suitable constitutive models to be defined for different soil types to determine the associated deformations and faces numerical problems if the soil has a low cohesion and angle of internal friction (Chang and Huang 2005; Cheng et al. 2007; Laouafa and Darve 2002).

Both strength reduction method and limit equilibrium method have their benefits and limitations. Although the strength reduction method is more sophisticated as compared to the limit equilibrium method, it cannot be declared to be superior (Krahn 2007). The strength reduction method is a new method and unlike limit equilibrium method has not withstood the test of time. The use of finite element method in the limit equilibrium framework (Krahn 2003) has thus been used in this research study.

2.5.3 Seismic slope stability analysis methods

The analysis methods for conducting seismic slope stability analysis includes the simple pseudo-static method, the more complicated and computationally intensive stress-deformation method and the permanent-displacement approach, which acts as a mediator to the other two methods (Cai and Bathurst 1996; Jibson 2011; Newmark 1965). Each of the aforestated methods has their benefits and limitations and hence co-exists as analysis tools in the geotechnical engineering community dealing with the stability of embankment slopes, in the event of an earthquake (Jibson 2011).

2.5.3.1 Pseudo-static method

The pseudo-static approach was introduced by Terzaghi (1950) by approximating the seismic excitation as a constant, unidirectional body force acting through the centroid of a rigid sliding mass, whose stability is to be evaluated (Cai and Bathurst 1996; FEMA 2005; Gazetas and Uddin 1994; Kramer and Smith 1997; Newmark 1965; Seed 1981). Since the effect of the vertical disturbances during the earthquake average out to zero, generally, this additional body force is applied only in the horizontal direction and incorporated in the limit equilibrium method of slope stability analysis (Babu et al. 2007; Jibson 2011). The horizontal acceleration is represented in terms of a seismic coefficient k_h, which is multiplied by the mass of slip surface to obtain the horizontal body force, and the stability of the mass is evaluated. Even though the pseudo-static approach is extremely simple, easy to use

and is widely used by practicing engineers, the effect of variation in the induced forces, throughout the body of the earthen embankment, cannot be apprehended. The stress-deformation method is used in such cases to have a better perception of the performance of the structure during seismic events.

2.5.3.2 Stress-deformation method

In the stress-deformation approach, the earthen embankment is discretized as a mesh and the stress and deformation at all the nodes are determined in response to an earthquake disturbance (time-history data) applied at the base of the structure (Jibson 2011). The earthquake-induced forces acting on a slip surface of interest are incorporated in this type of stability analysis, unlike the unidirectional constant body force used in the pseudo-static approach. This procedure hence provides a realistic modelling of the seismic response of the structure and is expected to provide a better understanding of the behavior of the embankment slope during an earthquake. However, the need for high-quality laboratory and field test data, and sophisticated constitutive models makes the stress-deformation approach suitable primarily for very important projects and is especially useful for research purposes (Baker et al. 2006; Gazetas and Uddin 1994; Jibson 2011; Shukha and Baker 2008).

2.5.3.3 Permanent displacement method

The permanent-displacement approach introduced by Newmark (1965) bridges the gap between the pseudo-static approach and the stress-deformation approach (Gazetas and Uddin 1994; Jibson 2011). The pseudo-static analysis alone does not

provide any information about the behavior of the slip surface during an earthquake, or the consequences of an event when the factor of safety (FOS) of the slip surface falls below unity (Gazetas and Uddin 1994; Kramer and Smith 1997; Seed 1981). Since the serviceability of the slope is related to the permanent deformation incurred, rather than the pseudo-static FOS, the permanent-displacement approach provides an understanding of the impact of the earthquake event on the embankment slopes (Kramer and Smith 1997; Marcuson III et al. 1992). A pseudo-static FOS less than one does not necessarily mean failure of the slope, rather the sliding mass incurs a permanent displacement (Gazetas and Uddin 1994; Newmark 1965; Seed et al. 1978). This method thus provides an estimate of the plastic deformation experienced by a sliding mass during an earthquake. The sliding mass incurs a permanent deformation when the earthquake-induced acceleration in the sliding mass exceeds the critical/yield acceleration (Gazetas and Uddin 1994; Jibson 2011; Kramer and Smith 1997; Seed 1981). The critical/yield acceleration is defined as the minimum horizontal acceleration at which the sliding mass is on the verge of imminent failure, i.e. the FOS is equal to unity. The critical acceleration can be obtained by iteratively varying the horizontal pseudo-static coefficient and determining the coefficient which results in a FOS of 1. The accumulated displacement is obtained by double integration of the acceleration (experienced by the sliding mass) over the time instances when the acceleration exceeds the yield acceleration (Jibson 2011; Kramer 1996; Seed 1979).

Initially, the sliding block (in Newmark type analysis) was assumed to behave as a rigid block and the variation of the earthquake-induced acceleration in the sliding mass was not considered in the permanent-displacement method (Gazetas and Uddin 1994; Jibson 2011; Kramer and Smith 1997). However, the decoupled method of analysis by Makdisi and Seed (1978) incorporates the non-rigid behavior of the sliding mass, which deforms internally during shaking. In such a process, a dynamic response analysis (for a particular earthquake time-history data) is performed without considering any failure of the slope (Jibson 2011; Kramer and Smith 1997; Seed 1979). The earthquake-induced acceleration obtained from the seismic response analysis is used to compute the average horizontal equivalent acceleration, which is then used in the Newmark type deformation analysis (Makdisi and Seed 1978; Seed 1979). Studies have shown that this decoupled approximation can lead to a conservative estimation of the permanent-displacement, especially when the frequency of base excitation is close to the natural frequency of the earthen structure (Gazetas and Uddin 1994; Kramer and Smith 1997; Lin and Whitman 1983). However, this over-prediction of permanent deformation was found to be insignificant when compared to the other associated uncertainties in the seismic response and sliding block analysis (Kramer and Smith 1997). Besides the aforementioned reasons, lack of available software packages capable of performing the computationally intensive coupled analysis, and need for complex constitutive models, make the decoupled approximation a

viable option to estimate the accumulated permanent-displacements of a sliding mass (Jibson 2011).

The permanent-displacement analysis overcomes some of the limitations of the pseudo-static analysis, but cannot capture the entire dynamic behavior of an earthen structure subjected to dynamic loading conditions (Xiong and Huang 2017). Nevertheless, the pseudo-static approach along with permanent-displacement analysis remains extremely popular among practicing engineers due to its simplicity. Different agencies, design manuals, and codes also recommend using pseudo-static analysis as a tool for preliminary screening, to justify the use of a rigorous stress-deformation based seismic response analysis, even for important projects (Baker et al. 2006; Christian and Urzúa 2017; Shukha and Baker 2008). Despite being a crude method, the pseudo-static approach is found to provide an index of the seismic stability of slopes (FEMA 2005; Kramer and Smith 1997), especially when the embankment materials does not incur significant strength loss and are not susceptible to liquefaction during earthquake (Baker et al. 2006; FEMA 2005; Seed 1981; USSD 2007). Hence the use of pseudo-static approach is justified where the embankment is made of clayey soil or dense sand (i.e. soils which are not susceptible to liquefaction). Earthen embankment structures present in low seismicity zones, where the intensity of earthquake excitation is not expected to be significant enough to cause soil liquefaction, can also be studied

using the traditional pseudo-static approach (Makdisi and Seed 1978; Seed 1981; Seed et al. 1978).

2.6 Reliability based analysis

Engineers are accustomed to performing deterministic stability analysis, in which the obtained analysis result solely depends on the mean (or estimated) value of the input parameters. However, there is a significant degree of uncertainty associated while performing an analysis due to the natural material variability, knowledge uncertainty or decision uncertainty (Baecher and Christian 2005; Christian 2004; Fenton and Griffiths 2010; Malkawi et al. 2000). Hence probabilistic theories are used to study the performance of a structure in terms of probability of failure and the reliability index (Babu and Srivastava 2010; Christian 2004; Christian et al. 1994). It should be noted that the term "failure" does not necessarily mean catastrophic failure of the structure, rather it is any unacceptable pre-defined criteria set by the user (Leonards 1982).

A brief overview of the theoretical background of reliability analysis is presented in this section. The resistance of the structure is denoted by R and the stress in the structure due to different loading conditions is denoted by S (Figure 2-22). Since the values of both R and S are uncertain, the mean values of S and R are also associated with their respective standard deviations, σ_S and σ_R, and their corresponding distributions (Figure 2-22). The standard deviation can be

considered as a measure of the uncertainty involved. A narrow standard deviation implies a higher confidence (or accuracy) in the estimated value and vice versa (Chakraborty et al. 2017a). The margin of safety, *M*, is defined as the difference of the resistance (*R*) and the stress (*S*) (equation 2.5) and the mean of the distribution of *M* is the difference in the mean values of *R* and *S* (equation 2.6) (Baecher and Christian 2005; Christian et al. 1994). The variance of *M*, can be obtained using equation 2.7, where ρ_{RS} is the correlation coefficient between *R* and *S*. The failure criteria is set at $M = 0$, i.e. when the stress is equal to the strength, representing the event when the safety margin is equal to 0 (considered as failures). The probability of failure p_f is the area of the distribution curve of *M*, which is below the safety margin of zero (Figure 2-22). The reliability index (β) is mathematically represented by equation 2.8. Graphically, the mean of the safety margin *M* is 'β times σ_M' away from the failure criteria (Figure 2-22).

$$M = R - S \tag{2.5}$$

$$\mu_M = \mu_R - \mu_S \tag{2.6}$$

$$\sigma^2_M = \sigma^2_R + \sigma^2_S - 2\rho_{RS}\,\sigma_R\,\sigma_S \tag{2.7}$$

$$\beta = \frac{\mu_M}{\sigma_M} = \frac{\mu_R - \mu_S}{\sqrt{\sigma_R^2 + \sigma_S^2 - 2\rho_{RS}\,\sigma_R\sigma_S}} \tag{2.8}$$

For geotechnical engineering problems, the margin of safety is most often represented in terms of the factor of safety (equation 2.9), instead of equation 2.5.

$$F = \frac{R}{S} \tag{2.9}$$

and failure happens when $F < 1$. The corresponding reliability index is then defined as

$$\beta = \frac{\mu_F - 1}{\sigma_F} \tag{2.10}$$

The calculation of reliability index is more complicated when the margin of safety is represented in terms of factor of safety, since the ratio of two uncertain quantities are involved (equation 2.9), instead of the difference (equation 2.5) (Baecher and Christian 2005; Christian 2013).

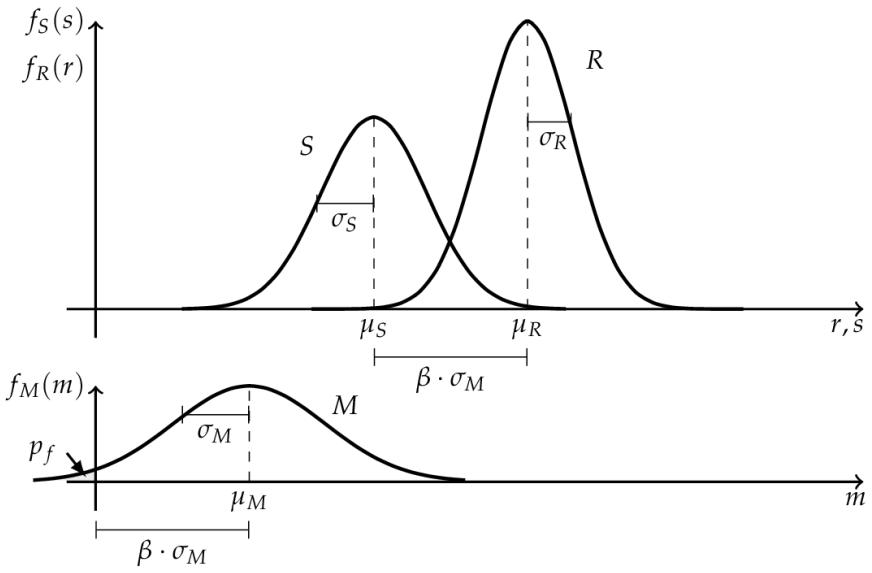

Figure 2-22: Distribution of R, S and M and graphical representation of reliability index and probability of failure
(Source: http://hackl.github.io/pyre/theory.html)

A brief overview of some of the different methods available to calculate the reliability index is presented here, however, interested readers may refer to Baecher and Christian (2005) for further details.

First order second moment (FOSM): This is the simplest and widely used method in practice. It involves only the first term of Taylor series expansion of the factor of safety function (the performance function) to obtain the mean and variance of the distribution and the higher terms are ignored (Chowdhury and Xu 1995; Duncan 2000; Malkawi et al. 2000; Phoon and Kulhawy 1999). The partial derivative of the performance function is evaluated N times at the respective mean values of the N uncertain variables which govern the performance function (Baecher and Christian 2005).

Second order second moment (SOSM): This method is similar to the FOSM, however, the first and second terms of the Taylor series expansion of the performance function, are used. The method is computationally intensive and does not provide additional accuracy in the obtained result (Baecher and Christian 2005; Bungenstab and Bicalho 2016) and hence rarely used in practice.

Point estimate method: The point estimate method requires estimating the moments of the performance function by evaluating the function at certain specific pre-determined discrete points (Baecher and Christian 2005; Christian 2004; Rosenblueth 1975). The function is estimated 2^N times, therefore involving a lot of computational effort when the number of variables involved (N) is high (Christian 2013).

Hasofer-Lind method: The reliability index obtained by FOSM gives different results if the safety function is represented in terms of margin of safety (M) and the factor of safety (F), even though M=0 and F=1 represent the same event. Moreover, the distribution of F is required to be assumed beforehand (e.g. normal, lognormal, etc.) in order to evaluate the reliability index and probability of failure. Both of these limitations are overcome by using the Hasofer-Lind method (Baecher and Christian 2005). This method provides a geometric representation of the reliability index as the distance between the function representing the failure condition and the 'peak of the multivariate distribution' of the uncertain parameters (Baecher and Christian 2005; Christian 2004; Hasofer and Lind 1974).

Monte Carlo simulation: In this method, the distribution of the uncertain input parameters, in terms of mean, standard deviation and the distribution pattern, is provided to the computer simulator (Baecher and Christian 2005; Christian 2004; Malkawi et al. 2000). A large number of data sets are used for these distributions to calculate the performance function (Christian 2013). The distribution of the performance function need not to known a priori, and the mean and its standard deviation are obtained at the end of the simulation (Babu and Srivastava 2010; Fenton and Griffiths 2010). The method is conceptually simple but requires significant computational effort to estimate the value of the performance function at each and every combination of the input data points. Usually, 30,000 to 40,000 simulations are found to be sufficient to obtain acceptable results of reliability index

and performance function (Babu et al. 2007). The performance function, as a mathematical function of the uncertain input parameters, is not required in the Monte Carlo simulation method. Due to this advantage, the Monte Carlo simulation has been used in this study.

The reliability index, obtained by any of the aforementioned methods, is considered as a measure of the probable performance of a structure under certain loading conditions. Hence the computed reliability index is often compared with the USACE (1997) guidelines (Figure 2-23) to judge the performance of the structure (Babu and Srivastava 2010; Babu et al. 2011; Wang and Kulhawy 2008). These guidelines are also be used in this study to evaluate the performance of the EM dam under different seismic loading conditions.

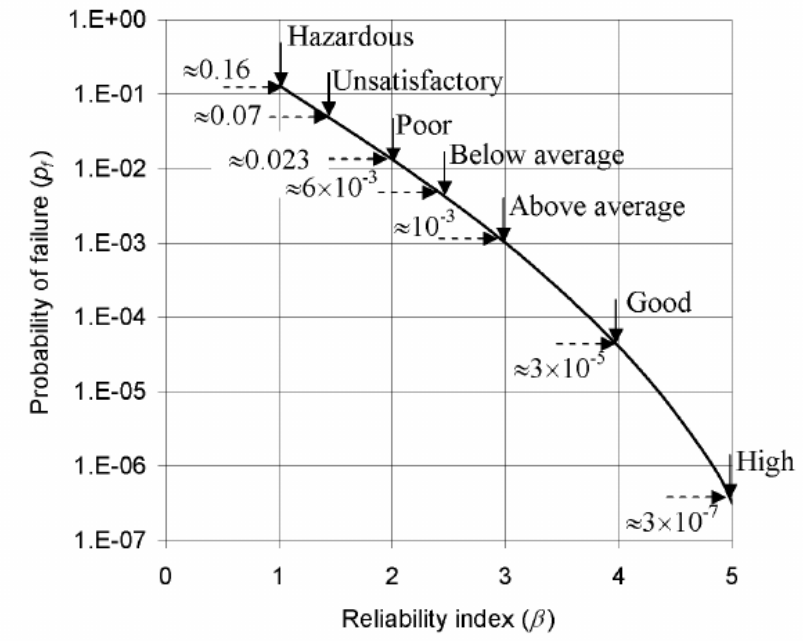

Figure 2-23: USACE (1997) guidelines for reliability index

2.7 Liquefaction analysis

Liquefaction analysis is one of the most interesting, yet complex topics in the field of geotechnical engineering (Chen et al. 2009; Kramer 1996; Xenaki and Athanasopoulos 2003). The effect of liquefaction first came to the attention of geotechnical engineers in 1964 when several structures such as slopes, bridges and building foundations were affected by the Good Friday earthquake in Alaska and the Niigata earthquake in Japan (Ayothiraman et al. 2012; Kramer 1996; Siegel 2013). The term 'liquefaction', originally coined by Mogami and Kubu (1953), encompasses different but related phenomena, in which the saturated soil loses it strength during cyclic, monotonic or transient undrained loading conditions (Kramer 1996). Liquefaction can be mainly classified into flow liquefaction, cyclic liquefaction and cyclic softening.

Flow liquefaction is not commonly observed in the field and is applicable to loose cohesion-less soils which exhibits strain softening behavior during undrained loading (Kramer 1996; Marcuson 1978; Robertson et al. 1995). This occurs when the in-situ static shear stress in loose sands is greater than the undrained steady-state shear strength. The undrained steady-state strength is the resistance offered by the soil at high strain levels during undrained shearing (Castro et al. 1992; Finno et al. 1996; Krahn 2004a; Kramer 1996; Thevanayagam 1998). Soils susceptible to flow liquefaction has a "collapsible soil-grain structure" and experiences significant strength loss on touching the collapse point (Figure 2-24)

(Krahn 2004a). The flow failure is also accompanied by high strain and deformation.

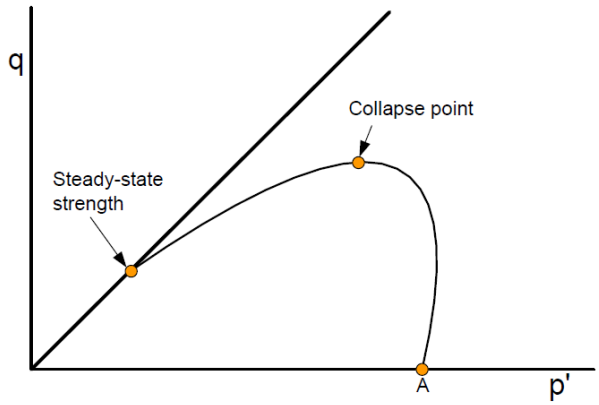

Figure 2-24: Stress path for loose-sand under monotonic loading (after Krahn 2004)

The flow liquefaction can be triggered by a dynamic loading condition, but once triggered, the static stresses can act as the driving force for the flow failure (Kramer 1996; Robertson and Cabal 2015). Laboratory tests on isotropically consolidated specimens, having different confining pressures, are found to reach the same undrained steady state shear strength, when the consolidated specimens have the same void ratios prior to shearing (Idriss and Boulanger 2008; Kramer 1996). The collapse point for the different specimens can be joined by a straight line to form the collapse surface (Figure 2-25). The collapse surface demarcates the stress-states in a soil which may be susceptible to flow liquefaction.

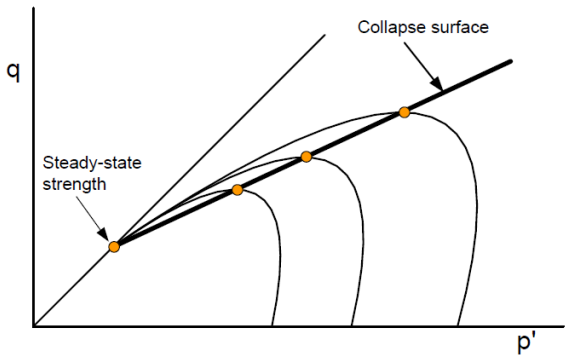

Figure 2-25: Definition of collapse surface
(after Krahn 2004)

The definition of the collapse surface is extremely important for performing a flow liquefaction analysis on loose sands having "collapsible soil-grain structure". The collapse surface is defined in terms of the undrained steady-state strength and the inclination of the collapse surface. Both of these parameters can be obtained by performing CU triaxial tests on specimens of loose sand (Krahn 2004a; Kramer 1996).

The collapse surface is used to determine if the soil is susceptible to flow liquefaction. If the stress state (p'-q values) lies below the collapse surface (point B in Figure 2-26), the soil will not experience flow liquefaction at its static stress condition (Chillarige et al. 1997; Krahn 2004a; Kramer 1996). However, if a trigger, such as dynamic loading condition, brings the new stress state on the collapse surface, the initial static stresses will drive the flow failure and will be accompanied with dramatically high values of deformation, till the steady state strength is mobilized (Figure 2-26). At the steady state, further deformation does

not result in any change in void ratio (critical void ratio) and the steady-state strength solely depends on the initial void ratio, before undrained shearing started (Kramer 1996).

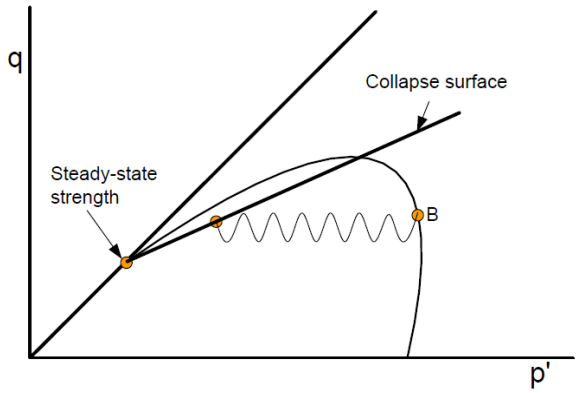

Figure 2-26: Undrained dynamic loading triggering flow liquefaction (after Krahn 2004)

Cyclic liquefaction is the other type of liquefaction which is more often observed in the field, as compared to flow liquefaction. The three different scenarios which may result in cyclic liquefaction, are shown in Figure 2-27. A brief overview has been provided in this section; interested readers may refer to Kramer (1996) for detailed explanation.

The first case (Figure 2-27a) occurs when the summation of static (τ_{static}) and the maximum cyclic shear stress (τ_{cyc}) is less than the undrained steady state shear strength and stress reversal does not occur. There may be scenarios when the summation of static (τ_{static}) and the maximum cyclic shear stress (τ_{cyc}), is greater than the undrained steady state shear strength but is not accompanied with stress reversal (Figure 2-27b). The third case occurs when the summation of static (τ_{static})

and maximum cyclic stress (τ_{cyc}), is less than the steady state strength but the magnitude of the peak cyclic stress is more than the static stress, resulting in stress-reversal (Figure 2-27c).

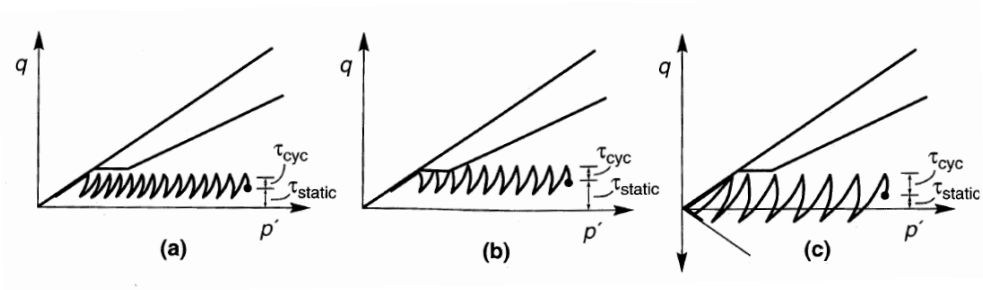

Figure 2-27: Three scenarios of cyclic liquefaction
(after Kramer 1996)

In all the cases, the dynamic loading results in an increase in pore water pressure and subsequent decrease in p' due to undrained conditions. In the first case, the generation of excess pore water pressure brings the stress path to the drained failure envelope. However, the stress path cannot move to the left of the failure envelope, hence continued dynamic loading causes the stress path to oscillate along the failure envelope. The low values of effective confinement (p') and reduced stiffness are associated with accumulation of permanent strain with each cycle of loading.

In the second case, the development of excess pore water pressure causes the stress path to move left (decrease in p') till the stress path touches the collapse surface (flow liquefaction surface). This results in flow liquefaction and the shear strength drops to the undrained steady state strength and it associated with large

deformations, typically observed in case of flow liquefaction. Further cyclic loading causes the stress path to move along the drained failure envelop, similar to the first case. In the third case, the sign of the shear stress changes with every cycle (i.e. compression and extension) as the stress path crosses the q=0 line and is associated with high rate of pore pressure generation. The stress path moves to the left and finally follows the compression and extension drained failure envelope. In each cycle, the stress path passes twice through the origin, which represents a state of zero effective stress. However, this state does not necessarily imply zero shear strength. Further application of monotonic load on the specimen, causes dilative behavior (since effective confinement is also 0), leading to the reduction in pore water pressure and movement of the stress path towards the undrained steady state strength.

Unlike flow liquefaction, cyclic liquefaction can occur in both loose and dense sand, when the initial static shear stress is less than the undrained steady state strength (Kramer 1996). Moreover, there is no definite initiation of cyclic liquefaction, as observed in cases of flow liquefaction (touching the collapse surface). The flow liquefaction is less commonly observed in the field as compared to cyclic liquefaction. However, the deformation associated with flow liquefaction is far greater than that observed in case of cyclic liquefaction (Kramer 1996).

Assessing the possibility of flow liquefaction requires identifying if the soil has a “collapsible soil-grain structure”, which requires performing undrained

triaxial tests on undisturbed loose sand samples. Moreover, commercially available software packages require the undrained steady state strength and inclination of the collapse surface as the input parameters for identifying the locations in an earthen structure which may be susceptible to flow liquefaction (Krahn 2004a). Due to the unavailability of undisturbed samples extracted from the upstream shell of the EM dam, it is not be possible to assess if the sand shell is susceptible to flow liquefaction.

The impact of cyclic liquefaction can be assessed using commercially available software packages. The analysis requires the use of suitable calibrated constitutive models and relations which can estimate the increase in pore water pressure, during seismic shaking simulations. Undrained cyclic triaxial tests on undisturbed samples are required to estimate the increase in pore water pressure and associated permanent strains, with each cycle of loading (Seed 1979). In absence of such test results, advanced constitutive models such as UBCSand or PM4sand cannot be used in the present study. Rather, the procedure outlined by De Alba et al. (1976) and Lee and Albaisa (1974) has been used to determine the pore pressure ratio function (equation 2.10).

$$r_u = \frac{1}{2} + \frac{1}{\pi}\ sin^{-1}\left[2\left(\frac{N}{N_L}\right)^{\frac{1}{\alpha}} - 1\right] \qquad (2.10)$$

where, N is the equivalent number of uniform cycles for laboratory tests at 0.65 τ_{max} for a given magnitude of earthquake (Figure 2-28) and N_L is the number of cycles

required to cause liquefaction corresponding to different shear stress ratios (cyclic number function).

The cyclic number function is supposed to be determined from laboratory test on undisturbed samples. However, due to lack of test results, the cyclic number functions have been adopted from the literature based on the type of sand (dense, medium dense, medium loose and loose) observed from bore log information.

Lastly, the third type of liquefaction, known as cyclic softening, occurs in the fine-grained soil when the shear stress due to dynamic loading conditions exceeds the undrained shear strength of the soil (Kramer 1996; Robertson and Cabal 2015). This type of liquefaction does not occur often. Even if it happens, the associated deformation is not significant due to the cohesive strength of the fine-grained soils (Robertson and Cabal 2015). Hence, this type of liquefaction is not considered in this study.

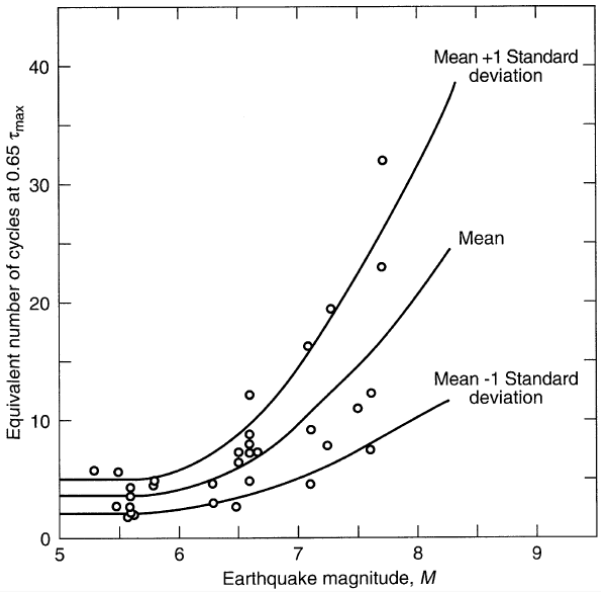

Figure 2-28: Equivalent number of cycles for laboratory testing for different earthquake magnitudes
(after Kramer 1996)

2.8 Recommendations by different agencies

This section presents the factor of safety (Table 2-4), pseudo-static coefficient (Table 2-5), allowable permanent deformation (Table 2-6 for Newmark type analysis) and reliability indices (Table 2-7) recommended by different agencies. Manuals, guidelines, reports and other types of existing literature were reviewed for different agencies including United States Society on Dams (USSD), United States Army Corps of Engineers (USACE), US Bureau of Reclamation (USBR), National Resources Conservation Services (NRCS), Federal Emergency Regulation Commission (FERC), Federal Emergency Management Agency (FEMA), California Division of Safety of Dams (CDSOD), Texas Commission on Environmental Quality (TCEQ) and California Geologic Survey (CGS).

Table 2-4: Recommended factor of safety for static and pseudo-static analysis (after USSD 2007)

Agency	Loading condition	Stress parameter	Factor of safety
USACE	Long-Term	Effective	1.5
USBR	Steady-State Seepage	Effective	1.5
NRCS	Steady-State Seepage	Composite	1.5
NRCS	Steady seepage with EQ	Total	1.1
FERC	Steady-State Seepage	Total and Effective	1.5
FERC	Steady seepage with EQ	Total and Effective	>1
FEMA	Steady-State Seepage	Effective	1.5
FEMA	Pseudo-static	Composite	>1
CDSOD	Steady-State Seepage	Effective	1.5
CDSOD	Pseudo-static	Total	1.1
TCEQ	Steady-State Seepage	Not specified	1.5
TCEQ	Pseudo-static	Not specified	>1

Table 2-5: Recommended values of horizontal seismic coefficient (after Melo and Sharma 2004)

Horizontal Seismic Coefficient, k_h	Description	
0.05 - 0.15	In the United States	
0.12 - 0.25	In Japan	
0.1	"severe" earthquakes	Terzaghi [4]
0.2	"violent, destructive" earthquakes	
0.5	"catastrophic" earthquakes	
0.1 - 0.2	Seed [2], FOS ≥ 1.15	
0.10	Major Earthquake, FOS > 1.0	Corps of Engineers [5]
0.15	Great Earthquake, FOS > 1.0	
½ to ⅓ of PHA	Marcuson [6], FOS >1.0	
½ of PHA	Hynes-Griffin [7], FOS > 1.0	
FOS = Factor of Safety. PHA = Peak Horizontal Acceleration, in g's.		

Table 2-6: Amount of deformation and corresponding post-earthquake condition (after USACE 2010)

Amount of Deformation	Significant Damage to Internal Structures (e.g. Cutoff Walls)	Remaining Freeboard for Post Seismic Evaluation (2-Year Flood Water Surface Elevation)	Post Seismic Flood Protection Ability
<1'	No	>1'	Probably Uncompromised
1' to 3'	Possibly	>1'	Possibly Compromised
3' to 10'	Likely if existing	None	Likely Compromised
Unlimited (flow side condition)	Yes	None	Compromised

CGS (2008) suggests that the Newmark deformation result should be used merely as an index to judge the post-earthquake serviceability of the structure and significant engineering judgement should be used to rely on the inferences drawn from the Newmark deformation analysis. It also suggests that a deformation of 0 to 15 cm should not be causing significant damage to the structure. However, a Newmark displacement over 30 cm is considered unstable, as suggested by USACE (Table 2-6).

Based on the above recommendations, the following target values of factor of safety, yield coefficient and Newmark displacement are selected and used to evaluate the condition of the dam:

(a) Static factor of safety > 1.5; (b) Pseudo-static factor of safety > 1; (c) Yield coefficient > 0.1 and (d) Newmark displacement < 30 cm

As described in section 2.6, reliability-based analysis has gained significant importance in the field of geotechnical engineering. The reliability-based approach

incorporates the effect of uncertainties associated with performing an analysis and the reliability index and the probability of failure are used to evaluate the expected performance of the structure (Table 2-7).

Table 2-7: Expected performance level of structure based on reliability index (after USACE 1997)

Expected Performance Level	Beta	Probability of Unsatisfactory Performance
High	5	0.0000003
Good	4	0.00003
Above average	3	0.001
Below average	2.5	0.006
Poor	2.0	0.023
Unsatisfactory	1.5	0.07
Hazardous	1.0	0.16

2.9 Summary and research needs

2.9.1 Improving coherence in a SASW field test

SASW test is a widely used non-intrusive and non-destructive testing technique to obtain the subsurface shear wave velocity (and small strain shear modulus). Very often, the SASW test trials need to be conducted several times due to unacceptable coherence (coherence < 0.95). In such scenarios, the test needs to be repeated until a result with acceptable coherence is obtained. Even performing the test several times may not guarantee an acceptable data. It is thus necessary to modify the current testing procedure to improve the efficiency and repeatability of a SASW field test. Laboratory tests in a controlled test box and in-situ testing on the field

needs to be performed to study the improvement in the quality of data by suitably modifying the test procedure. The impact of erroneous estimation of G_{max} on seismic response of an earthen embankment structure, subjected to a free-field acceleration time history data, also needs to be studied to comprehend the impact of erroneous estimation of the modulus values.

2.9.2 Impact of erroneous estimation of G_{max} values

Review of existing literature provided some insight on the possibility of erroneous estimation (both underestimation and overestimation) of V_s using different methods available. Although the extent of deviation of the estimated V_s may depend on the testing technique or correlations used and vary from one site to another, it is evident from the available literature that a significant uncertainty remains in the estimation of shear wave velocity profile and small strain shear modulus. Since the shear wave velocity and small strain shear modulus are important parameters in seismic response analysis and slope stability analysis of earthen structures, it is expected that error in estimation of G_{max} will affect the behavior of the structure to dynamic loading. Hence, the impact of such errors needs to be studied.

Moreover, the in-situ tests (SASW, SCPT etc.) are mostly conducted on the crest of the dam; hence simplified assumptions are made regarding the G_{max} of the shell of the dam. The dam is often idealized to consist of horizontal layers, and the material is assigned with the G_{max} values obtained from in-situ tests conducted on

the dam crest. In some cases, the shell is considered to have uniform G_{max} properties, whereas some analyses assume G_{max} to increase as a function of effective mean stress. Hence it is necessary to study the influence of inaccurate estimation of G_{max} of the shell of an earthen dam, on its seismic response. A sensitivity analysis is required to gain some understanding on the impact of erroneous estimation of G_{max}, on the response of the earthen structure and the stability of its slopes under seismic loading conditions.

2.9.3 A method to determine strain-dependent natural frequency

The existing methods used to determine the natural frequency of an earthen embankment structure can provide the natural frequency corresponding to low strain levels. Due to non-linear behavior of soil, the response of an earthen dam to an earthquake excitation depends on the strain level experienced by different zones of the dam. For a zoned dam, hydraulic-fill dam or any other highly non-homogeneous dam, the natural frequency obtained by free vibration analysis or Eigen value analysis, may not suitably portray the response of the structure at various strain levels experienced by different zones/segments of the dam, during an earthquake event (Abdel-Ghaffar and Scott 1979b; Mejia and Seed 1983). A method is hence required to predict the natural frequency of an earthen embankment structure taking into account the effect of non-linear behavior of soil.

2.9.4 Seismic slope stability analysis of the hydraulic-fill dam

Earthen dams made of clayey soils, build on clay-rock foundations have been found to be safe during strong earthquakes when compared to dams having significant zones of sand (Seed 1981; Seed et al. 1978). Well-built dams, including some hydraulic-fill dams, have shown resilience to moderate shaking without significant damage (Ambraseys 1960a; Seed 1981). However, some hydraulic-fill dams such as the Lower San Fernando dam have been found to be extensively damaged by earthquakes (Foster et al. 2000; Seed et al. 1978). The susceptibility of earthquake-induced damage was found to depend on the location of the dam. Recently in 2016, the United States Geological Survey (USGS) indicated Oklahoma-Kansas, the Raton Basin, North Texas, North Arkansas, and New Madrid to be high seismic hazard zone due to induced seismicity. This necessitates the evaluation of earthen dams located in this region, which at the time of construction might not have been specifically designed to withstand earthquake loading conditions. In this study, the stability of Eagle Mountain Dam, an eighty-five-year-old hydraulic-fill dam located in Fort Worth, Texas is evaluated. Pseudo-static approach along with permanent-displacement method have been used to perform the preliminary seismic slope stability analysis.

Although commercially available software packages have made it easy to perform seismic stability analysis, the efficacy of the analysis depends on the accuracy with which the dam is modelled. The embankment structure is often

idealized as a zoned structure with the respective averaged material properties assigned to the individual zones, such as shell, core and foundation (Babu et al. 2007; Boulanger and Montgomery 2016; Pelecanos 2013; Tezcan et al. 2001). The accuracy of a subsequent analysis result may be questionable since this crude approximation of assigning averaged values of different material properties at different zones of a dam section may not portray the actual field conditions.

The epistemic uncertainty, that includes site characterization uncertainty, model uncertainty, and parameter uncertainty (Baecher and Christian 2005), makes the evaluation of the safety of the hydraulic-fill structures even more challenging. Significant engineering judgement, based on prior experience, is thus required in such cases and a substantial degree of uncertainty is associated in estimating the material properties (Babu and Srivastava 2010; Duncan 2000; Griffiths et al. 2010; Wolff 1996; Xiong and Huang 2017; Zhenyu et al. 2015). A probabilistic approach in terms of reliability-based analysis can provide important information on the impact of erroneous estimation of different material properties (Babu et al. 2007; Garevski et al. 2013; Liang et al. 1999; Yegian et al. 1991).

A research study is required to address some of the key uncertainties including the material variability and seismic coefficient uncertainty. Probabilistic concepts need to be used to evaluate the stability of hydraulic-fill dams. Pseudo-static approach along with decoupled permanent-displacement method is required

to perform the preliminary seismic slope stability analysis and assess the condition of the dam. The probability of failure of the slopes and the probable performance of the dam should be evaluated, based on the reliability index, to identify the critical sections of the dam, which may require proactive measures to avoid any catastrophic consequences. Furthermore, dynamic slope stability analysis with estimation of excess pore water pressure is also required to study the effect of strength loss in liquefiable soils, on the stability of the structure, during different earthquake events.

Chapter 3: Research Methodology

3.1 Analysis steps

This chapter presents the steps involved in performing the seismic response and stability analysis of hydraulic-fill dams, incorporating the effect of material variability and induced-seismicity. The necessities of the individual tasks and the link between the different steps are explicitly explained in this chapter. The major tasks involved in this study are shown in Figure 3-1 and the steps followed to perform the stability analysis is depicted in Figure 3-2.

The first and most crucial step for performing seismic response and stability analysis was to determine the geomaterial properties required for the analysis. Extensive in-situ and laboratory tests database on samples collected along the crest and downstream toe of the dam was available for the present study. The relevant information on material properties, such as coefficient of permeability, volumetric water content, unit weight, shear strength parameters and Atterberg limits, were compiled and grouped based on the soil types. Small strain shear modulus values were determined from the shear wave velocity profile determined from spectral analysis of surface waves (SASW) tests.

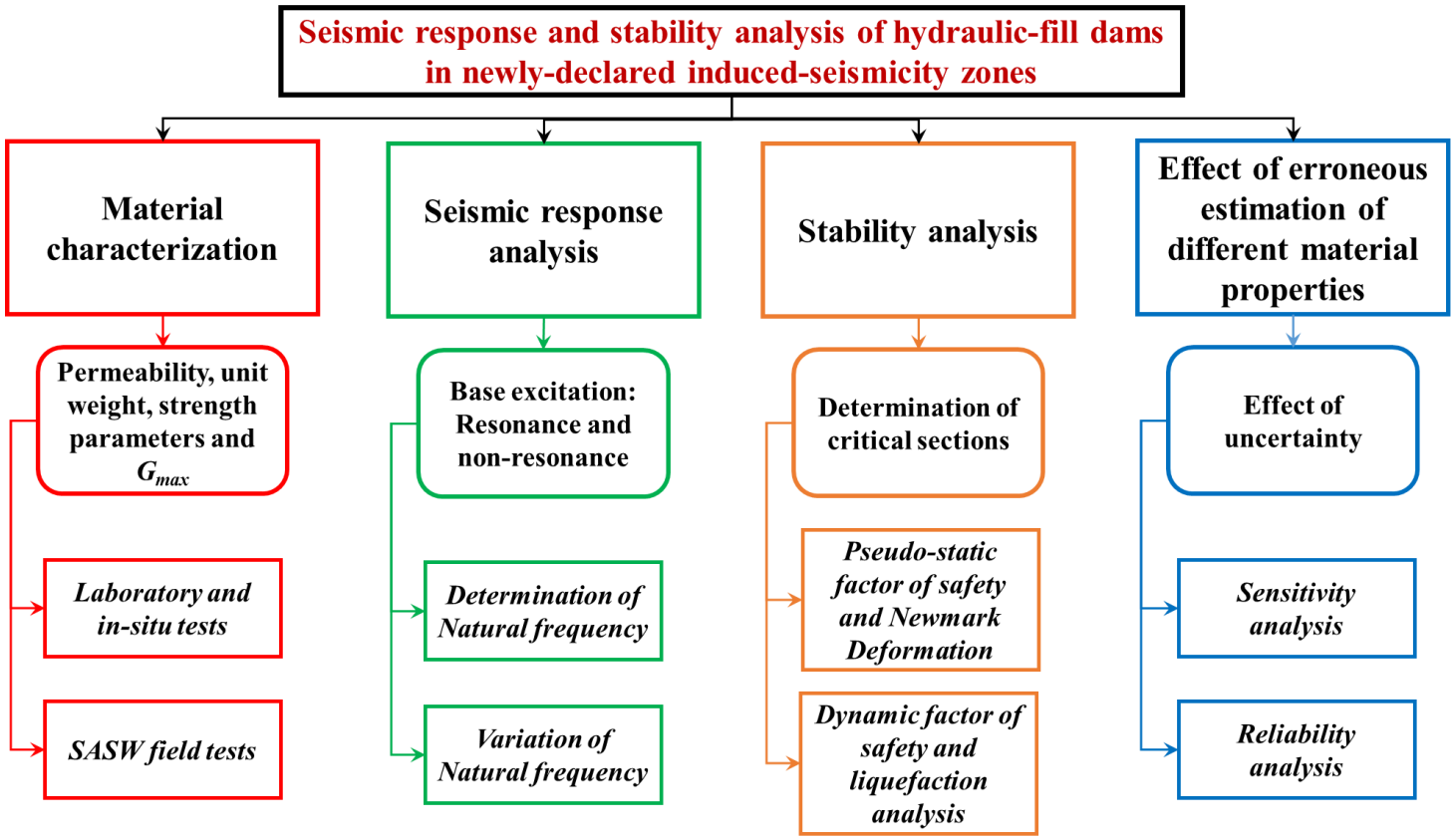

Figure 3-1: Major tasks involved in the study

The SASW test procedure involves striking the ground surface with an impact source (typically a hand-held hammer) to generate Rayleigh waves of a wide range of frequencies. However, the test needs to be repeated several times to attain an acceptable value of coherence (> 0.95). The testing technique had to be modified to improve the repeatability and efficiency of the SASW test before conducting the in-situ test on the crest of the dam. The necessity of improving the efficiency of the testing method and its impact on seismic response analysis had to be evaluated to justify the importance of accurately determining the small strain shear modulus.

A significant uncertainty and chance of variability were associated with the assessment of shear strength parameters, owing to the hydraulic-fill method of construction. Even though geostatistics-based kriging analysis was used to interpolate the material properties interpreted from in-situ tests, a reliability-based analysis was necessary to obtain valuable information on the impact of the uncertainties involved in estimating the shear strength parameters, on the slope stability analysis results. A reliability-based pseudo-static static analysis was thus performed to evaluate the probability of failure during different earthquake events and assess the probable performance of the dam.

Although the pseudo-static analysis provides an index of probable performance of a dam during seismic events, it does not include the effect of the response of the structure during earthquake excitations. Hence a time-history based

shaking analysis was required to study the behavior of the structure during seismic events. Time-history data needed for dynamic analysis is usually available for dams located in earthquake-prone zones. However, the EM dam is located in Texas, a state which does not have a considerable history of strong earthquake motions. Nevertheless, Texas has been declared to be a seismic hazard zone due to induced seismicity (USGS 2016). Hence a natural frequency based approach was required to select time-history data to be used for the analysis.

The earthquake data, with varying peak ground accelerations, had to be selected such that predominant frequency of some of the earthquakes were close to the natural frequency of the dam. This would facilitate the study of the stability of the slopes in the event of a resonance condition. Thus, the natural frequency of the structure had to be estimated for the different sections of the EM dam. The conventional methods to determine the natural frequency does not include the effect of non-linear material behavior, experienced during seismic loading conditions. It was thus necessary to develop a method which can predict the earthquake-induced strain-dependent degradation of natural frequency. Newmark deformation and dynamic slope stability analysis were then performed using suitable earthquake excitations to estimate the accumulated earthquake-induced deformations and evaluate the stability of the slopes, respectively.

Several hydraulic-fill dams around the world have a history of unsatisfactory performance during seismic events due to liquefaction of the sand layers. Hence liquefaction analysis was necessary, especially for the saturated upstream sand shell of the EM dam. Cyclic liquefaction analysis with the estimated increase in pore water pressure was required to study the stability of the dam when some portions of the sand shell get liquefied. Furthermore, flow liquefaction analysis was necessary for the foundation sand layers to assess the chances of flow type failure, which is usually associated with excessive deformation. Finally, the probable performance of different sections of the dam had to be comprehensively evaluated from the results obtained from static, pseudo-static, Newmark deformation, reliability-based analysis, dynamic stability and liquefaction analysis. The critical zones had to be identified which may require pro-active remedial measures to avoid any unwanted circumstances.

The entire regime of dynamic analyses were performed using the shear modulus estimated from SASW field tests conducted along the crest of the dam. However, previously published literature suggested/indicated that the small strain shear modulus determined by different techniques (in-situ tests, laboratory tests, and correlation equations) usually differs from one another, resulting in significant uncertainty in the estimated values. Hence a sensitivity analysis was performed to assess the effect of inaccurate estimation of small strain shear modulus, stemming out of the inter-method or intra-method variability. It was also necessary to evaluate

the relative importance of the accuracy of the estimated modulus values at different locations of the dam and determine the location from which undisturbed samples should be extracted and tested in the laboratory, in case of critical projects.

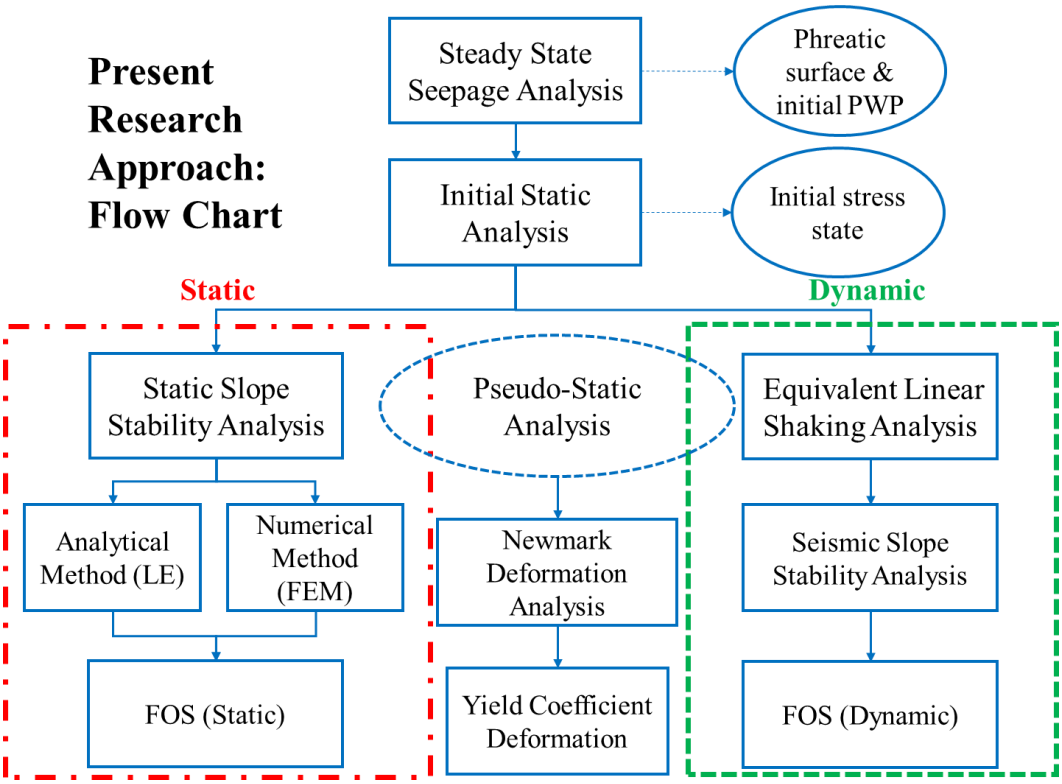

Figure 3-2: Stability analysis steps

3.2 Summary

This chapter presented the analyses steps and tasks involved in this research study. The shear wave velocity profile of the EM dam and the method proposed to improve the quality and repeatability of SASW field test are presented in chapter 4. The obtained subsurface shear moduli were used as input parameters for the finite

element models of the dam, to determine the natural frequency of the dam sections and for performing the dynamic analyses.

The novel method developed to determine the strain-dependent natural frequency of embankment structures is elucidated in chapter 5. The variation of natural frequency along the length of the dam, owing to the material variability and method of construction, is also provided in chapter 5. The earthquake time-history data, required for performing a dynamic analysis were selected based on the estimated natural frequency of the dam sections. The behavior of the structure under resonance and non-resonance condition was studied to evaluate the performance of the dam under probable seismic events. The results of the comprehensive slope stability analyses are presented in chapter 6.

The sections of the dam, which may be critical during seismic events, were first identified using the simple pseudo-static slope stability analysis. Reliability analyses were subsequently used in this study to capture the effect of uncertainty associated with the estimated shear strength parameters, on a pseudo-static slope stability analysis. Although pseudo-static analysis provides an index of the performance of dam during probable earthquake events, it does not include the effect of the response of the dam during seismic shaking. Moreover, the chances of liquefaction and its influence on the stability of the slopes cannot be studied using a pseudo-static approach. The dynamic stability analyses results, incorporating the

effects of cyclic liquefaction and flow liquefaction of the sand layers of the dam, are also presented in chapter 6. Based on the analysis results, the critical sections of the dam were evaluated, and the earthquake conditions which may have the most detrimental impact on the dam were also determined.

The analyses results presented in chapters 5 and 6, and their implications, were solely based on the subsurface shear modulus values estimated from the SASW test results (chapter 4) and used for performing the analyses. However, the literature suggests the chance of making a wide margin of error while estimating the modulus values using different estimation techniques. The impact of inter-method and intra-method variability, associated with the estimation of subsurface shear moduli, on the seismic response and slope stability analyses results, is thus explored using a sensitivity analysis in chapter 7. Lastly, the conclusions are drawn from the analyses results of this research study, and scope of future research are highlighted in chapter 8.

Chapter 4: Estimation of Shear Modulus of Dam Embankment Layers

4.1 Introduction

This chapter presents the subsurface V_s profiles determined by conducting SASW field tests on the crest of the EM dam. The trial tests conducted using conventional hand-held hammers suggested the coherence to be unacceptable for many of the trials. Hence the test had to be repeated several times to achieve an acceptable result (coherence > 0.95). A method to improve the efficiency and acceptability of the SASW test was therefore needed. This chapter details the technique developed to improve the quality of the SASW test result, by using constant impact energy for each strike/repetition. The applicability of the method in enhancing the coherence in a SASW field test was verified by conducting extensive tests in a controlled test box in the laboratory, as well as by performing the tests on the crest of the EM dam. The shear wave velocity profile obtained by conducting the SASW test at different sections of the dam is provided at the end of this chapter. These results will be later used in chapter 5 for determining the natural frequency of the dam and in chapter 6 for the time-history based dynamic stability analysis of the dam slopes. The contents of this chapter have been accepted for publication in ASTM Geotechnical Testing Journal and are being re-used with permission from ASTM GTJ (Appendix A).

4.2 Background

Small strain shear modulus (G_{max}), which refers to strain levels less than 0.001 %, is an important parameter used in geotechnical engineering projects dealing with dynamic loading conditions (Addo and Robertson 1992; Aouad et al. 1993; Chakraborty et al. 2019a; Hiltunen and Woods 1988; Joh 1996; Nazarian and Stokoe II 1983; Nazarian and Stokoe 1985; Sanchez-Salinero et al. 1986; Stokoe et al. 1991). Over the last few decades, several advancements have been made in determining G_{max} by field tests, including the crosshole test, downhole test, and seismic cone penetration test, and laboratory tests such as the resonant column and bender element tests. These field tests are intrusive in nature (Stokoe et al. 1991), whereas the laboratory tests require undisturbed samples and hence do not accurately provide the modulus values at actual field conditions. Under such circumstances, a non-destructive testing technique, like the spectral analysis of surface waves (SASW), is a feasible option for determining the subsurface stiffness profile.

SASW is a non-intrusive and non-destructive testing technique widely used to determine the in-situ shear wave velocity and small strain shear moduli of subsurface layers. The test philosophy is based on the dispersive nature of Rayleigh waves, which are used to calculate the shear wave velocity (Addo and Robertson 1992; Al-Hunaidi 1993; Kramer 1996; Kumar and Hazra 2014; Kumar and Rakaraddi 2013; Nazarian and Stokoe II 1983; Nazarian and Stokoe 1985; Stokoe

et al. 1991). Rayleigh waves are used because two-thirds of the impact energy of a vertically oscillating impact source emanates as Rayleigh waves, and Rayleigh wave energy varies as $1/\sqrt{r}$ when compared with shear wave energy, which varies as $1/r^2$, where r is the distance from the impact source (Miller and Pursey 1955). Hence, at a given distance from the source of the impact, most of the energy received by geophones is in the form of Rayleigh waves. A brief overview of the test procedure is presented here; a detailed description can be found elsewhere (Heisey et al. 1982; Nazarian and Stokoe II 1983; Nazarian and Stokoe 1985; Sheu 1987; Stokoe et al. 1991).

The first and most important step for SASW testing is to conduct the test on the field and obtain an acceptable representative subsurface information about the site. The test is performed by placing a pair of geophones at a predetermined spacing on the ground surface and using an impact source to generate Rayleigh waves. Subsequent tests are conducted to get information about deeper subsurface layers by increasing the distance between the geophones to twice of that used for the previous test, following common receiver midpoint geometry (Mancuso and Vinale 1993; Nazarian and Stokoe 1985; Stokoe et al. 1991). Hand-held hammers or sledge hammers of varying weights are the impact sources most commonly used, and the quality and acceptability of the test are judged based on the coherence and wrapped phase information obtained at the time of the test.

The coherence function is a measure of the quality of the signal, and is an important parameter used for deciding the acceptability of a SASW field test (Heisey et al. 1982; Joh 1996; Kumar and Hazra 2014; Kumar and Rakaraddi 2013; Mukherjee and Prashant 2009; Nazarian and Stokoe II 1983; Nazarian and Stokoe 1985; Stokoe et al. 1991; Suits et al. 2008). A coherence close to 1 implies that the wave of a certain frequency was received by both the geophones used for the SASW test (Kumar and Hazra 2014; Kumar and Rakaraddi 2013). A high coherence also ensures a high signal to noise (S/N) ratio, which is required for the acceptability of a field test. This confirms that the power of the output signal (far geophone) was actually due to the input signal (near geophone), of the same frequency.

The primary reason for a low value of coherence is that the frequencies that are excited at the input are not received/measured at the output. Background noise, improper excitation of waves of certain frequencies, or inadequate frequency resolution during signal digitization, or combinations thereof also lead to decrease in coherence (Heisey et al. 1982; Kumar and Hazra 2014; Nazarian and Stokoe II 1983). A threshold value of coherence greater than 0.95 is thus recommended, and has been used by other researchers to decide the frequency range where the phase data can be used for further analysis (Addo et al. 1993; Mukherjee and Prashant 2009; Sayyedsadr and Drnevich 1989; Sheu 1987; Thorel et al. 2006).

For a given geophone spacing, the same test is repeated four to five times in order to strengthen the signal and reduce the effect of background noise by averaging the data in the frequency domain (Al-Hunaidi 1993; Heisey et al. 1982; Marosi and Hiltunen 2004; Mukherjee and Prashant 2009). Figure 4-1a shows typical raw data plots in the time domain, for four repeated strikes in a SASW test. The coherence and phase plot obtained after accepting the four repetitions (stacked signals) is provided in Figure 4-1b and Figure 4-1c, respectively. The frequency range having coherence > 0.95 (shown by dashed red line in Figure 4-1b) can be used for generation of the dispersion curve, after masking the region having unacceptable coherence (Figure 4-1c). A dispersion curve, depicting the variations of phase velocity with respective wavelengths, is then obtained from the data collected from field testing. The dispersion curves for all of the varying distances between geophones are combined to obtain the global dispersion curve (Marosi and Hiltunen 2004; Nazarian and Stokoe II 1983; Nazarian and Stokoe 1985; Stokoe et al. 1991; Suits et al. 2008).

For each geophone spacing (D), a maximum wavelength of $3D$ may be used for generating the dispersion curves. An upper limit of $3D$ is generally used since it is expected that a surface wave of higher wavelength may not fully develop for a geophone spacing of D (Addo and Robertson 1992; Al-Hunaidi 1993; Rix 1990; Sheu 1987). The number of subsurface layers, layer thickness, density, Poisson's ratio, and V_s are assumed, and the theoretical dispersion curve is determined by

performing the inversion analysis (Addo and Robertson 1992; Al-Hunaidi 1993; Joh 1996; Nazarian and Stokoe II 1983; Nazarian and Stokoe 1985; Stokoe et al. 1991).

The assumed material properties for the different layers are initially assigned over a depth equal to the maximum wavelength (=3D) of the Rayleigh wave, which is expected to develop during field testing (Brown et al. 2000). The layer thickness, V_s and Poisson's ratio are modified after each iteration so that the theoretical and field dispersion curves almost match. The final V_s profile, which provides a dispersion curve similar to that obtained from field tests (Root Mean Square (RMS) error between the field and theoretical dispersion curves < 10), is used for subsequent analysis.

One of the key challenges of SASW testing is obtaining a coherence value close to one (1) for the frequency range of interest. Very often, due to unacceptable coherence (coherence < 0.95), the test trials need to be conducted several times, until a result with an acceptable coherence value is obtained (Al-Hunaidi 1992; Joh 1996; Nazarian and Stokoe 1985). Even performing the test several times may not guarantee an acceptable data. The purpose of the current study was to study the effect of using an impact source of constant energy (for all four repetitions in a test) in order to generate Rayleigh waves with almost identical sets of frequencies.

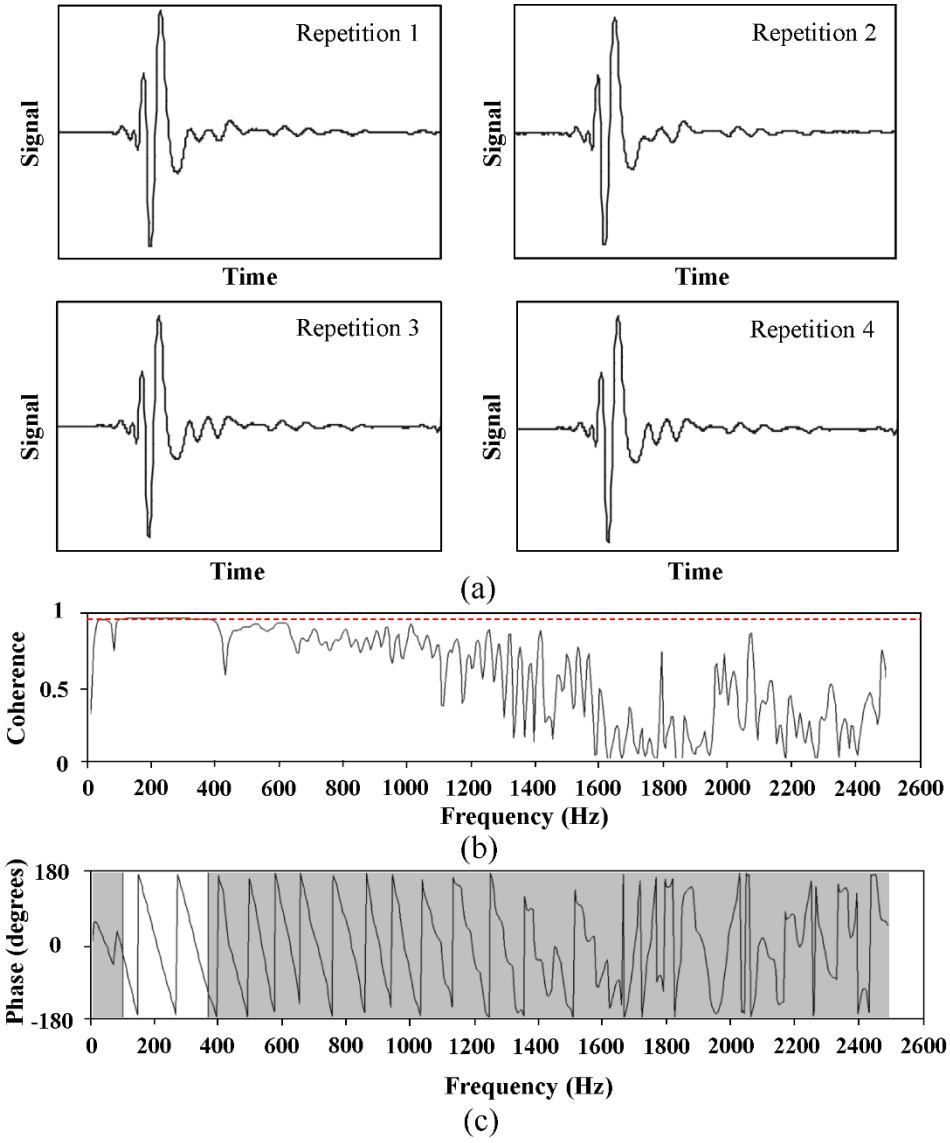

Figure 4-1: (a) Typical raw signals in time domain; (b) Coherence function and (c) Wrapped phase of stacked signals

Laboratory tests in a controlled test box and in-situ testing at a field site were performed to study the improvement in the quality of data obtained by using

a constant impact energy source. The following sections present the experimental studies, test results, and analyses performed in this study.

4.3 Experimental Program

The experimental program was designed and conducted to study the improvement in coherence value upon using an impact source of constant energy. A series of laboratory and field tests were conducted to study the effects of constant and varying-impact energy on the quality of data, based on coherence value. Laboratory tests were performed in a metal box filled with compacted soil, while the field tests were performed on the crest of EM dam in North Texas. The following sections present the details of the tests that were performed.

4.3.1 Laboratory testing

The laboratory test studies were performed in a metal box with dimensions of 1.5 m by 0.60 m by 0.45 m. The soil, with a water content of 21 % and bulk density of 18.3 kN/m^3, was manually compacted in six layers, using a square head rammer. Basic soil characterization tests, including Atterberg limits, specific gravity, standard Proctor compaction, and the composition of soil were determined in accordance with ASTM standards (ASTM D4318 - 10e1; ASTM D854 – 14; ASTM D698-12e2; ASTM C136/C136M-14; ASTM C117-13; ASTM D7928-17). The results are reported in Table 4-1. The soil was classified as fat clay with sand (CH), as per USCS soil classification (ASTM D2487 – 11).

Table 4-1: Basic soil characterization results

Property	Magnitude
Specific Gravity	2.72
Liquid Limit (%)	60
Plastic Limit (%)	26
Plasticity Index (%)	34
Optimum Moisture Content (%)	21
Maximum Dry Density (KN/m^3)	20.2
Gravel (%)	0.1
Sand (%)	16.2
Silt (%)	31.4
Clay (%)	52.3

The main intent of the box testing was to have a controlled test section for studying the effects of using constant and varying impact energies to generate Rayleigh waves, for four repetitions in a SASW test, on coherence value and dispersion curves. Changes in the coherence and quality of data were observed when an impact source of constant energy was used for all four of the repetitions. A random height for the fall of the hammer was used for all four repetitions, to simulate the effect of using a hand-held hammer (referred to as V-L test, implying variable impact energy applications for four repetitions in the laboratory test). A constant energy of 2.8 J was delivered by dropping a 2.2 kg drop hammer from a height of 13 cm (referred to as C-L test, implying constant impact energy application for four repetitions in the laboratory test). Figure 4-2 shows the metal box with the drop hammer used for performing SASW tests in the laboratory.

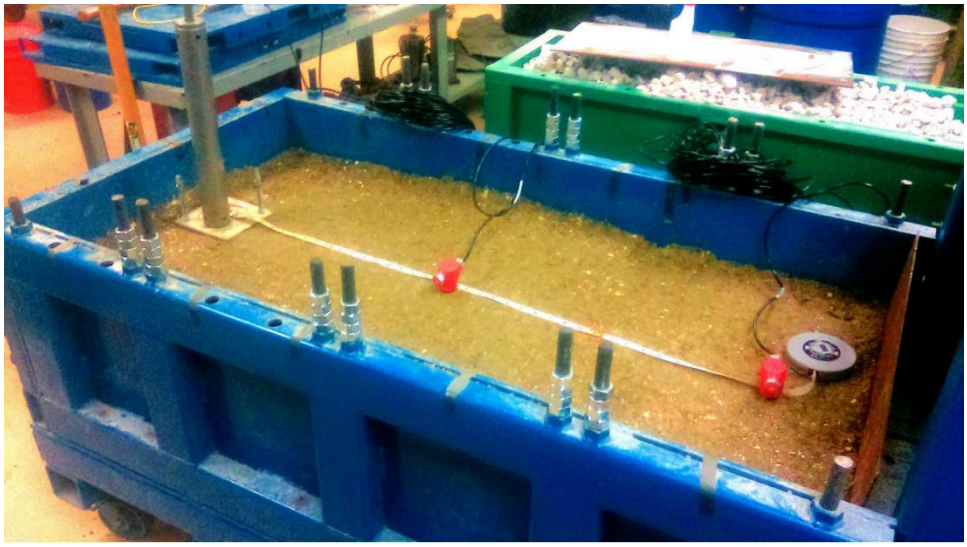

Figure 4-2: Experimental setup for laboratory test

SASW tests were conducted on the surface of the soil compacted in the test box. The distance from the impact source to the first geophone and the spacing between geophones were maintained at 0.6 m for all of the tests. The impact source and pair of geophones were aligned in a straight line. The hammer was dropped on a metal plate that was placed on the soil surface, instead of directly striking the surface of compacted soil (Kumar and Rakaraddi 2013).

Series of tests were performed with both random and constant height of fall of the hammer, and the data was analyzed. It should be noted that the V_s profile was not determined (i.e., inversion analysis was not performed) for the tests performed in the metal box, as the presence of the metal confining box could result in an erroneous estimation of the V_s profile. Since both types of tests, V-L and C-L, were conducted in the presence of the metal box, it is reasonable to assume that

performing a comparative study on the effect of using constant and varying impact energy on coherence would not be significantly affected by the boundary effects of the box, since the boundary effect of the box are expected to affect both the type of test results to the same degree.

4.3.2 Field testing

The main objective of conducting field tests was to study the effects of the two test methodologies on coherence value and subsequent estimation of V_s profile. G_{max}, an important parameter for seismic response analysis of an earth dam, is often determined by the SASW test. Hence, the SASW field tests for both constant and varying impact energy sources were conducted at an earthen dam site. The tests were conducted on the crest of Eagle Mountain Dam located in Tarrant County, Texas, USA. The dam was built in early 1930's, using the hydraulic-fill construction procedure. Eagle Mountain Lake and its facilities serve as a water supply resource for Fort Worth, Texas, for municipal, industrial, and irrigation purposes, and also act as a resource for public transportation and recreational facilities, such as fishing and boating. The natural geological profile of this site consists of Paluxy sandstone and shale.

Two sets of SASW tests were conducted on the crest of the dam, similar to those conducted in the laboratory test setup. The first set was performed with a random height of fall of a hammer in the test (referred to as the V-F test and

implying variable impact energy for four repetitions in a field test). A constant drop height of drop hammer was used for the second set of tests (referred to as the C-F test and implying constant impact energy for four repetitions in a field test). The tests were conducted with three different spacing between the two geophones, 0.6 m, 1.2 m, and 2.4 m, following common receiver midpoint geometry, as shown in Figure 4-3 (Mancuso and Vinale 1993; Nazarian and Stokoe 1985; Stokoe et al. 1991). A 2.2 kg hammer, with a drop height of 0.3 m, was used for conducting tests with a geophone spacing of 0.6 m and 1.2 m. Whereas, for conducting tests with a geophone spacing of 2.4 m, a 4.5 kg hammer and a drop height of 0.45 m, was used to impart a higher energy required to obtain information of deeper layers. The signal sensitivity of the geophones was modified based on geophone spacing, weight of the hammer used and site conditions. Figure 4-4 presents the test setup in the field, with a spacing of 2.4 m between the geophones. G1 and G2 shown in Figure 4-3 and Figure 4-4, denotes the near and far geophones (from impact source), respectively. It should be noted that the spacing selected in this study is considered adequate to demonstrate the effectiveness of using constant impact energy in SASW field tests. Additional tests were conducted with the aid of a sledgehammer for greater spacing between geophones to get information of deeper layers. The effectiveness of a constant impact energy was however studied based on the test conducted with the drop hammer, for receiver spacing of 0.6m, 1.2m and 2.4m.

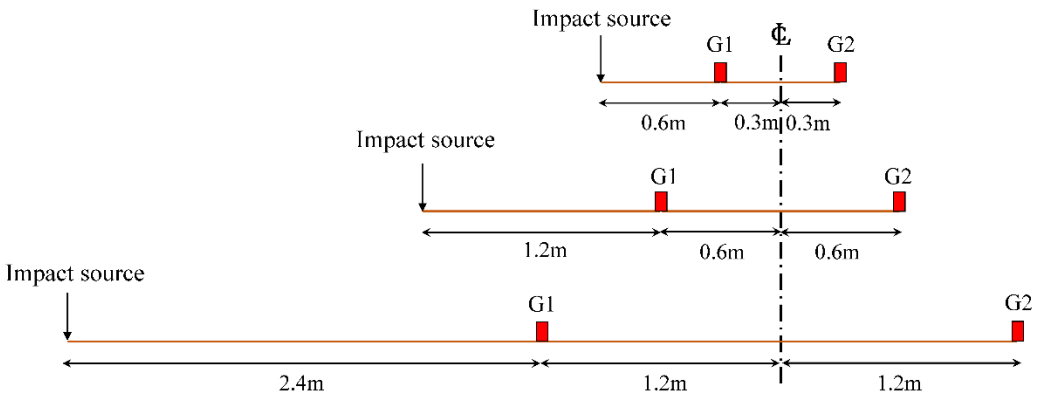

Figure 4-3: Layout of common receiver midpoint geometry

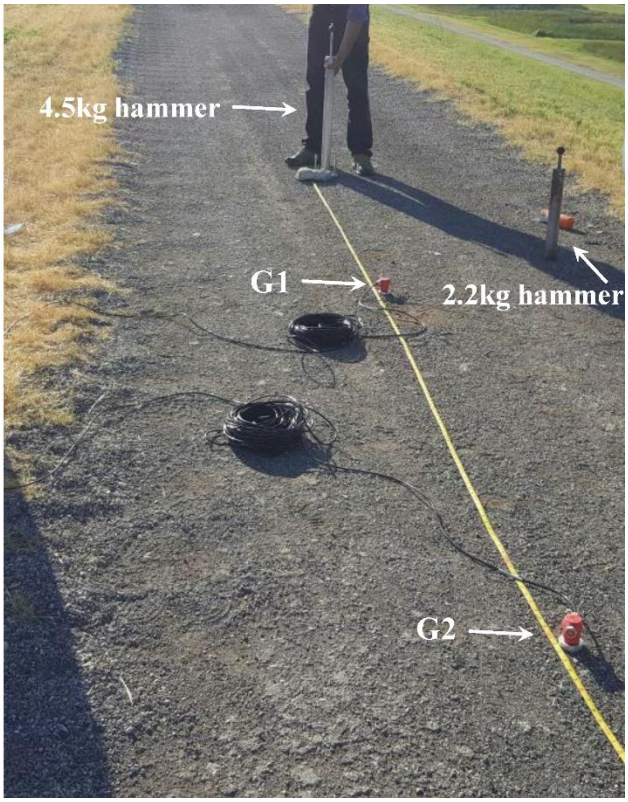

Figure 4-4: Field SASW test setup

The distance from the impact source to the nearest geophone (G1) was equal to the distance between geophones for each of the tests (Figure 4-3). Similar to the laboratory box testing, the hammer was dropped onto a steel plate, rather than onto the ground surface. In addition to comparing the coherence function for the two sets of tests, the dispersion curve and the V_s profile were also determined. For each geophone spacing, the ground surface was struck four times (i.e. four repetitions) and the test was accepted or rejected solely based on the coherence displayed on the data logger.

4.4 Analysis and discussion of results

4.4.1 Laboratory tests

This section presents the laboratory test results and analyses performed to investigate the effect of impact energy on the coherence function. The preliminary judgment of accepting or rejecting the test was made from the plot of coherence values versus frequency (generated after accepting four repetitions for each test). Figure 4-5 depicts the two representative SASW test results obtained for the V-L tests.

In each set of test results, two plots are shown: one presenting the coherence data plot (Figure 4-5a and Figure 4-5c) and the other showing the wrapped phase plot (Figure 4-5b and Figure 4-5d). The phase data and the corresponding coherence plot, which are shown in the following sections are obtained after accepting each

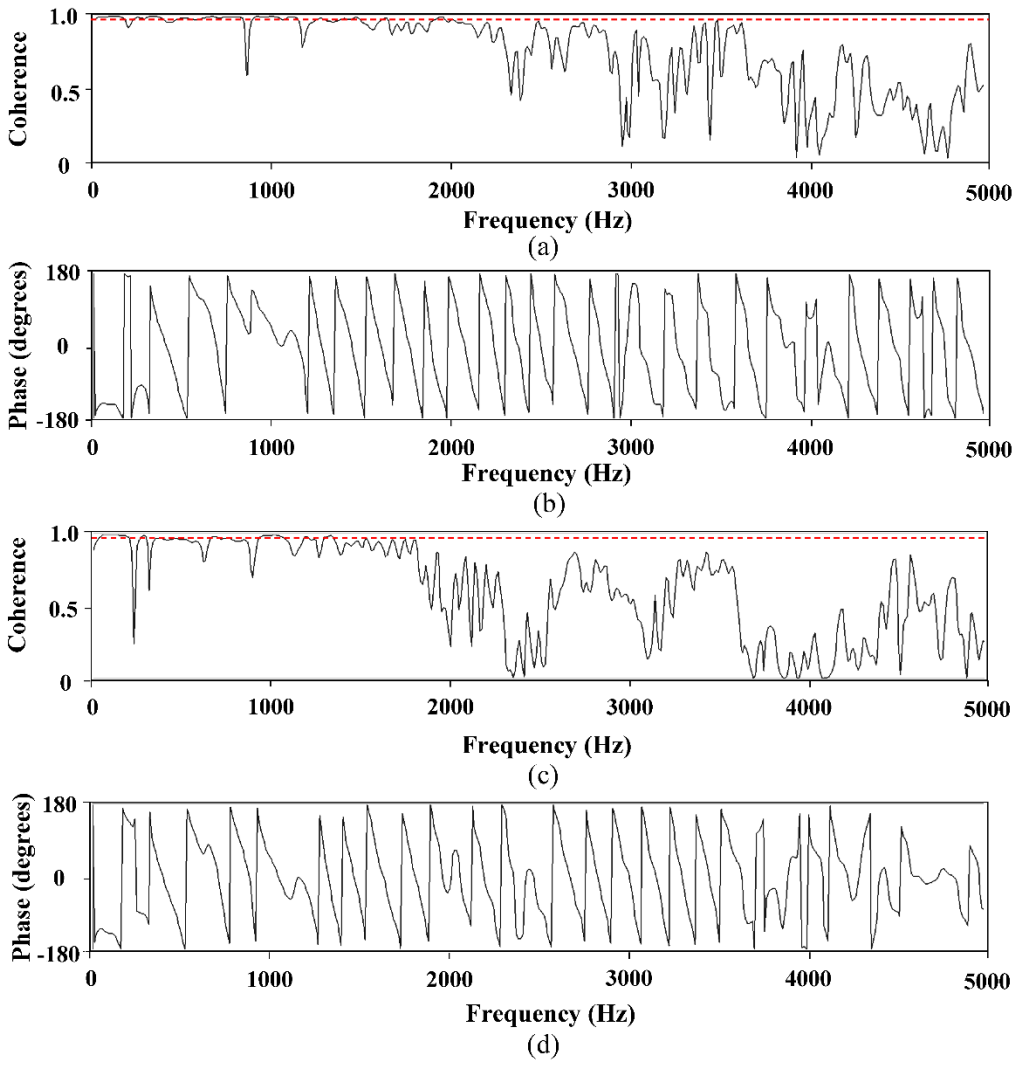

Figure 4-5: Results from two V-L Tests: (a) and (c) Coherence function; (b) and (d) Wrapped phase (0.6m geophone spacing)

of the four repetitions and is based on the result obtained after averaging the data in the frequency domain. The coherence plot represents the quality of the test data, and the wrapped phase plot represents the phase lag of a Rayleigh wave of a given frequency between the two geophones. The acceptable threshold value of coherence

(0.95) has been marked by a red dashed line in all the following plots of coherence function. The phase lag was determined by unwrapping the phase data and identifying the number of 360˚ jumps.

The mathematical equations used to calculate the coherence and wrapped phase are provided in Equations 4.1 to 4.5. The detailed explanation of coherence and unwrapping of phase data can be found elsewhere (Heisey et al. 1982; Joh 1996; Kumar and Hazra 2014; Kumar and Rakaraddi 2013; Nazarian and Stokoe II 1983; Nazarian and Stokoe 1985; Stokoe et al. 1991; Suits et al. 2008).

$$G_{Y_1Y_1}(f) = Y_1^*(f) \,.\, Y_1(f) \tag{4.1}$$

$$G_{Y_2Y_2}(f) = Y_2^*(f) \,.\, Y_2(f) \tag{4.2}$$

$$G_{Y_1Y_2}(f) = Y_1^*(f) \,.\, Y_2(f) \tag{4.3}$$

$$Coherence = \frac{|G_{Y_1Y_2}(f)|^2}{G_{Y_1Y_1}(f).G_{Y_2Y_2}(f)} \tag{4.4}$$

$$\Phi_{\text{wrapped}}(f) = \tan^{-1} \frac{\text{Imaginary}(G_{Y_1Y_2})}{\text{Real}(G_{Y_1Y_2})}, \text{ in degrees} \tag{4.5}$$

Where:

$Y_1(f)$ and $Y_2(f)$ are the FFT of the signals received by the pair of geophones,

$Y_1^*(f)$ and $Y_2^*(f)$ are the complex conjugates of $Y_1(f)$ and $Y_2(f)$, respectively,

$G_{Y_1Y_1}(f)$ and $G_{Y_2Y_2}(f)$ are the auto spectrum (power at each frequency *f*) of the signals Y_1 and Y_2, respectively,

$G_{Y_1Y_2}(f)$ is the cross power spectrum, a measure of mutual power between two signals.

Figure 4-5 presents the coherence and phase data of two V-L tests and illustrates that there is a significant variation in coherence function and wrapped phase plots that were generated. As stated earlier, only data for the frequency range having a coherence value greater than 0.95 can be used for generating the dispersion curves. The phase data having an unacceptable coherence or having broken discontinuous phase should be masked and not used for further analysis (Figure 4-1c). Hence, only two cycles of the wrapped phase, as shown in Figure 4-5a, can be used to generate the dispersion curve.

Figure 4-5c depicts the data that was of such poor quality that it could not be further processed and used for analysis. It can be observed from Figure 4-5 that the coherence plots for the two tests are different, even though both the tests were conducted on the same test setup, using the same impact source. Hence, it can be concluded that the repeatability of the test is affected in case of V-L tests, and a greater number of tests is thus required to obtain an acceptable test with reliable SASW data.

Figure 4-6 represents a typical set of data obtained from C-L tests. Unlike the tests performed with varying height of fall of hammer (V-L tests), the tests conducted with constant height of fall (C-L tests) showed a coherence very close to

one (1) for a wide range of frequency. It can be observed in Figure 4-6 that the coherence was almost equal to one (1) over a wide frequency bandwidth for C-L tests. Thus, a greater number of cycles of the wrapped phase can be effectively used for generating the dispersion curve. This would facilitate generating the dispersion curve over a wider range of wavelengths, subsequently providing better overlap in dispersion curves generated for varying distances between geophones.

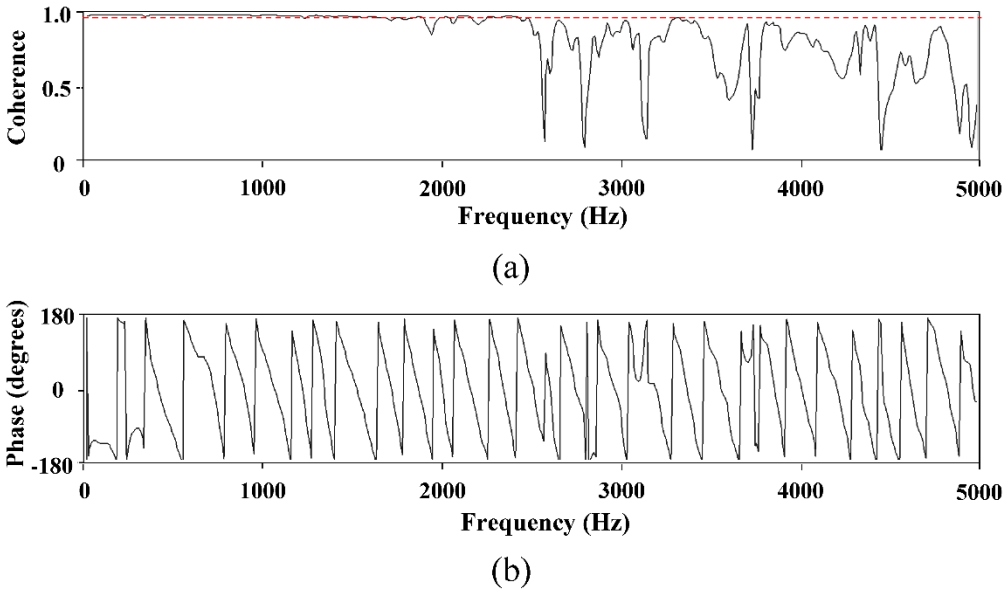

Figure 4-6: Results from C-L tests: (a) Coherence function and (b) Wrapped phase

Figure 4-7 shows the dispersion curves for three tests determined from the V-L and C-L tests. Figure 4-7a shows a significant deviation in the dispersion curve, using test results with low coherence. Conversely, Figure 4-7b shows identical dispersion curves generated for three C-L tests. The repeatability of the

SASW testing is hence significantly improved when an impact source of constant energy is used for all of the repetitions. The dispersion curve obtained for Test 1 of the V-L test (Figure 4-7a) is similar to those obtained for C-L tests (Figure 4-7b). Hence, multiple tests must be conducted with hand-held hammers at a given location to produce reliable test results. Conversely, using an impact source, which can impart constant energy for all of the repetitions in a SASW test, can render the test efficient, reliable, and repeatable.

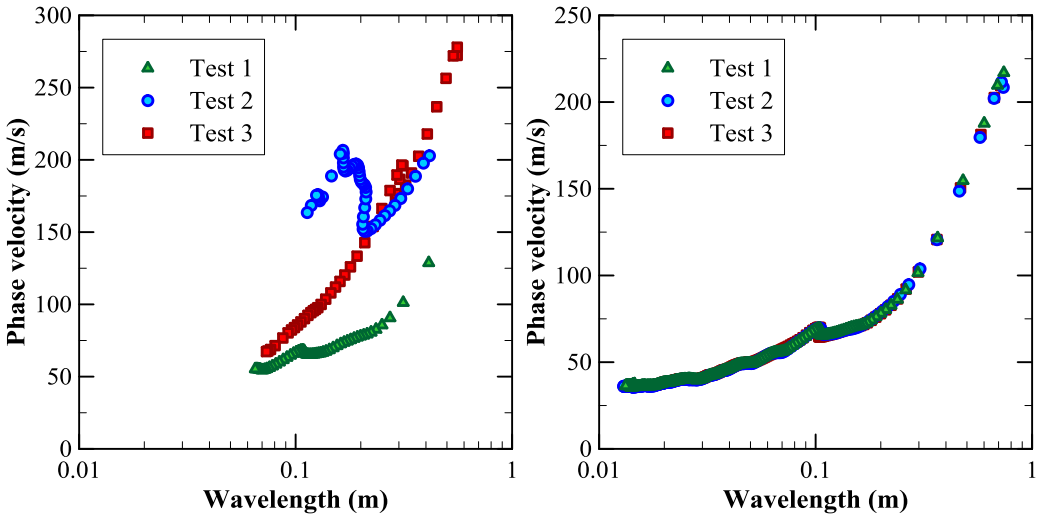

(a) (b)

Figure 4-7: Dispersion curves: (a) V-L tests (b) C-L tests

Figure 4-7 shows the significant improvement in the C-L test results when compared with V-L test results. In order to further investigate the reasons for this, a Fourier analysis was performed on the waveforms received by the geophones for each of the four repetitions of the V-L and C-L tests (Figure 4-8). It was observed that waves of different sets of frequencies were excited for each of the four

repetitions of the V-L test, due to the different levels of energy of impact (Figure 4-8a). Whereas, Figure 4-8b shows that waves of very similar sets of frequencies were excited during the C-L tests. Hence, the Fourier analysis plot of the average of the four repetitions (in frequency domain) was almost identical to that obtained for each repetition of the C-L test.

Since the same set of frequencies was excited by using constant impact energy, averaging the signal in the frequency domain reinforced the signal and reduced the noise in the signal. This led to an improvement in the coherence and quality of data, as shown in Figure 4-5 and Figure 4-6. However, the reduction in coherence (Figure 4-6) and deviation in FFT plots (Figure 4-8b) beyond 2500 Hz can probably be attributed to the attenuation of low wavelength (high frequency) surface waves (Heisey et al. 1982).

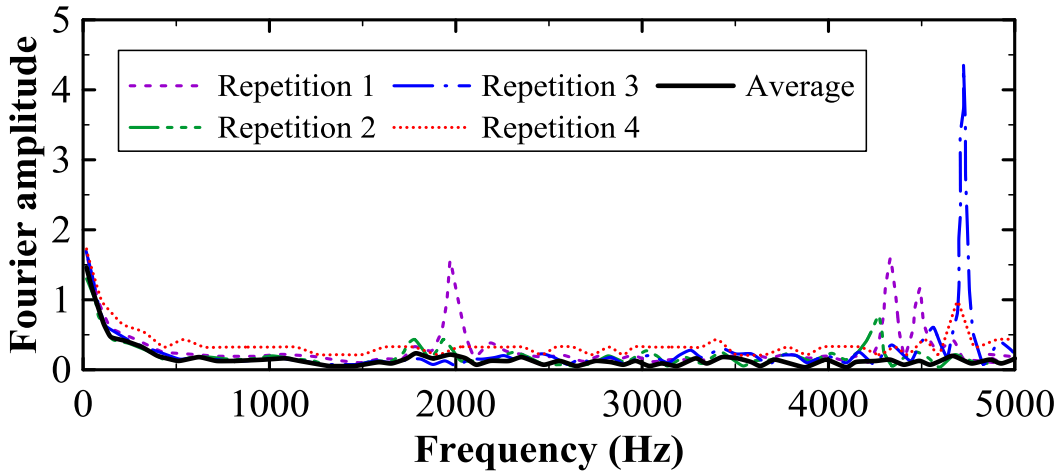

(a)

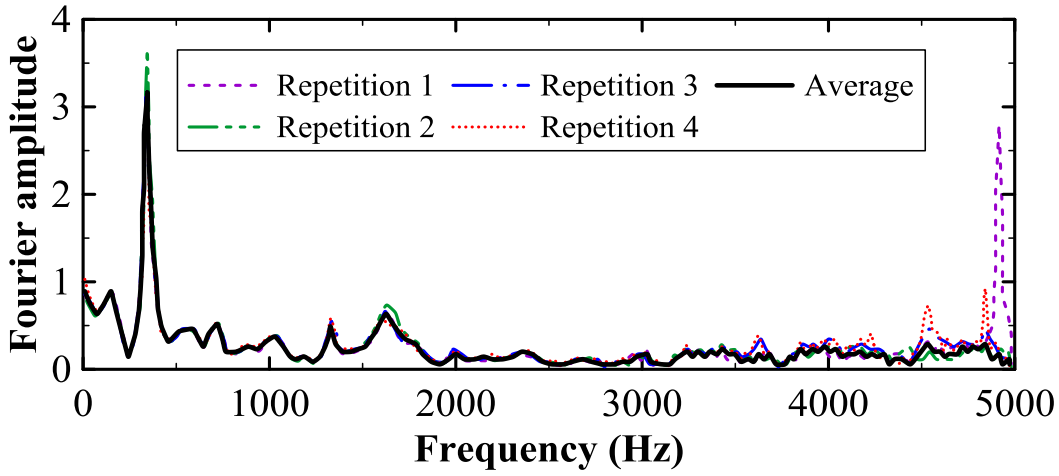

(b)

Figure 4-8: Fast Fourier Transform (FFT) of signal received by geophone (a) V-L test; (b) C-L test

4.4.2 Field tests

SASW tests were conducted at different sections along the crest of the dam. The improvement in the quality of the tests was similar to those of the laboratory tests. The SASW tests conducted in the field with constant impact energy (C-F) resulted in greater improved coherence than those conducted using variable impact energy (V-F). Figure 4-9 represents a typical set of results obtained, using the V-F method for 0.6 m geophone spacing. Several trials were required to obtain an acceptable test using variable impact energy, with the best test result having an acceptable coherence only for the initial cycles (Figure 4-9). It can be observed from Figure 4-10 that coherence of one (1) was achieved for most of the frequencies for geophone spacing of 0.6 m for the C-F tests.

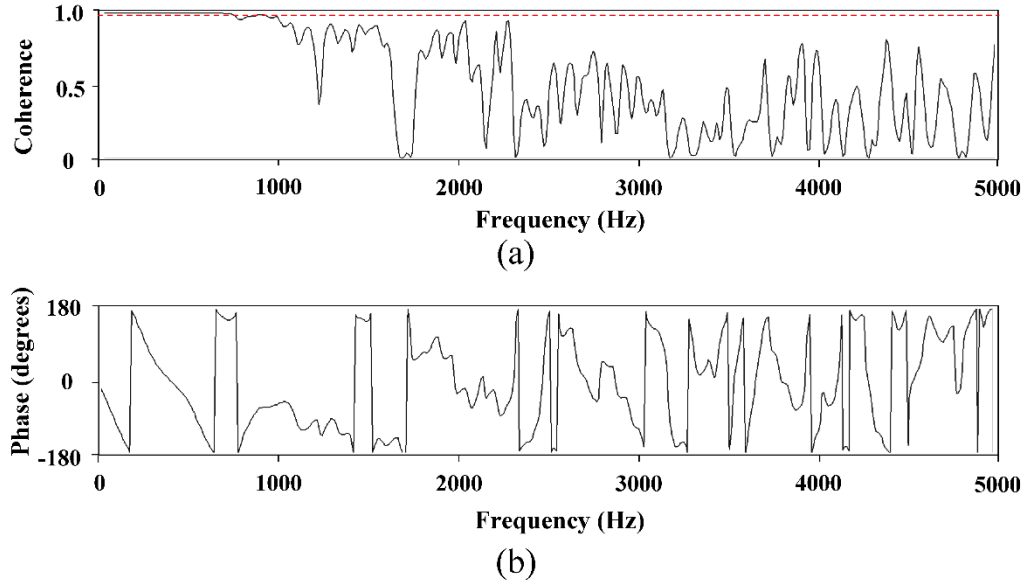

Figure 4-9: Test results from V-F tests: (a) Coherence function and (b) Wrapped phase (0.6m spacing)

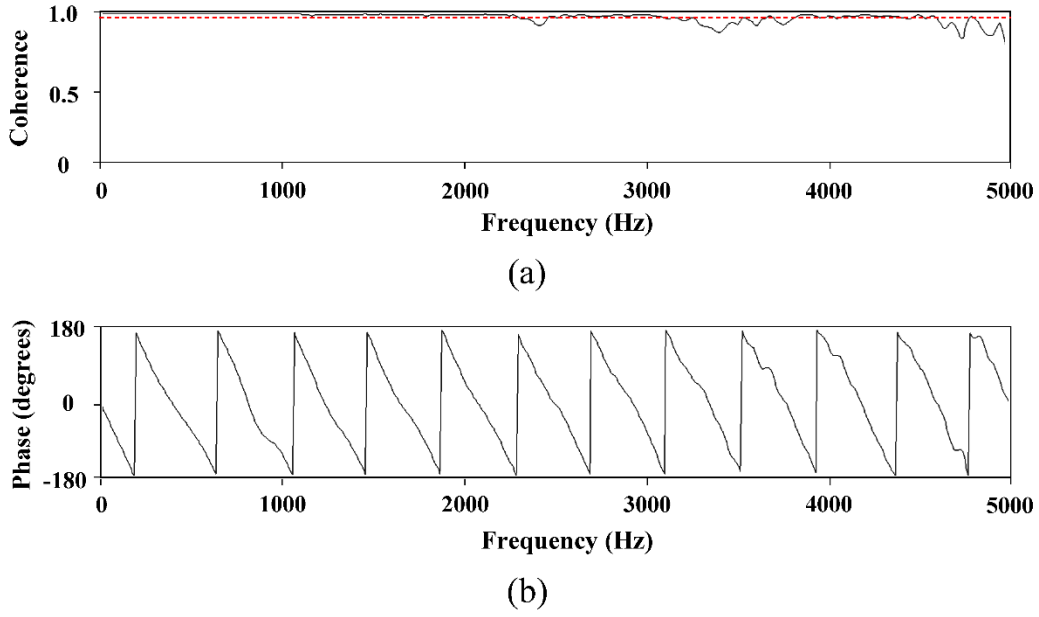

Figure 4-10: Test results from C-F tests: (a) Coherence function and (b) Wrapped phase (0.6m spacing)

Figure 4-11 and Figure 4-12 represent the typical V-F and C-F test results performed with geophone spacing of 2.4 m. When the geophone spacing was increased to 1.2 m or greater, the coherence was found to decrease after a few initial cycles (Figure 4-12), even upon using a constant energy source. This can be mainly attributed to the attenuation of high frequency (low wavelength) waves, which becomes significant when the geophone spacing is increased (Heisey et al. 1982). Such attenuation of high-frequency waves would result in low power in the signal received by the farthest geophone (G2), even though, the signal was received by the geophone close to the impact source (G1).

Although a coherence of one (1) was not obtained for the entire frequency range, an improvement in the quality of data can be observed by comparing Figure 4-11 (V-F) and Figure 4-12 (C-F), especially for a frequency less than 700 Hz. The results depicted in Figure 4-11a and Figure 4-11b were used for generating the dispersion curves and performing inversion analyses. The test results shown in Figure 4-11c and Figure 4-11d were rejected and could not be used for further analysis due to poor coherence. There was no significant impact of neglecting the low coherence data (at high-frequency range) for higher geophone spacing (e.g., 2.4 m), since information about shallow layers was obtained from the data pertaining to lower geophone spacing (e.g., 0.6 m or 1.2 m).

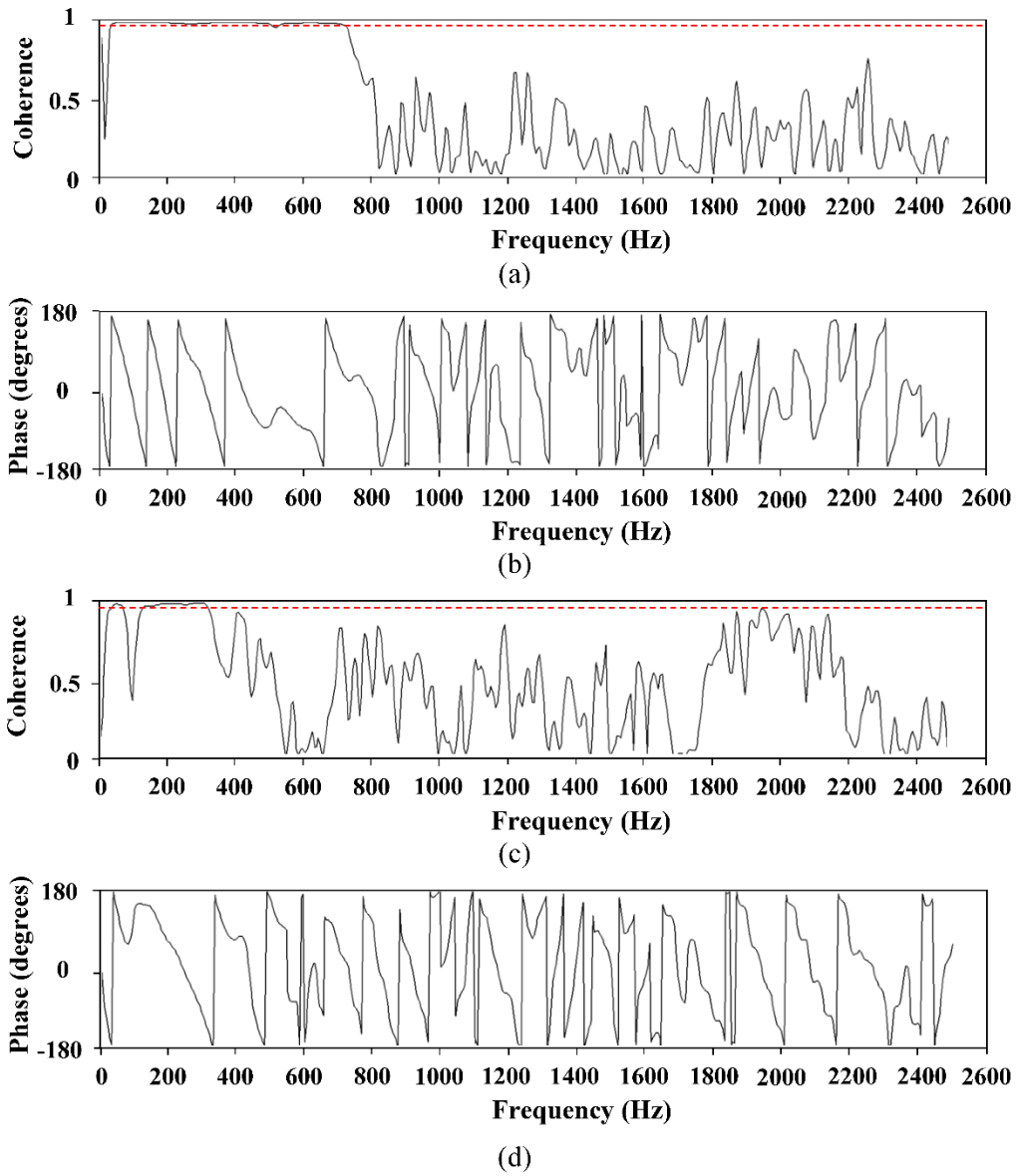

Figure 4-11: Test results from two V-F tests: (a) and (c) Coherence function; (b) and (d) Wrapped phase (2.4m geophone spacing)

Figure 4-13 shows the dispersion curves obtained by using the transfer function from the C-F and V-F tests for tests conducted at a particular section of the dam. The tests conducted with constant impact energy offered a good coherence

over a wide range of frequencies; hence, the dispersion curve was spread over a wide range of the wavelengths (Figure 4-13). A 0.6 m spacing between the geophones provided a dispersion curve of a minimum wavelength of 0.07 m for the C-F test, as compared to the minimum wavelength of 0.4 m for the V-F test. Some of the data pertaining to subsurface layers are hence lost, due to unacceptable coherence, when performing tests with hand-held hammers. A greater number of V-F tests with shorter geophone spacing may be required under such circumstances.

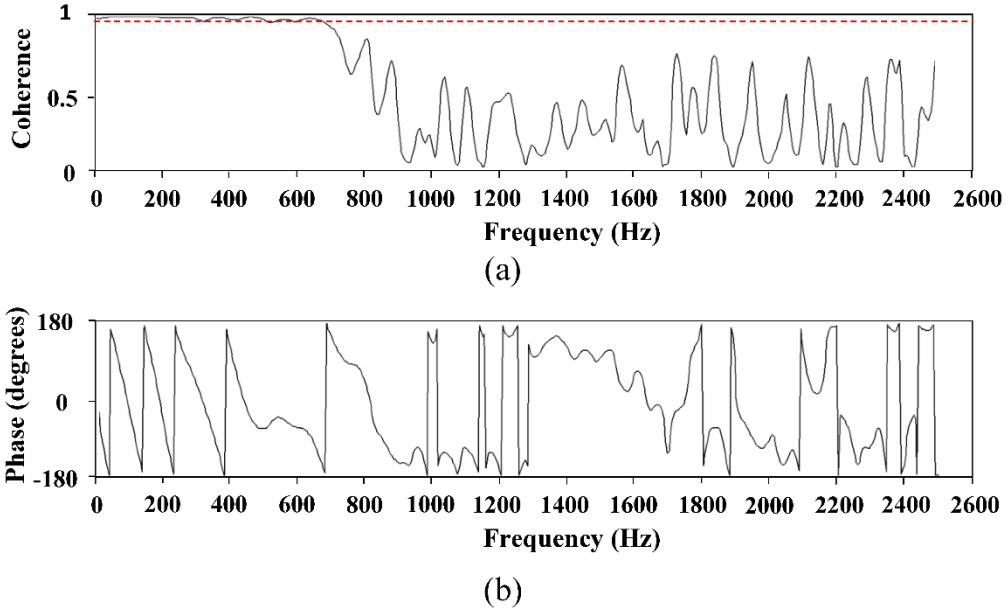

Figure 4-12: Test results from C-F tests: (a) Coherence function and (b) Wrapped phase (2.4m geophone spacing)

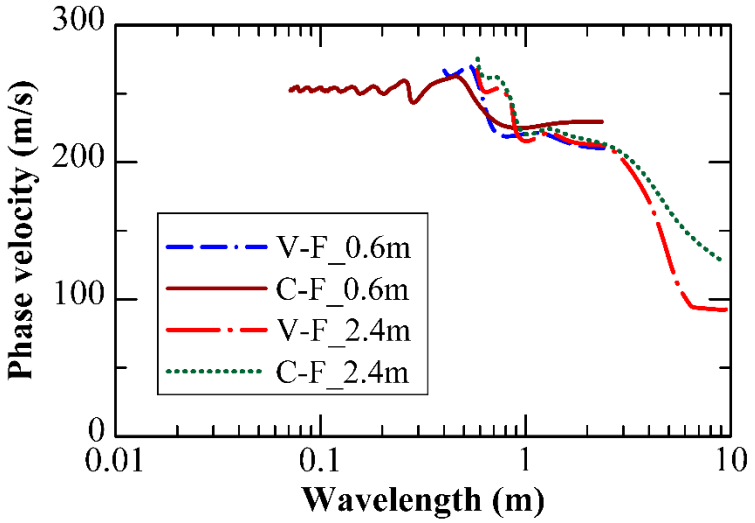

Figure 4-13: Dispersion curves used for inversion analysis

A deviation in the dispersion curves can be observed between the C-F and V-F tests for 0.6 m geophone spacing (C-F_0.6m and V-F_0.6m, Figure 4-13). The dispersion curve for the two sets of tests for 2.4 m geophone spacing (C-F_2.4m and V-F_2.4m) were found to be similar up to a wavelength of 3 m. A prominent difference in the dispersion curves can be observed beyond wavelengths of 3 m, due to poor coherence in the low frequency zone (Figure 4-11a and Figure 4-11b). Inversion analysis was performed for tests conducted with constant and variable impact energy conditions.

The inversion analysis of the respective entire global dispersion curves provided significantly different V_s profiles (Figure 4-14) due to the aforementioned reasons. The variation in V_s (and hence G_{max}) fluctuated significantly and

underestimated or overestimated the V_s of subsurface layers at various depths. A similar difference in the V_s profile was also observed for tests conducted at other sections of the dam. The V_s profiles obtained by C-F and V-F tests are estimated values of the actual V_s existing in the field; it was not possible to determine the actual in-situ V_s profile. Although the V_s profile obtained by the C-F tests may not be absolute, it is expected that the test results accurately portray the subsurface V_s profile because of the improvement in coherence (close to one (1) for C-F tests).

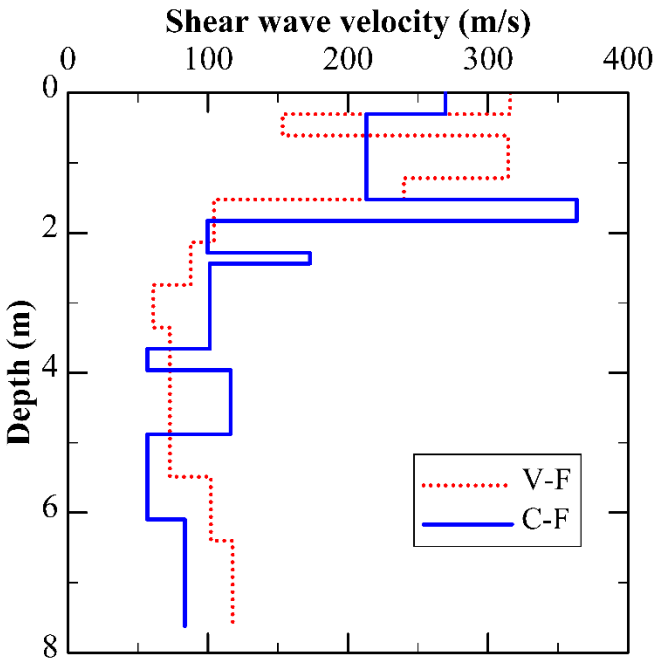

Figure 4-14: Shear wave velocity profile obtained for C-F and V-F tests

4.4.3 Shear wave velocity profile

The modified SASW testing technique was used to determine the subsurface shear wave velocity profile at eight different sections of the dam. The sections are designated by the station numbers, namely Stn. 5, Stn. 9, Stn. 14.5, Stn. 18, Stn. 22, Stn. 27, Stn. 33 and Stn. 39. The location of the station can be determined by multiplying the station number by 100 ft. (30.48 m) from the west end of the dam. The shear wave velocity profile at each of the stations is provided in Figure 4-15. These shear wave velocity profiles will be used in the subsequent analyses to obtain the small strain shear modulus of the dam embankment layers.

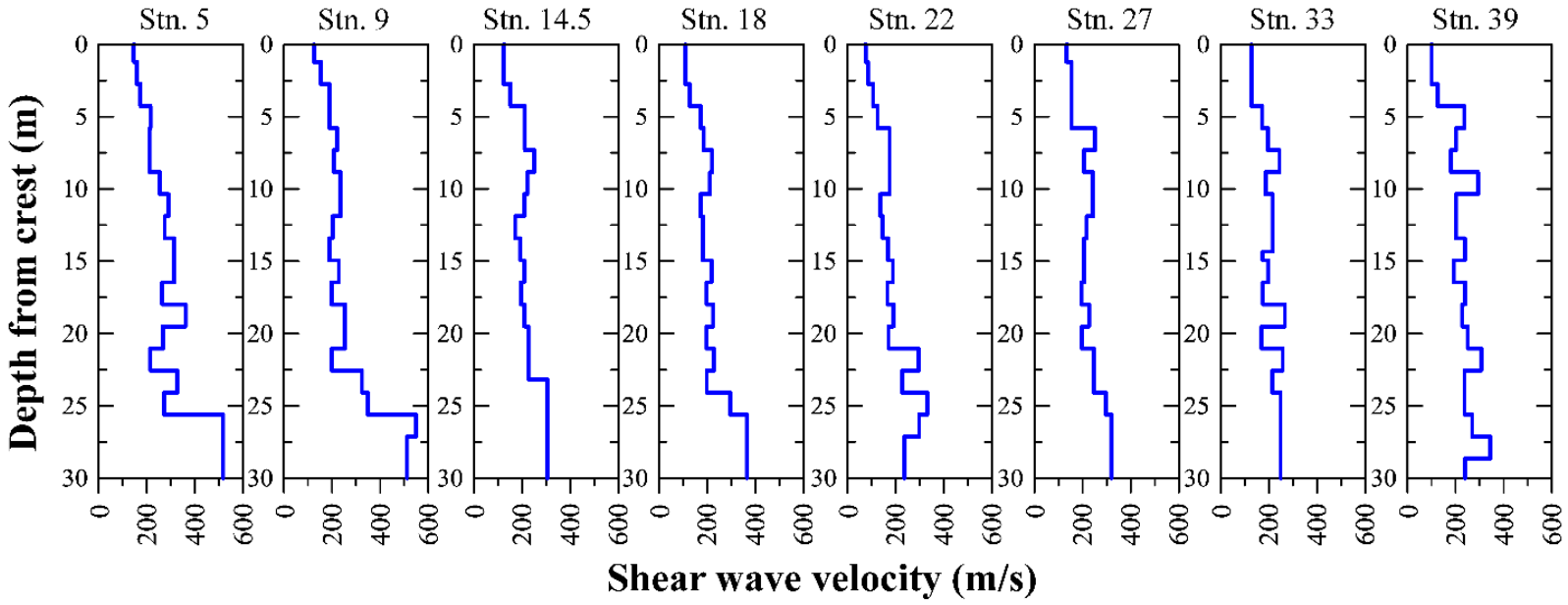

Figure 4-15: Shear wave velocity profile at different sections of the dam

4.5 Summary

The quality and acceptability of a SASW test result are preliminarily judged based on the coherence and wrapped-phase data plots displayed on the data logger at the time of testing. Very often, test data needs to be rejected, due to unacceptable coherence displayed at the end of the test, and repeated until acceptable data with coherence > 0.95 (for the frequency range of interest) is obtained. The purpose of this research work was to study the improvement in coherence values when striking the ground surface with the same impact energy for four repetitions of a SASW test. Unlike the current SASW testing procedure, which uses impact sources like hand-held hammers or sledge hammers, a drop hammer with a constant height of fall was used to maintain constant impact energy to generate Rayleigh waves.

- The variability in the coherence data was significant for tests conducted with variable impact energy. Conversely, a significant improvement in coherence was observed upon using an impact source capable of maintaining constant impact energy for multiple repetitions in a SASW test. The repeatability of the test at a given site was also found to improve by maintaining the impact energy used to strike the ground to generate Rayleigh waves. Consequently, this modified testing technique was found to be efficient and reliable.
- Unlike the tests conducted with hand-held hammers, four strikes with identical impact energy generated waves with the same set of frequencies. This

strengthened the signal, while reducing the signal noise, resulting in a more accurate test with a high coherence value. This ensured the accurate determination of shear wave velocity profiles of subsurface layers.

- Employing a source of constant impact energy facilitates a greater number of wrapped-phase cycles, with a wider frequency range, to generate dispersion curves. The loss of data pertaining to subsurface layers which could have occurred without the use of an impact source of constant energy can hence be minimized. A better overlap in the dispersion curves, generated for various geophone spacing, facilitates the formation of a continuous global dispersion curve, thereby rendering the test results more reliable.
- The shear wave velocity profiles obtained at eight different sections of the dam will be used in chapters 5 and 6 to obtain the small strain shear modulus of the dam embankment layers. These values will be used as input parameters for determination of the natural frequency of the two-dimensional plane strain models of the dam and for performing time-history based dynamic stability analyses.

Chapter 5: Estimation of Natural Frequency of the Dam

5.1 Introduction

Any time-history based dynamic analysis requires the acceleration time-history data of real earthquakes. These data are readily available for earthquake-prone regions, which has a history of past earthquakes. However, no such recorded data were available at the EM dam site. This necessitated developing a natural frequency based approach to select the time-history data for dynamic analysis. The natural frequency of the different sections of the dam had to be determined based on the shear wave velocity profile estimated in chapter 4. Earthquake data recorded at different stations in Oklahoma, Arkansas, and surrounding states were selected to encompass a broad spectrum of predominant frequency contents, which would enable the study of the response of the EM dam under resonance and non-resonance conditions.

It is a well-established fact that the natural frequency of a structure decreases with an increase in strain levels, induced during seismic loading conditions. However, the current methods cannot predict the strain-dependent natural frequency of an earthen structure. This chapter presents a novel method which can predict the degradation of the natural frequency with an increase in strain levels. The variation of strain-dependent natural frequency along the length of the EM dam is also presented at the end of this chapter.

5.2 Background

Dams and levees are among the most crucially important engineered structures that serve the society by primarily providing flood protection, hydroelectric power, water for irrigation purposes and as recreation sites (FEMA 2017). They are stable under normal operating conditions, but are susceptible to failure when subjected to seismic excitations. Not all earthquake events cause significant damage to existing structures; however, the occurrence of near resonance condition, where the predominant frequency of an earthquake excitation is close to the natural frequency of the structure, may result in amplified vibrations that may cause extensive structural damage (Banerjee 2017; Banerjee et al. 2018a; Chakraborty et al. 2018, 2019b; Dakoulas and Gazetas 1985; Gazetas 1987; Parish et al. 2009; Wood 1973). Hence, it is essential to study the seismic response of earthen dams and estimate their natural frequencies and mode shapes of vibration.

Seismic response of dams has been studied by: (a) simple analytical methods, such as the shear beam method; (b) numerical approaches, such as the finite element and finite difference methods; (c) field studies, using the ambient vibration or forced vibration method; and (d) analysis of seismograms/accelerograms recorded at different segments of the dam during earthquake events (Abdel-Ghaffar and Scott 1981; Abdel-Ghaffar et al. 1980; Cetin et al. 2005; Chopra 1967; Clough and Chopra 1966; Gazetas 1987; Ishizaki and

Hatakeyama 1962; Keightley 1966; Mononobe et al. 1936; Okamoto et al. 1969; Okamoto 1984).

With the shear beam method, the dam is considered as a beam that has a variable wedge-shaped cross section (Ambraseys 1960b; Ike 2008; Okamoto 1984). Closed-form solutions of the natural frequencies and mode shapes of the structure are obtained, and the effect of heterogeneity is incorporated in terms of variation in shear modulus as a pre-defined function of depth. Hence, variations in the shear wave velocity profiles obtained from in-situ tests, such as the seismic cone penetration test (SCPT) and spectral analysis of surface waves (SASW) test, which may not necessarily follow a definite trend, cannot be incorporated into the shear beam method. This limitation can be addressed by using numerical approaches, such as finite element/finite difference methods (FEM/FDM), which are capable of incorporating the effects of variations in shear modulus, zones with different material properties, unequal side slopes, and arbitrary geometric configurations (Chopra 1967; Clough and Chopra 1966). Seismic excitation, with both horizontal and vertical components of earthquake motion, can also be dealt with by using numerical methods (Chopra 1967; Gazetas 1987; Yiagos and Prevost 1991). Seismic response analyses with FEM/FDM are considered more accurate and to more effectively portray the realistic behaviour of the structure than the shear beam method (Ishizaki and Hatakeyama 1962). In the numerical methods, the natural frequencies are obtained by Eigen value analysis, modal analysis, or free-vibration

analysis (Bybordiani and Arıcı 2017; Charatpangoon et al. 2014; Chopra 1967; Prevost et al. 1985; Vijayasri et al. 2017; Woodward and Griffiths 1993; Xiao et al. 2008).

The seismic response of an earthen dam can also be studied, based on the data recorded during earthquake events by accelerographs/seismographs that are placed in different locations of the dam (Okamoto et al. 1969; Abdel-Ghaffar & Scott 1979a; Abdel-Ghaffar & Scott 1979b; Cetin et al. 2005; Pelecanos et al. 2015; Yang et al. 2017), or by conducting ambient vibration or forced vibration tests (Abdel-Ghaffar and Koh 1981; Abdel-Ghaffar and Scott 1981; Castro et al. 1998; Jafari and Davoodi 2006). Accelerograph data is not usually available for dams that are located in newly identified regions of induced seismicity, and in such cases, ambient vibration or forced vibration tests may be utilised as an alternative approach. Ambient vibration test uses natural sources of excitation such as wind, low intensity tectonic movements, microtremors, water release from reservoirs, and other sources of vibration (Abdel-Ghaffar and Koh 1981; Jafari and Davoodi 2006; Trifunac 1972).

In the forced vibration test, excitations are induced along the upstream-downstream directions, by rotating eccentric-mass vibration generators that are attached to the crest of the dam (Abdel-Ghaffar and Scott 1981; Abdel-Ghaffar et al. 1980; Gauron et al. 2018; Gazetas 1987; Jafari and Davoodi 2006; Keightley 1966). The acceleration induced at the crest and at different locations of the side

slopes are recorded, and the data is analysed to determine the natural frequency and mode shapes of the structure (Abdel-Ghaffar and Scott 1981; Petrovski et al. 1974). The forced vibration tests require sophisticated instruments for performing the tests and collecting the data, which might not be feasible for all projects. A brief overview of the evolution of the techniques employed to determine natural frequency is presented in Table 5-1; however, readers may also refer to other pertinent literature (Gazetas 1987; Okamoto 1984; Pelecanos 2013) for detailed information.

Most of the existing methods can estimate the natural frequency of a structure at low strain levels, where the shear modulus of the materials can be represented by the small strain shear modulus (G_{max}) (Ishibashi and Zhang 1993; Jafari and Davoodi 2006; Kramer 1996; Puppala et al. 2006). The linear elastic seismic response analysis does not account for the strain-dependent reduction in the shear modulus or an increase in the damping ratio of the dam materials during earthquakes. These effects can be incorporated into the analysis by using the iterative equivalent linear method and the coupled or decoupled non-linear method (Gazetas 1987; Idriss 1973; Jibson 2011; Prevost et al. 1985). The fully coupled non-linear method of dynamic analysis can capture the actual behaviour of soil in a more realistic manner, but it requires high quality test data and 'sophisticated soil-constitutive models' to predict the behaviour of the structure (Elia et al. 2011; Jibson 2011), neither of which are commonly available in real projects. Many

studies have found that the simple equivalent linear method converges well and predicts real problems satisfactorily (Abdel-Ghaffar and Scott 1979b; Mejia and Seed 1983; Prevost et al. 1985; Rathje and Bray 2000) and hence this method is widely used in practice, and is also adopted in this study.

Due to non-linear behaviour of the soil, the response of an earthen dam subjected to an excitation depends on the strain level experienced by different regions of the dam. Hence, the natural frequency corresponding to the low strain linear elastic range may not accurately exhibit the response of the dam during real earthquake conditions (Abdel-Ghaffar and Scott 1979b; Jafari and Davoodi 2006). The purpose of this study is to develop a procedure to determine the natural frequency of an earthen embankment structure by taking into account the influence of material non-linearity and estimating the strain-dependent natural frequency of the earthen structure.

The proposed method is based on the theory that earthen dams have filtering effects for seismic waves of certain frequencies that are not close to the natural frequency of the structure (Zhu and Zhou 2010). In other words, only those waves (excitations) having frequencies close to the natural frequencies of the structure are amplified because of resonance. Accordingly, a synthesised wave, henceforth referred to as the ‘sum of sines’ wave, obtained by superimposing sinusoidal waves of varying frequencies, is used to simulate horizontal seismic excitation at the base of the dam.

Table 5-1: Natural frequency determination methods reported in literature

Authors	Topic of study	Natural frequency determination method
Ambraseys 1960	Theoretical study on 2D wedge with different truncation ratios subjected to arbitrary disturbance	Shear beam method
Ishizaki and Hatakeyama 1962	Comparative study on vibration of dam using finite difference method and shear beam approach	Finite difference method
Clough and Chopra 1966	Response of a triangular dam under free vibration when subjected to El Centro Earthquake, using finite element method	Finite element method
Keightely 1966	Forced vibration tests on Bouquet Canyon Dam	Forced vibration test
Chopra 1967	Comparative study on vibration of dam, using 2D finite element method and shear beam approach	Finite element method
Okamoto et al. 1969	Seismic response analysis of Sannokai Dam, using data collected from seismometer placed at crest, mid-slope, and on banks.	Shear beam method and Fourier analysis data recorded by seismometer
Abdel-Ghaffar and Scott 1979	Seismic response analysis of Santa Felicia Dam, using accelerometer reading recorded during two earthquakes	Fourier analysis of data recorded by accelerometer
Gazetas 1981	Modification of classical, homogeneous shear beam model to incorporate heterogeneity; shear modulus increased as 2/3rd power of distance from crest	Shear beam method
Abdel-Ghaffar and Scott 1981	Forced vibration tests on Santa Felicia Dam	Forced vibration test
Tsiatas and Gazetas 1982	Dynamic response of 5 different earth dams of 90m height and avg. V_s = 324 m/s, compared using plane strain and shear beam method	Shear beam method and finite element method
Makdisi et al. 1982	Dynamic response of embankment dams in narrow triangular canyon, studied using 3D finite element analysis	Finite element method
Mejia and Seed 1983	2D and 3D dynamic analysis of earthen dams compared for two different earthquake motions	Finite element method
Dakoulas and Gazetas 1985	Inhomogeneous shear beam model and plane-strain FEM analysis results compared	Shear beam method and Finite element method
Prevost et al. 1985	2D and 3D dynamic analysis of Santa Felicia Dam subjected to two earthquakes, based on non-linear hysteretic analysis and using multi-surface plasticity theory	Finite element method
Gazetas 1987	An overview of different methods for estimating seismic response of earthen dams to seismic excitations	Shear beam method, finite element method and forced vibration tests
Woodward and Griffith 1993	Comparison between 2D and 3D FEM analysis of non-homogeneous earth dams with values measured at site	Finite element method
Castro et al. 1998	Natural frequency determination from spectral amplitudes of 13 earthquakes	Spectral amplitude of data recorded for 13 earthquakes and finite element method
Cetin et al. 2005	Seismic response of Kiralkizi Dam studied from available crest acceleration data, 2D finite difference analysis, and shear-beam method	Fourier analysis of acceleration data, finite difference method and shear beam method
Xiao et al. 2008	1D shear-wedge theory and FEM results compared for hardfill dam, incorporating effect of water on upstream face of dam	Shear beam method and finite element method
Parish et al. 2009	Seismic response of earth dam studied using finite difference model; behaviour of shell and dam studied when subjected to real earthquake data; effect of plasticity considered	Finite difference method
Charatpangoon et al. 2014	Dynamic analysis of Fujinama Dam, using field data and FEM analysis	Finite element method

The acceleration-time plots, obtained from the crest of the dam after performing a time-history analysis, are analysed on the frequency domain, using Fast Fourier Transform (FFT) to obtain the set of frequencies that are most excited for a given structure (i.e. natural frequencies). The validity of the 'sum of sines' method was first tested by performing the analysis of well-documented embankment structures obtained from the published literature. It was later utilized to determine the strain-dependent natural frequencies of different sections of the EM dam. The following sections present the methodology employed, analysis of results, and the salient findings of the study.

5.3 Methodology

5.3.1 Generation of synthesised 'sum of sines' wave

The acceleration versus time data for performing a time-history analysis was synthesised by the superimposition of sinusoidal waves of frequencies ranging from 0.01 Hz to 25 Hz, with increments of 0.01 Hz. MATLAB was used to generate data for each frequency for a time duration of 20 s. The data was recorded every 0.02 s for each frequency present in the synthesised wave, and the acceleration-time data was then obtained by adding the acquired data for these 2500 frequencies over a time period of 20 s. The final data obtained from the superimposition of sinusoidal waves was scaled to different values of peak acceleration to simulate different levels of seismic excitation. Figure 5-1 shows the acceleration versus time data (peak acceleration = 0.1g) obtained by superimposition of sinusoidal waves having

frequencies ranging from 0.01 to 25 Hz (Equation 5.1). A generalised equation of the synthesised wave is presented in Equation 5.2.

$$\text{Acc}\,(t) = \sum_{i=1}^{i=2500} \sin\,(2 \text{ x } \pi \text{ x } 0.01 \text{ x } i \text{ x } t);\ 0 \text{ s} \leq t \leq 20 \text{ s} \qquad (5.1)$$

$$\text{Acc}\,(t) = \frac{PHA}{\max\left[\sum_{i=1}^{i=F/f} \sin(2\pi \text{ x } f \text{ x } i \text{ x } t)\right]} \sum_{i=1}^{i=F/f} \sin(2\pi \text{ x } f \text{ x } i \text{ x } t)\ ;\ 0 \text{ s} \leq t \leq T \text{ s} \qquad (5.2)$$

where, *PHA* = Peak horizontal acceleration; *F* = maximum expected frequency range to be scanned; *f* = least count of frequency scale; *t* = time steps; and *T* = Duration of synthesised wave.

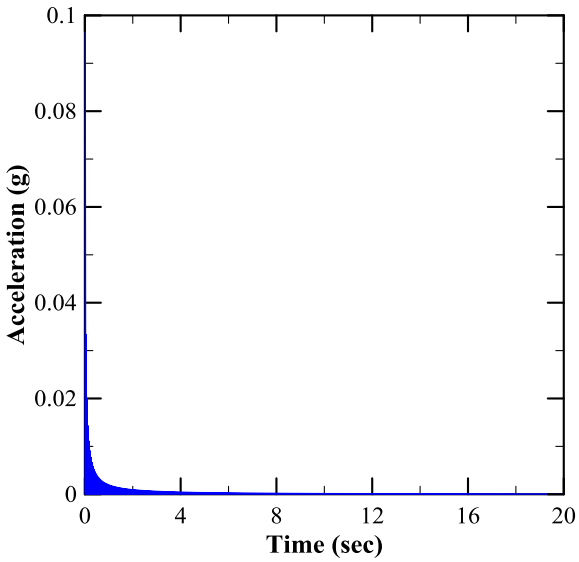

Figure 5-1: Synthesised wave ('sum of sines') used for determination of natural frequency

5.3.2 Validation with published literature

The applicability of the developed methodology for determining the natural frequencies of a structure was demonstrated by using a basic single degree of freedom (SDOF) system. It was further validated by performing analyses on

different earthen structures whose natural frequencies have been reported in previously published literature. A commercially available finite-element-based software was used to perform time-history analysis on these earthen structures. The acceleration-time data obtained from the summation of sine waves (Figure 5-1) was used as the forcing function for the SDOF systems and to simulate a horizontal earthquake excitation applied at the base of an earthen embankment structure. The frequencies of vibration that were most excited were determined by identifying prominent frequency peaks of the obtained FFT plot of the response of the structures. The location of the first strong peak in the FFT plot of the crest acceleration in the frequency domain or the last prominent peak in the time-period domain has provided a measure of natural frequency/time-period for the first mode of vibration (Mejia and Seed 1983; Mejia et al. 1982). The natural frequencies or time periods obtained by the 'sum of sines' method were compared with those reported in the literature. The details of the SDOF systems and earthen dams, along with their material properties, are presented in subsequent sections.

5.3.3 Application of 'sum of sines' method on EM dam

The 'sum of sines' method was extended to determine the natural frequencies of a section of the EM dam, as shown in Figure 5-2. Series piezocone penetration tests were conducted at the crest of the dam, and the soil behaviour type (SBT) and effective friction angle were then interpreted from the CPT data. A database of other soil properties including unit weight and plasticity index, was prepared for

different soil types based on laboratory tests conducted on soil samples extracted from different locations of the earthen dam. A two-dimensional (2D) section, for which a shear wave velocity profile and an as-built drawing were available, was selected for the analysis (Figure 5-2). The geometry of the dam was obtained from the drawing, and this section was further subdivided into numerous zones to incorporate the variations in small strain shear modulus which had been determined from shear wave velocity profiles ($G_{max} = \rho V_s^2$). The material properties of the subdivided zones were assigned, based on the compiled material property database, the SBT values, and available bore log information.

A 2D, plane strain, time-history analysis was performed, using the same software that was used to validate the proposed methodology. Linear elastic analyses using G_{max} values of the respective soil layers were performed to obtain the natural frequency of the structure that corresponded to the low strain levels. Equivalent linear analyses were then performed to determine the natural frequency of the dam section, incorporating the effect of non-linear behaviour of the dam materials (Gazetas 1987; Kramer 1996; Mejia and Seed 1983). The modulus degradation curve and the variations of damping ratios with strain levels were defined for the equivalent linear analysis, based on the effective confining stress and plasticity index of the individual zones (Ishibashi and Zhang 1993).

The synthesised wave was scaled to various peak accelerations and applied at the base of the dam to create a variety of strain levels, enabling the study of the

effect of non-linear behaviour of soil on the natural frequencies. The natural frequency of the first mode, obtained by the 'sum of sines' method, was plotted against the root mean square (RMS) strain value obtained at the crest of the dam. Real earthquake time-history data (21 scenarios) with widely different frequency contents were then used to induce the horizontal acceleration at the base of the earthen dam model (Table 5-2). The frequency corresponding to the first prominent peak in the FFT plot of the crest acceleration was plotted against the corresponding RMS strain for all of the real earthquake cases, and was compared with that predicted by using the 'sum of sines' method. This approach provided insights into the strain-dependent characteristic of the natural frequency of earthen dams, and was used to justify the applicability of the developed methodology.

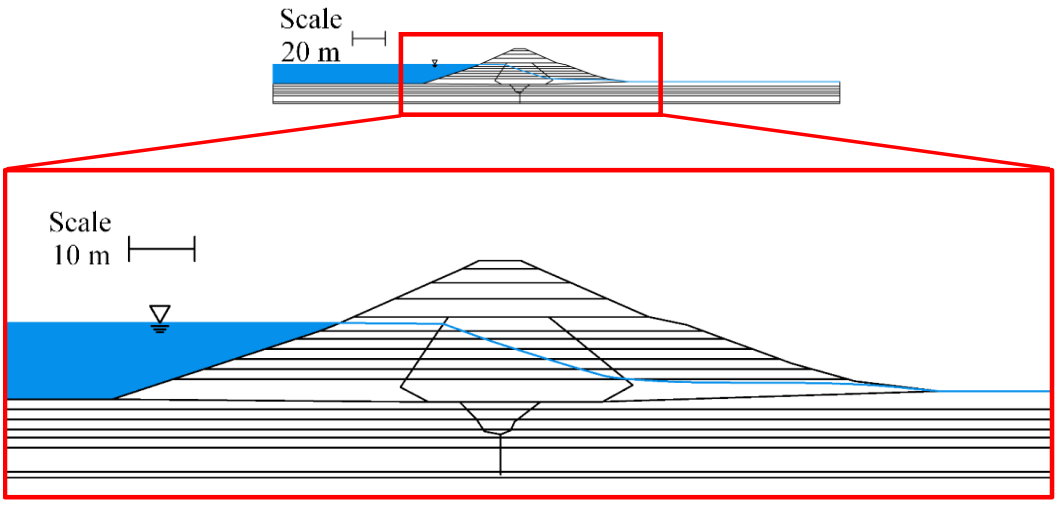

Layer	Depth (m)	V_s (m/s)	Unit weight (kN/m^3)	Density (kg/m^3)	G_{max} (kN/m^2)
1	0-1.3	124.9	20.4	2082	32,492
2	1.3-2.7	153.5	20.4	2082	49,071
3	2.7-5.7	189.6	20.7	2114	76,032
4	5.7-7.3	221.2	20.7	2114	103,489
5	7.3-8.8	207.7	20.7	2114	91,204
6	8.8-10.6	207.5	20.4	2082	89,696
7	10.6-11.9	234.8	19.0	1938	106,836
8	11.9-13.3	201.6	20.3	2066	84,039
9	13.3-14.9	188.1	20.3	2066	73,130
10	14.9-16.4	227.2	20.3	2066	106,716
11	16.4-18.0	197.1	20.3	2066	80,319
12	18.0-21.1	252.8	20.6	2098	134,145
13	21.1-22.5	198.6	20.4	2082	82,182
14	22.5-24.0	323.6	20.4	2082	218,026
15	24.0-25.6	347.7	20.4	2082	251,682
16	25.6-27.1	549.3	20.7	2114	638,038
17	Rest of Foundation	510.2	21.2	2162	562,835

Figure 5-2: Section of hydraulic-fill dam used for analysis

5.4 Analysis and discussion of results

5.4.1 Validation

Before applying the proposed methodology to the hydraulic-fill dam, it was important to assess the efficacy of the 'sum of sines' method in providing realistic natural frequency values. Hence, three SDOF systems and five embankment dam cases from previously published literature were investigated. The case studies were selected because their natural frequencies were readily available for comparison with results obtained from the 'sum of sines' method.

5.4.1.1 SDOF system

The SDOF systems with mass (m) of 80 kg, damping ratio (d) of 5%, and stiffness values (k) of 400 N/m, 4,000 N/m and 40,000 N/m were considered for the analysis. The resonant frequency (f_r) for forced vibration of a damped SDOF system was obtained analytically using Equation 5.3 (Richart et al. 1970). The synthesised wave excitation was used as the forcing function on the 80 kg mass, and its response to the wave excitation was determined using MATLAB Simulink (Figure 5-3a). The FFT of the acceleration response of the 80 kg mass provided the natural frequencies of the respective SDOF systems. The analytical solutions and those obtained by using the 'sum of sines' method (Figure 5-3b) provided similar natural frequencies of 0.35 Hz, 1.12 Hz, and 3.56 Hz, for the three SDOF systems, respectively. This validated the utility of the developed methodology to estimate the natural frequency of simple SDOF systems. The natural frequency of embankment structures was determined by using the 'sum of sines' method and is compared with that reported in the literature in the following section.

$$f_r = \frac{1}{2\pi}\sqrt{\frac{k}{m}}\left(\sqrt{1 - 2d^2}\right) \tag{5.3}$$

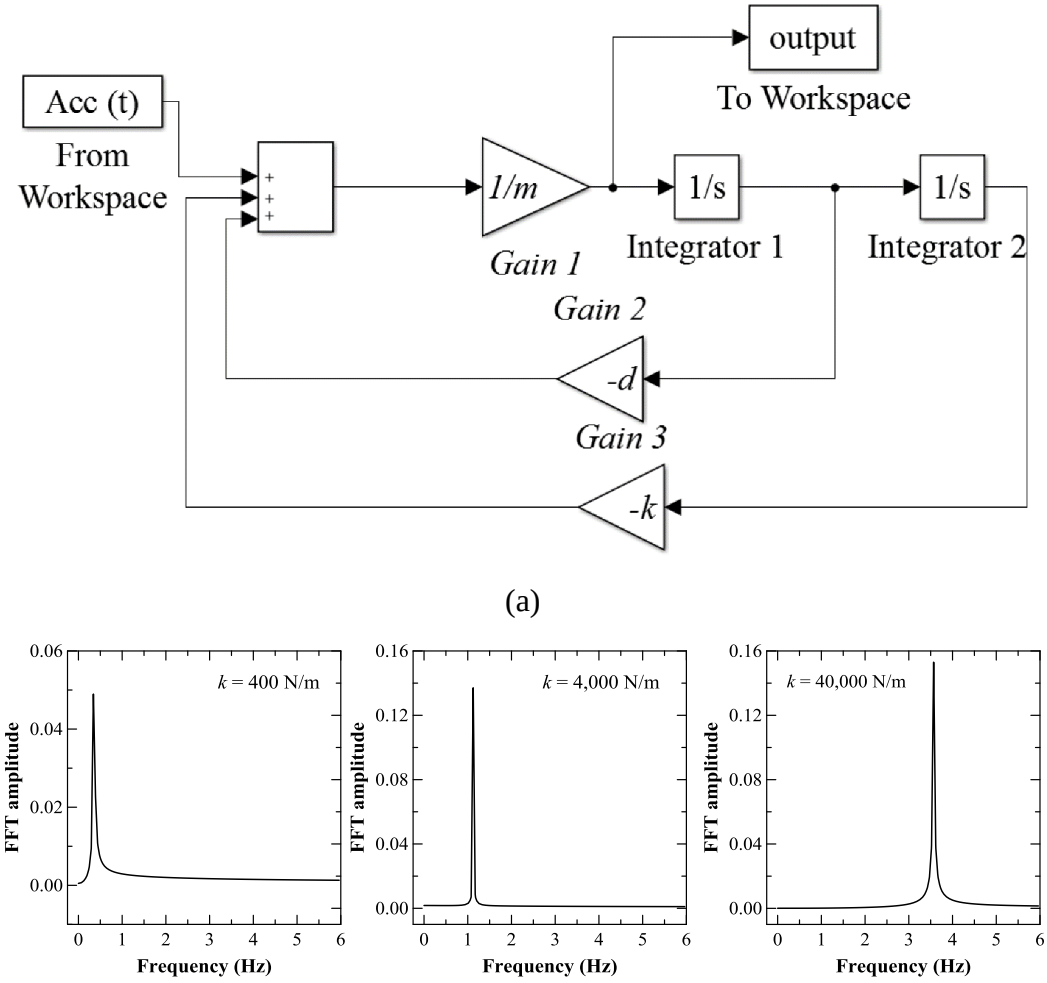

Figure 5-3: (a) Simulink model used for analysis; (b) Natural frequency obtained using 'sum of sines' method for SDOF system of mass m = 80 kg, d = 0.05, and stiffness k of 400 N/m, 4,000 N/m and 40,000 N/m

Table 5-2: List of earthquakes used for validating the applicability of the 'sum of sines' method

Region	Station	Date	Compone	Scaled	F_1(Hz	F_2(Hz	F_3(Hz	T_m (s)
Arkansas	Enola	26th June 1982	0	0.001g	*2.68	3.37	6.98	0.279
Arkansas	Enola	26th June 1982	0	0.01g	*2.68	3.37	6.98	0.279
Arkansas	Enola	26th June 1982	0	0.03g	*2.68	3.37	6.98	0.279
Arkansas	Enola	26th June 1982	0	0.1g	*2.68	3.37	6.98	0.279
Arkansas	Enola	26th June 1982	0	†0.5g	*2.68	3.37	6.98	0.279
Arkansas	Enola	5th July 1982	90	0.05g	*1.96	*4.54	*6.69	0.319
Arkansas	Enola	5th July 1982	90	0.3g	*1.96	*4.54	*6.69	0.319
Arkansas	Enola	5th July 1982	90	0.6g	*1.96	*4.54	*6.69	0.319
Missouri	Dexter	6th November	360	0.02g	1.14	*1.807	-	0.638
Missouri	Dexter	6th November	360	0.07g	1.14	*1.807	-	0.638
Missouri	Dexter	6th November	360	0.1g	1.14	*1.807	-	0.638
Missouri	Dexter	6th November	360	†0.5g	1.14	*1.807	-	0.638
Missouri	Dexter	6th November	360	†0.8g	1.14	*1.807	-	0.638
Oklahoma	SW Harper	19th November	90	0.0009g	Multiple peaks			0.108
Oklahoma	SW Harper	19th November	90	0.04g	Multiple peaks			0.108
Oklahoma	SW Harper	19th November	90	0.08g	Multiple peaks			0.108
Oklahoma	SW Harper	19th November	90	†0.25g	Multiple peaks			0.108
Oklahoma	Mehan	7th November	90	0.15g	2.39	5.03	*9.57	0.128
Oklahoma	Mehan	7th November	90	0.4g	2.39	5.03	*9.57	0.128
Oklahoma	Mehan	7th November	90	†0.65g	2.39	5.03	*9.57	0.128
Oklahoma	Mehan	7th November	90	†1.5g	2.39	5.03	*9.57	0.128

* Predominant frequency of the earthquake time-history data

† Earthquake cases with higher modes of vibration

$$T_m = \frac{\Sigma\left[C_i^2.\left(\frac{1}{f_i}\right)\right]}{\Sigma C_i^2}$$

5.4.1.2 Embankment Case Studies

Case 1 – Clough and Chopra (1966)

Figure 5-4a depicts the triangular dam model described by Clough and Chopra (1966). The height and width of the dam were 91.4 m and 274.3 m, respectively, and it had a symmetric cross-section with a side slope of 1.5H:1V. The dam was assumed to be homogeneous and isotropic, and two-dimensional linear elastic plane strain condition was used for the analysis. The material properties used for the model were: unit weight of 20.4 kN/m^3, Poisson's ratio of 0.45, damping ratio of embankment of 0.05, shear wave velocity of 304.8 m/s, and small strain shear modulus (G_{max}) of 193,387 kPa. This model was analysed by using the synthesised wave signal (Figure 5-1) as the horizontal base excitation.

Figure 5-4b describes the natural time period of the dam as reported in the literature (Clough and Chopra 1966) and presents the natural time period obtained by performing FFT of the crest acceleration when the dam model was subjected to the synthesised horizontal acceleration time-history data. It may be noted from Figure 5-4b that no peak matches were found for modes 2, 5, 6, 9, and 10. This could be attributed to zero modal participation, meaning that they were not excited by horizontal earthquake motion (Gasparini and Sun 1982). The natural time periods for the remaining modes were found to be in consonance with those observed in the previous studies (Clough and Chopra 1966; Gasparini and Sun 1982).

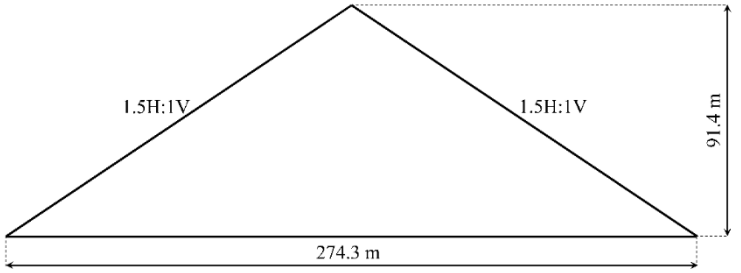

(a)

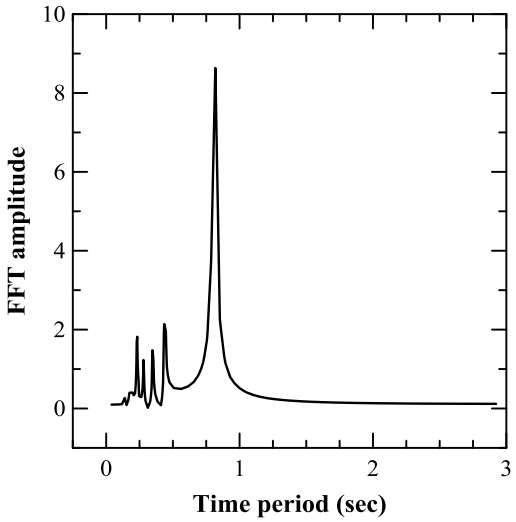

Mode	Circular frequency (rad/s)	Frequency (Hz)	Time period reported (s)	Time period observed (s)
1	7.715	1.23	0.81	0.79
2	12.52	1.99	0.50	-
3	14.6	2.32	0.43	0.43
4	19.31	3.07	0.33	0.34
5	20.12	3.20	0.31	-
6	23.1	3.68	0.27	-
7	23.75	3.78	0.26	0.27
8	25.95	4.13	0.24	0.24
9	26.76	4.26	0.23	-
10	28.77	4.58	0.22	-

(b)

Figure 5-4: Case 1 (a) Dam model after Clough and Chopra (1966); (b) Natural period determination

Case 2 – Okamoto (1984)

Figure 5-5a shows a triangular dam model described by Okamoto (1984). The height and width of the dam were 90 m and 540 m, respectively, with side slope of 3H:1V. The material properties used for the analysis include unit weight of 20.4 kN/m^3, Poisson's ratio of 0.45, damping ratio of 0.05, shear wave velocity of 300 m/s, and small strain shear modulus (G_{max}) of 187,264 kPa. Similar to the previous case, the dam was assumed to be homogeneous and isotropic, and was analyzed using a 2D plane strain condition.

The first and second natural periods were reported as 0.88 s and 0.47 s, respectively (Okamoto 1984). Figure 5-5b illustrates the natural time periods obtained from 'sum of sines' method: 0.86 s and 0.40 s, with a small kink around 0.47 s. The minor divergence in the value of the second natural period could be attributed to the insignificant excitation of the second mode by horizontal base motion, similar to that observed in Case 1. Apart from some minor peaks, the other significant peaks were noticed at 0.27 s and 0.23 s. For the higher order modes, the natural period information was not reported, and hence, it could not be validated with the present 'sum of sines' method.

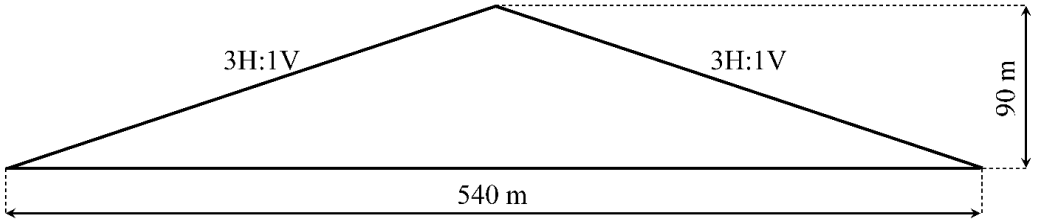

(a)

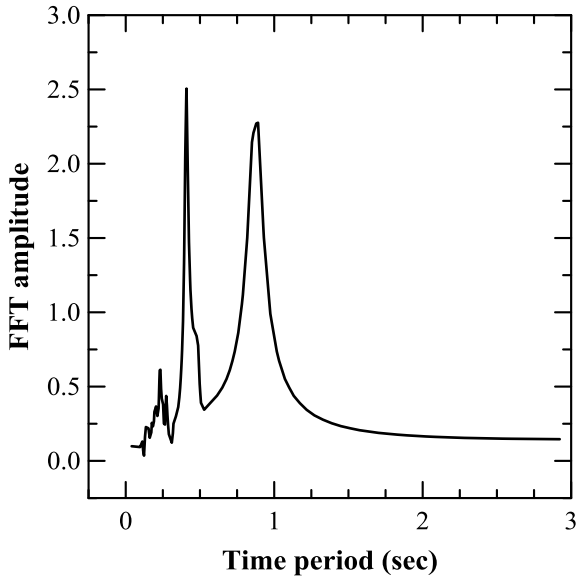

(b)

Figure 5-5: Case 2 (a) Dam model; (b) Natural period determination

Case 3 – Tsiatas and Gazetas (1982)

Figure 5-6a presents a non-homogeneous dam section analysed by Tsiatas and Gazetas (1982), using 2D plane strain finite element analysis. Of the five different cases highlighted in their research paper, case A was only analysed as part of the present study. Other cases (B, C, D and E) were not considered due to the lack of requisite data for the input parameters and analysis. The dam section had a height and base width of 90 m and 405 m, respectively. The cross section was asymmetric,

with a side slope of 2.5H:1V to the left, and 2H:1V to the right. The shear modulus was assumed to vary in direct proportion to the square root of mean stress (Tsiatas and Gazetas 1982). A unit weight of 17.66 kN/m^3, Poisson's ratio of 0.3, damping ratio of 0.05, and average shear wave velocity of 324 m/s (weighted area average) were used to model the dam.

The first and third natural periods, obtained from the 'sum of sines' method (Figure 5-6b), are in agreement with those reported by Tsiatas and Gazetas (1982), with a marginal error of 6%. This slight discrepancy in the first natural period could be further reduced if the exact distribution of G_{max} used by Tsiatas and Gazetas (1982) was known. The paper suggested the use of an average shear wave velocity of 324 m/s; therefore, to obtain the distribution of G_{max}, a weighted average shear wave velocity of 324 m/s was used in conjunction with a criterion of G_{max} variation that was proportional to the square root of the mean stress. It is expected that the difference in the distribution of G_{max} values used by Tsiatas and Gazetas (1982) and those used in the present analysis will lead to a slight variation in the predicted time periods. Hence the accuracy of the obtained natural frequency (or time period) of vibration will depend on the distribution of G_{max} values of the embankment material. Nevertheless, the analysis showed that the proposed method can be used to analyse asymmetric dam sections.

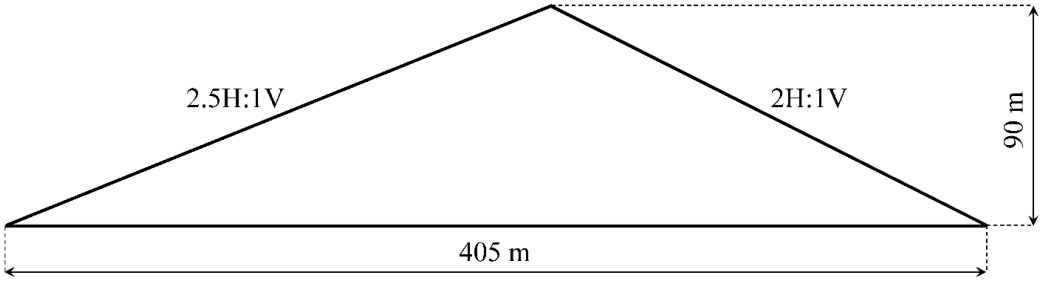

(a)

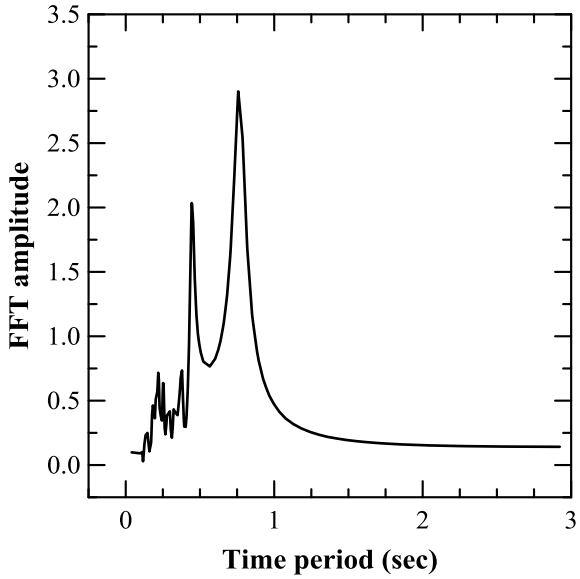

Mode	Time period reported (s)	Time period observed (s)
1	0.790	0.74
2	0.500	-
3	0.449	0.44

(b)

Figure 5-6: Case 3 (a) Dam model after Tsiatas and Gazetas (1982); (b) Natural period determination

Case 4 – Parish et al. (2009)

Figure 5-7a shows a comparatively complex dam section that was analysed using 3D finite difference modelling by Parish et al. (2009). This dam was comprised of different zones, such as foundation, shell, and core; each zone contained a different material with distinct properties. The crest width, base width, and height of the dam were 20 m, 240 m, and 50 m, respectively. The slopes on both of the sides were 2.2H:1V. The core of the dam had a top width of 10 m and a base width of 30 m. The material properties of the core, shell, and foundation of the dam are illustrated in Figure 5-7a.

Response spectra of free horizontal vibration of the dam revealed three major peaks near 0.7 Hz, 1.4 Hz, and 2.1 Hz, with a high spectral velocity between 1.4 Hz and 2.1 Hz (Parish et al. 2009). A similar trend was observed in the FFT plot of dam crest acceleration, using the present approach. Figure 5-7b depicts the major peaks at 0.68 Hz, 1.37 Hz, 1.66 Hz, 2.1 Hz, and 2.39 Hz. This demonstrates the applicability of the 'sum of sines' method for determining the natural frequency of a zoned earthen dam.

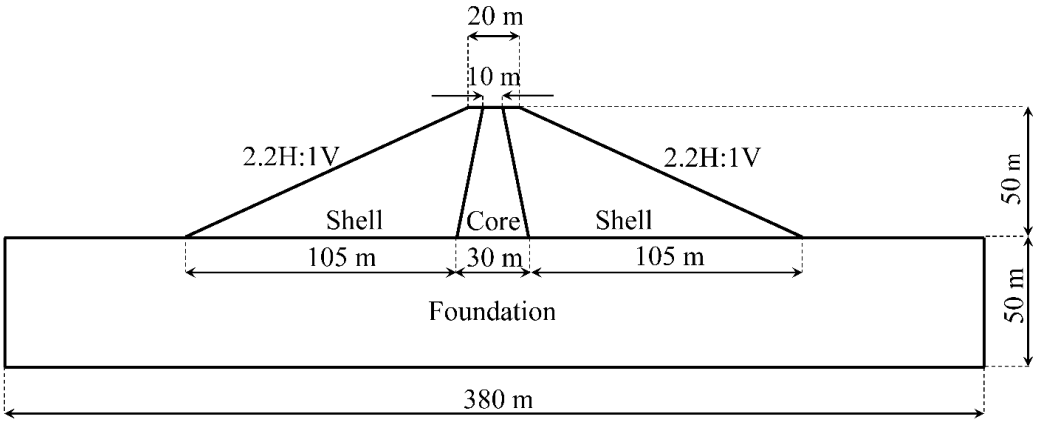

Zone	Unit Weight (kN/m^3)	Poisson's ratio	Damping ratio	G_{max} (kPa)
Core	17.65	0.3	0.02	13,073
Shell	19.62	0.3	0.02	23,080
Foundation	21.58	0.25	0.02	400,000

(a)

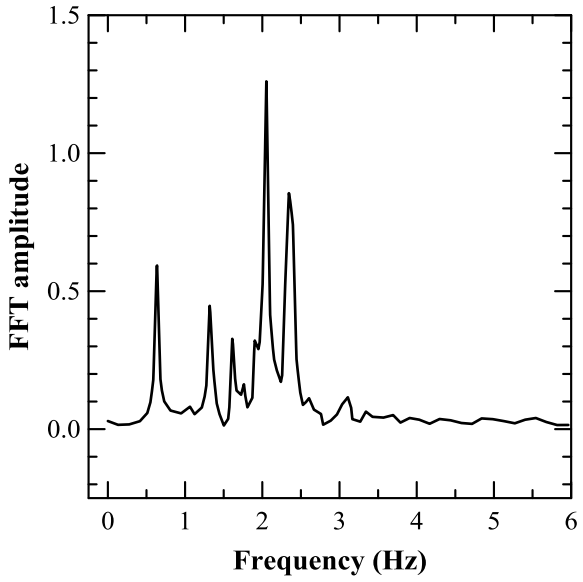

(b)

Figure 5-7: Case 4 (a) Dam model after Parish et al. (2009); (b) Natural period determination

Case 5 – Cetin et al. (2005)

The Kiralkizi Dam in Turkey was analysed by Cetin et al. (2005), using a 2D finite difference model. Unlike the previous cases, this dam is a real existing structure, where the zones of the dam have different material properties, which adds to the complexities of the analysis. The dam geometry and material properties are presented in Figure 5-8.

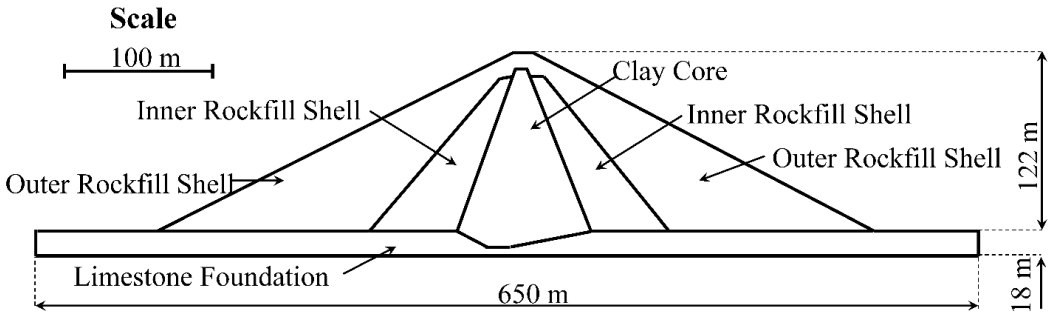

Zone	Unit Weight (kN/m^3)	Poisson's ratio	Damping ratio	G_{max} (kPa)	c' (kPa)	ϕ' (deg.)
Clay Core	19	0.48	0.02	78,000	80	0
Inner Rockfill Shell	22	0.33	0.02	202,000	0	42
Outer Rockfill Shell	22	0.33	0.02	560,000	100	45
Limestone foundation	23	0.33	0.02	1,498,000	500	45

Figure 5-8: Case 5 dam model after Cetin et al. (2005)

Figure 5-9a describes the spectral response for the crest acceleration and foundation base excitation observed by Cetin et al. (2005). The response of the dam was assessed, using an advanced finite-difference-based software. The natural period for the first mode of vibration was reported as 0.55 s (Figure 5-9a). The natural periods of the dam, determined by the 'sum of sines' method, are shown in

Figure 5-9b. Major peaks are indicated at different time periods: 0.22 s, 0.31 s, 0.58 s, and 1.02 s, with 1.02 s being the natural period of first mode of vibration according to the 'sum of sines' method. With the exception of the peak at 1.02 s, the peaks revealed by the 'sum of sines' method in Figure 5-9b closely resemble those shown in Figure 5-9a.

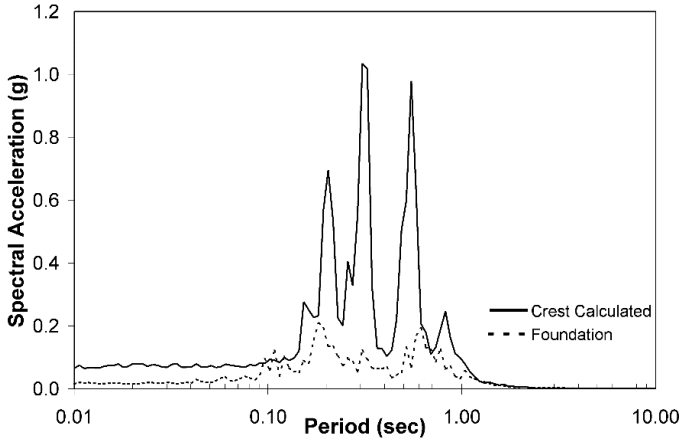

(a)

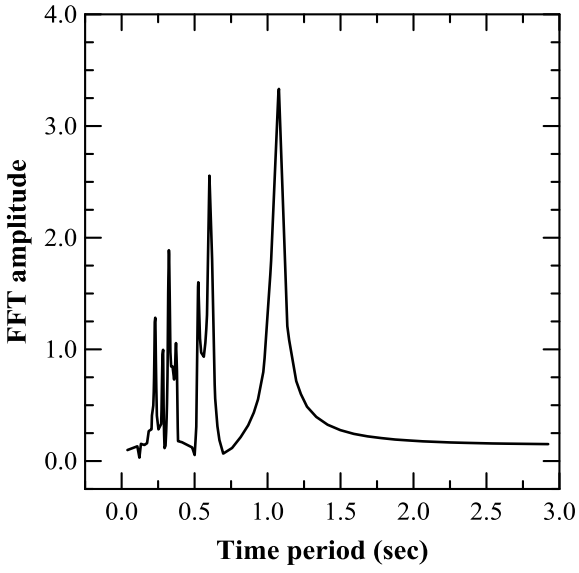

(b)

Figure 5-9: (a) Crest spectral amplitude (after Cetin et al. 2005); (b) Natural period determination Case 5

The reason for this discrepancy was further analysed by studying the mode shapes of vibration. It is important to note that the prominent peaks in the spectral response for the crest acceleration, shown in Figure 5-9a, stem from the particular earthquake excitation applied to the dam foundation, denoted as 'Foundation' in Figure 5-9a. Furthermore, the response spectra for the earthquake time-history data does not exhibit any major peak at or near a period of 1 s. As the earthquake excitation did not have any major component waves with a time period close to 1 s, the dam did not vibrate significantly in the first mode. It should be noted that a small peak was recorded around 0.9 s in the spectral response for the crest acceleration (denoted as 'Crest Calculated' in Figure 5-9a).

Component waves in close proximity to the second and third modes caused the dam to vibrate with a time period of 0.55 s (second mode) and 0.3 s (third mode). This was in addition to the small peak corresponding to the first mode of vibration having a time period of approximately 0.9 s. Sinusoidal waves with time periods of 1 s and 0.58 s were used as the base excitation to study the mode shapes of vibration and the response of the structure. Figure 5-10 shows the FFT data of the crest acceleration, and Figure 5-11 presents the variations of the absolute value of the relative displacement with time, along the centre line of the dam. The absolute value of the relative displacement along the centre line of the dam, for the entire duration of excitation, was used to examine the mode shape of vibration. Figures 5-10 and 5-11 suggest that 1.02 s and 0.58 s were indeed the natural periods for the first and

second modes of vibration, respectively. This confirms that the ‘sum of sines’ method is capable of correctly identifying the different modes of vibration which may be excited by a horizontal seismic excitation. Therefore, it can be concluded that the ‘sum of sines’ method provides more reliable information about the natural time period of the dam, without missing any possible modes of vibration.

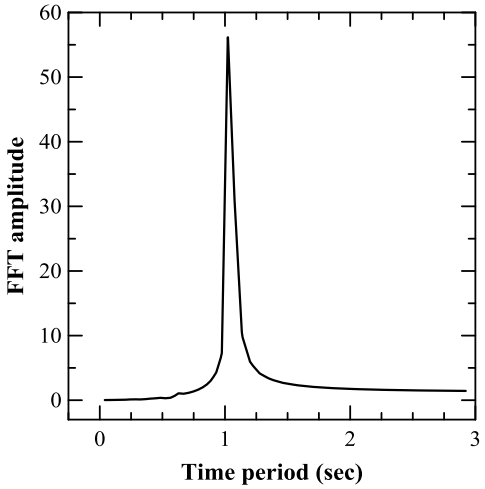

(a)

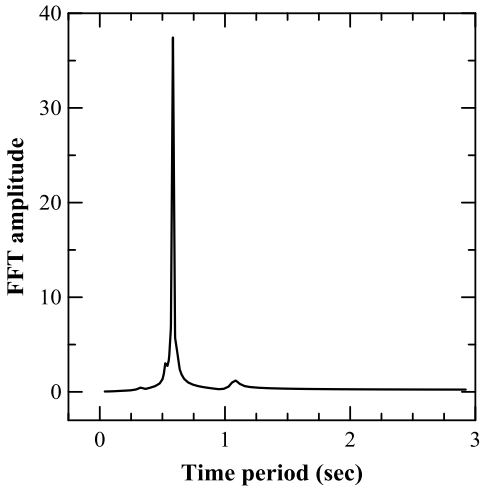

(b)

Figure 5-10: FFT of crest acceleration of dam subjected to sinusoidal waves having time period of (a) 1 s and (b) 0.58 s

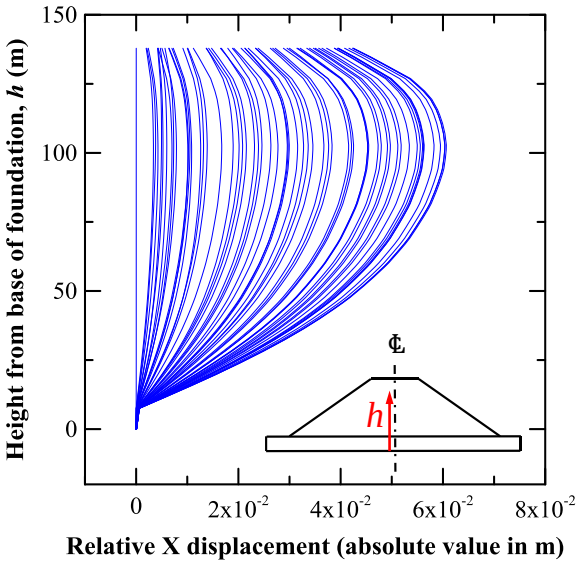

(a)

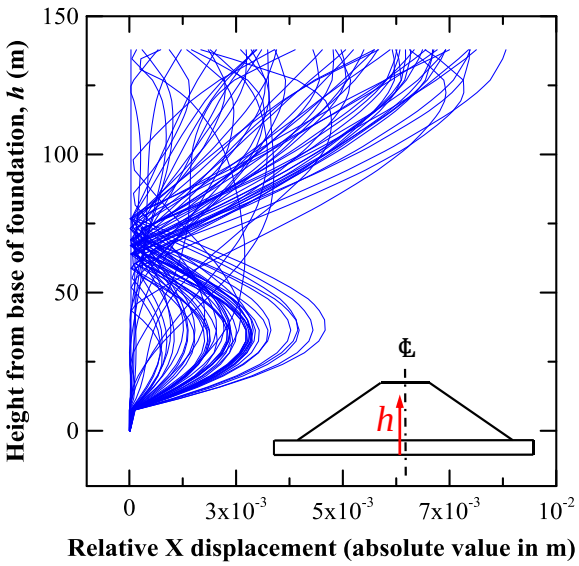

(b)

Figure 5-11: (a) First mode of vibration and (b) predominant second mode of vibration when subjected to sinusoidal waves having time periods of 1 s and 0.58 s, respectively

The five different cases were studied in the increasing order of their complexity. Case 1 and 2 involved homogeneous dams with symmetric cross sections, and Case 3 focused on non-homogeneous asymmetric structures having different side slopes. Cases 4 and 5 were studied to test the applicability of the proposed 'sum of sines' method to real dam sections, where the core, shell and foundation have widely different properties. Results indicate that the proposed approach can be used to determine the natural frequency of an earthen structure. However, the veracity of the results depends on the accuracy with which the dam model with its material properties depicts the actual dam characteristics.

5.4.2 Application of 'sum of sines' method on EM dam

The synthesised acceleration time-history data (Equation 1) was used as horizontal acceleration applied at the base of the 2D FEM model of the hydraulic-fill dam section (Figure 5-2) to determine the natural frequencies of the first mode of vibration. It was noted that, under small strain conditions (crest RMS strain $< 10^{-6}$), linear elastic analysis provided the same natural frequencies as those obtained from equivalent linear analysis. The rationale behind this observation, $G = G_{max}$, is used in equivalent linear analysis (i.e. $G/G_{max} = 1$ at low strain level) for very low intensity excitations, where the strain level attained by different sections of the dam does not cause significant non-linear response of the earthen structure. Non-linear behaviour of the dam was recorded for scaling the synthesised wave to peak ground accelerations of 0.1*g* and above. A reduction in stiffness and an increase in damping

at higher strain levels lead to an increase in the time period of oscillation, which is in agreement with that observed by Mejia and Seed (1983). The reduction in natural frequency of the first mode with an increase in the RMS strain recorded at the crest of dam is presented in Figure 5-12. The natural frequency for the first mode of vibration was constant at 2.39 Hz, up to a RMS strain of 10^{-6}. However, with further increase in the RMS strain, plotted in logarithmic scale, the natural frequency decreased, following a linear trend in a semi-logarithmic plot. This can be attributed to the non-linear behaviour of the dam embankment material at higher levels of disturbance, caused by increased peak ground acceleration of the base excitation.

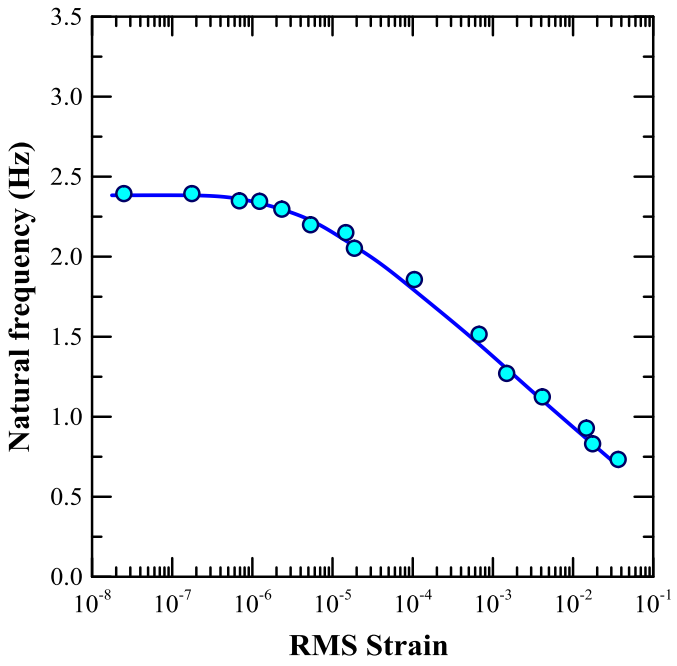

Figure 5-12: Natural frequency for first mode of vibration with RMS strain at crest of dam

Figure 5-12 was obtained by using the synthesised acceleration time data as the horizontal base excitation. However, real earthquake excitations are random in nature, and hence different sets of frequencies are present in the waves. Hence, it was necessary to compare the natural frequency of first mode of vibration when subjected to real earthquake scenarios with those predicted by the 'sum of sines' method at different strain levels. Acceleration time-history data for five different earthquakes was scaled to different peak accelerations and used as base excitation for the given dam section. The acceleration-time data of these earthquakes and their corresponding FFT plots are shown in Figures 5-13 and 5-14, respectively. Twenty-one earthquake time-history scenarios were used for validating the applicability of the developed methodology and are summarised in Table 5-2. The natural frequency was obtained from the FFT of the crest acceleration-time data. The first prominent peak observed for each of the 21 cases of earthquake excitations was also plotted against the respective RMS strain calculated at the crest (Figure 5-15). It can be observed in Figure 5-15 that the variations of natural frequency with RMS strain followed a similar trend for most of the different earthquake excitations. As the synthesised acceleration-time data had the same amplitude for all of the component waves of different frequencies, the vibration of the dam subjected to the synthesised wave had a significant component of vibration in the first mode. Since the first strong peak in the FFT plot was used to obtain the data points in Figure 5-

12, it can be concluded that the trends highlighted in Figures 5-12 and 5-15 correspond solely to the first mode of vibration.

As evidenced in Figure 5-15, there were a few cases where the natural frequency deviated significantly from the trend indicated by the 'sum of sines' method (Figure 5-12). In order to comprehend this behaviour, the displacement along the centre line of the dam was studied to determine the mode shapes of vibration. Figures 5-16 through 5-19 show the absolute value of the displacement pattern of the centre line of the dam and the corresponding FFT plot of crest acceleration time-history data when the dam is subjected to different scaled peak ground accelerations (PGA) generated by using the Enola EQ and Mehan EQ time-history data. The acceleration-time data for these two earthquakes were specifically selected due to their widely different predominant frequencies (Table 5-2 and Figure 5-14). The Enola EQ data had a predominant frequency of 2.68 Hz, and the Mehan EQ data had a predominant frequency of 9.57 Hz (Table 5-2).

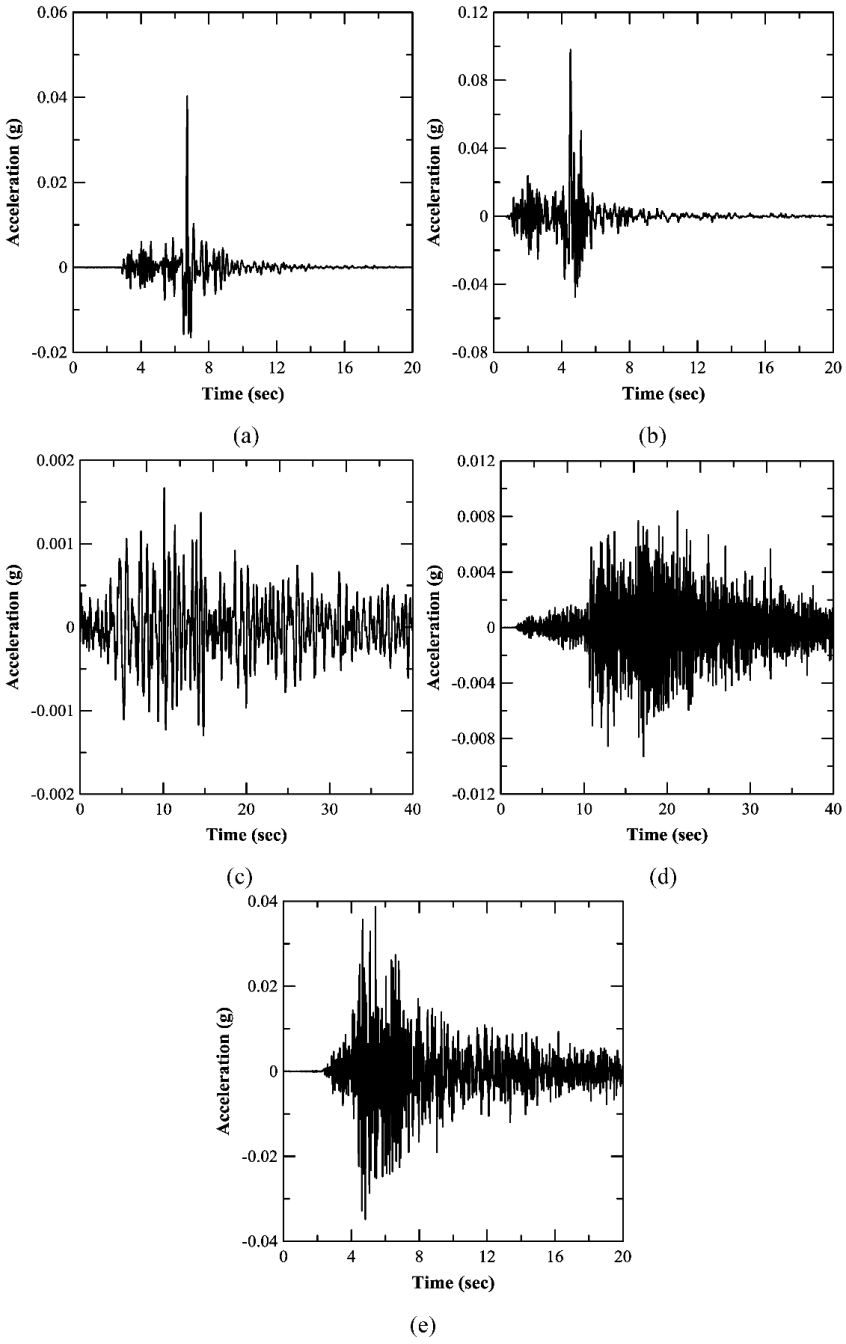

Figure 5-13: Earthquake acceleration-time data for (a) Enola, June 1982; (b) Enola, July 1982; (c) Dexter, November 2011; (d) SW Harper, November 2015; and (e) Mehan, November 2016

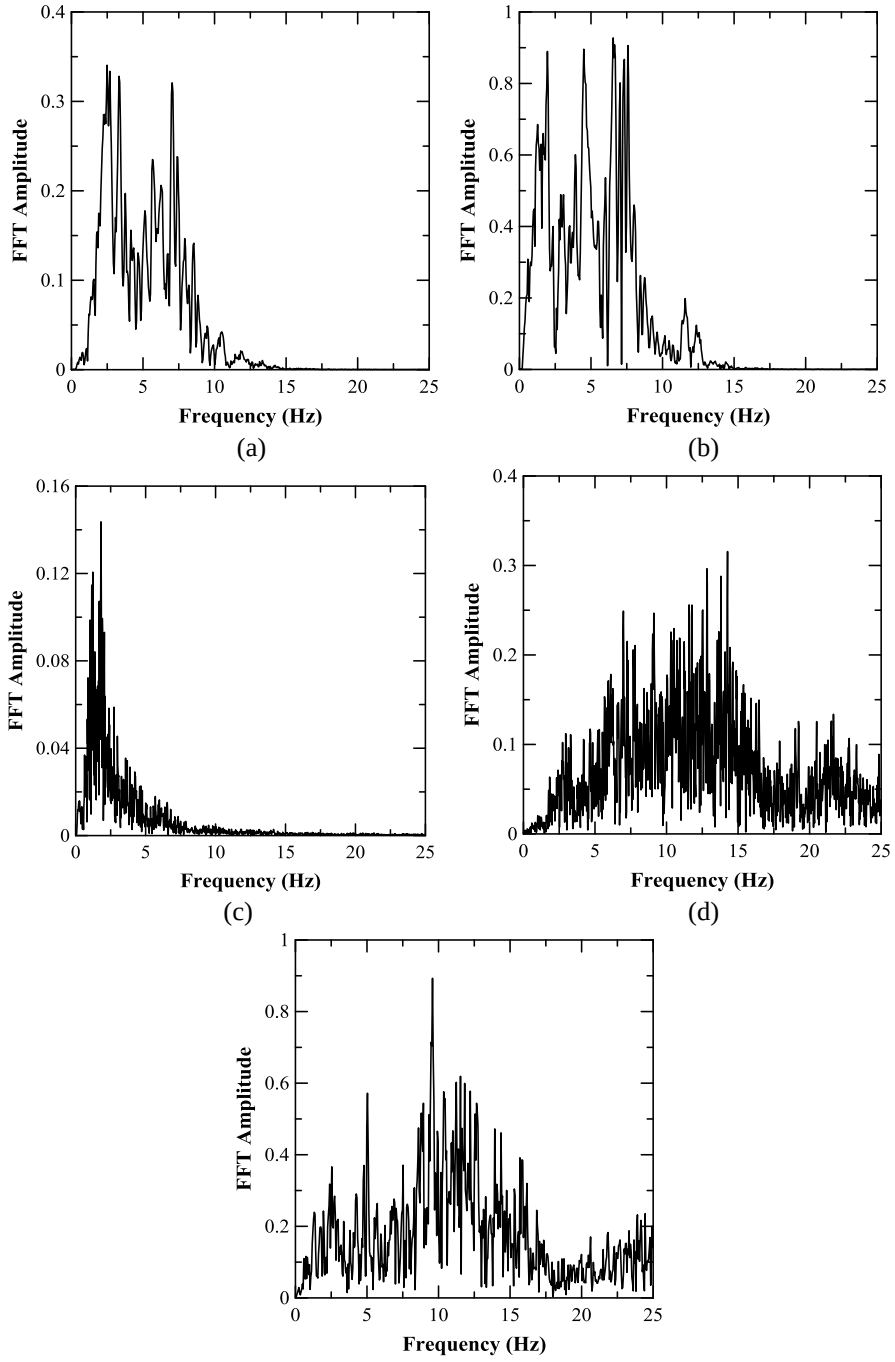

Figure 5-14: FFT plot of earthquake acceleration-time data for (a) Enola, June 1982; (b) Enola, July 1982; (c) Dexter, November 2011; (d) SW Harper, November 2015; and (e) Mehan, November 2016

The absolute displacement along the centre line of the dam, in conjunction with the FFT plot, facilitated understanding the rationale behind the observed deviation in natural frequency of vibration from that predicted by the ‘sum of sines’ method (Figure 5-15).

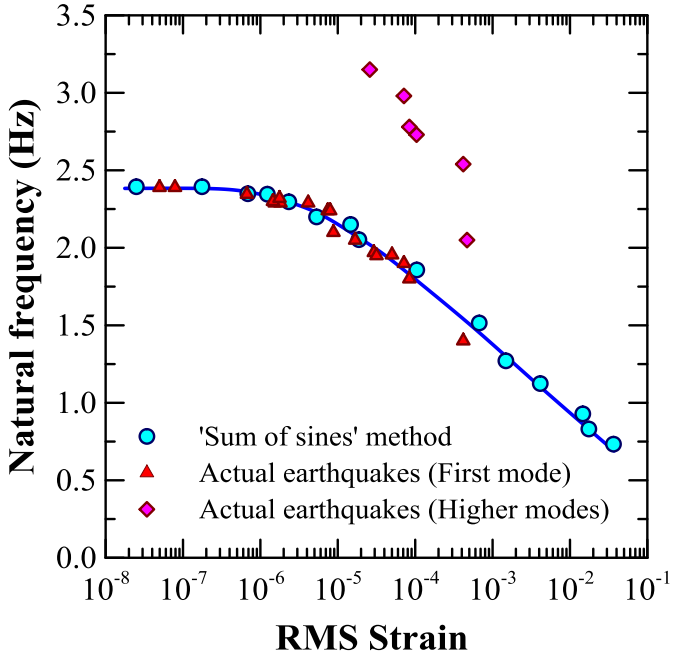

Figure 5-15: Applicability of ‘sum of sines’ method to determine strain-dependent natural frequency for actual earthquake cases

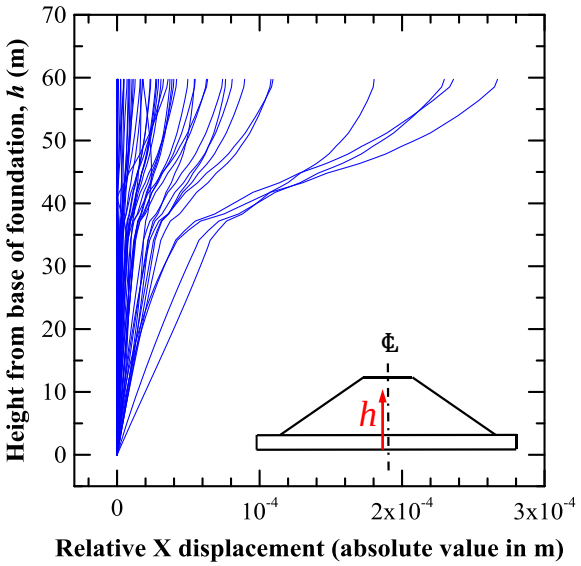

(a)

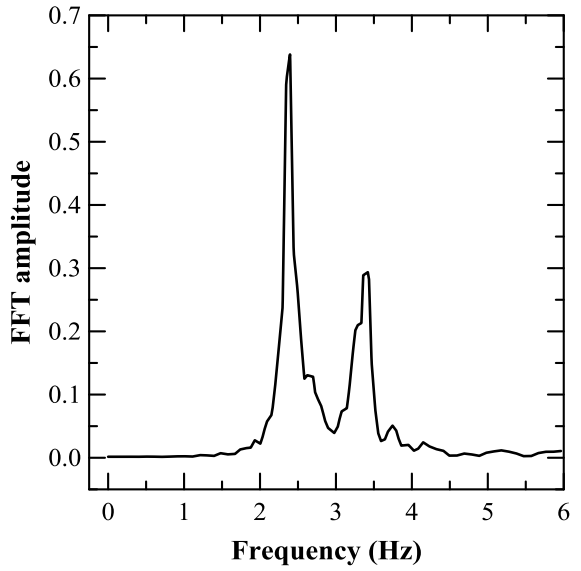

(b)

Figure 5-16: (a) First mode of vibration and (b) FFT of acceleration at crest of dam for Enola EQ (PGA= 0.001g)

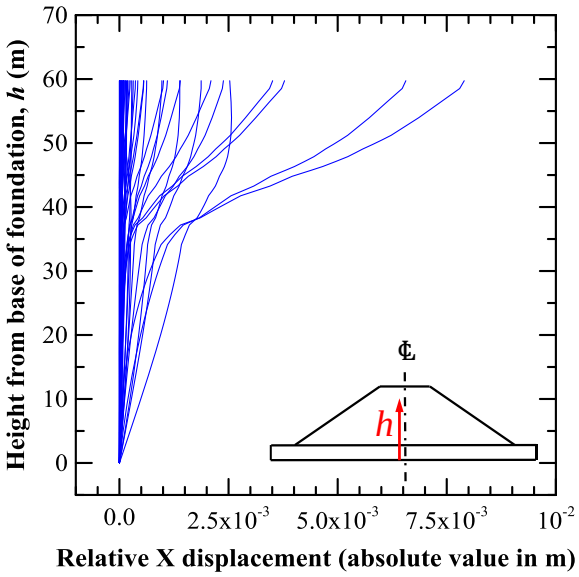

(a)

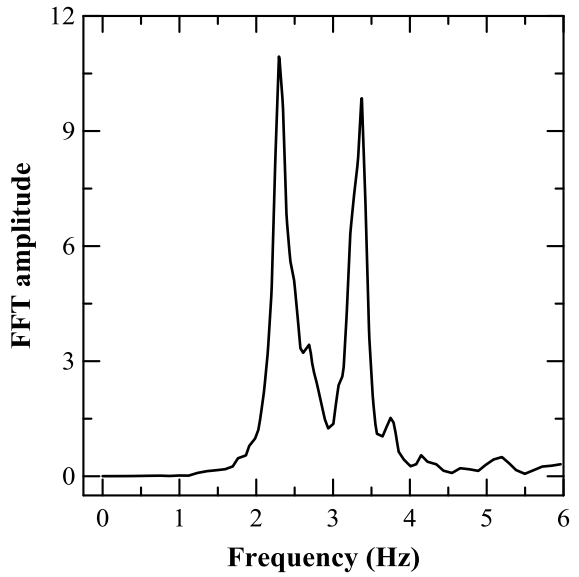

(b)

Figure 5-17: (a) First mode of vibration and (b) FFT of acceleration at crest of dam for Enola EQ (PGA= 0.03g)

The dam vibrated in the first mode for low PGA; the natural frequency for the first mode of vibration was 2.39 Hz and 2.29 Hz (Figures 5-16 and 5-17), when subjected to Enola EQ, scaled to two different low values of PGA. The decrease in natural frequency from 2.39 Hz to 2.29 Hz was due to the increase in PGA from $0.001g$ to $0.03g$ for the Enola EQ data, resulting in non-linear behaviour of the soil. However, with an increase in PGA, the structure tended to vibrate predominantly at higher modes (Figures 5-18 and 5-19). This effect is manifested in the FFT plots, which depicts the distinctive and strong peaks at 2.74 Hz and 3.14 Hz, corresponding to the higher modes of vibration. The outliers in the results presented in Figure 5-15 were found to correspond to the higher modes of vibration. For those cases, the FFT plot of the crest acceleration time-history data did not show any definite peaks for the first mode of vibration. Hence, the first detectable strong peaks (shown as outliers in Figure 5-15) do not always represent the first mode of vibration. There are two different scenarios where the dam might vibrate at higher modes: a) when the peak ground acceleration is high, simulating earthquakes of higher intensity (Prevost et al. 1985), and b) where the major constituent frequency peaks of the earthquake time-history data are close to the natural frequencies of the higher modes of vibration (Figures 5-9 to 5-11 and Table 5-2).

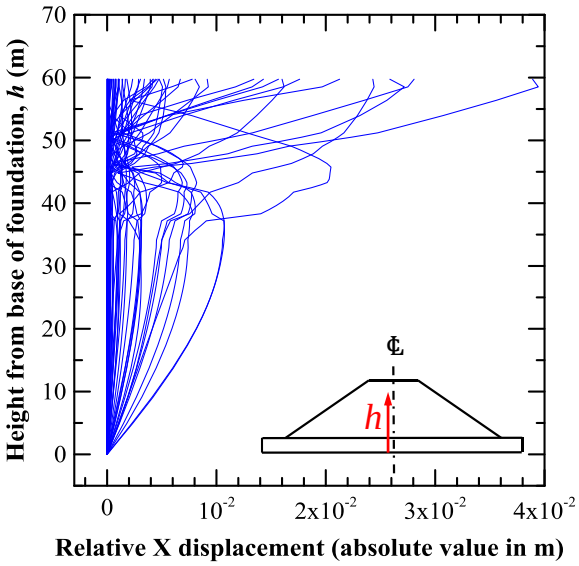

(a)

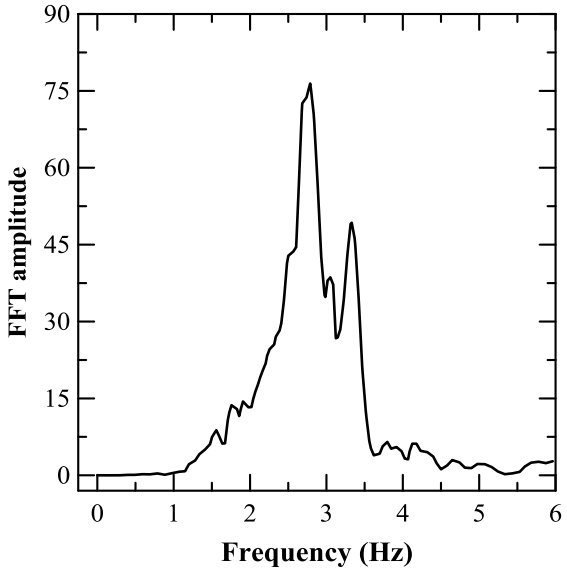

(b)

Figure 5-18: (a) Higher modes of vibration and (b) FFT of acceleration at crest of dam for Enola EQ (PGA= 0.5g)

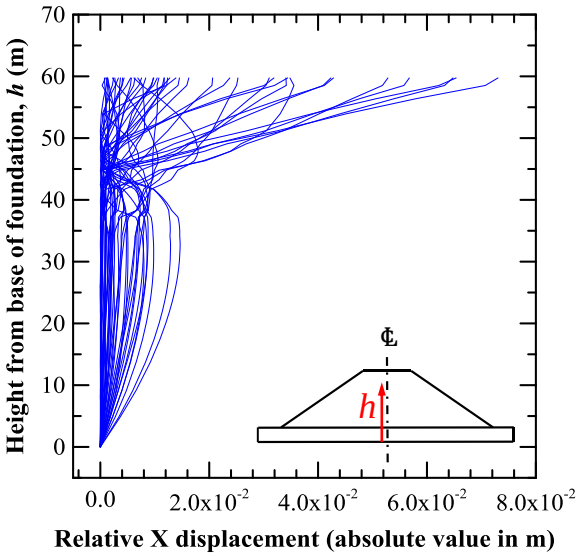

(a)

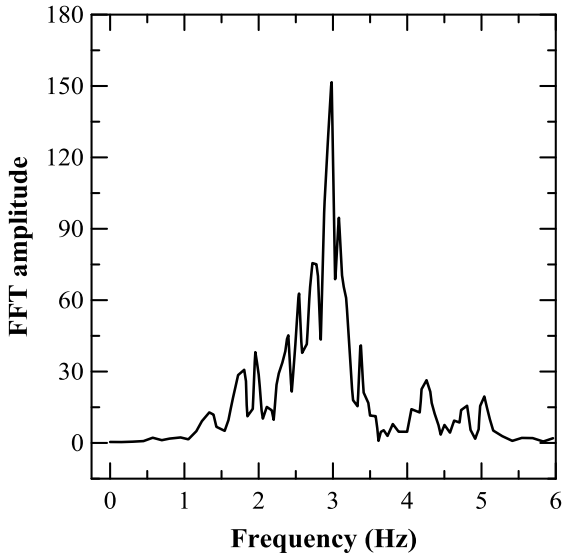

(b)

Figure 5-19: (a) Higher modes of vibration and (b) FFT of acceleration at crest of dam for Mehan EQ (PGA= 0.65g)

5.4.3 Natural frequency of EM dam

The sum of sines method was applied to determine the strain-dependent natural frequency of eight different section of the EM dam. The shear wave velocity profiles for each of the sections is presented in Figure 4-15 of chapter 4. The natural frequency corresponding to low strain levels and the strain-dependent degradation of the natural frequency of the individual sections are provided in Figure 5-20.

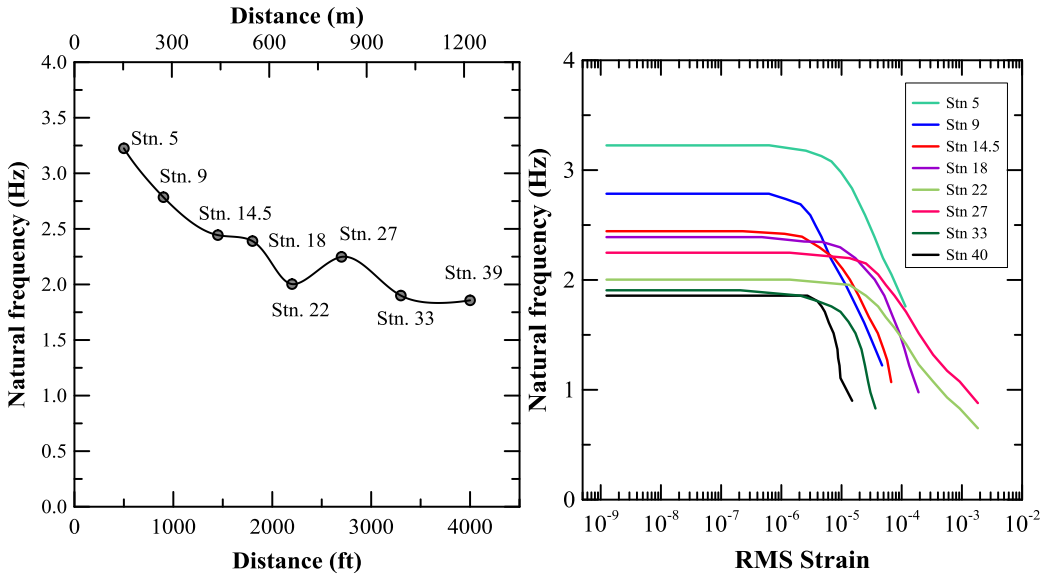

(a) (b)

Figure 5-20: Variation of (a) First natural frequency at low strain levels and (b) strain-dependent natural frequency along the length of the dam

The natural frequency was observed to be the highest for Station 5, which was constructed by wetting and rolling the dam embankment geomaterials. Whereas, the natural frequency of the hydraulic-fill segment of the dam (Station 14.5 to 39) was observed to exhibit a comparatively lower natural frequency. This

can be attributed to the hydraulic-fill method of construction of the different segments of the dam. Wetting and rolling the dam material provides a higher control on achieving the target degree of compaction, leading to higher stiffness and subsequently higher natural frequency. Contrarily, the hydraulic-fill segment of the dam had a lower natural frequency due to the lower stiffness when compared to the wetted and rolled section (Figure 4-15). The comparatively low values of stiffness were due to the lack of control associated with placing the embankment material by hydraulic-fill. The natural frequency of Station 9, which had a wetted and rolled shell, coupled with a hydraulic fill core, was found to lie in between that observed for the Station 5 and Stations 14.5 to 39 (Figure 5-20).

The actual variation of the natural frequency of the EM dam may be different from that estimated in this study using 2D plane strain models of the different sections. A two-dimensional plane strain analysis implicitly assumes same material property along the entire length of the dam, which may not be a reasonable assumption in case of a highly heterogeneous dam, as the EM dam. A comprehensive three-dimensional analysis is thus required, since it is expected to provide a better representation of the natural frequency of the dam, incorporating the effect of the material variability along the length of the dam.

5.5 Practical implications

The developed method, ‘sum of sines’, was proven to accurately determine the natural frequency of the vibration modes of an earthen embankment structure when

excited by horizontal disturbances, and can be used as an alternative to the Eigen value analysis or free vibration analysis. In addition to providing the natural frequency corresponding to the free vibration analysis, the method was extended to predict the first natural frequency of earthen structures when subjected to different extents of seismic disturbances. The results provide an understanding of the behaviour of structures exhibiting nonlinear behaviour when subjected to earthquake motions. Any software capable of performing a time-history-based equivalent linear type of non-linear analysis can incorporate the developed method to predict the variations of the natural frequency of the first mode of vibration with different degrees of disturbances (varying strain levels). Earthen structures incur an unrecoverable loss in stiffness at high strain levels. Hence, the behaviour of the structure, when exposed to the first earthquake excitation, is different from that during the aftershocks. This method can thus provide understanding of the post-earthquake natural frequency of vibrations of an earthen dam after it has exhibited nonlinear behaviour during the earthquake.

5.6 Summary

The objective of this study was to determine the natural frequency of an earthen structure for the first mode of vibration, incorporating the effect of non-linear behavior of the structure. A synthesized acceleration time-history data, formed by superimposing 2500 sinusoidal waves with frequencies ranging from 0.01Hz to 25

Hz (increment of 0.01Hz), was scaled to different peak accelerations to induce different degrees of disturbances and different levels of strain within the structure. The study was implemented in two parts (a) validating the applicability of the proposed methodology in determining the natural frequency (corresponding to G_{max} at low strain levels) of different earthen structures studied by previous researchers; and (b) determination of strain-dependent natural frequency of a section of a hydraulic-fill dam using 2D plane strain equivalent linear analysis. The following major conclusions were drawn from this study:

- The natural frequencies of the three SDOF systems and the five earthen embankment structures were estimated through the 'sum of sines' method, developed as a part of the research. Results show that these natural frequencies are in good agreement with the corresponding frequency values obtained from analytical solutions and those reported in literature, respectively.
- When the scaled, synthesised wave was applied as base excitation to the dam, the structure vibrated primarily at frequencies that were close to the natural frequency of the structure at the particular strain level. Fast Fourier transform of the acceleration time-history data at the crest of the dam provided an accurate estimate of the natural frequencies.

- Due to the difference in strain levels attained at different regions of the dam at different modes, a parameter was selected to act as a surrogate measure of the degree of disturbance experienced by the dam. For the first mode of vibration, the root mean square (RMS) strain was designated as one such suitable parameter.
- The natural frequency for the first mode of vibration remained constant until a certain RMS strain at the crest, implying linear behaviour of the structure at small magnitudes of disturbances. However, the natural frequency of the dam decreased with an increase in the peak acceleration of the synthesised wave, and decreased with a subsequent increase in the strain at different zones. The reduction in natural frequency with crest RMS strain was observed to follow a linear trend on a semi-logarithmic scale.
- The variation of the natural frequency of the structure with crest RMS strain depends on the modulus degradation curve and the variation of damping ratio with strain. The accuracy with which the 'sum of sines' method predicts the strain-dependent natural frequency will depend on the material properties used to model the dam.
- The variation of the first natural frequency with RMS strain followed the same trend as that obtained from the proposed 'sum of sines' method, when actual earthquake cases, with varying peak crest accelerations and significantly different frequency content, were used as base excitation. This

demonstrates the effectiveness of the approach in estimating the strain-dependent natural frequency for the first mode of vibration of an earthen structure subjected to a real earthquake event. The 'sum of sines' method of natural frequency determination can be used to study the post-earthquake behaviour of a dam and to gain insight into the performance of the dam at different strain levels.

- The first natural frequency of the dam, at low strain levels, was found to decrease from 3.25 Hz to 1.8 Hz along the length of the dam. The natural frequency of the wetted and rolled segment was found to be higher than that corresponding to the hydraulic-fill portion. The rationale behind this observed variation was attributed to the difference in construction procedures adopted to build the structure and consequent difference in the stiffness of the subsurface layers at different segments (stations) of the dam. These estimated natural frequency values will be used to select the earthquake time-history data for dynamic stability analysis in next chapter.

Chapter 6: Stability Analyses of the EM Dam

6.1 Introduction

This chapter presents the results of the analyses performed to assess the stability of the slopes of the EM dam. The method adopted to include the effect of material variability in creating the finite element model of the dam is elucidated in this chapter. The stability analyses consist of three major parts: (a) static analysis, (b) pseudo-static analysis and (c) dynamic stability analysis. The critical sections of the dam are identified based on these analyses results and are compared. The reliability analysis results, which captures the effect of uncertainty associated with the estimation of shear strength parameters, is also provided.

The dynamic analysis was performed using the small strain shear modulus profiles obtained from chapter 4. Real earthquake time-history data of eight earthquakes recorded in Oklahoma and Arkansas were selected for the analysis, in the absence of data recorded at the dam site. The earthquakes were chosen such that some of their predominant frequencies were close to the first natural frequency of the dam, presented in chapter 5. The effect of peak acceleration, earthquake magnitude and frequency contents of the earthquake, on the excess pore water pressure generated in the sand layers and its impact on the stability of the slopes during earthquakes, were studied and is presented in this chapter. Lastly, the state parameter was estimated from CPT results to evaluate the chances of flow liquefaction.

6.2 Background

Evaluating the stability of slopes of earthen embankment structures, such as dams and levees, is of paramount importance since the failure of these megastructures can have catastrophic consequences. These water-retaining structures, which are usually stable under normal working conditions, may become unstable during earthquake events (Chatterjee and Choudhury 2014; Choudhury et al. 2007; Fell et al. 2005; Hack et al. 2007; Meehan and Vahedifard 2013; Seed and Martin 1966; Seed 1981). The seismic stability of slopes is usually evaluated using the pseudo-static method, the stress-deformation method or the permanent-displacement method (Cai and Bathurst 1996; Jibson 2011; Newmark 1965). The pseudo-static approach, introduced by Terzaghi (Terzaghi 1950), incorporates the effect of earthquake shaking as a constant horizontal force on a slip surface, which is obtained by multiplying an appropriate horizontal seismic coefficient k_h with the weight of the sliding mass. The stability is subsequently evaluated by static limit equilibrium analysis (Cai and Bathurst 1996; FEMA 2005; Gazetas and Uddin 1994; Jibson 2011; Kramer and Smith 1997; Newmark 1965; Seed 1981). However, approximating the effect of earthquake excitation as an equivalent horizontal force is a crude assumption, which cannot capture the response of the structure during seismic events. The computationally intensive, stress-deformation approach is then considered to be a suitable option for such analysis. In the stress-deformation approach, the earthen embankment is discretized as a mesh using a

commercially available finite element or finite difference based software and the stress and deformation at all the nodes are determined in response to an earthquake disturbance (time-history data) applied at the base of the structure (Jibson 2011). However, the need for high-quality laboratory and field soil property test data, and sophisticated constitutive models makes the stress-deformation approach suitable primarily for high-risk projects (Baker et al. 2006; Gazetas and Uddin 1994; Jibson 2011; Shukha and Baker 2008).

The permanent-displacement approach introduced by Newmark (Newmark 1965) bridges the gap between the pseudo-static approach and the stress-deformation approach (Gazetas and Uddin 1994; Jibson 2011). The method provides an estimate of the plastic deformation experienced by a sliding mass when the earthquake-induced acceleration exceeds the yield acceleration (Gazetas and Uddin 1994; Jibson 2011; Kramer and Smith 1997; Seed 1981). The yield acceleration is defined as the minimum acceleration at which the sliding mass is on the verge of imminent failure, i.e., the factor of safety (FOS) is equal to unity.

The sliding block in the Newmark type of deformation analysis (Newmark 1965) was assumed to behave as a rigid block and the variation of the earthquake-induced acceleration in the sliding mass was not considered in the permanent-displacement method (Gazetas and Uddin 1994; Jibson 2011; Kramer and Smith 1997). The decoupled method of analysis by Makdisi and Seed (Makdisi and Seed

1978) incorporates the non-rigid behavior of the sliding mass, which deforms internally during shaking. In the decoupled method, a dynamic response analysis is performed at first without considering any failure of the slope (Jibson 2011; Kramer and Smith 1997; Seed 1979). Subsequently, the earthquake-induced acceleration is used to compute the average horizontal equivalent acceleration, which is then used in the Newmark type deformation analysis (Makdisi and Seed 1978; Seed 1979).

Despite being a crude method, the pseudo-static approach provides an index of the seismic stability of slopes (FEMA 2005; Kramer and Smith 1997), especially when the embankment materials does not incur significant strength loss and are not susceptible to liquefaction during earthquakes (Baker et al. 2006; FEMA 2005; Seed 1981; USSD 2007). The pseudo-static approach along with permanent-displacement analysis remains extremely popular among practicing engineers due to its sheer simplicity. Different agencies and design guidelines recommend using pseudo-static analysis as a preliminary screening tool for justifying the use of a rigorous stress-deformation type of analysis, even for important projects (Baker et al. 2006; Christian and Urzúa 2017; Shukha and Baker 2008). Earthen embankment structures present in low seismicity zones, where the intensity of earthquake excitation is not expected to be significant enough to cause soil liquefaction, can also be studied using the traditional pseudo-static approach (Makdisi and Seed 1978; Seed 1981; Seed et al. 1978).

Well-built dams, including some hydraulic-fill dams, have shown resilience to moderate shaking without significant damage (Ambraseys 1960a; Seed 1981). However, some hydraulic-fill dams such as the Lower San Fernando dam have been extensively damaged by earthquakes (Foster et al. 2000; Mejia et al. 2005; Seed et al. 1978). Hence hydraulic-fill dams need to be evaluated for seismic risks related to slope stability issues.

Recently in 2016, the United States Geological Survey (USGS) indicated Oklahoma-Kansas, the Raton Basin, North Texas, North Arkansas, and New Madrid to be high seismic hazard zone due to induced seismicity (USGS 2016). This necessitates the evaluation of the stability of earthen dams, especially hydraulic-fill dams located in these regions, which at the time of construction might not have been specifically designed to withstand earthquake loading conditions.

Although commercially available software has made it easy to perform seismic stability analysis of slopes, the efficacy of the analysis results depends on the accuracy with which the dam is modelled. The dam is often idealized as a zoned structure with the representative material properties assigned to the respective individual zones, such as shell, core and foundation (Babu et al. 2007; Boulanger and Montgomery 2016; Pelecanos 2013; Tezcan et al. 2001). The accuracy of the analysis result may be questionable since this crude approximation may not portray the actual field conditions. The epistemic uncertainty, that includes site

characterization uncertainty, model uncertainty, and soil parameter uncertainty (Baecher and Christian 2005) makes the evaluation of safety even more challenging for these inherently heterogeneous, hydraulic-fill structures. Significant engineering judgement, based on prior experience, is thus required in such cases and a substantial degree of uncertainty is associated in estimating the material properties (Babu and Srivastava 2010; Duncan 2000; Griffiths et al. 2010; Wolff 1996; Xiong and Huang 2017; Zhenyu et al. 2015). A probabilistic approach in terms of reliability-based analysis can provide important information on the impact of uncertainty associated with the estimation of different material properties (Babu et al. 2007; Garevski et al. 2013; Liang et al. 1999; Yegian et al. 1991).

In this chapter, the stability of the slopes of the EM dam is evaluated. This study also addresses some of the key uncertainties including the material variability and seismic coefficient uncertainty. Probabilistic concepts are used to evaluate the stability of the hydraulic-fill dam. Pseudo-static approach along with decoupled permanent-displacement method are used to perform the preliminary seismic stability analysis, assess the condition of the dam and determine the critical sections. The probability of failure of the slopes is determined using Monte Carlo simulations, when different sections of the dam are subjected to a wide range of seismic conditions. The probable performance of the dam is also evaluated, based on the reliability indices, to further identify the problematic sections of the dam.

The pseudo-static and Newmark deformation analyses can provide information about the stability of the structure, in case the geomaterials do not incur significant strength loss and are not susceptible to liquefaction. However, it was also necessary to evaluate the stability of the slopes in the event of cyclic liquefaction, by performing a time-history based dynamic analyses and estimating the subsequent increase in pore water pressure in the saturated sand layers. Flow liquefaction susceptibility also had to be evaluated for the foundation sand layers, by estimating the state parameter from the cone penetration test results. The following sections present the site details, methodology, and analysis and discussion of results.

6.3 Site details

This section presents the site details of the EM dam that is considered for performing the stability analyses. The construction of this 26m high and 1463m long dam started in January 1930 and was completed in October 1932. Based on the United States Geological Survey (USGS) seismic hazard report published in 2016 (USGS 2016), this site is located in high seismic hazard zone due to induced seismicity. Probabilistic seismic hazard analysis suggests that in one year, there is one percent chance of experiencing an earthquake that exceeds peak ground acceleration (PGA) of 0.3*g* (Caballero 2017; Petersen et al. 2017). This critical infrastructure was not specifically designed to withstand earthquake loading conditions at the time of construction, as the construction was done 85 years ago.

Thus it was necessary to evaluate the stability of the slopes of this dam under probable seismic events, due to an increase in the rate of induced seismic events in north Texas and adjacent regions, over the last few years (USGS 2016).

This dam was partially built by wetting and rolling the embankment soil and partly by hydraulic-fill method of construction. Figure 6-1 present four different zones including Zone A, Zone B, and Zone C_1 and C_2, that are categorized based on the construction process adopted. Zone A of the dam was built by wetting, rolling and compacting the embankment soil material. Whereas, Zone B has a wetted and rolled shell, with the core constructed by hydraulic-fill method. Unlike Zone B, both the shell and core of Zone C_1 and C_2 were built by hydraulic-fill method, with the use of starter dykes. Extensive laboratory and field tests were conducted at the dam site to comprehensively determine the material properties of the dam.

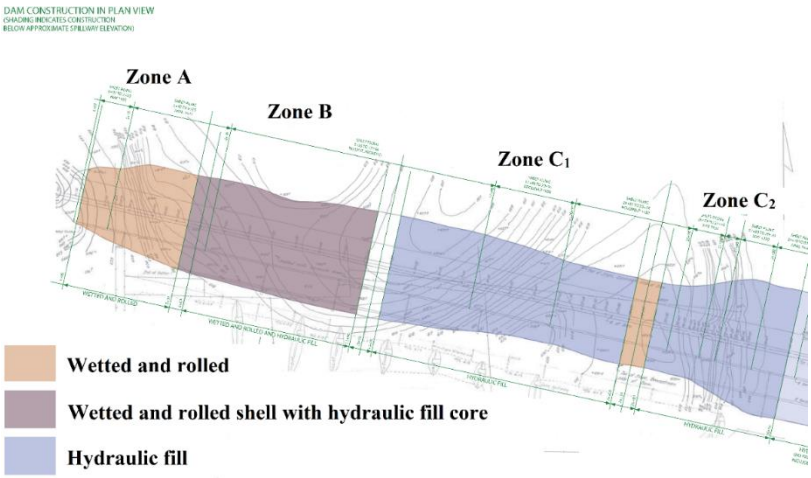

Figure 6-1: Plan view of dam showing the different zones based on the method of construction

6.4 Methodology

Hydraulic-fill was a popular method of construction when the dam was constructed in the early 20th century. The borrow soil used to build the dam was mixed with water, transported through flumes and discharged along the outer edge of the embankment, at suitable intervals. The course-grained soil particles settled first, close to the edges of the embankment to form the outer shell. Whereas the fine-grained soil, which takes longer time to settle, got deposited near the center of the embankment to form the low-permeability core of the dam. Hydraulic-fill dams exhibit a high degree of inherent variability in material properties owing to this method of construction (Caballero 2017; Caballero et al. 2017; Küpper 1991; Marcuson et al. 1990; Morgenstern and Küpper 1988; Vick 1996). The high degree of heterogeneity necessitated comprehensive determination of the material properties present at different sections of the dam.

6.4.1 Material characterization of the dam

Series of piezocone penetration tests (CPTu) were performed along the crest (39 soundings) and downstream toe of the dam (29 nos.). In addition to the CPTu results, several undisturbed samples were obtained from 18 boreholes (5 along the crest, 6 along the downstream toe and 7 along the dam slopes), which were used to determine index, hydraulic and shear strength properties of various soil types. Laboratory tests were conducted to determine the Atterberg limits, unit weight, saturated volumetric water content, saturated coefficient of permeability, and shear

strength parameters from triaxial and direct shear tests of different soil types, extracted from different boreholes. Furthermore, the unconfined compressive strength of the sandstone and shale layers present in the dam foundation were also determined.

The CPTu data was analyzed to determine the soil behavior types (SBTs) in the dam embankments (Robertson et al. 1986a), effective friction angle (ϕ') (Kulhawy and Mayne 1990), and undrained shear strength (s_u) (Robertson and Cabal 2015), employing the widely used and readily available correlations. Ordinary Kriging analysis, which is based on geostatistics, was performed to interpolate the obtained data (SBT, ϕ' and s_u) to generate 3D models of the dam, depicting the variation of the respective properties. 2D cross-sectional slices (for plane strain analysis) at the eight locations where the SASW tests were conducted, were further used to perform 2D seismic slope stability analysis using a commercially available finite element analysis software. The software was capable of performing pseudo-static analysis, decoupled permanent-displacement analysis, and dynamic stability analysis with excess pore water pressure estimation, for any given earthquake time-history data.

6.4.2 Construction of plane strain models of the dam

The most challenging and critical part of this study was to construct each of the eight two-dimensional sections of the dam in the software and assign the respective

material properties of such a heterogeneous dam. The as-built construction drawings were used to draw the outline of each of the sections to scale, which were then used for performing stability analysis. Each section was further sub-divided into several horizontal layers based on the shear wave velocity profile obtained from the SASW tests conducted on the crest of the dam (Figure 4-15). Unlike the wetted and rolled segment of the dam (Figure 6-2a), the zones of the dam built by hydraulic-fill construction method namely Zones B, C_1, and C_2 were found to be constructed with a core of fine-grained soil, and the shell section made up of primarily coarse-grained material (Figure 6-2b). Hence, the stratified sections for the hydraulic-fill zones of the dam were further divided into the shell, core and puddled trench core, based on the information available from the respective as-built drawings. Rigid base boundary condition was used for the dynamic analysis, assuming the earthquake time-history data to represent "within motion" (Mejia and Dawson 2006). The element size was selected such that it was smaller than one-tenth the wavelength corresponding to the highest frequency component of the input wave (Kuhlemeyer and Lysmer 1973). Before performing the seismic slope stability analysis, it was necessary to determine the pre-earthquake factor of safety (FOS) using pore water pressure evaluated from long-term steady state seepage conditions.

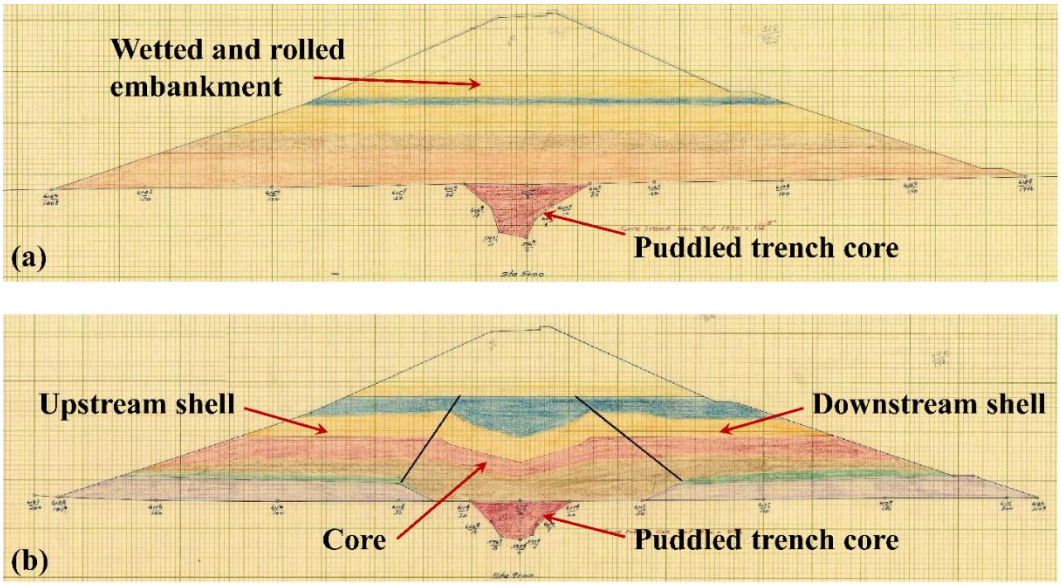

Figure 6-2: As-built drawing showing typical (a) wetted and rolled section and (b) hydraulic-fill section having a distinct core.

6.4.3 Determination of location of phreatic surface

The phreatic surface location was determined for each of the eight sections by performing the steady-state seepage analysis using a saturated-unsaturated model. The fully saturated permeability and volumetric water content of different soil types were assigned to the different segments of a particular dam cross section based on the respective SBT profile (2D slices obtained from a 3D model of SBT of the dam) and borelog data, wherever available. The variation of coefficient of permeability and volumetric water content with matric suction was defined depending on the soil type and data available from existing literature. The average coefficient of permeability obtained from laboratory testing of various undisturbed samples are reported in Table 6-1. The reservoir water elevation on the upstream side of the

dam was assumed to be the same as the top of the spillway level, which is at a distance of 10 m below the crest of the dam (freeboard).

Table 6-1: Mean values of saturated coefficient of permeability and volumetric water content for different soil types

	Sandy lean clay	Lean clay with sand	Fat clay	Sandstone	Shale	Sandy Silt	Sand
# samples	4	5	4	5	2	CPT guide*	CPT guide*
Mean k (m/s)	5.36 $x10^{-9}$	1.67 $x10^{-8}$	6.83 $x10^{-11}$	5.28 $x10^{-6}$	9.69 $x10^{-11}$	1.02 $x10^{-7}$	1.02 $x10^{-5}$
Mean volumetric water content	0.31	0.32	0.377	0.29	0.193	0.3	0.3

* Robertson and Cabal (2014)

6.4.4 Stability analysis

6.4.4.1 Determination of static FOS

The pre-earthquake static FOS was determined prior to performing the pseudo-static and permanent deformation analysis. Effective strength parameters c' and ϕ' were used for the pre-earthquake analysis, using the long-term steady-state pore water pressure conditions (FEMA 2005; USSD 2007). The strength contribution of the matric suction in the unsaturated soil above the phreatic surface was not considered for the stability analysis. The unit weight of different soil types, required to estimate the initial static stress-state of the dam, under steady-state seepage conditions are provided in Table 6-2. The data provided in Table 6-2 was obtained by compiling the unit weights of different soil types available from the undisturbed sample cores, extracted from different locations of the dam. The variation of

effective friction angle, for a particular section of the dam, was obtained from the 2D slice of the corresponding section obtained from the 3D model developed using kriging analyses of cone penetration sounding parameter based strength property interpretations. The effective cohesion was assumed to be zero unless specific results obtained from the triaxial or direct shear tests on undisturbed samples were available (USSD 2007).

Table 6-2: Unit weight of different soil types

	Sandy lean clay	Lean clay with sand	Fat clay	Silty clay with sand	Lean clay	Sandy silt	Fat clay with sand	Clayey sand
# samples	27	5	3	6	2	3	3	3
Mean (kN/m^3)	20.6	20.2	18.9	20.7	19.0	20.0	19.2	21.2
Std. dev. (kN/m^3)	0.50	0.21	0.28	0.09	0.06	0.86	0.35	0.28
CoV (%)	2.43	1.07	1.49	0.47	0.34	4.34	1.84	1.33

6.4.4.2 Determination of pseudo-static FOS

The pseudo-static factor of safety for the dam slopes was determined under three different conditions:

(1) Effective stress analysis, using c'=0 kPa for all the soil types (unless specific data was available from laboratory tests), and ϕ' as obtained from the 3D model of effective friction angle of the dam (using CPT correlations). This condition is termed here as Case 1;

(2) Effective stress analysis using effective friction angle (similar to the previous case), but using small value of c' (5 kPa to 10 kPa) for layers of clayey soil. This condition is termed here as Case 2; and

(3) Effective stress analysis using effective friction angle and c'=0 for the sandy soil (coarse-grained materials) and soils above phreatic surface, and undrained shear strength parameters (s_u) for the saturated clayey soil layers present below phreatic surface, since soils of low permeability are assumed to exhibit undrained behavior during seismic events (Babu et al. 2007; Duncan et al. 2014; FEMA 2005; Newmark 1965; Seed 1979; USSD 2007). This condition is termed as Case 3.

For all three cases, an increase in excess pore water pressure was not estimated during earthquake shaking, to be consistent with the requirements of pseudo-static analysis.

6.4.4.3 Decoupled permanent-displacement analysis

The serviceability of the dam depends on the deformation incurred by a slip surface during seismic events (Chowdhury et al. 2009; Kramer and Smith 1997; Mansour 2016; Park 2016). Hence, it was important to determine the permanent deformation incurred by the sliding mass, besides computing the pseudo-static FOS. The decoupled permanent-displacement analysis was performed for both the upstream and downstream slopes, for all the eight sections of the dam. Previous studies have shown that this decoupled approximation can lead to a conservative estimation of

the permanent-displacement, especially when the frequency of base excitation is close to the natural frequency of the earthen structure (Gazetas and Uddin 1994; Kramer and Smith 1997; Lin and Whitman 1983). However, this over-prediction of permanent deformation was found to be insignificant when compared to the other associated uncertainties in the seismic response and sliding block analysis (Kramer and Smith 1997).

Two different earthquake time-history records, having significantly different predominant frequencies were used as base excitations for permanent-displacement analysis. Due to the absence of strong motion data recorded at EM dam, earthquake records recorded at Enola, AR and Norfolk, OK during Arkansas Earthquake on 26th June, 1982 and Oklahoma Earthquake on 7th November, 2016, respectively were modified and used for this study. These two earthquakes were specifically selected because the Enola EQ had a predominant frequency close to the natural frequency of the dam sections (Figure 5-20), whereas the Norfolk EQ had a frequency that is distinct from that of the dam. The earthquake time-history data was modified and scaled to a peak acceleration of 0.3*g*, based on the probabilistic seismic hazard analysis (Caballero 2017; Petersen et al. 2017). The time-history data and the frequency of the earthquakes are shown in Figure 6-3. In order to incorporate the effect of non-linear behavior, an equivalent linear type of analysis was performed. The modulus degradation and variation of damping with

strain were specified based on the effective mean confining pressure and plasticity index of different soil types (FEMA 2005; Ishibashi and Zhang 1993).

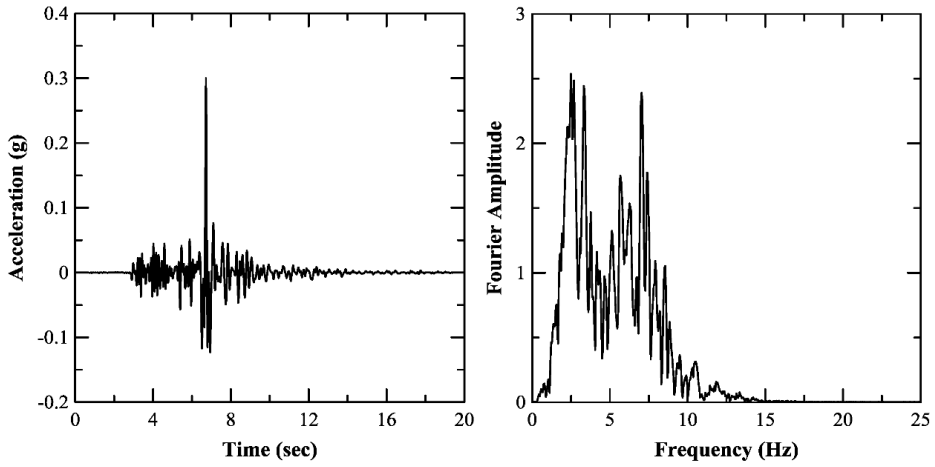

(a)

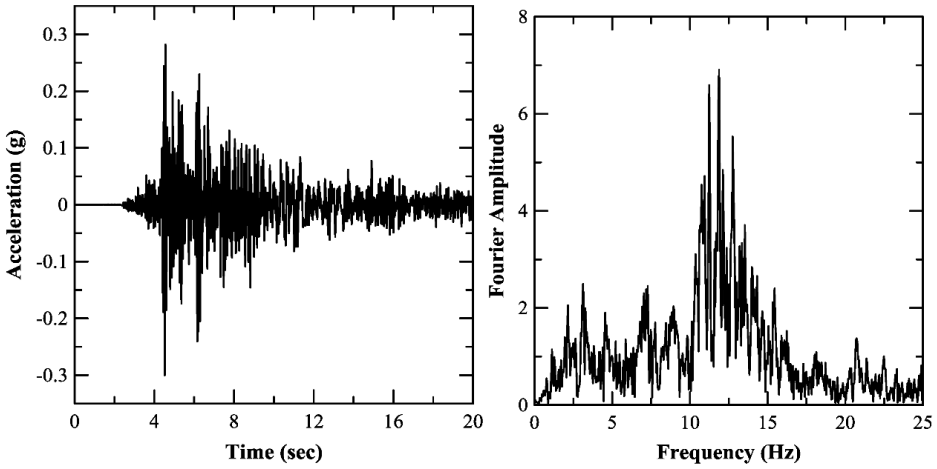

(b)

Figure 6-3: Modified earthquake time-history (PGA = 0.3*g*) and FFT data for (a) Enola and (b) Norfolk

6.4.4.4 Reliability-based analysis

The reliability analysis was performed for the critical slip surfaces determined from the Case-3 analysis, for both the upstream and downstream slopes of the dam sections. The mean values of the shear strength parameters were kept same as that used for the deterministic analysis. The standard deviation for effective friction angle of different soil types were assessed based on limited number of test results, following the method outlined by Chakraborty et al. (2017) (Appendix B). The population standard deviations of effective friction angle, estimated for different soil types, are reported in Table 6-3. The estimated values were found to lie within the range of standard deviation values recommended by Duncan (2000). The coefficient of variation for undrained shear strength was assumed to be 30% (Duncan 2000) due to the lack of laboratory test data. The standard deviation of undrained shear strength was obtained by multiplying 0.3 with the respective assigned mean values of undrained shear strength. Both the friction angle and undrained shear strength were assumed to follow a normal distribution, a reasonable assumption for most geotechnical engineering problems (Baecher and Christian 2005; Chakraborty et al. 2017a). The reliability index and probability of failure were obtained with respect to the pseudo-static factor of safety, by performing 35,000 cycles of Monte Carlo simulations for different values of horizontal seismic coefficients. The process was repeated for all of the sections including upstream and downstream slopes and the performance indices of the

different dam sections was classified from hazardous to highly safe, as recommended by USACE (1998).

Table 6-3: Standard deviation of effective friction angle for different soil types

Soil type	lean clay with sand	sandy lean clay	fat clay	sandy silt	clayey sand
Average friction angle (in degrees)	25.9	26.6	19.1	35.3	27.7
Number of samples tested	13	17	7	2	3
Chakraborty (2017) Population std. dev.	2.59	2.66	3.82	1.76	1.38
Lower limit of std. dev. as per Duncan (2000)	0.52	0.53	0.38	0.71	0.55
Upper limit of std. dev. as per Duncan (2000)	3.37	3.45	2.48	4.58	3.60

6.4.4.5 Liquefaction assessment and dynamic stability analyses

Cyclic liquefaction

The analysis was performed using the same finite element based software package, used for performing the pseudo-static and permanent deformation analyses. Drained shear strength parameters were assigned to the soil layers above the phreatic surface, for the stability analysis. Whereas, the clay layers in the core of the dam were assigned undrained shear strength parameters for the dynamic analysis. The saturated regions of the sand shells are expected to be subjected to undrained loading conditions during earthquake events. Hence, effective stress analysis with estimated excess pore water pressure was suitable for the saturated upstream and downstream sand shell layers, and for the sand layers in the

foundation. Cyclic liquefaction analysis requires suitable constitutive models and relations which can predict the increase in pore water pressure, in the sand layers, during seismic shaking simulations. Undrained cyclic triaxial tests on undisturbed samples of sand are required to calibrate the model based on the increase in pore water pressure and associated permanent strains, with each cycle of loading (Seed, 1979). In the absence of such test results, advanced constitutive models such as UBCSand or PM4sand were not used in the present study. Instead, the procedure outlined by Lee and Albaisa (1974) and De Alba et al. (1976) has been used to estimate the excess pore water pressure, in the sand layers (equation 6.1 and 6.2). This method is widely used in practice (Dash and Sitharam 2009; Krahn 2004a; Polito et al. 2008) and hence adopted in this study.

$$r_u = \frac{1}{2} + \frac{1}{\pi}\ sin^{-1}\left[2\left(\frac{N}{N_L}\right)^{\frac{1}{\alpha}} - 1\right] \quad (6.1)$$

$$\Delta u = r_u\ x\ \sigma'_3 \quad (6.2)$$

where, N is the equivalent number of uniform cycles for laboratory tests at 0.65 τ_{max} for a given magnitude of earthquake (Figure 2-28); N_L is the number of cycles required to cause liquefaction corresponding to different shear stress ratios (cyclic number function, Figure 6-4); $\alpha = 0.7$; Δu is the change in pore water pressure and σ'_3 is the effective confining stress, obtained from initial static analysis.

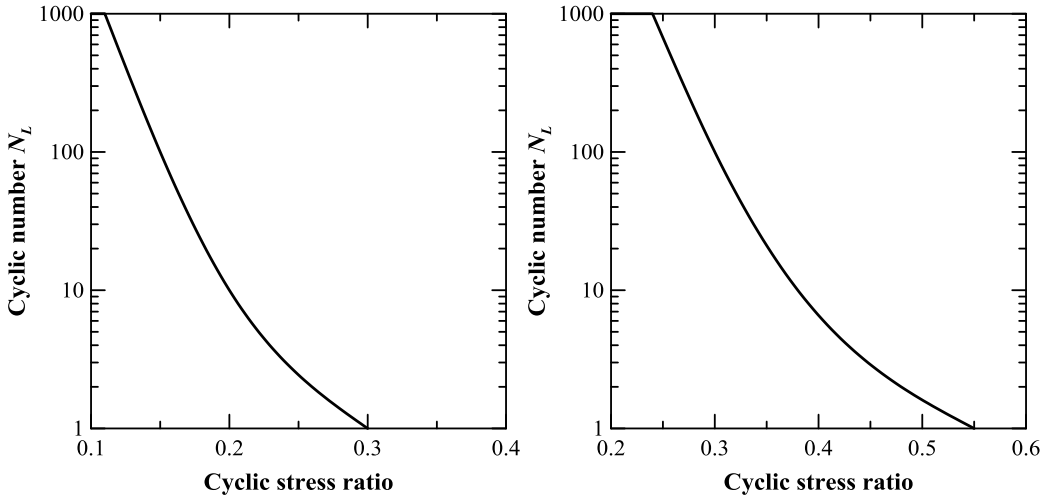

Figure 6-4: Cyclic number function for (a) loose sand and (b) medium dense sand

The cyclic number function is supposed to be determined from laboratory test on undisturbed samples. However, due to lack of test results, the cyclic number functions have been adopted from the literature based on the type of sand (dense, medium dense, medium loose and loose) observed from bore log information (Figure 6-4). The analyses were performed for eight different sections of the dam, where shear wave velocity profiles were available. Two different earthquake magnitude conditions were considered (a) $M < 6.5$ ($N = 4$) and (b) $M = 7$ ($N = 10$) (Figure 2-28). For each earthquake magnitude scenarios, eight different earthquake time-history data were used as the base excitation (Table 6-4). Due to the absence of strong motion records registered at the dam site, earthquake time-history data from different earthquakes in Oklahoma and Arkansas were used in this study. The data were selected to encompass a wide range of peak accelerations and frequency contents, with some earthquakes having a predominant frequency close to the

natural frequency of the dam (Figure 5-20). However, unlike the Newmark deformation analysis, the earthquake time-history data were not modified and scaled to peak acceleration of 0.3g. It is expected that the probability of having an earthquake with a peak acceleration of 0.3g and that earthquake excitation causing a resonance condition will be extremely low. Such a rare event may cause extensive liquefaction of sand layers, in case the sand layers in the field are susceptible to liquefaction. The time-history data and the frequency contents of the different earthquakes are shown in Figure 6-5.

Table 6-4: Earthquake data used for analysis

Earthquake details	**Designated as**
Component 360; Peak acc. = 0.001g; Station Dexter (Oklahoma); Date 2011-11-06	A
Component 0; Peak acc. = 0.035g; Station Enola (Arkansas); Date 1982-07-05	B
Component 90; Peak acc. = 0.038g; Station Mehan (Oklahoma); Date 2016-11-07	C
Component 0; Peak acc. = 0.04g; Station Enola (Arkansas); Date 1982-06-26	D
Component 360; Peak acc. = 0.05g; Station Mehan (Oklahoma); Date 2016-11-07	E
Component 90; Peak acc. = 0.097g; Station Enola (Arkansas); Date 1982-07-05	F
Component 90; Peak acc. = 0.146g; Station S Brethren Rd. (Oklahoma); Date 2016-11-07	G
Component 90; Peak acc. = 0.402g; Station CUH Airport (Oklahoma); Date 2016-11-07	H

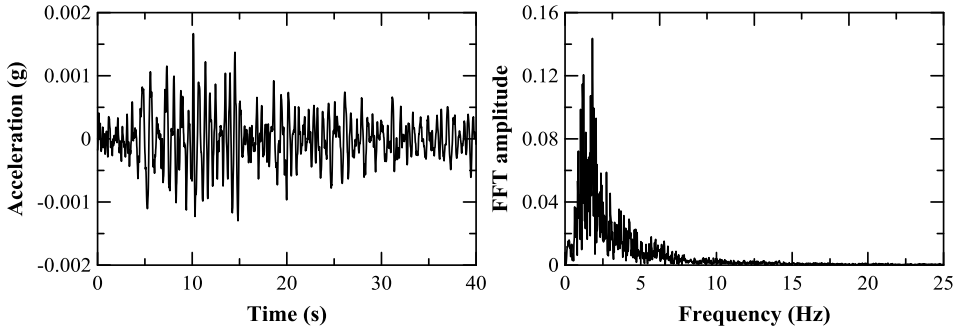
Acceleration (g)
0.002
0.001
0
-0.001
-0.002
0
10
20
30
40
Time (s)
FFT amplitude
0.16
0.12
0.08
0.04
0
0
5
10
15
20
25
Frequency (Hz)

(a)

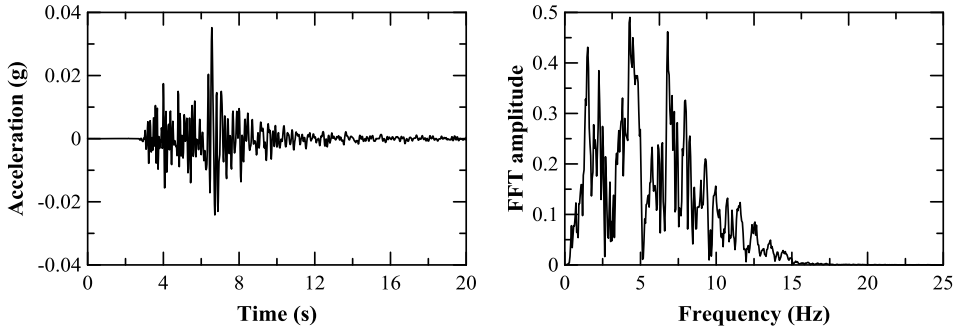
Acceleration (g)
0.04
0.02
0
-0.02
-0.04
0
4
8
12
16
20
Time (s)
FFT amplitude
0.5
0.4
0.3
0.2
0.1
0
0
5
10
15
20
25
Frequency (Hz)

(b)

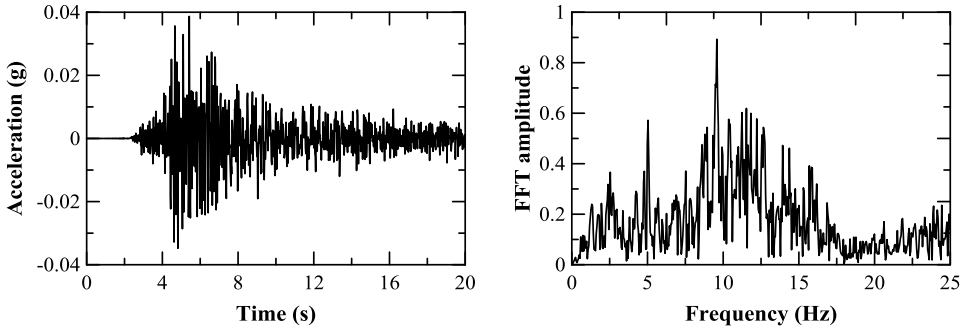
Acceleration (g)
0.04
0.02
0
-0.02
-0.04
0
4
8
12
16
20
Time (s)
FFT amplitude
1
0.8
0.6
0.4
0.2
0
0
5
10
15
20
25
Frequency (Hz)

(c)

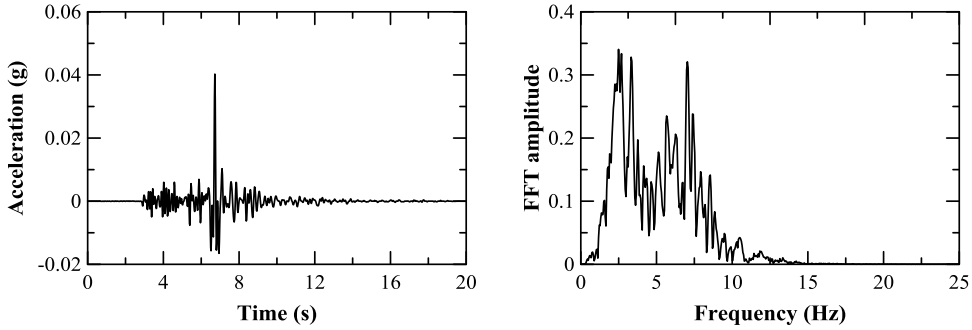
Acceleration (g)
0.06
0.04
0.02
0
-0.02
0
4
8
12
16
20
Time (s)
FFT amplitude
0.4
0.3
0.2
0.1
0
0
5
10
15
20
25
Frequency (Hz)

(d)

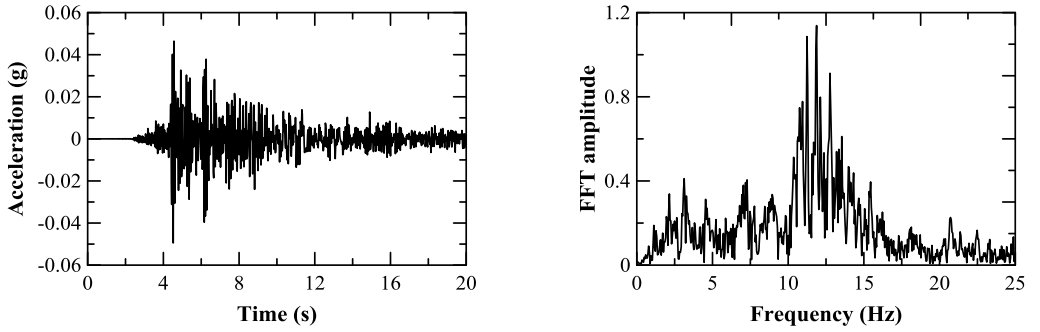

(e)

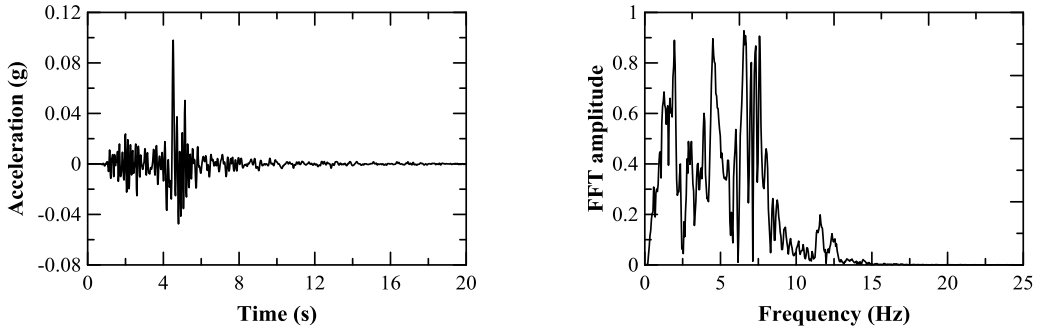

(f)

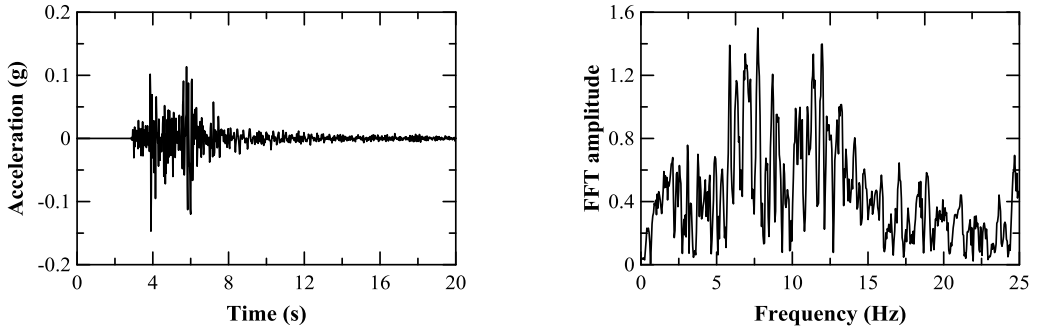

(g)

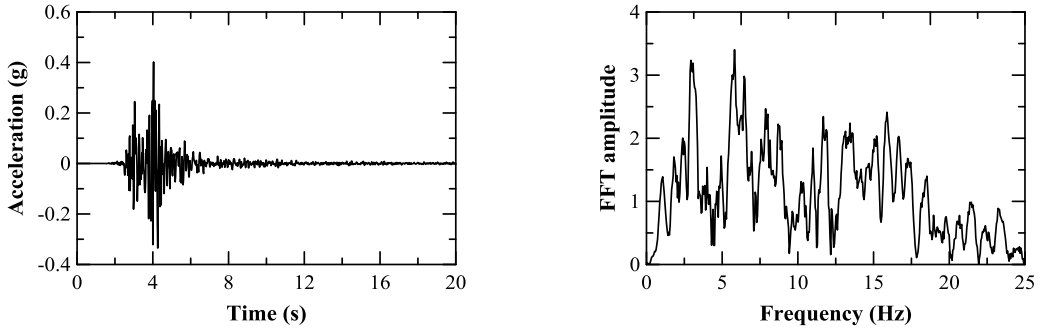

(h)

Figure 6-5: Earthquake time-history and frequency content data for earthquakes (a) A, (b) B, (c) C, (d) D, (e) E, (f) F, (g) G and (h) H

Flow liquefaction analysis

Flow liquefaction is not commonly observed in the field and applies to loose cohesion-less soils which exhibits strain softening behavior during undrained loading (Kramer 1996; Marcuson 1978; Robertson et al. 1995). This occurs when the in-situ static shear stress in loose sands is greater than the undrained steady-state shear strength. The undrained steady-state strength is the resistance offered by the soil at high strain levels during undrained shearing (Castro et al. 1992; Finno et al. 1996; Krahn 2004a; Kramer 1996; Thevanayagam 1998). Soils susceptible to flow liquefaction has a "collapsible soil-grain structure" and experiences significant strength loss on touching the collapse point (Krahn 2004a). The flow failure is also accompanied by high strain and deformation. The flow liquefaction can have catastrophic consequences, and hence it was necessary to evaluate the chances of flow liquefaction of the foundation sand layers. In the absence of triaxial test results on undisturbed sand samples collected from the foundation layers, state parameter was used as a measure of studying the contractive behavior of the sand. The state parameter is defined as the difference in the void ratio in the field and the critical state void ratio (Robertson and Cabal 2014). A positive value of state parameter suggests contractive behavior of the sand, with chances of flow liquefaction. The state parameter of the foundation sand layers was hence determined using the CPT data available along the downstream toe of the dam. The

normalized cone resistance and normalized friction ratio were plotted on Figure 6-6 to check if the state parameter was greater than 0.

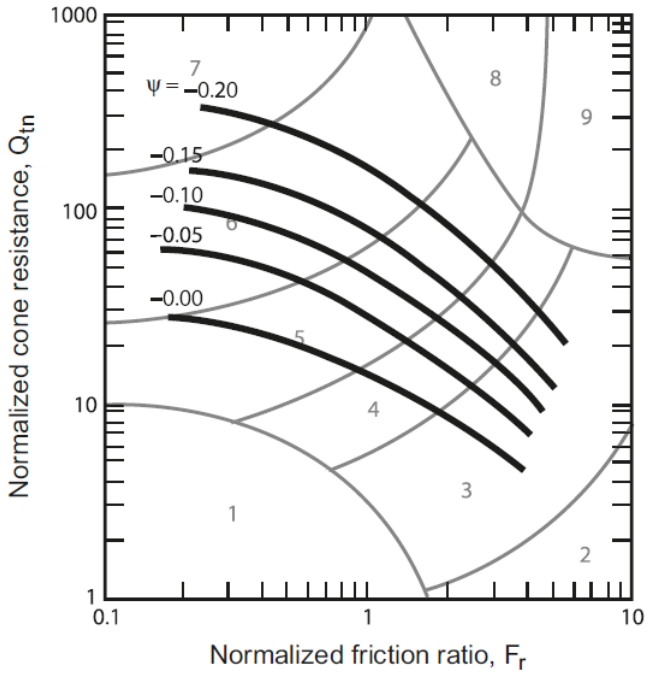

Figure 6-6: Determination of state parameter based on CPT data (after Robertson and Cabal 2014)

6.5 Analysis and discussion of results

This section presents the static and pseudo-static factor of safety results, along with the permanent deformation incurred by the critical slip surfaces of different segments of the dam, when subjected to the two earthquake events (scaled to 0.3g) considered in this study. The 2D sections used for the analysis are represented by the respective station numbers. The analysis was performed for those sections where SASW test results were available, namely, Stations 5, 9, 14.5, 18, 22, 27, 33 and 39. Station 5 and 9 lies in Zone A and B respectively, whereas Stations 14.5 to

22 belong to Zone C_1 and the rest of the stations fall in Zone C_2. The location of a particular station can be determined by multiplying the station number by 100 ft (or 30.48m); the station 0 is located at the start of the dam (left/west end of the dam in Figure 6-1).

The soil behavior type (SBT), effective friction angle (ϕ') and undrained shear strength (s_u) values, used for assigning the material properties to the FEM model of the dam, are presented for the respective sections. Additionally, the as-built drawings used to construct the model of the dam section, the location of the phreatic surface for long-term steady state condition and the critical deep slip surfaces are also provided. Typical results are presented in detail for sections belonging to each zone. The analysis results for all of the eight sections are also summarized and presented in graphical format. The dynamic stability and liquefaction analyses results are provided at the end of this section.

6.5.1 Static and pseudo-static FOS of typical sections

Zone A: Station 5

Station 5 is located at a distance of 152 m (500 ft) from the left (west) end of the dam. The section lies in Zone A, which was constructed by wetting and rolling the embankment fill (Figure 6-1). Due to the nature of construction, this zone does not have a distinct core or shell. Hence the model of the dam was constructed by dividing the body of the dam into horizontal layers, as per the shear wave velocity

profile. The variation of SBT, s_u, ϕ' profile of the section, the as-built drawings and the critical slip surfaces of the upstream and downstream slopes, whose FOS were determined, are shown in Figure 6-7.

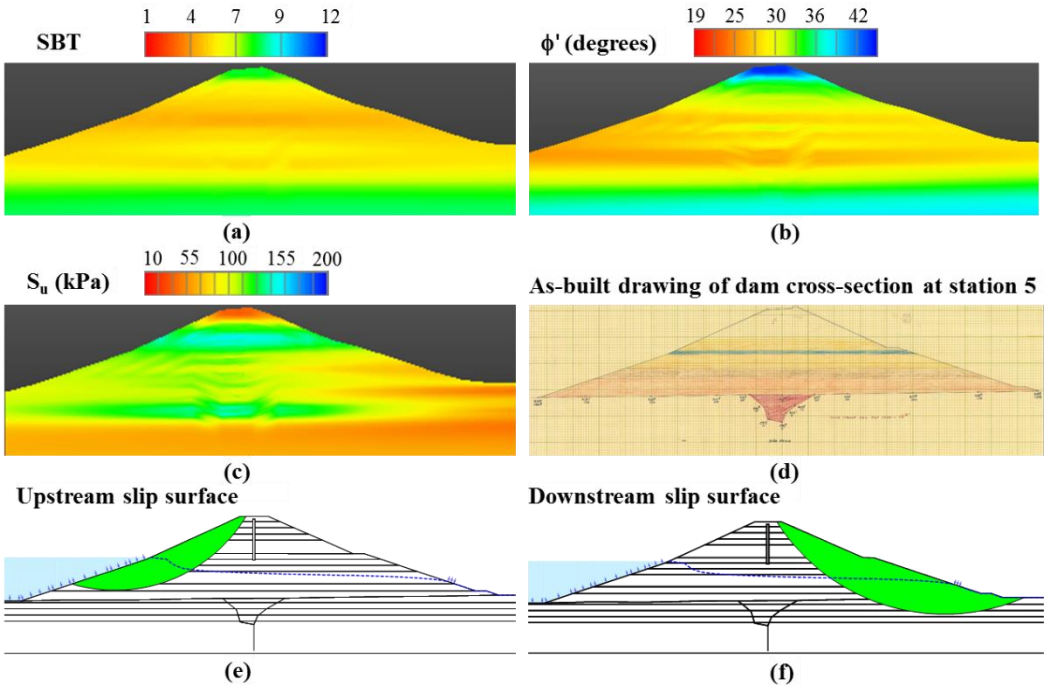

Figure 6-7: 2D sections of (a) SBT, (b) effective friction angle, (c) undrained shear strength, (d) as-built drawings, (e) upstream critical slip surface and (f) downstream critical slip surface at Station 5

Figure 6-8 presents the variation of pseudo-static FOS with horizontal seismic coefficient, for the upstream and downstream slopes at station 5. No bore log information or laboratory test results on extracted soil samples were available for this section; hence the stability analysis for Case-1 was performed with zero effective cohesion, resulting in low values of static FOS and yield coefficient, especially for the downstream slope. The Case 3 analysis using s_u values for the

clayey soil layers resulted in unrealistic high FOS values. The static FOS (seismic coefficient = 0) for Cases 1, 2 and 3 for the upstream and downstream slopes are 1.58, 1.64 and 4.25; and 1.22, 1.43 and 3.47, respectively. The yield coefficients for the slopes are shown in Figure 6-8.

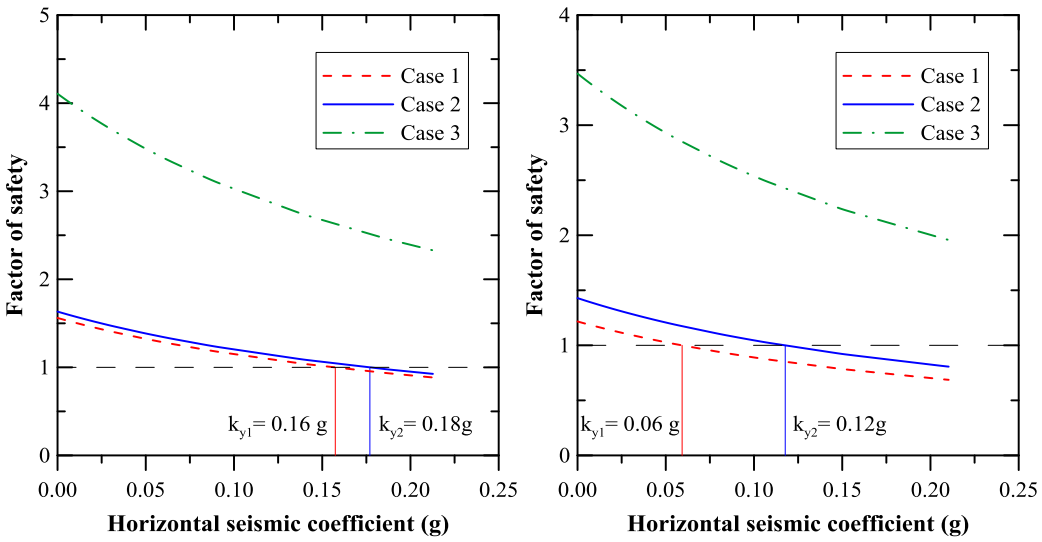

Figure 6-8: Pseudo-static FOS for station 5 (a) upstream slope and (b) downstream slope

Zone B: Station 9

Station 9 is located in Zone-B of the dam, at a distance of 274m (900 ft) from the left (west) end. Unlike Station-5, this section has a shell made up of wetted and rolled coarse-grained soil and a hydraulic-fill core, primarily consisting of fine-grained soil. Since the CPTs were conducted along the crest and downstream toe of the dam, the properties of the shell were not assigned using the visualization models of the respective parameters; rather the properties were assigned solely based on limited information obtained from bore logs/borings on the slope. The 2D models

of SBT, s_u and ϕ' were primarily used to assign the properties along the core of the dam and the wetted and rolled section above the core. The core of the dam is made up of clay to clayey silt (SBT 4 to 6), with ϕ' ranging from 20 to 27 degrees. The variation of different soil properties along with the as-built drawings, demarcating the shell and the core of the dam is shown in Figure 6-9.

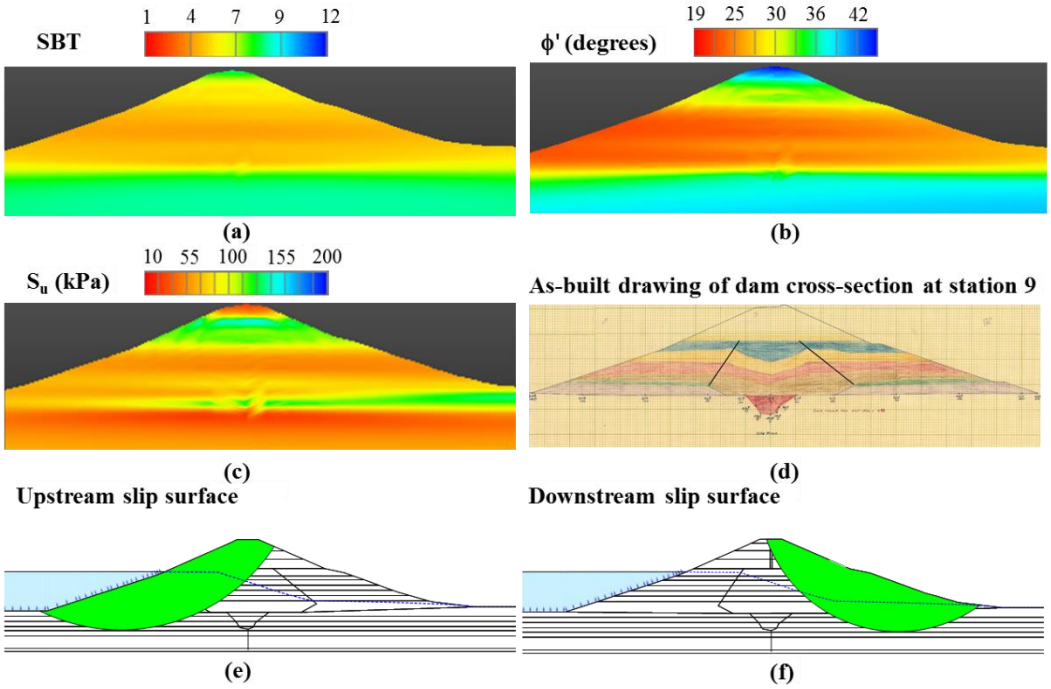

Figure 6-9: 2D sections of (a) SBT, (b) effective friction angle, (c) undrained shear strength, (d) as-built drawings, (e) upstream critical slip surface and (f) downstream critical slip surface at Station 9

Figure 6-10 presents the variation of pseudo-static FOS with horizontal seismic coefficient for the upstream and downstream slopes of the dam at station 9. The static FOS for the upstream and downstream slopes for Case 1, 2 and 3 were 1.45,

1.54 and 2.21; and 1.41, 1.49 and 1.82, respectively. Direct shear tests on a representative undisturbed sample, collected from the downstream toe, at a depth of 5m, revealed an effective cohesion of 30 kPa for a fat clay layer. Hence this value was assigned to the fat clay layer in the foundation section of Case-1 and Case-2 analyses. The presence of the fat clay layer can also be observed in the 2D model of s_u values, as represented by green layer near the downstream toe, with s_u value of 120 kPa (Figure 6-9c). The Case-3 static FOS for station 9 was less than that of Station 5 because of the difference in s_u values, as observed on comparing Figure 6-7c and 6-9c.

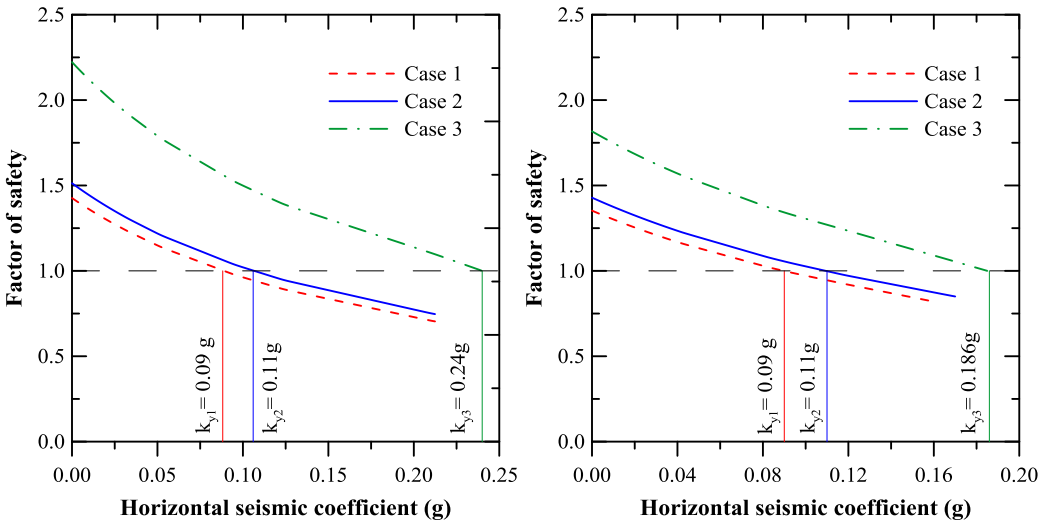

(a) (b)

Figure 6-10: Pseudo-static FOS for station 9 (a) upstream slope and (b) downstream slope

Zone C_1: Station 14.5

Station 14.5 marks the beginning of Zone C_1, which has both the core and shell constructed by hydraulic-fill method, with the aid of starter dykes. A significant number of direct shear and triaxial test results of undisturbed samples were available and hence used for FOS determination (Case-1 and Case 2). A layer of lean clay with sand (c'=33 kPa, $\phi' = 20°$ from CD test) and a layer of sandy lean clay (c'=52kPa, $\phi' = 18°$ from DS test) were identified from the bore log, at a depth of 12.5m and 15.5m from the crest of the dam, respectively. Bore logs available at the downstream slope and near the toe of the dam suggests the presence of a layer of fat clay (c'=62kPa, $\phi'=14°$ DS test) overlain by a layer of over-consolidated lean clay (c'=167kPa, $\phi'=12°$ DS test) at the foundation of the dam (downstream side). Due to the availability of this information, these layers were assigned with the respective effective cohesion and friction angle values. The presence of clayey layers near the downstream foundation, possessing high cohesive strength can also be observed from the 2D slice depicting the variation of SBT and s_u values for this section (Figure 6-11a and c). Presence of clayey soil layers in the downstream toe of the dam is not apparent from the visualization model depicting the variation of effective friction angle values (Figure 6-11b); nevertheless, effective friction angle values obtained from DS test were assigned for these layers.

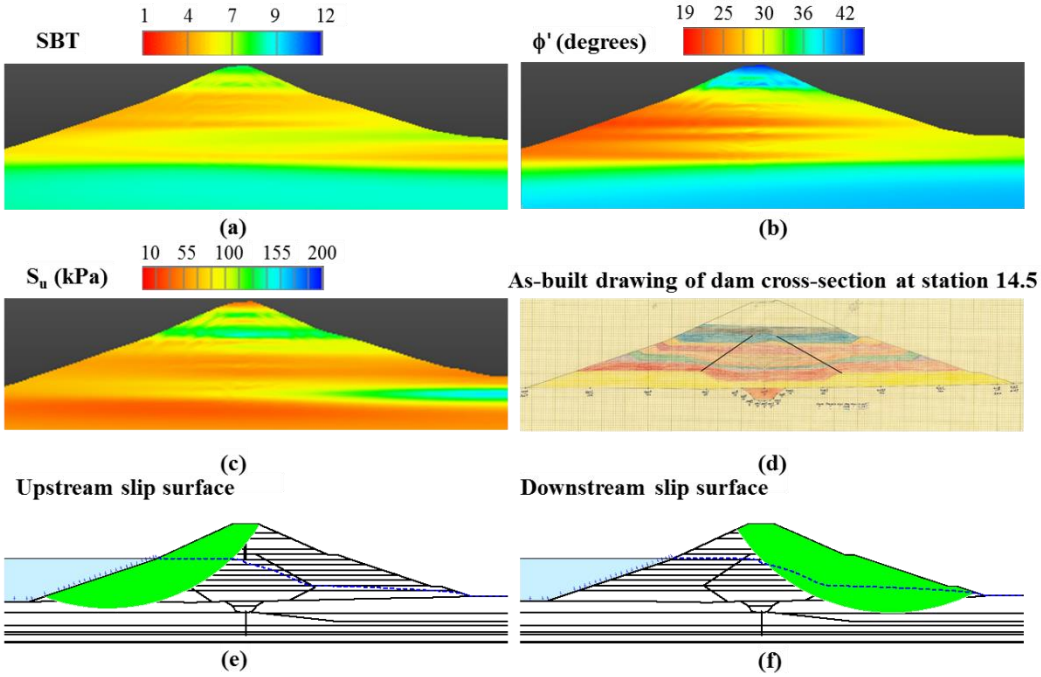

Figure 6-11: 2D sections of (a) SBT, (b) effective friction angle, (c) undrained shear strength, (d) as-built drawings, (e) upstream critical slip surface and (f) downstream critical slip surface at Station 14.5

The pseudo-static FOS for Case 1 and Case 2 were almost similar for the downstream slope due to the use of high effective cohesion values, obtained from laboratory test results (Figure 6-12b). The pseudo-static FOS of the downstream slope for Case-3, was significantly higher than that obtained for Case-1 and Case 2, due to the high value of s_u for the foundation clay layers (near downstream toe). The static FOS for the upstream and downstream slopes for the analysis performed using three different strength parameters are 1.41, 1.54 and 1.6; and 1.73, 1.75 and 2.12, respectively. The static FOS of the downstream slope for Case 1 and Case 2 were significantly higher than the corresponding values for Station 5 and 9 due to

the availability of information about the effective cohesion of the foundation clay (downstream side).

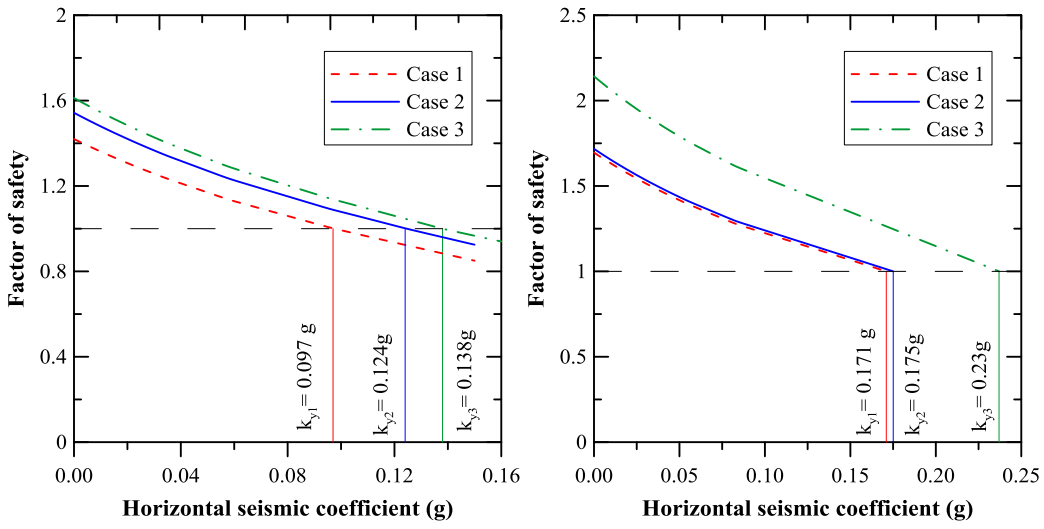

(a) (b)

Figure 6-12: Pseudo-static FOS for station 14.5 (a) upstream slope and (b) downstream slope

Zone C_2: Station 27

Station 27 belongs to Zone C_2, which is similar to Zone C_1, with both the shell and core constructed by hydraulic-fill method of construction. A few laboratory test results for effective cohesion and friction angle were available and hence used for analysis. Direct shear test results revealed that a sandy lean clay layer, at a depth of 12.5m from the crest, had an effective cohesion of 45 kPa and effective friction angle of 20°. Triaxial test result on an undisturbed sample, collected from a sandy lean clay layer, at a depth of 3m from the ground surface, at the downstream toe of the dam showed an effective friction angle of 32° and zero effective cohesion. These strength parameters led to a higher pseudo-static coefficient and static FOS

of the critical slip surfaces for Case-1 and Case-2 analysis. The pseudo-static FOS for Case 3 analysis was found to be higher than Case-1 and Case-2 analysis for the upstream slope due to the presence of layers with high s_u values (Figure 6-13c). Contrarily, the s_u values were found to be low for downstream toe of the dam, resulting in lower pseudo-static FOS (Figure 6-14). The static FOS for the upstream and downstream slopes for the analysis performed using three different strength parameters are 1.63, 1.75 and 1.73; and 1.55, 1.69 and 1.43, respectively.

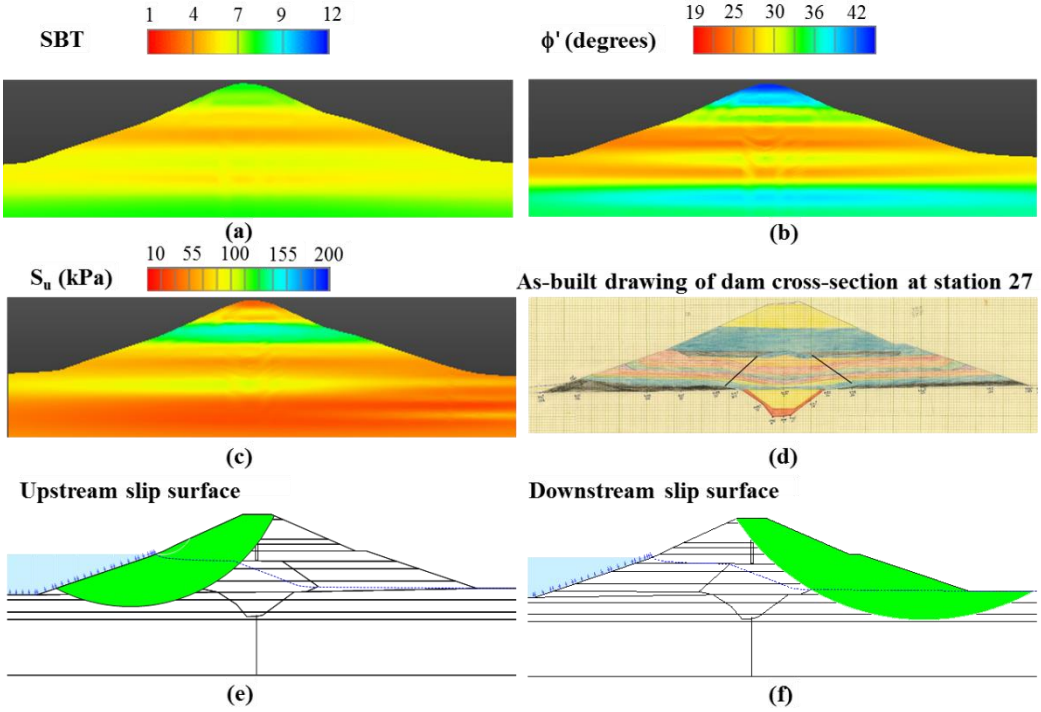

Figure 6-13: 2D sections of (a) SBT, (b) effective friction angle, (c) undrained shear strength, (d) as-built drawings, (e) upstream critical slip surface and (f) downstream critical slip surface at Station 27

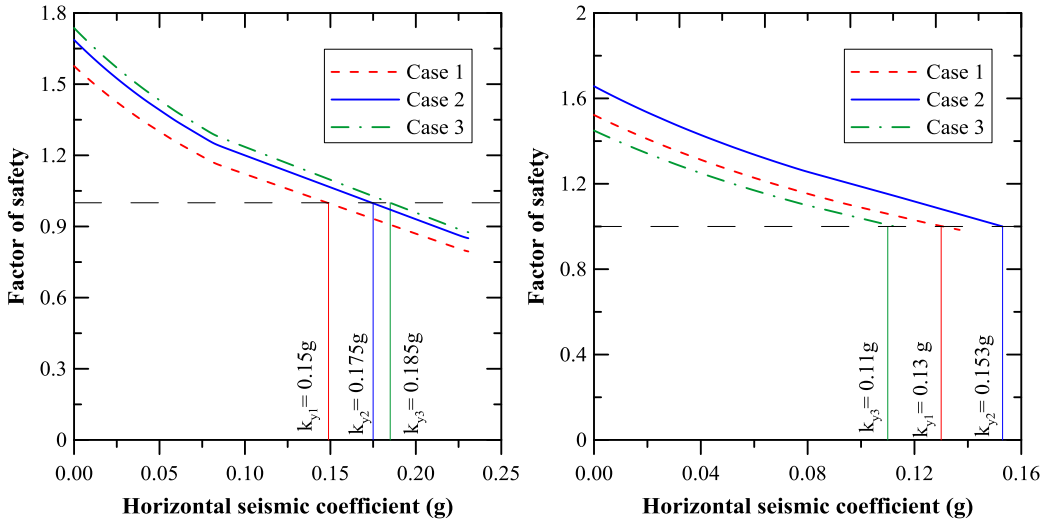

(a) (b)

Figure 6-14: Pseudo-static FOS for station 27 (a) upstream slope and (b) downstream slope

Zone C_2: Station 33

Station 33 had both its shell and core constructed by hydraulic-fill method; additional granular fill materials were placed on the upstream and downstream toe of the dam after construction. These additional fill material can be observed in Figure 6-15. Triaxial and direct shear test results on undisturbed samples were available for a fat clay layer and layer of lean clay with sand, located at a depth of 12m below the crest of the dam and 14m below the surface of the downstream fill material, respectively. The effective cohesion intercept of 19 kPa and 40 kPa, and effective friction angle of 22° and 20°, were used for the respective layers, for Case-1 analysis. The variation of pseudo-static FOS was almost similar for three types of analysis for the critical section on the upstream slope of the dam (Figure 6-16a).

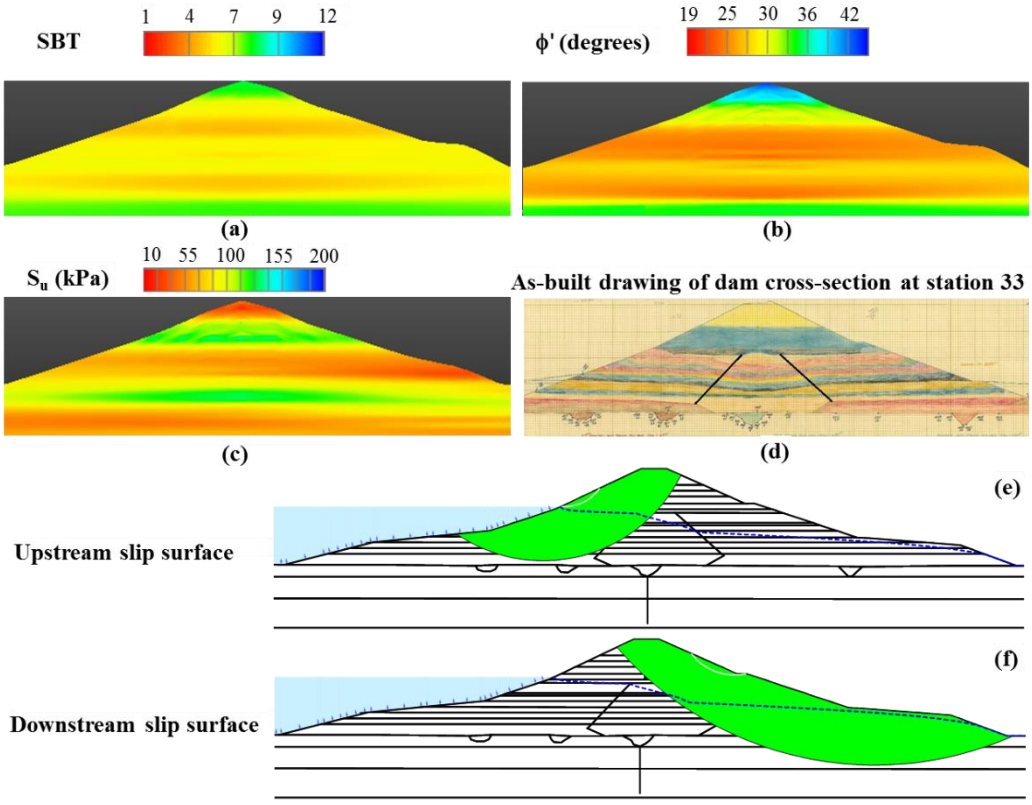

Figure 6-15: 2D sections of (a) SBT, (b) effective friction angle, (c) undrained shear strength, (d) as-built drawings, (e) upstream critical slip surface and (f) downstream critical slip surface at Station 33

Contrarily, the pseudo-static FOS for the Case-3 analysis for the downstream slope was found to be significantly higher than that obtained by Case-1 and Case-2 analysis. The rationale behind this can be comprehended on observing the location of critical slip surfaces shown in Figure 6-15e and f. The critical slip surface of the downstream slope can be observed to pass through the foundation clay layer, where high values of s_u are assigned for the undrained analysis. However, the most part of the upstream critical slip surface passes through the sandy shell, where effective friction angle is used even for Case-3 analysis, instead of the undrained shear

strength. The static FOS for the upstream and downstream slopes for the analysis performed using three different strength parameters are 1.91, 1.95 and 1.93; and 1.75, 1.78 and 2.15, respectively. The FOS for both the slopes were higher than that observed for the other sections of the dam due to high s_u values (when compared to other sections) and due to the presence of extra fill materials near toe of the dam; hence improving the stability of the slopes.

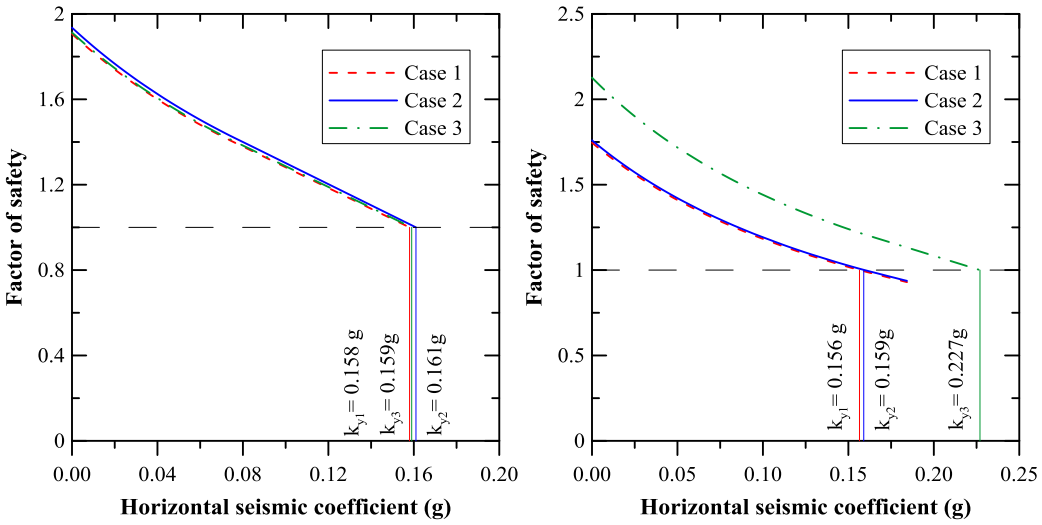

Figure 6-16: Pseudo-static FOS for station 33 (a) upstream slope and (b) downstream slope

6.5.2 Static FOS and yield coefficient of the dam

Although there were some surficial slip-surfaces with very low FOS, those cases were not considered as a part of this study. Only the deep slip surfaces having the lowest FOS were of interest and have been presented (USSD 2007).

Figure 6-17 and 6-18 shows the variation of the static FOS and yield coefficient, for the critical slip surfaces analyzed for different sections of the dam. The red

dashed line in both the figures denotes the FOS and yield coefficient criteria used in this study to judge the stability of the slopes. The safety criteria of FOS>1.5 and yield coefficient>0.1 were adopted based on the recommendations made by different agencies (USSD 2007).

There were some stations which did not satisfy the two criteria used for checking the safety of the sections (FOS>1.5 and yield coefficient>0.1), and those sections may be considered critical. The sections which did not satisfy the safety criteria for Case-1 analysis may not be alarming, since c' was assumed to be 0, unless laboratory test data was available. Hence, on assuming small values of c' (Case-2 analysis), most of the sections satisfied the safety criteria. The downstream slopes of Stations 18, 22 and 27 were however observed to have a FOS < 1.5 and yield coefficient < 0.1 for Case-3 analysis, and may be considered critical under earthquake conditions. The static FOS for Case-3 analysis does not have any physical significance since drained condition will prevail in an 85 years old dam, under long-term steady state seepage conditions. Nonetheless, the Case-3 analysis provides a surrogate measure of the stability of the slopes during earthquakes and is also required for performing a pseudo-static analysis.

It is important to note that the data presented in Figure 6-17 and 6-18 corresponds to the particular slip surface which had the lowest static FOS for Case-1 analysis. However, it is not mandatory for the same slip surface to have the least FOS, among

all the deep slip surfaces, for both Case-1 and Case-3 analysis. Hence it was necessary to separately determine the critical slip surface for Case-3 analysis. Moreover, studying the FOS of a single slip surface for each section of the dam does not provide any information about the remaining probable slip surfaces. Hence the FOS is represented in the following section, in terms of distribution of FOS. An approach to determine the critical sections during earthquakes is also elucidated.

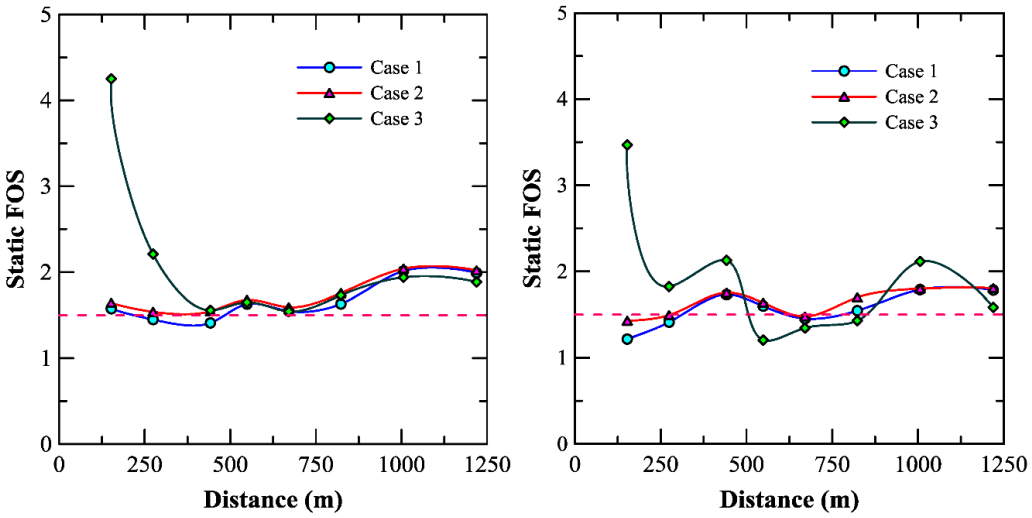

Figure 6-17: Static FOS for different stations analysed (a) upstream slope and (b) downstream slope

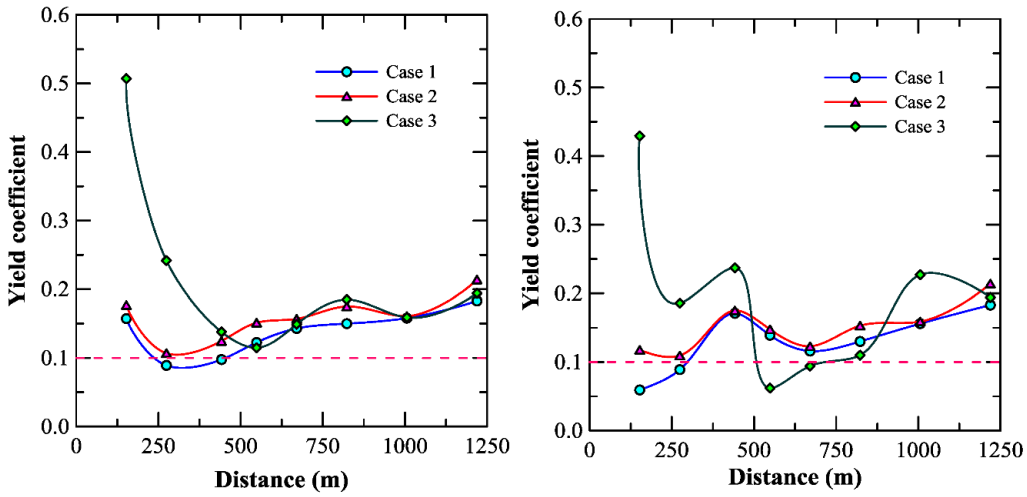

Figure 6-18: Yield coefficient for different stations analysed (a) upstream slope and (b) downstream slope

6.5.3 Determination of critical sections

6.5.3.1 Representation of FOS

An effective way of representing the static FOS was adopted to present the FOS of a slope. The method of representation is illustrated in Figure 6-19, using the FOS results obtained for the slip surfaces of downstream slope of station 27. The FOS of all the slip surfaces, ranging from the least value to a FOS of 2, were arranged in ascending order and distributed into intervals of 0.1, as shown in Figure 6-19. The percentage of slip surfaces lying within the respective range of static FOS is plotted to obtain the distribution of FOS. A slope is declared safe if the least FOS for a deep slip surface is greater than 1.5, otherwise, it is declared as critical. For the same distribution of FOS, two typical cases are shown; a safe section and a critical

section. The judgment on the safety of a section is made based on the FOS of the deep slip surface with the least FOS. For the section marked as safe, even though there was a significant portion of slip surfaces having FOS < 1.5, these were surficial slip surfaces, which were ignored for this study. The variation of FOS of the critical sections, for the upstream and downstream slopes, along the length of the dam, is presented in the following section.

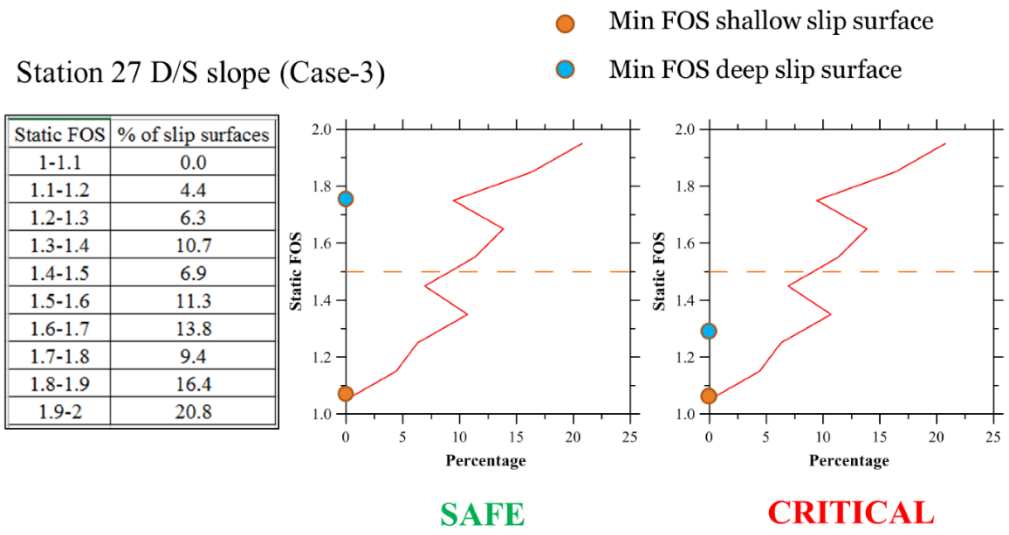

Static FOS	% of slip surfaces
1-1.1	0.0
1.1-1.2	4.4
1.2-1.3	6.3
1.3-1.4	10.7
1.4-1.5	6.9
1.5-1.6	11.3
1.6-1.7	13.8
1.7-1.8	9.4
1.8-1.9	16.4
1.9-2	20.8

Figure 6-19: Representation of FOS of a slope

The variation of FOS is presented in Figure 6-20 using the same representation technique as described in Figure 6-19. Since the FOS results for all the stations are shown at the respective location along the crest of the dam, the percentage of slip surfaces having a certain range of FOS is represented on the distance scale, for all the three analysis cases. The percentage values can be obtained for the respective

cases using the ‘Scale’ provided in Figure 6-20. The distribution of FOS for the three analysis cases are shown by black, blue and red, respectively.

6.5.3.2 Critical sections

Figure 6-17 and 6-18 suggested that all the sections satisfied the recommended FOS and yield coefficient criteria for Case-1 and Case-2 analysis. Hence, it can be reasonably concluded that the dam is safe based on static steady-state seepage conditions. The probable stability problems of a dam section, in the event of an earthquake, was hence studied for the deep slip surface with the lowest FOS for Case-3 analysis (purple line in Figure 6-20). As represented in Figure 6-19, only those sections which had the least FOS (for the deep slip surface) < 1.5 was considered critical. It can be observed that the upstream slope of Station 5, 33 and 39 had a significant percentage of slip surface below 1.5, however, the least FOS of the deep slip surface was greater than 1.5, and hence can be considered to be safe during earthquake events.

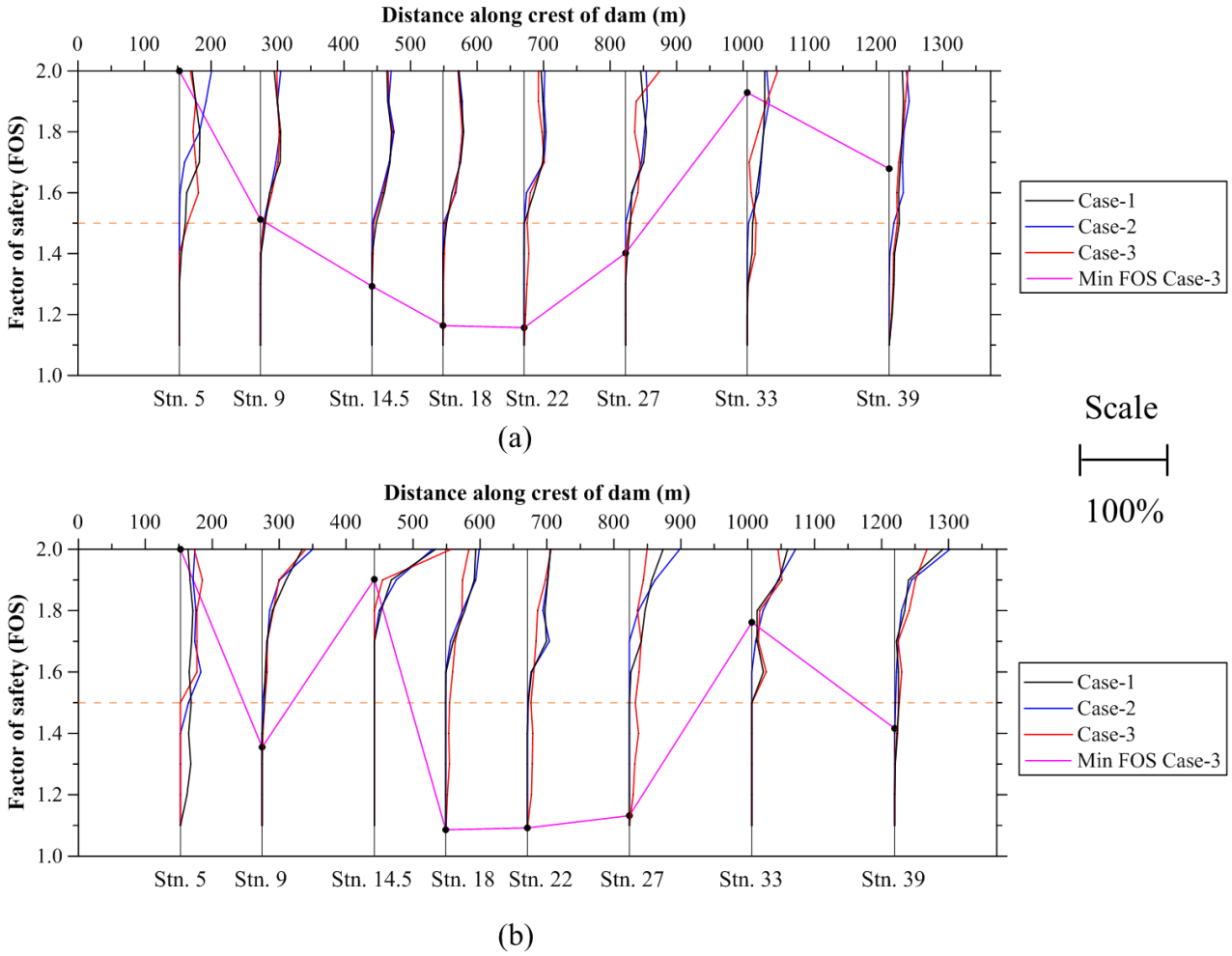

Figure 6-20: Variation of FOS along length of dam (a) upstream slope and (b) downstream slope

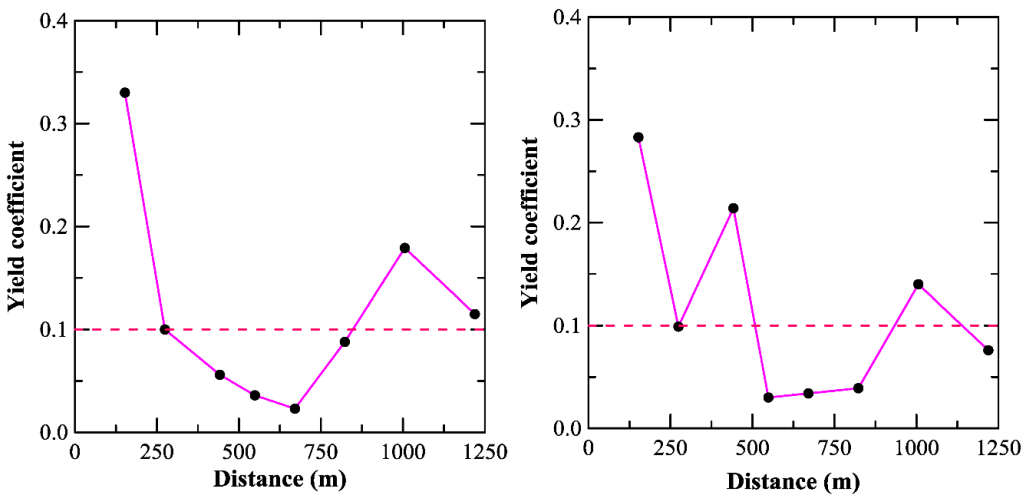

Figure 6-21: Yield coefficient for different stations analysed (a) upstream slope and (b) downstream slope for Case-3 (deep slip surface with least FOS)

The critical slip surfaces along the length of the dam can be easily determined by observing the location of the stations which have FOS < 1.5 and yield coefficient < 0.1 (Figure 6-20 and 6-21). The portion of the dam lying between Station 14.5 and 27 may become critical during earthquakes, although their static FOS and yield coefficients, for Case-1 and Case-2 analysis, were greater than 1.5 and 0.1 respectively. It is important to note that this critical region of the dam was constructed by hydraulic-fill method. During construction of the hydraulic-fill core, provision was kept for draining out the very fine-grained clay fraction of the soil after depositing the fill material in the core. This was purposefully done to reduce the construction time since such fine clay particles would have taken a significant amount of time to settle. The values of undrained shear strength for this zone of the

dam was thus less than other sections of the dam, leading to lower FOS and yield coefficient.

In this analysis, the effect of increase in pore water pressure in the shell of the dam was not incorporated, to be consistent with the requirements of pseudo-static analysis. However, in the event of earthquakes, excess pore water pressure may develop in the shell of the dam, in addition to the undrained behavior of core of the dam. Further study was thus performed to incorporate the effect of excess pore-water pressure generation. During the time-history analysis of some of the sections of the dam, there were some time instants when the average acceleration was greater than the respective yield acceleration. Although this would not mean the complete collapse of the dam, there would be some accumulated deformations. The deformation obtained by Newmark deformation analysis of the downstream and upstream slopes, for the two earthquake cases is presented in Figures 6-22 and 6-23.

6.5.4 Deformation analysis and serviceability criterion

The deformation for all the sections were found to be less than the tolerable deformation limit of 30 cm (1 ft) recommended by USACE. The high value of deformation for station 5, case 1 analysis was due to unavailability of c' data. The low yield coefficient and low static FOS resulted in such high values of deformation as compared to other sections. However, it should be noted that deformation is

associated with earthquake-induced shaking, and hence Case-1 and Case-2 deformations are not of practical significance since effective stress analysis was performed for these cases. The deformation incurred by the critical sections for Case-3 analysis was significantly higher than that observed for Case-1 and Case-2 analysis (Figure 6-22 and 6-23); nevertheless, the deformation was less than 30 cm (1 ft), and hence the dam can be assumed to be safe based on the serviceability condition. The deformation in case of Enola earthquake was found to be more than that for Norfolk since the predominant frequency of the earthquake was close to the natural frequency of the dam section, resulting in amplified vibration. The deformation of the downstream side of the dam was also observed to be more than that of the upstream slope. The load of the impounding water, which facilitates in increasing the stability of the upstream slope, lead to higher static FOS and yield coefficient, when compared to the downstream slope (Fell et al. 2005; Pinyol et al. 2008). However, the saturated upstream shell may be susceptible to cyclic liquefaction during an earthquake, and hence may become unstable. Such analysis, which includes the effect of excess pore water pressure, is presented towards the end of this chapter.

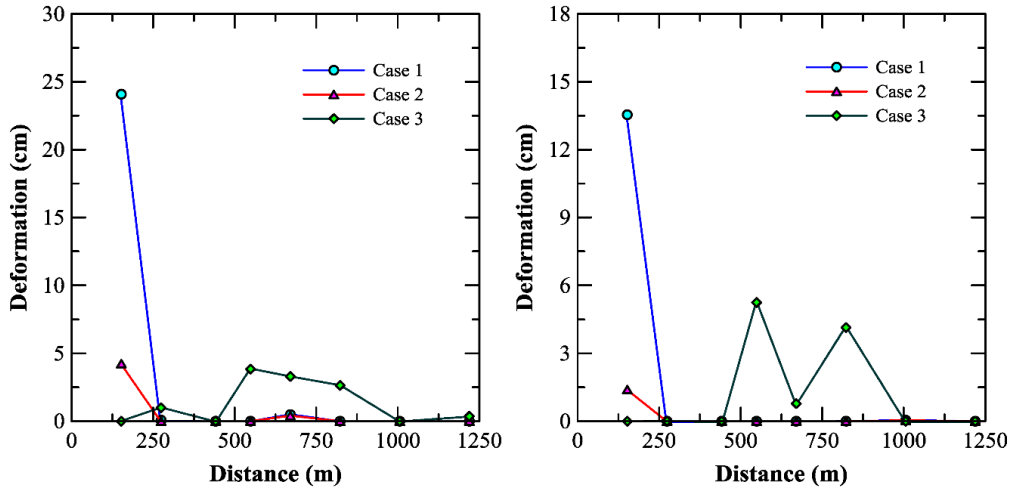

Figure 6-22: Plastic deformation of downstream slope for (a) Enola and (b) Norfolk earthquake

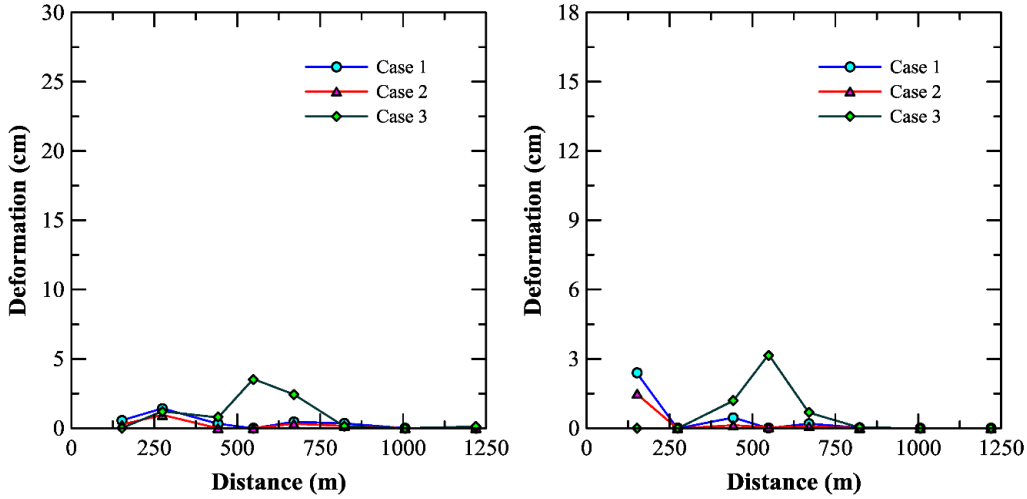

Figure 6-23: Plastic deformation of upstream slope for (a) Enola and (b) Norfolk earthquake

6.5.5 Reliability-based analysis

The analyses results presented so far were solely based on the average estimated values of the respective shear strength parameters. However, there is a significant uncertainty and variability associated with the estimation of the shear strength parameters. A reliability analysis was thus performed to incorporate the effect of such uncertainties, in the pseudo-static analysis.

Figures 6-24 and 6-25 depicts the variation of reliability index and the corresponding probability of failure with an increase in horizontal pseudo-static seismic coefficient, for the critical slip surfaces of the downstream and upstream slopes, respectively. It should be noted that term 'failure' denotes the event when the factor of safety falls below unity, for a given seismic coefficient. As mentioned earlier, the pseudo-static factor of safety less than unity doesn't necessarily imply a catastrophic failure of the dam. The reliability index can be observed to decrease following a perfect linear trend, with the increase in seismic coefficient, for all the sections considered for the analysis. This can be attributed to the increase in the constant horizontal body force considered in the pseudo-static analysis, which affects the stability of the structure and reduces the mean value of factor of safety obtained from the Monte Carlo simulations. The rate of reduction of reliability index was found to vary from one section to another. This may be due to the difference in location of the critical slips surface and changes in mean and standard deviation values of the material properties through which the critical slips surface

passes, at different sections of the dam. A shift in the mean factor of safety close to 1 implies the inclusion of a greater area of the normal distribution curve of the probability density function of the factor of safety to fall below unity. Hence, the probability of failure can be observed to drastically increase with an increase in horizontal seismic coefficient. Figure 6-24b and 6-25b suggest that the hydraulic-fill segment of the dam, from Station 14.5 to Station 27, may be considered hazardous even for very low seismic coefficients (Table 2-7). These observations are in agreement with that represented in Figure 6-20, which was used to determine the critical sections along the length of the dam. The plots shown in Figure 6-24b and 6-25b can be used to judge the expected performance level of the dam (Table 2-7) during seismic events and detect the sections which may require immediate attention and pro-active remedial measures. Furthermore, the reliability analysis provided important information on the effect of uncertainty associated with the material properties used for the analysis, on the stability of the structure.

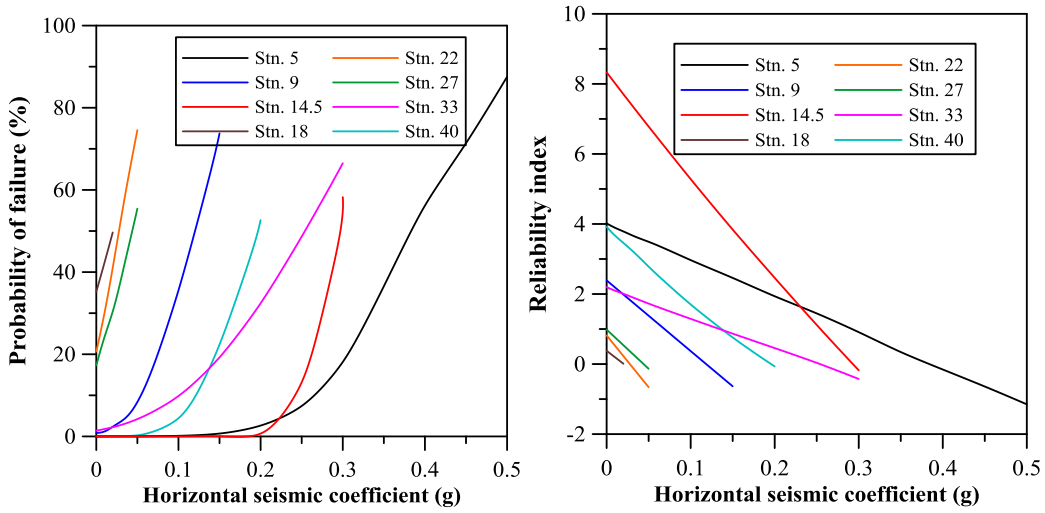

(a) (b)

Figure 6-24: Variation of (a) Probability of failure and (b) reliability index with horizontal seismic coefficient for critical downstream slope

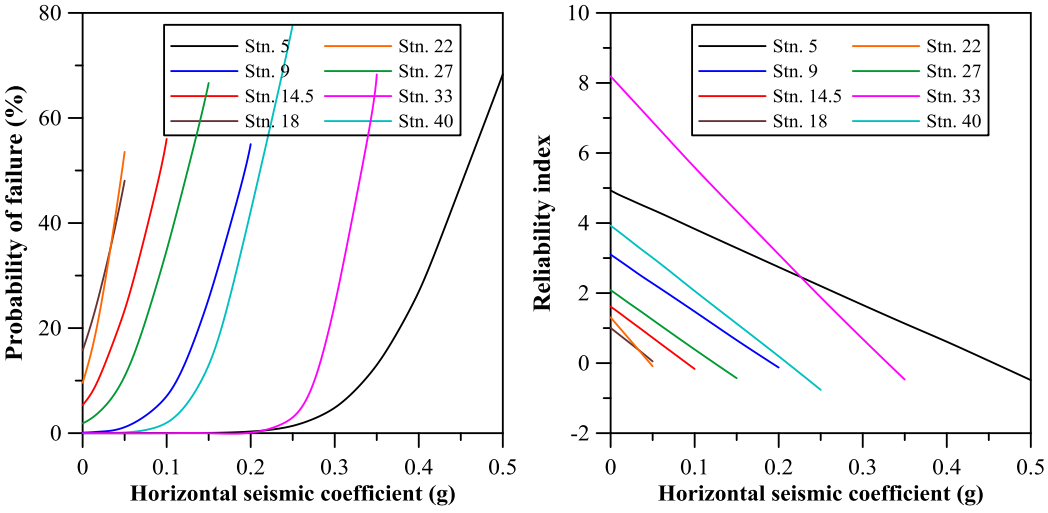

(a) (b)

Figure 6-25: Variation of (a) Probability of failure and (b) reliability index with horizontal seismic coefficient for critical upstream slope

6.5.6 Liquefaction assessment

The pseudo-static analyses, performed to evaluate the performance of different sections of the EM dam does not capture the effect of the time-dependent response of the structure during earthquake events. Moreover, the impact of accumulation of excess pore water pressure, in the sand shell or foundation sand layers is not accounted for in the analysis. Since the primary reason behind the failure of several hydraulic-fill and tailing dams around the world was attributed to the liquefaction of sand layers, it was imperative to reassess the stability of the EM Dam during probable earthquake events, including the effect of cyclic liquefaction. Unlike the Newmark deformation analysis, which was performed with two earthquake time-history data, scaled to a PGA of 0.3g, the dynamic analysis was performed using actual earthquake time-history data (unscaled), recorded at different stations in Oklahoma and Arkansas (Figure 6-5). The following section presents the cyclic liquefaction and flow liquefaction analysis results. The critical sections of the dams are determined and are compared with the findings of the pseudo-static and Newmark deformation analysis.

6.5.6.1 Cyclic liquefaction analysis

The earthquake time-history data (Figure 6-5) were selected to cover a wide range of frequency contents, to study the effect of the frequency content of the earthquake, in addition to the intensity of the earthquake excitation (peak acceleration and magnitude). For each of the eight sections, the analysis was performed for eight

different excitations, considering two different earthquake magnitudes (M<6.5 and M=7). The variation of the factor of safety with the time of earthquake was recorded for the critical slip surfaces determined from the static and pseudo-static analysis. A color coding scheme was used to represent the performance of the dam during different earthquake events. The green color was assigned when the FOS of a slip surface under consideration did not fall below 1, for any time instant of the earthquake excitation (Figure 6-26a). A yellow ochre color was assigned when the FOS marginally dropped below 1 for a time instant of the earthquake, and was designated as critical (marked with red) when the FOS dropped significantly below 1 (Figure 6-26b and c).

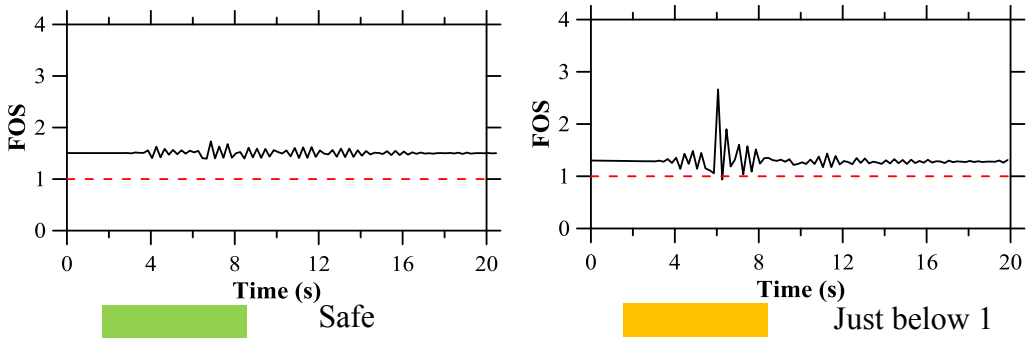

(a) (b)

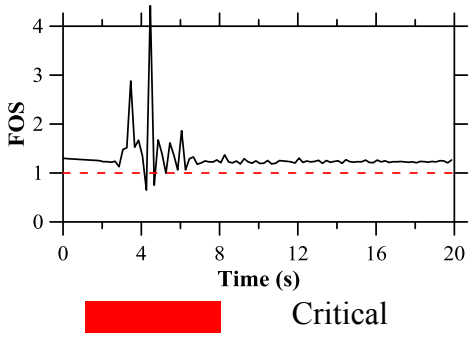

(c)

Figure 6-26: Color coding used to represent the stability of the slip surfaces (a) Safe, (b) FOS just below 1, and (c) critical

The event of the factor of safety falling below does not necessarily mean a catastrophic failure, rather some permanent accumulation of deformation is expected. In this study, the deformation of the slip surface is not estimated, rather the variation of FOS has been used as a surrogate measure of the performance of the dam during seismic events. Since laboratory test data of undrained cyclic triaxial test on undisturbed samples of sand extracted from the shell was unavailable, it was not possible to estimate the accumulated strain/deformation during earthquake shaking. In case of real earthquakes, the cases marked green are expected to have the least deformation, followed by the yellow ochre and red color coded cases.

Figure 6-27 and 6-28 illustrate the results of variation of FOS of the upstream and downstream critical surfaces at Station 9, respectively, when subjected to earthquakes A through H (M<6.5). The impact of the peak acceleration

of the earthquake is apparent from these figures, with an increase in fluctuations in the dynamic FOS when subjected to earthquakes A (PGA = 0.001g) to H (PGA = 0.402g). The increase in peak acceleration results in an increase in the earthquake-induced forces on the critical slip surface. Moreover, a higher peak acceleration leads to an increase in the cyclic stress ratio, estimated at different Gauss integration points of the FEM model of the dam shell. This results in an increase in excess pore water pressure and subsequent reduction in shear strength provided by the segment of the slip surface passing through the sand layers. The combined effects of these two factors resulted in a higher fluctuation in the FOS and also lead to a decrease in FOS below 1, for some time instants (Figure 6-27h and 6-28h).

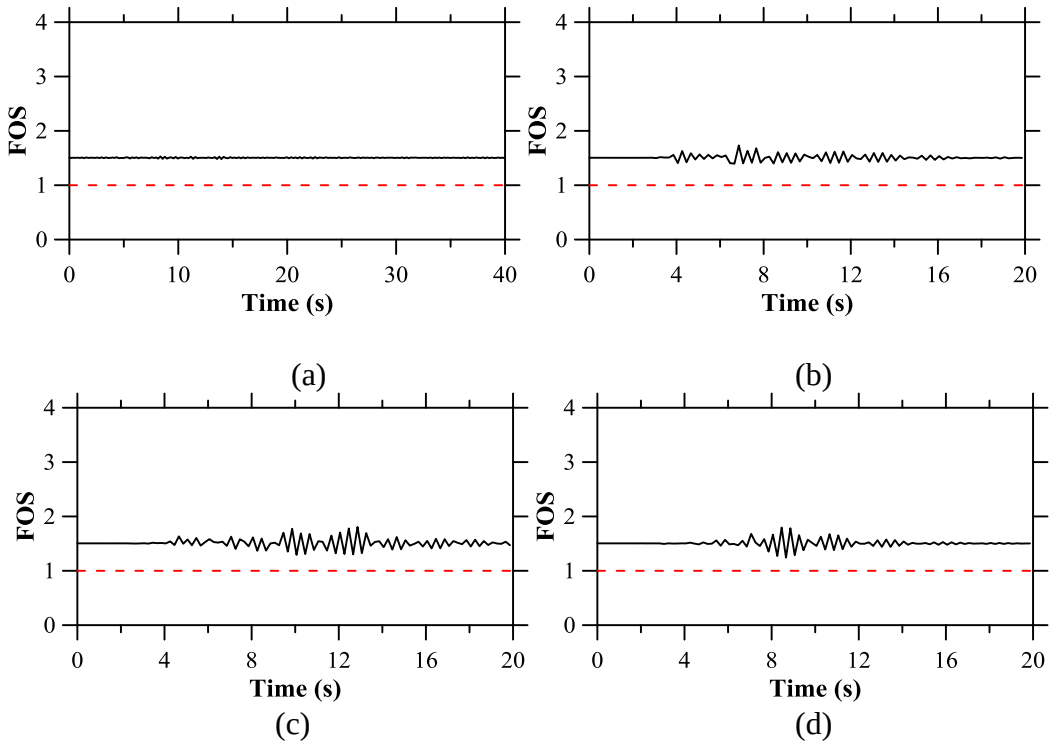

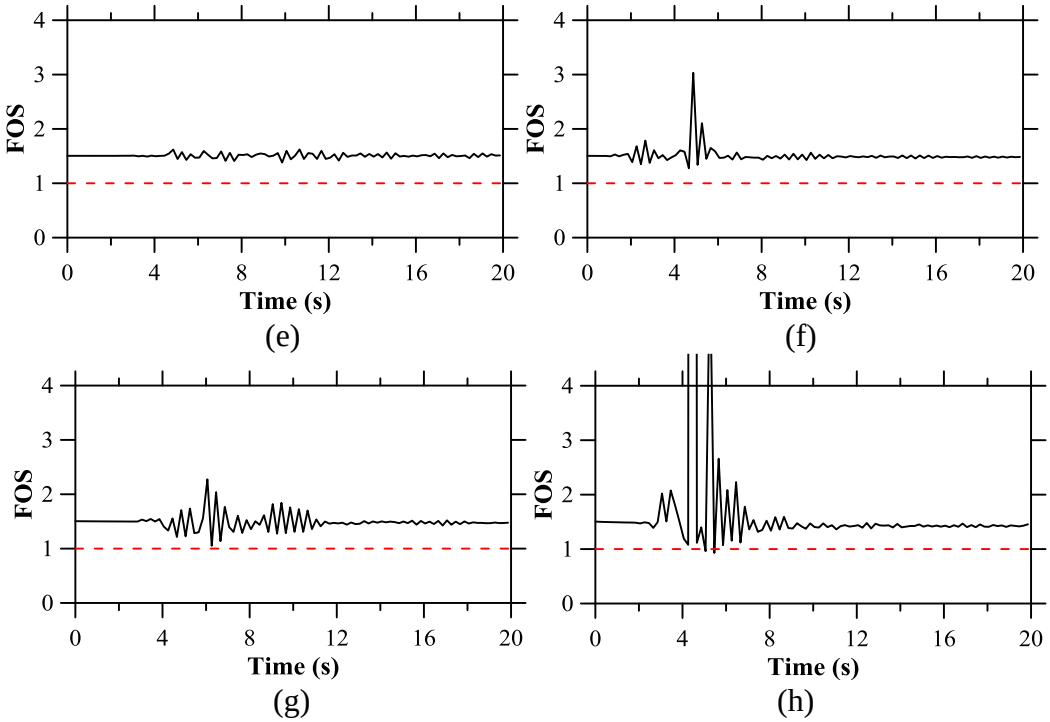

Figure 6-27: Dynamic factor of safety of critical upstream slope of Stn. 9 when subjected to earthquakes (a) A, (b) B, (c) C, (d) D, (e) E, (f) F, (g) G and (h) H

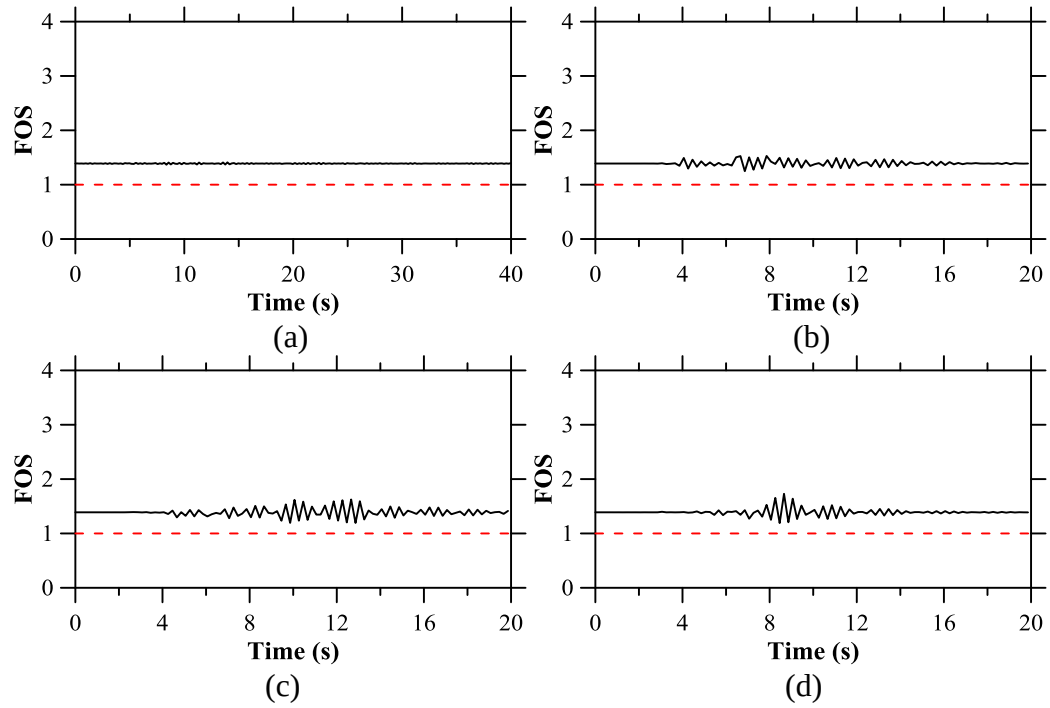

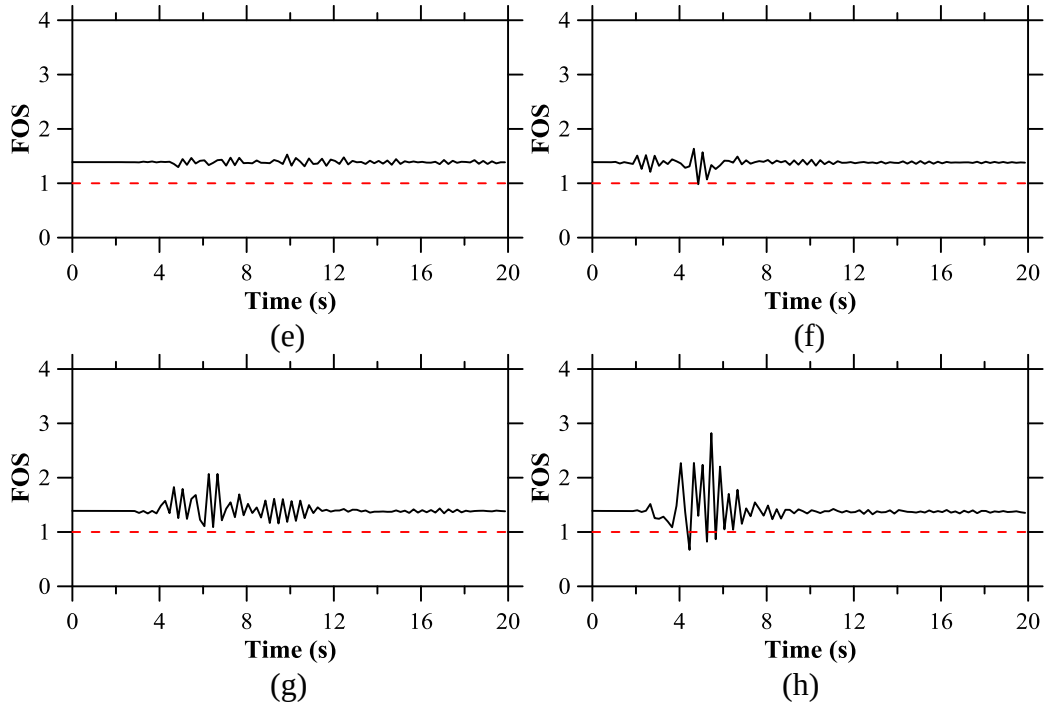

Figure 6-28: Dynamic factor of safety of critical downstream slope of Stn. 9 when subjected to earthquake (a) A, (b) B, (c) C, (d) D, (e) E, (f) F, (g) G and (h) H

An apparent anomaly in the variation of FOS can be observed by comparing the dynamic FOS results of Figure 6-27 and Figure 6-28 c, d, and e. Despite having a higher PGA, the variations in the dynamic FOS results for earthquake E (PGA = 0.05g) is less significant as compared to that observed for earthquakes C (PGA = 0.038g) and D (PGA = 0.04g). The rationale behind this behavior can be comprehended by comparing the predominant frequencies of earthquakes C, D and E, with the first natural frequency of Station 9 (Figure 5-20). The predominant frequency of earthquakes C and D were close to 2.7 Hz, the first natural frequency of Station 9. This resulted in an amplified vibration due to a near-resonance condition. Contrarily, the predominant frequency of earthquake E was close to 11.8

Hz, which was significantly different from the first natural frequency of the structure. The near-resonance amplification resulted in a higher earthquake-induced force/acceleration to act on the body of the slip surface, causing the observed fluctuations in the FOS (against the time of the earthquake). The effect of the predominant frequency of the earthquake excitation can be better observed by studying the figures depicting the excess pore water pressure accumulated in the sand layers of the dam.

Figure 6-29 presents the excess pore water pressure developed in the sand layers of the dam (Station 9), when subjected to earthquake excitations A through H. An increase in excess pore water pressure can be observed in the shell and foundation sand layers, with an increase in the peak acceleration of the earthquakes. Despite having a lower PGA, the excess pore water pressure generated in the upstream shell of the dam in case of earthquakes B, C, and D, were significantly higher than that for earthquake E. This suggests that the predominant frequency of an earthquake excitation plays a significant role in the seismic stability of the slopes of a hydraulic-fill dam, especially when the comparison is being made between two earthquake excitations with the similar peak accelerations.

However, the excess pore water pressure developed near the surface of the upstream shell, for earthquakes with PGA less than 0.06g, would merely cause surficial failures, with raveling of the surface sand, which should not hamper the overall stability of the dam. Moreover, the presence of rip rap and near-surface clay

layer of soil was not taken into consideration. The generation of excess pore water pressure was significant for earthquake H; however, such strong earthquake excitations with PGA of 0.402g are not expected for the EM dam site and may be considered a hypothetical case. Based on deterministic seismic hazard analysis, the peak ground acceleration of an earthquake was estimated as 0.02g (Caballero 2017). Hence the EM dam is expected to be safe during possible earthquakes with PGA less than 0.06g. The analysis results are based on the cyclic number function assumed for the study. Further studies with undrained cyclic triaxial test results would be needed to accurately estimate the increase in pore water pressure, assess the chances of liquefaction and estimate the associated deformations.

The excess pore water pressure in the foundation sand layers and deeper layers of the sand shells can be observed to be insignificant for earthquakes A through E. However, an increase in peak acceleration of the earthquake excitation to 0.09g and above, may lead to liquefaction of the sand layers and cause stability issues, especially for the upstream shell of the dam. Figure 6-30a shows that the FOS of a slip surface passing entirely through the upstream shell degraded from 1.8 to 0.35 at the end of the earthquake excitation. The reason behind the drop in FOS can be attributed to increase in excess pore water pressure in the upstream shell of the dam (Figure 6-30b). The foundation sand layer, especially below the dam embankment, was observed to be more stable as compared to the upstream shell due to the high effective overburden pressure and initial confining stresses.

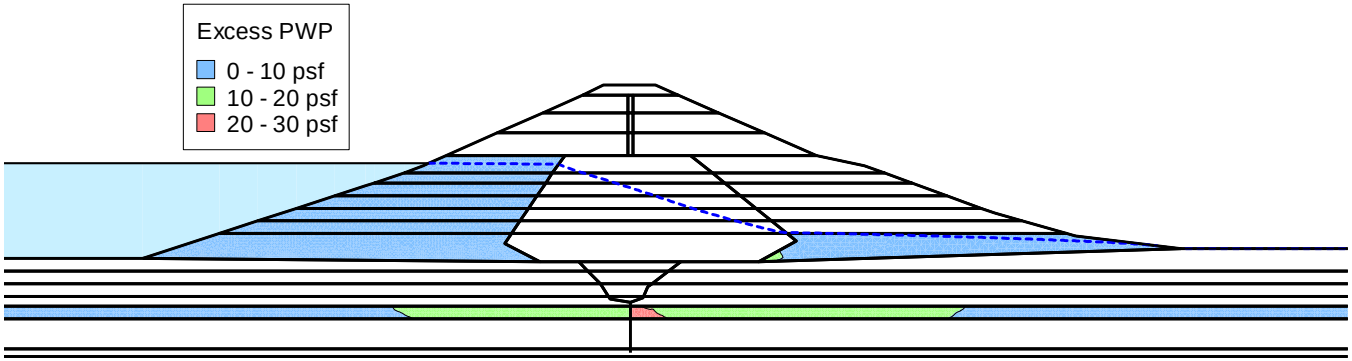
Excess PWP
0 - 10 psf
10 - 20 psf
20 - 30 psf

(a)

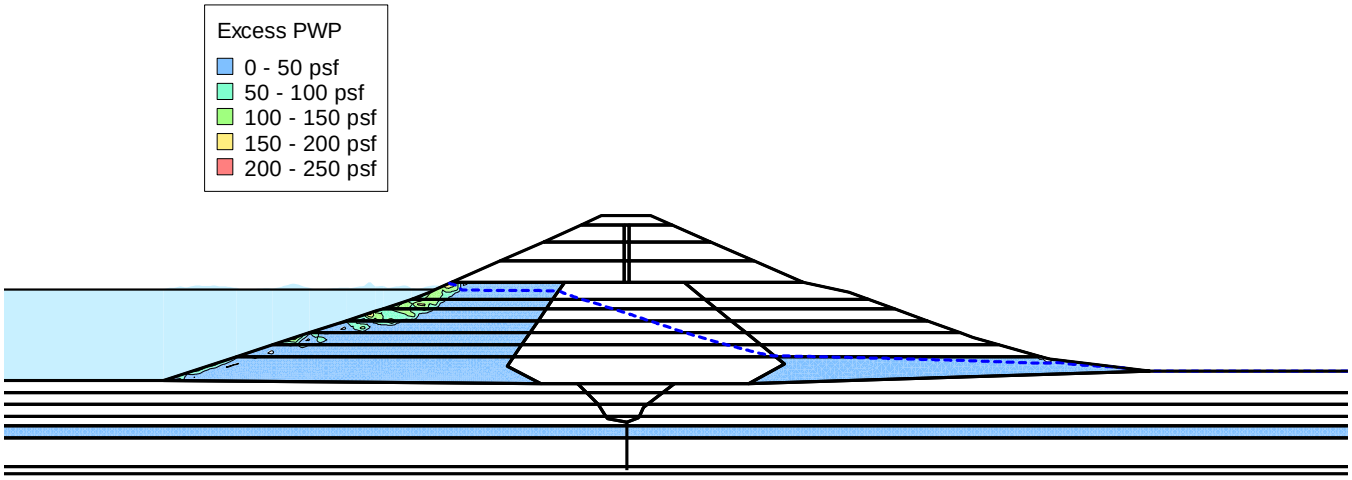
Excess PWP
0 - 50 psf
50 - 100 psf
100 - 150 psf
150 - 200 psf
200 - 250 psf

(b)

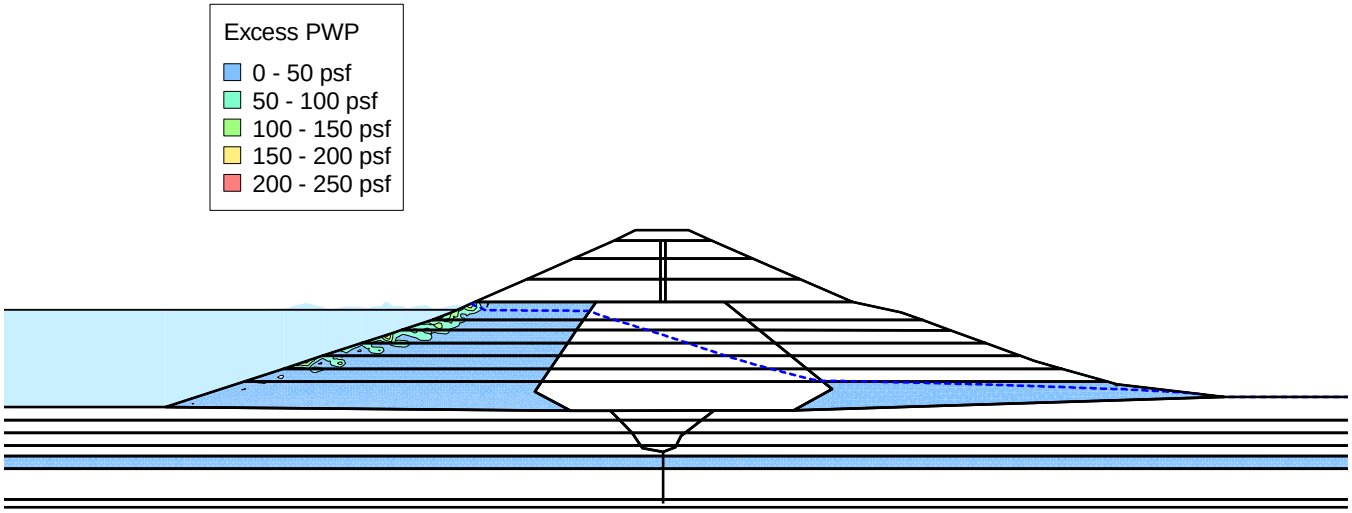
Excess PWP
0 - 50 psf
50 - 100 psf
100 - 150 psf
150 - 200 psf
200 - 250 psf

(c)

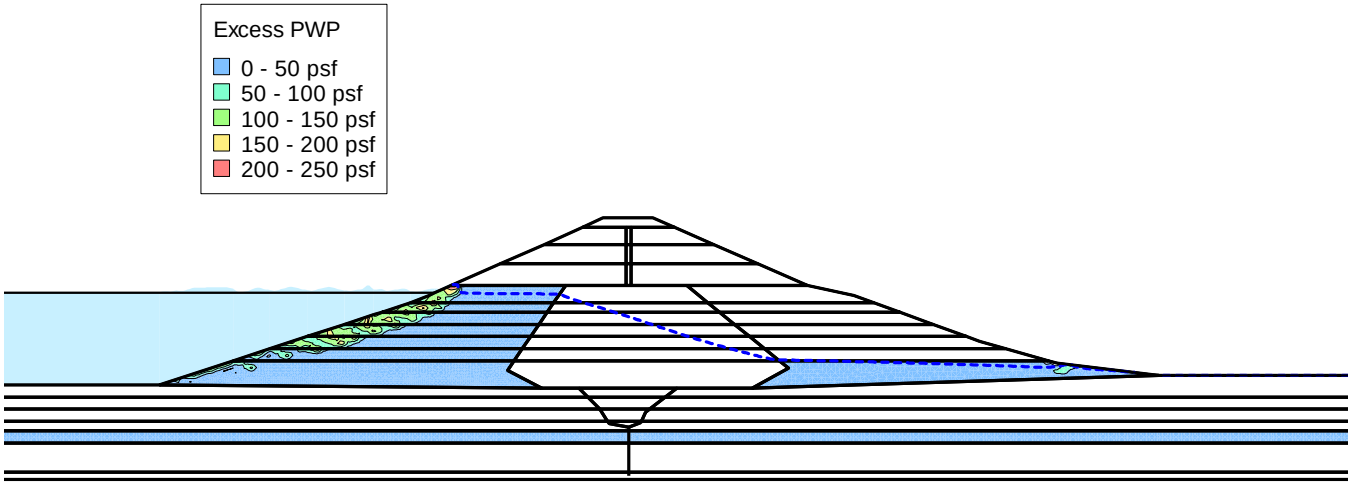
Excess PWP
0 - 50 psf
50 - 100 psf
100 - 150 psf
150 - 200 psf
200 - 250 psf

(d)

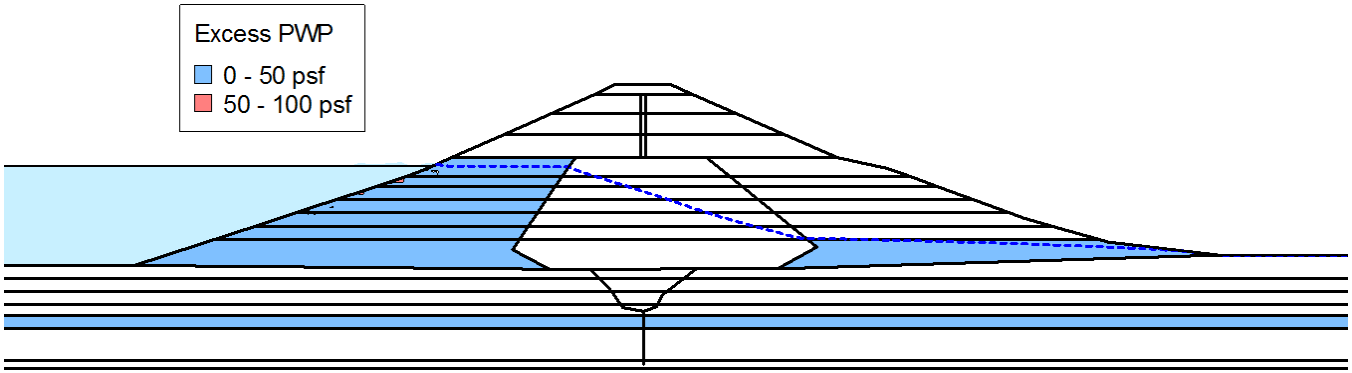
Excess PWP
0 - 50 psf
50 - 100 psf

(e)

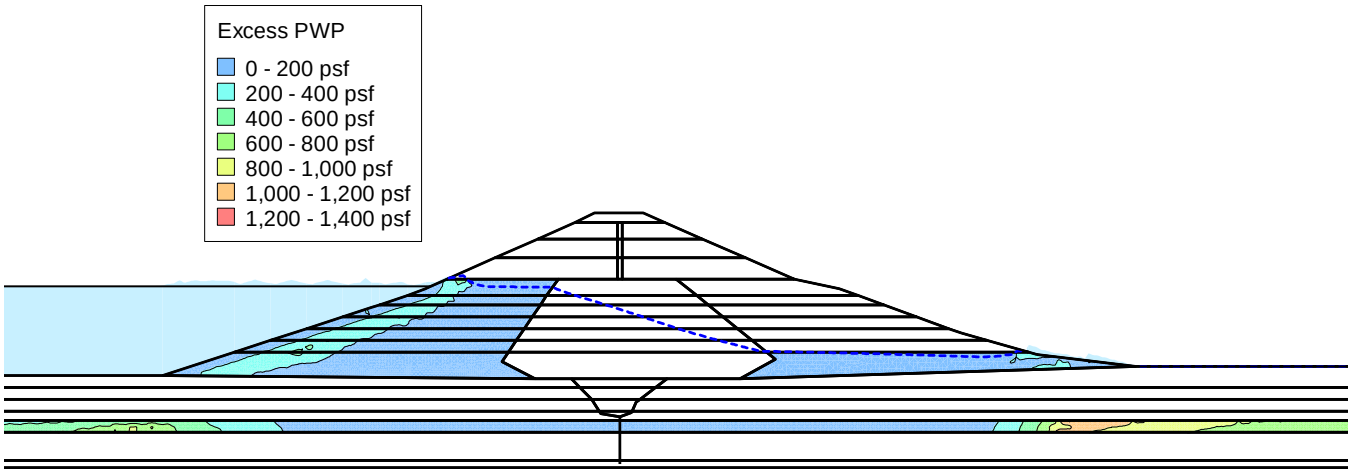
Excess PWP
0 - 200 psf
200 - 400 psf
400 - 600 psf
600 - 800 psf
800 - 1,000 psf
1,000 - 1,200 psf
1,200 - 1,400 psf

(f)

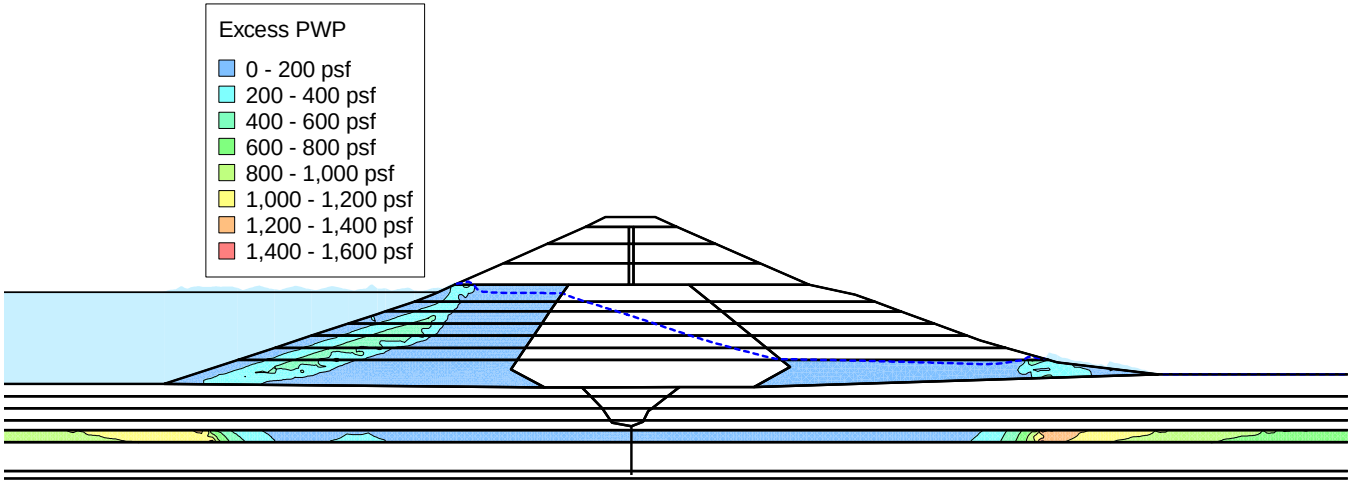

(g)

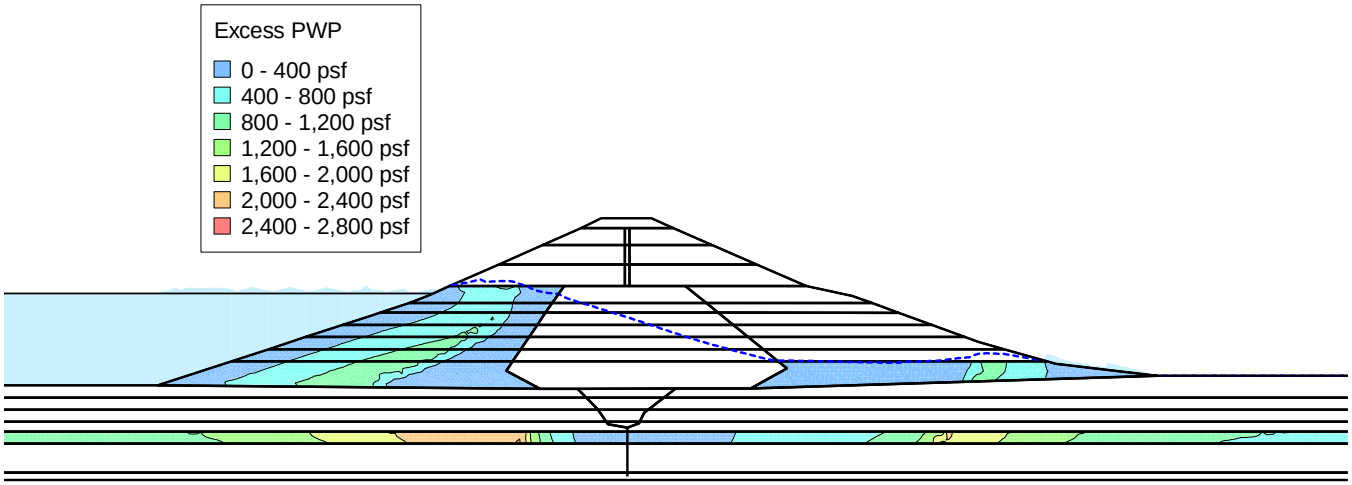

(h)

Figure 6-29: Excess pore water pressure generated in the upstream shell, downstream shell and foundation sand layer of Stn. 9 when subjected to earthquake (a) A, (b) B, (c) C, (d) D, (e) E, (f) F, (g) G and (h) H

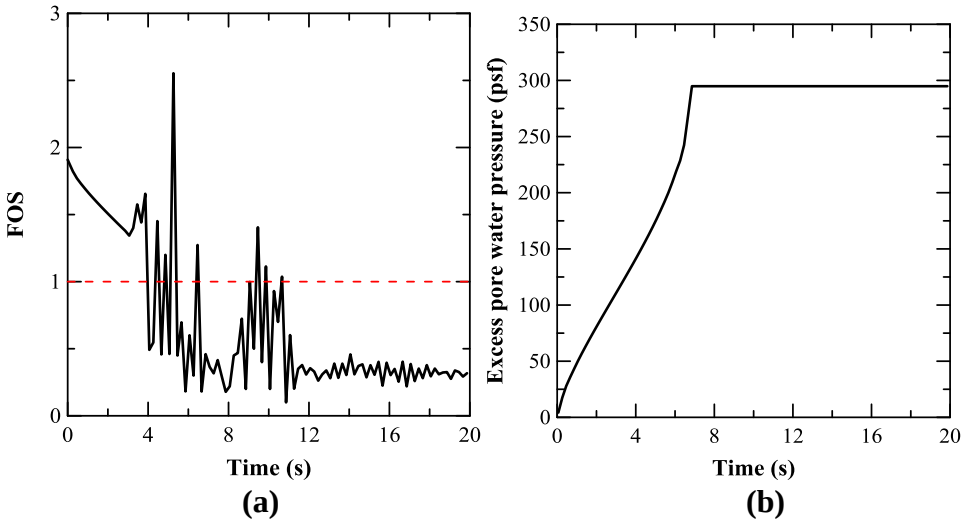

Figure 6-30: (a) Dynamic factor of safety of a surficial slope passing through upstream shell of Stn. 9; (b) Variation of excess pore water pressure at a point near the surface in the upstream slope, when subjected to earthquake G

The performance of the dam sections under different earthquake events have been compiled and presented using color-coded tables in Figure 6-31. The FOS during different earthquake events were observed to be higher than 1 for most earthquakes with PGA less than 0.06g. However, there were some events (marked with yellow ochre) when the FOS just stooped below one for a small instant of time. The FOS significantly dropped below one for some of the sections in the hydraulic-fill zone of the dam (Zone C_1) when the peak acceleration of the earthquake was greater than 0.09g. The stations ranging from 14.5 to 27 were found to be the most critical sections, which is in agreement with the observations made from the pseudo-static analysis. The detrimental effect of an earthquake with high magnitude, peak acceleration, and the event with the predominant frequency of the earthquake close to the natural frequency of the earthen dam, can be observed in Figure 6-31.

Earthquakes	A	B	C	D	E	F	G	H
Predominant frequency (Hz)	1.14, 1.80	1.51, 2.24, 4.25	2.5, 5.03, 9.57	2.5, 3.37, 7.08	11.82, 11.87	1.95, 4.49, 6.64	5.86, 7.72, 11.38	2.98, 5.81
Peak acceleration (g)	0.001	0.035	0.038	0.04	0.05	0.097	0.146	0.402
Station 5								
Station 9								
Station 14.5								
Station 18								
Station 22								
Station 27								
Station 33								
Station 39								

(a)

Earthquakes	A	B	C	D	E	F	G	H
Predominant frequency (Hz)	1.14, 1.80	1.51, 2.24, 4.25	2.5, 5.03, 9.57	2.5, 3.37, 7.08	11.82, 11.87	1.95, 4.49, 6.64	5.86, 7.72, 11.38	2.98, 5.81
Peak acceleration (g)	0.001	0.035	0.038	0.04	0.05	0.097	0.146	0.402
Station 5								
Station 9								
Station 14.5								
Station 18								
Station 22								
Station 27								
Station 33								
Station 39								

(b)

Earthquakes	A	B	C	D	E	F	G	H
Predominant frequency (Hz)	1.14, 1.80	1.51, 2.24, 4.25	2.5, 5.03, 9.57	2.5, 3.37, 7.08	11.82, 11.87	1.95, 4.49, 6.64	5.86, 7.72, 11.38	2.98, 5.81
Peak acceleration (g)	0.001	0.035	0.038	0.04	0.05	0.097	0.146	0.402
Station 5								
Station 9								
Station 14.5								
Station 18								
Station 22								
Station 27								
Station 33								
Station 39								

(c)

Earthquakes	A	B	C	D	E	F	G	H
Predominant frequency (Hz)	1.14, 1.80	1.51, 2.24, 4.25	2.5, 5.03, 9.57	2.5, 3.37, 7.08	11.82, 11.87	1.95, 4.49, 6.64	5.86, 7.72, 11.38	2.98, 5.81
Peak acceleration (g)	0.001	0.035	0.038	0.04	0.05	0.097	0.146	0.402
Station 5								
Station 9								
Station 14.5								
Station 18								
Station 22								
Station 27								
Station 33								
Station 39								

(d)

Figure 6-31: Dynamic stability analyses results for different sections of the dam when subjected to different earthquake conditions for upstream slope (a) M < 6.5, (b) M = 7; and downstream slopes (c) M < 6.5 and (d) M = 7

6.5.6.2 Flow liquefaction analysis

The cyclic liquefaction analyses suggested chances of liquefaction-induced stability issues in the different sections of the dam, especially for earthquake events with high peak accelerations and when the predominant frequency of the earthquake excitation is close to the first natural frequency of the dam sections. The effect was pronounced when the peak accelerations of the earthquake were 0.09g and above. In addition to cyclic liquefaction assessment, the susceptibility for flow liquefaction was also assessed based on the state parameter of the foundation sand layers. The CPT data was used to determine the soil behavior type (SBT), and the CPT data corresponding to predominantly sand type soils, having an SBT value ranging from 7 to 10 (on a scale of 1 to 12), was used to obtain the normalized friction factor and normalized cone resistance. The obtained data suggest that other than station 39, the foundation sand layers had a negative value of state parameter, which implies that the foundation sand of the dam can be considered to be safe against flow liquefaction (Figure 6-32). A more thorough analysis would have been possible if laboratory test results on the undrained steady state shear strength and inclination of the flow liquefaction surface were available. Further studies are required to comprehensively evaluate the chances of flow liquefaction.

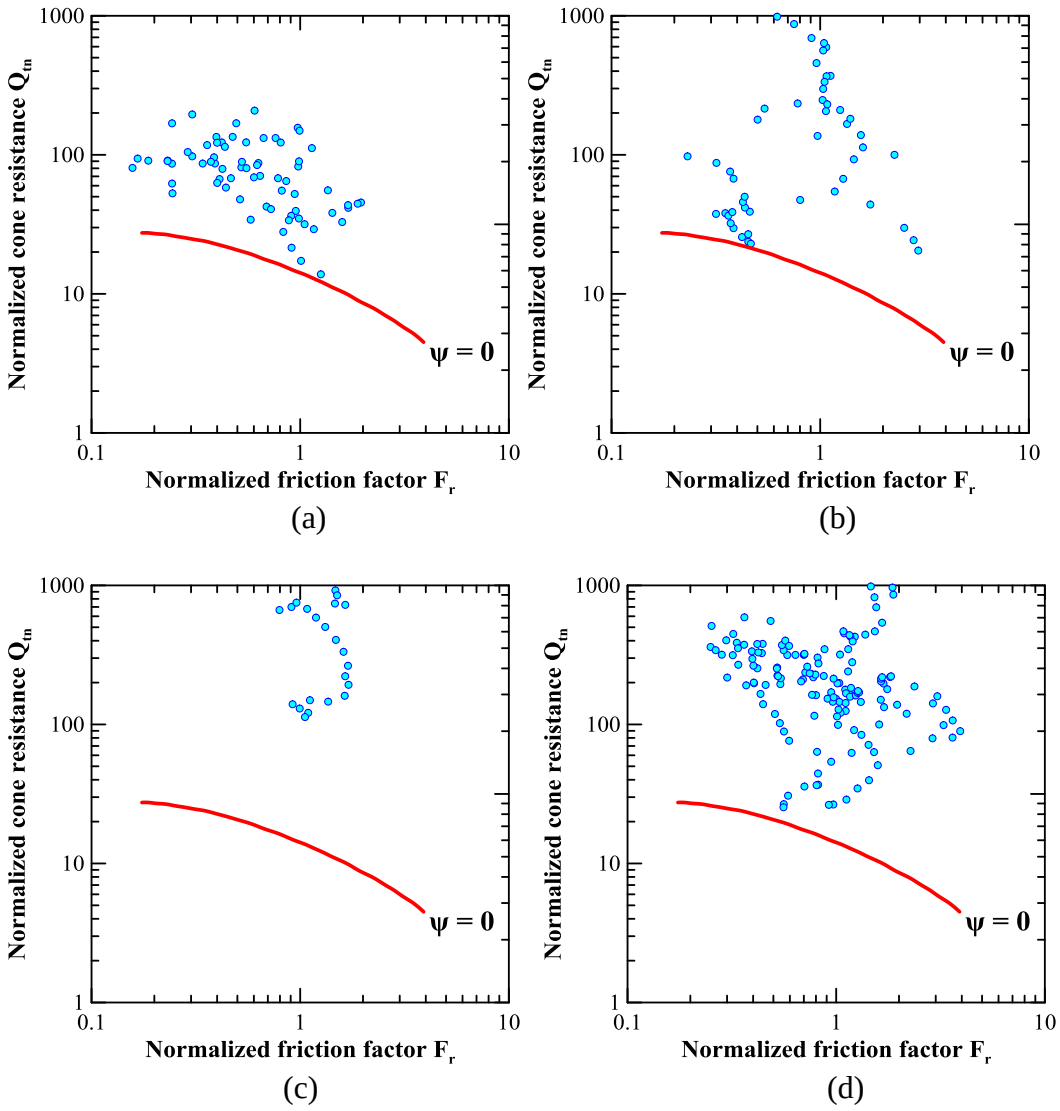
1000
100
10
1
0.1
1
10
Normalized cone resistance Q_{tn}
Normalized friction factor F_r
ψ = 0
(a)
(b)
(c)
(d)

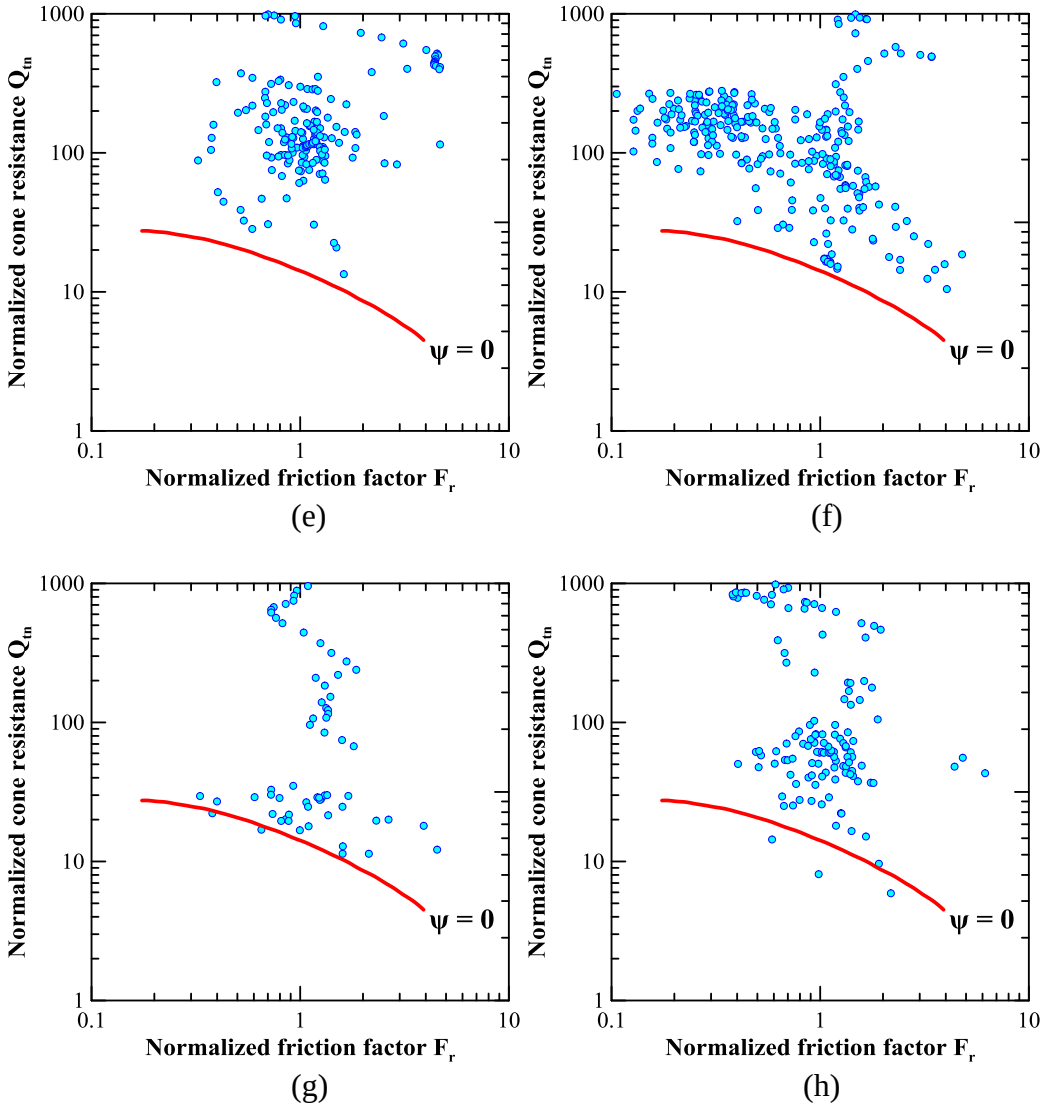

Figure 6-32: Flow liquefaction susceptibility check for foundation sand layers in (a) Stn. 5, (b) Stn. 9, (c) Stn. 14.5, (d) Stn. 18, (e) Stn. 22, (f) Stn. 27, (g) Stn. 33 and (h) Stn. 39, based on state parameter

6.6 Summary

In this chapter, pseudo-static, decoupled Newmark deformation type of analyses, and dynamic stability analyses were performed to evaluate the stability of the slopes of the EM dam for probable seismic events. The effect of material variability was

incorporated into the analysis using three-dimensional visualization models of different strength parameters of the dam, generated using in-situ test results, and interpolated using geostatistics-based kriging analysis. Two earthquake time-history data, having significantly different predominant frequencies, were scaled to PGA of 0.3g based on PSHA, and used for performing the decoupled Newmark deformation analysis. Eight earthquake time-history data (unscaled), were used to estimate the excess pore water pressure in the sand layers and for performing the dynamic stability analysis. The following conclusions can be drawn based on the analysis results:

- The strength parameters obtained from the three-dimensional visualization models created using kriging analysis was able to capture the variation in different strength properties along the length of the hydraulic-fill dam. Assigning the respective material properties in the stability analysis is expected to give accurate results when compared to the traditional method of assigning representative material properties at different zones of the dam.
- The hydraulic-fill dam can be considered to be stable during normal working condition. However, some sections of the dam, especially in Zone C_1, may be critical during the earthquake loading conditions. The new method of representing the factor of safety results, in terms of the distribution of factor of safety was found to be effective for identifying the critical sections.

- The factor of safety obtained on performing a static analysis using undrained shear strength parameters was found to be a good surrogate measure of the stability of the dam during seismic events. The sections which had low values of factor of safety for the Case-3 analysis, were also found to have low yield coefficients and higher plastic deformations during an earthquake, as compared to the other sections. This shows the importance of performing a static stability analysis with undrained strength parameters for the clay layers below the phreatic surface, even though such an analysis does not have any physical significance.
- The dam can be considered to be safe based on the serviceability criteria of plastic deformation, provided that significant excess pore water pressure does not generate during seismic events. However, if the effect of increase in pore water pressure and associated loss in shear strength in the sand shell is significant, the deformations need to be re-evaluated.
- The probability of failure of the dam sections were found to drastically increase and the reliability index was observed to decrease with an increase in the horizontal seismic coefficient. The decline in the reliability index was found to follow a perfectly linear trend, for all the sections of the dam.
- The reliability analysis suggests that the Zone C_1 of the dam falls in the hazardous zone, even for low horizontal seismic coefficients, as per the USACE recommendations. Stations 9 to 27 of the dam was also found to be

in the hazardous zone, for a seismic coefficient of 0.1*g*, which roughly corresponds to an earthquake with PGA of 0.3*g*. Hence proactive remedial measures are required for this sections of the dam to avoid any catastrophic consequence during a 0.3*g* PGA earthquake.

- Based on the dynamic slope stability analysis results, the different sections of the dam should be safe for earthquakes with PGA of 0.06g and below. The dam may withstand earthquakes with even higher peak ground accelerations, provided that the predominant frequency of the earthquake is distinct from the natural frequency of the dam.
- The critical sections identified based on the pseudo-static analysis and dynamic stability analysis were found to be similar. This justifies the effectiveness of the simple pseudo-static analysis, for being used as a screening tool and obtaining an index on the performance of dams during earthquake events. Both the methods of the analysis found the hydraulic-fill zone C_1 to be critical.
- The upstream shell of the dam may be susceptible to cyclic liquefaction and there may be certain portions of the upstream shell which may collapse due to build-up of excess pore water pressure and subsequent strength loss. The foundation sand layer, especially near the toes of the dam, where the effective overburden pressure is not significant, may also be susceptible to cyclic liquefaction. The chances of cyclic liquefaction induced instability

issues will increase with the increase in peak acceleration and magnitude of the earthquake. Even for an earthquake with low peak acceleration (about 0.03g), cyclic liquefaction may happen in the sand layers if the predominant frequency of the earthquake excitation is close to the natural frequency of the dam. However, based on the state parameter estimated for the sand layers, the foundation sand seems to be not susceptible to flow liquefaction.

- All the analysis performed in this section were based on the shear modulus values estimated for the layers of the dam embankment. However, literature suggests chances of a wide margin of deviation in the estimated results due to inter-method and intra-method variability. Hence a sensitivity is required to comprehend the impact of incorrect estimation of the small strain shear modulus values on seismic response and stability analysis. This topic is discussed in detail in the next chapter.

Chapter 7: Evaluation of uncertainty associated with seismic stability analysis

The contents of this chapter has been published in IFCEE 2018: Developments in Earth Retention, Support Systems, and Tunneling, ASCE Geotechnical Special Publication 297 and is being re-used with permission from ASCE (Appendix A).

Title of article: "Impact of Variation of Small Strain Shear Modulus on Seismic Slope Stability Analysis of a Levee: A Sensitivity Analysis"

DOI of the full article: 10.1061/9780784481608.029

7.1 Introduction

Shear wave velocity (V_s) and small strain shear modulus (G_{max}) are important fundamental soil properties, which are widely used in geotechnical engineering problems involving dynamic loading conditions (Banerjee 2017; Chaney et al. 1996; Kayen et al. 2013; Mayne and Rix 1995). The maximum shear modulus (G_{max}) corresponds to the shear modulus of the soil at strain level less than 0.001% (Mayne and Rix 1995; Robertson et al. 1986b; Stokoe et al. 1991).

The G_{max} (and V_s) values are used for estimating the response of earthen structures, such as dams and levees subjected to earthquake loading conditions, assess the stability of slopes and evaluate soil liquefaction potential (Gazetas 1981; Kayen et al. 2013; Piao et al. 2006; Raptakis and Makra 2015). The G_{max} (and V_s) values can be estimated by different methods, such as laboratory tests on undisturbed soil samples, in-situ tests or by using empirical or semi-empirical correlation equations. Maximum shear modulus is related to the shear wave velocity as shown in equation 4.7.

$$G_{max} = \rho . V_s^2 \quad (4.7)$$

where ρ is the bulk density of the soil.

Laboratory tests include bender element tests or resonant column tests on undisturbed soil samples, performed under similar confining pressure conditions as expected in the field (Chaney et al. 1996; Suits et al. 2005). However, sample disturbances and incorrect estimation of the stress state of the soil under in-situ condition may lead to erroneous estimation of G_{max}, with a difference of 100% or more as compared to field test results (Anderson et al. 1978; Hryciw 1990). The best method to estimate these parameters is to conduct in-situ tests with minimum soil disturbance (Hryciw 1990; Mayne and Rix 1995). Thus, the tests carried out under field conditions are expected to provide a better estimation of the G_{max} values. It is essential to incorporate the effect of anisotropic stress conditions existing in the field, which may result in variation in V_s with the direction of propagation of the waves (Roesler 1979; Stokoe et al. 1985; Yan and Byrne 1991). The in-situ tests include invasive methods such as crosshole test, downhole test, suspension logging test, or seismic cone penetration test (SCPT) (Hryciw 1990; Mayne and Rix 1995; Moss 2008; Robertson et al. 1986b); and non-invasive techniques such as spectral analysis of surface waves (SASW), multichannel analysis of surface waves (MASW), frequency-wavenumber method (f-k method), refraction microtremor (ReMi), seismic reflection/refraction test or microtremor array measurements (MAM) (Marosi and Hiltunen 2004; Moss 2008; Stokoe et al. 1991).

It may not be feasible to conduct in-situ tests under certain circumstances, such as economic constraints or unavailability of specialized equipment. The G_{max} values are estimated using semi-empirical or empirical correlations in such cases (Mayne and Rix 1995). Semi-empirical correlations relate G_{max} values to mean effective stress, void ratio, relative density, plasticity index, over consolidation ratio, and other factors which influence the shear wave velocity of soil (Hryciw 1990; Robertson et al. 1995; Seed and Idriss 1970; Seed et al. 1986).

The values of V_s or G_{max} can also be estimated from empirical correlations with standard penetration tests (SPT), cone penetration tests (CPT), dilatometer test (DMT), pressuremeter test (PMT) or Becker penetration test (BPT) (Ahmed 2016; Akin et al. 2011; Hryciw 1990; Robertson and Cabal 2015; Rollins et al. 1998). A vast database of V_s (and G_{max}) values for different types of soil from around the globe and their corresponding test results (SPT, CPT, BPT, DMT, PMT, etc.) were used by researchers to perform regression analysis and obtain these correlations. The choice of a particular method for determining the shear wave velocity profile of subsurface layers depends on several factors, including the type and importance of the project, associated costs and budget, expertise and experience of engineers.

There are several methods available for estimation of G_{max} values. However, a significant difference is observed in the result obtained by these methods. Several researchers have studied the intra method and inter method variability in estimated

G_{max} values. The inherent variability and heterogeneity of subsurface soil layers, the fundamental difference in the philosophy of various testing methods, and differences in interpretation of results by different individuals primarily lead to the variability in the estimated G_{max} values obtained from different methods (Moss 2008). Moreover, the extent of the difference in estimated V_s varies with depth and complexity of the subsurface soil profile (Marosi and Hiltunen 2004; Moss 2008; Raptakis and Makra 2015). Robertson et al. (1986) reported that V_s obtained from CPT downhole tests was consistently higher than those obtained from the crosshole tests by a margin of 20%, leading to a deviation of about 40% in the estimated G_{max} values. The average error in G_{max} obtained using empirical correlations with Dilatometer test was found to be around 23% (Hryciw 1990). A study by Mayne and Rix (1995) showed that V_s obtained from CPT correlations deviated from those obtained using SASW test; with an error margin upto 50%. The difference in the V_s profile was found to decrease with prior knowledge about the void ratio profile of the site. However, such an information is seldom available beforehand for any projects.

Correlation equations used to obtain shear wave velocity from equivalent N_{60} from Becker penetration test was reported to vary within a margin of ± 30% of that obtained from field tests (Rollins et al. 1998). The deviation was found to be as high as ± 50% for some cases. The intra-method variability for SASW tests was reported to have a coefficient of variation of 5 to 6%, while those for downhole

tests and SCPT varied from 1 to 3% (Moss 2008). The study by Moss (2008) also provides an excellent compilation of inter-method variability (using various invasive and non-invasive field testing techniques) in the estimated V_s, that has been reported by several researchers. Other studies have stated that the margin of error in determining shear wave velocity may vary from -30% up to +110% (Ahmed 2016; Raptakis and Makra 2015).

The existing literature hence provides some insight on the possibility of inaccurate estimation (both underestimation and overestimation) of V_s (and G_{max}) using the different methods available. Although the extent of deviation of the estimated V_s (and G_{max}) depends on the testing technique or correlations used and vary from one site to another, it is evident from the available literature that a significant uncertainty remains in the estimation of shear wave velocity profile and small strain shear modulus. Since the shear wave velocity and small strain shear modulus are important parameters in seismic response analysis and seismic slope stability analysis of earthen structures like dams and levees, it is expected that errors in estimation of G_{max} values will affect the behavior of these structures under dynamic loading conditions.

Sensitivity analyses in slope stability studies are often performed to gauge the relative importance of different parameters in the analysis and understand the impact of erroneous estimation of a particular input parameter. Commercially available software provide the option to implement sensitivity studies and

determine the effect of variation of different parameters such as cohesion, angle of internal friction, and unit weights. However, no such analyses are usually performed to study the effect of erroneous estimation of G_{max} values of different layers of an earthen structure.

Furthermore, G_{max} is an important parameter for seismic stability analysis, and existing literature clearly portray the possibility of high deviation in the estimated G_{max} values using different existing methods. Hence in this study, a sensitivity analysis was performed on an earthen embankment structure in North Texas to gain some understanding of the impact of inaccurate estimation of G_{max} values, on the response of the structure and the stability of its slopes under seismic loading conditions.

7.2 Methodology

This section describes the tasks conducted to study the impact of variation of small strain shear modulus on seismic response and stability of the slopes of an earthen embankment structure. A section perpendicular to the axis of a 15m high levee located in North Texas was used for the analysis. A plane strain, equivalent linear analysis was performed using a finite element based software. The embankment section was divided into eleven horizontal layers, based on the shear wave velocity profile obtained from in-situ tests. The shear strength parameters of the corresponding layers were obtained using CPT correlations, corroborated by consolidated undrained triaxial tests conducted in the laboratory.

The modulus degradation curve and the damping ratio curve for equivalent linear analysis were obtained from the available literature (Ishibashi and Zhang 1993). Before conducting the dynamic analysis, the factor of safety (FOS) under static stress conditions was determined for both the side slopes of the structure using the Morgenstern-Price method. The layered geometry of the embankment section, the corresponding material properties used for the analysis and the slip surfaces which had the least FOS (critical slip surfaces) under static condition are shown in Figure 7-1.

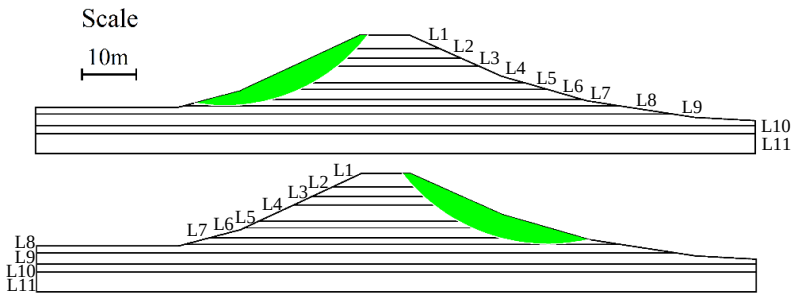

Layer	c' (kPa)	ϕ'	γ (kN/m^3)	V_s (m/s)
L1	0.0	36°	19.6	146
L2	0.0	35°	19.6	122
L3	5.0	34°	20.7	177
L4	5.0	33°	20.2	213
L5	2.5	32°	20.2	223
L6	5.0	30°	20.2	259
L7	5.0	28°	20.2	207
L8	10.0	27°	20.2	244
L9	15.0	27°	20.7	213
L10	5.0	25°	20.4	232
L11	5.0	26°	20.4	290

Figure 7-1: Embankment section with critical slip surfaces under static condition

The embankment structure was subjected to two earthquake excitations to perform the sensitivity analysis. The time history data and corresponding frequency

content data for M4.7 Oklahoma earthquake of 19th November 2015, recorded at Caldwell, KS and M4.5 Oklahoma Earthquake of 2nd November 2016, recorded at Pawnee, OK are shown in Figure 7-2. Both time-history data were scaled to a peak acceleration of 0.05g.

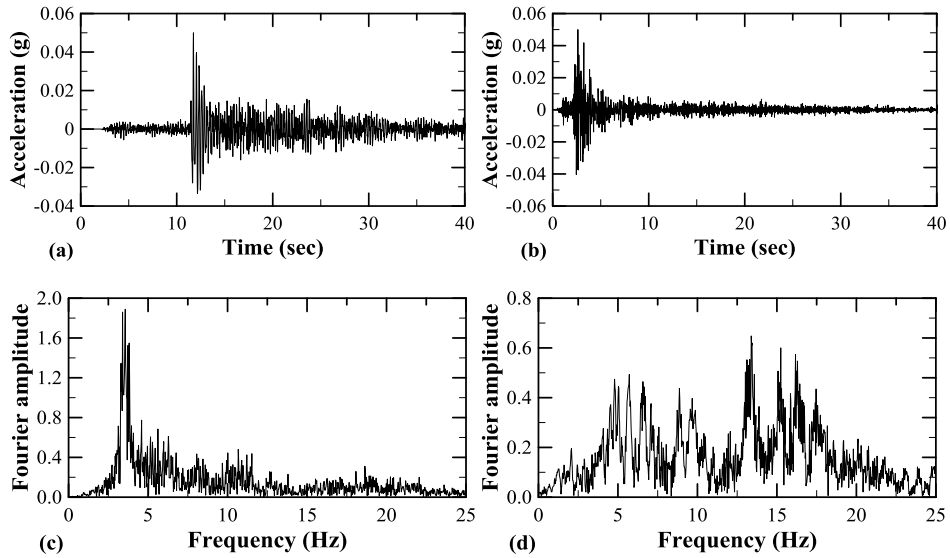

Figure 7-2: Time history data of (a) Caldwell and (b) Pawnee earthquake; FFT data for (c) Caldwell and (d) Pawnee earthquake

Two different types of G_{max} variation regimes were followed. The first type of variation involved varying the G_{max} values for each of the eleven layers, one at a time, without any change in the properties assigned to the remaining ten layers. This would provide some understanding of the impact of an erroneous estimate of G_{max} values of a particular layer. The second type of variation involved varying the G_{max} values of the layers as a group. The first (top) four layers (L1, L2, L3 and L4) formed the first group, L1-G; the following (middle) four layers (L5, L6, L7 and

L8) formed the second group, L2-G; and the remaining (bottom) three layers (L9, L10 and L11) formed the third group, L3-G. Unlike the first type of variation, the G_{max} values for the second type of variation were altered as a group, i.e. the G_{max} values of all the layers of a group were varied at a time, without changing the G_{max} values of other layers of the remaining two groups. For both the types of variation, the G_{max} values (of each layer for the first type of variation and each group of layers for the second type of variation) were varied from 60% to 140% of that obtained from in-situ tests, in increments of 10%. This would simulate the effect of overestimation and underestimation of G_{max} values existing in the field. The natural frequency, peak crest acceleration and the minimum FOS (for both the slopes), when subjected to seismic loading were determined for each of the G_{max} combinations.

In a time-history analysis, the FOS of a slip surface varies with time due to variation in the horizontal forces induced owing to the seismic excitation. The minimum FOS of the slip surfaces (shown in Figure 7-1) over the entire time duration of the earthquake was used to study the effect of inaccurate estimation of G_{max} values on seismic stability of the slopes. The slip surfaces have been named as L (for left slip surface) and R (for right slip surface) in the following section. Effect of water on the upstream side of the structure was not considered in this study. It was expected that including the effect of water on the upstream side would affect the sensitivity analysis due to the variation in excess pore water pressure

developed during seismic loading. This would result in a change in the shear strength of soil for different G_{max} combinations, which is undesirable for this sensitivity analysis.

7.3 Analysis and discussion of results

This section presents the results obtained from the sensitivity analysis performed by varying the G_{max} values following two different variation regimes mentioned in the previous section. The consequent changes in natural frequency and peak acceleration recorded at the crest of the earthen embankment were used as surrogate measures of variation in seismic response of the earthen structure when subjected to earthquake loading conditions. The effect of such variations was manifested in the variation of the minimum FOS of the left (L) and right (R) slip surfaces shown in Figure 7-1. Figure 7-3a illustrates the change in natural frequency of the structure for the first type of variation in G_{max} values. It is evident from Figure 7-3a that the maximum deviation in natural frequency occurred when the G_{max} value of L11 (the bottom most layer) was altered from 60% to 140% of that obtained from in-situ tests. However, it was observed that the change in natural frequency for the first type of variation was less significant when compared to that observed for the second type of variation (Figure 7-3b). The deviation in natural frequency was most prominent for L3-G, where the natural frequency was found to increase from 2.9 Hz to 3.67 Hz. It should be noted that the natural frequency of the structure (Figure 7-3b) was close to the predominant frequency of the Caldwell EQ (Figure 7-2c)

when G_{max} values of L11 ranged from 100% to 140% of that obtained from in-situ tests. A near resonance condition would occur in such a scenario, resulting in a higher peak acceleration as compared to that obtained for G_{max} value of L11 varying from 60% to 90% of that estimated from in-situ tests (Figure 7-3a). Thus, the peak acceleration at crest remained almost constant for G_{max} values of 100% to 140% (L11, Figure 7-4a). A similar trend was also observed for variation in natural frequency with change in G_{max} values for L1-G. In the case of L2-G and L3-G, the natural frequency of the structure was found to increase with an increase in the corresponding G_{max} values (Figure 7-3b), resulting in an increase in the peak acceleration for Caldwell Earthquake (Figure 7-4a).

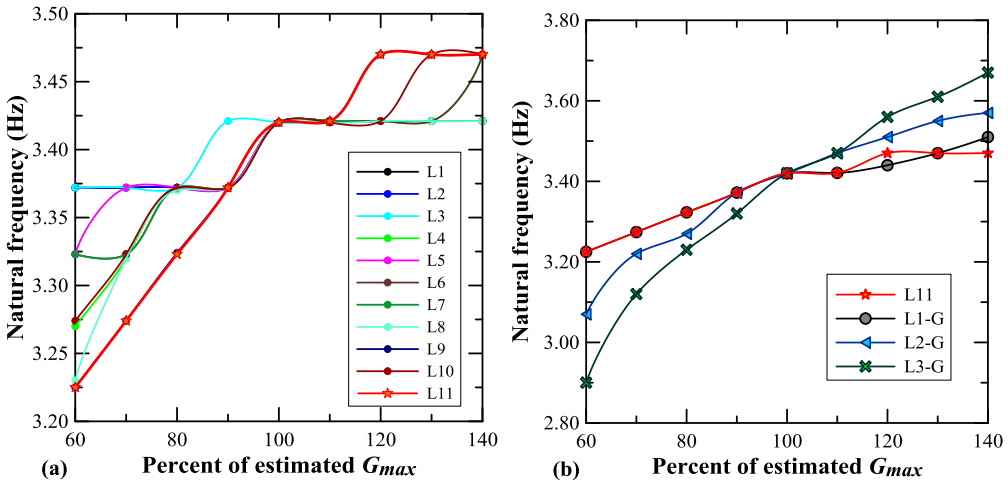

Figure 7-3: Variation of natural frequency for G_{max} variation in (a) Individual layers (b) Grouped layers

The amplification and peak acceleration at the crest of the structure was low for Pawnee EQ. (Figure 7-4b) for both the types of variation in G_{max} values, as

compared to those for Caldwell EQ (Figure 7-4a). The reason for such observation can be attributed to the noticeable difference in the natural frequency of the structure (Figure 7-3b) from the predominant frequency of the Pawnee EQ (Figure 7-2d). There was no appreciable effect of the variation in G_{max} values on peak crest acceleration for L11, L2-G and L3-G when the embankment structure was subjected to Pawnee EQ (Figure 7-4b). However, a higher peak acceleration at the crest of the structure was observed for L1-G when the G_{max} values were varied from 60% to 80% of those obtained from in-situ tests.

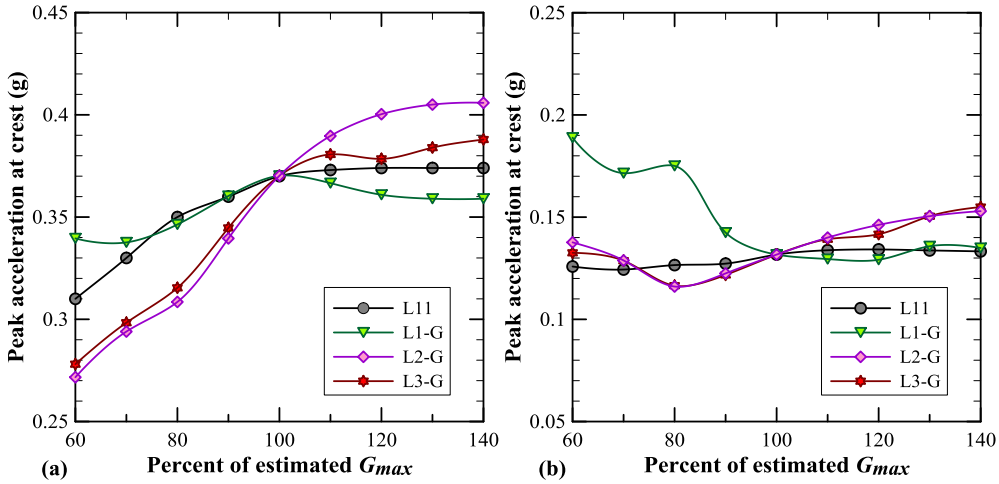

Figure 7-4: Variation of peak acceleration at crest for (a) Caldwell and (b) Pawnee earthquake

The observed variation in natural frequency and peak crest acceleration with G_{max} values can be explained by studying the factors affecting the natural frequency of the structure and analyzing the propagation of the seismic disturbance. For a given earthen structure (i.e. fixed geometry), the natural frequency primarily depends on the distribution of mass and stiffness. A higher mass at the base of the

structure is responsible for the higher variation in natural frequency in case of L3-G. This behavior can be comprehended by considering the embankment structure as a cantilever beam (crest of the structure as the free end) with variable stiffness (G_{max} values) and higher moment of inertia (I) toward the base (higher width at the base of trapezium cross-section of structure). The seismic excitation at the base (foundation) of the structure propagates to the crest via shear waves. The shear deformation at the top of each layer, in turn, depends on the shear modulus and the thickness of that particular layer. Hence the change in shear modulus of a thinner layer does not significantly affect its seismic response. Thereby, the effect of erroneous estimation of G_{max} values becomes more pronounced for the variation of G_{max} values of a group of layers. Moreover, the response at the crest of the structure depends on the accumulated response of each of the underlying layers. Therefore, the effect of change in G_{max} values of the deeper layers is more prominent, when compared to the same degree of change in a near-surface layers.

Figure 7-5 shows the variation of the minimum FOS for the two pre-defined slip surfaces (Figure 7-1), under different earthquake conditions due to a change in G_{max} values of L11. The FOS under static condition, for left and right slip surfaces, was 1.79 and 1.96, respectively. The decrease in FOS (from static FOS) due to earthquake loading is higher when there is an increase in the induced horizontal forces acting on the slip surfaces. Hence, the minimum FOS for Caldwell EQ (L and R) were found to be less than that for Pawnee EQ (Figure 7-5). Moreover, the

effect of variation of G_{max} values on the minimum FOS was observed to be more prominent for Caldwell EQ than Pawnee EQ. This could be attributed to the near resonance condition for Caldwell EQ, in which the natural frequency of the structure (Figure 7-3b, L11) was close to the predominant frequency of the earthquake (Figure 7-2c), resulting in an amplification of the vibration (Figure 7-4a).

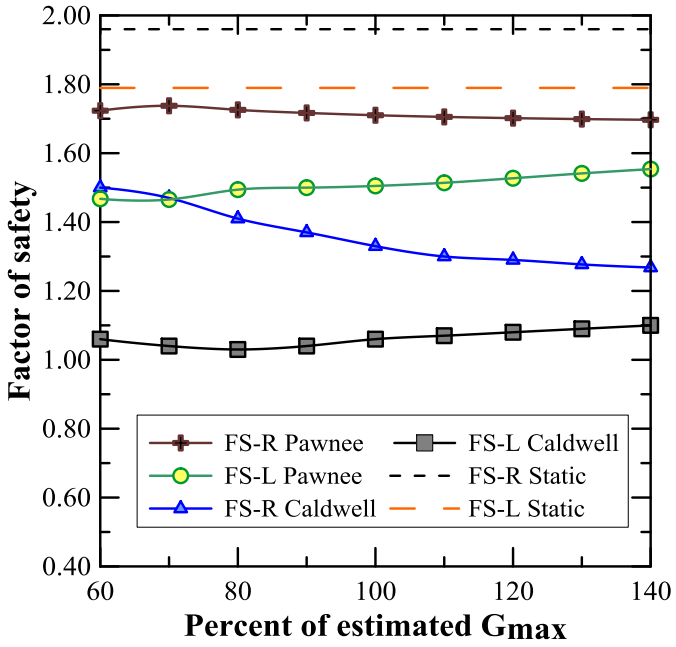

Figure 7-5: Variation of minimum FOS for Caldwell and Pawnee earthquake due to variation of G_{max} value in L11 of the embankment structure

The change in minimum FOS for both the slip surfaces was found to be more pronounced for the second type of variation, in which the G_{max} values were varied in a group (Figure 7-6). A significant variation in minimum FOS for the left slip surface can be observed for L1-G when subjected to Caldwell EQ (Figure 7-

6a). A factor of safety less than one was observed for G_{max} values ranging from 120% to 140% of that obtained from in-situ tests. Although this might not cause complete failure of the slope, there would be some associated permanent deformation for the time duration when FOS was less than 1.

For the right slip surface, the minimum FOS for all the second type of variations was found to decrease with an increase in G_{max} values (Figure 7-6b), probably due to the increase in the horizontal acceleration (as shown in Figure 7-4a). Unlike the variation in natural frequency and peak acceleration at the crest of the structure, the variation of G_{max} values in near surface layers (L1-G) resulted in a significant variation in FOS. This can be attributed to the fact that a large portion of the slip surface lies in the first four layers; therefore variation in G_{max} values (of L1-G) would alter the acceleration induced in the slip surface by the seismic loading. However, the variation in minimum FOS was not prominent for Pawnee EQ, when compared to that observed for Caldwell EQ (Figure 7-6c and d). A small value of PGA (0.05g), coupled with low seismically induced forces on the slip surface may be the result of such minor variation in FOS when subjected to Pawnee EQ.

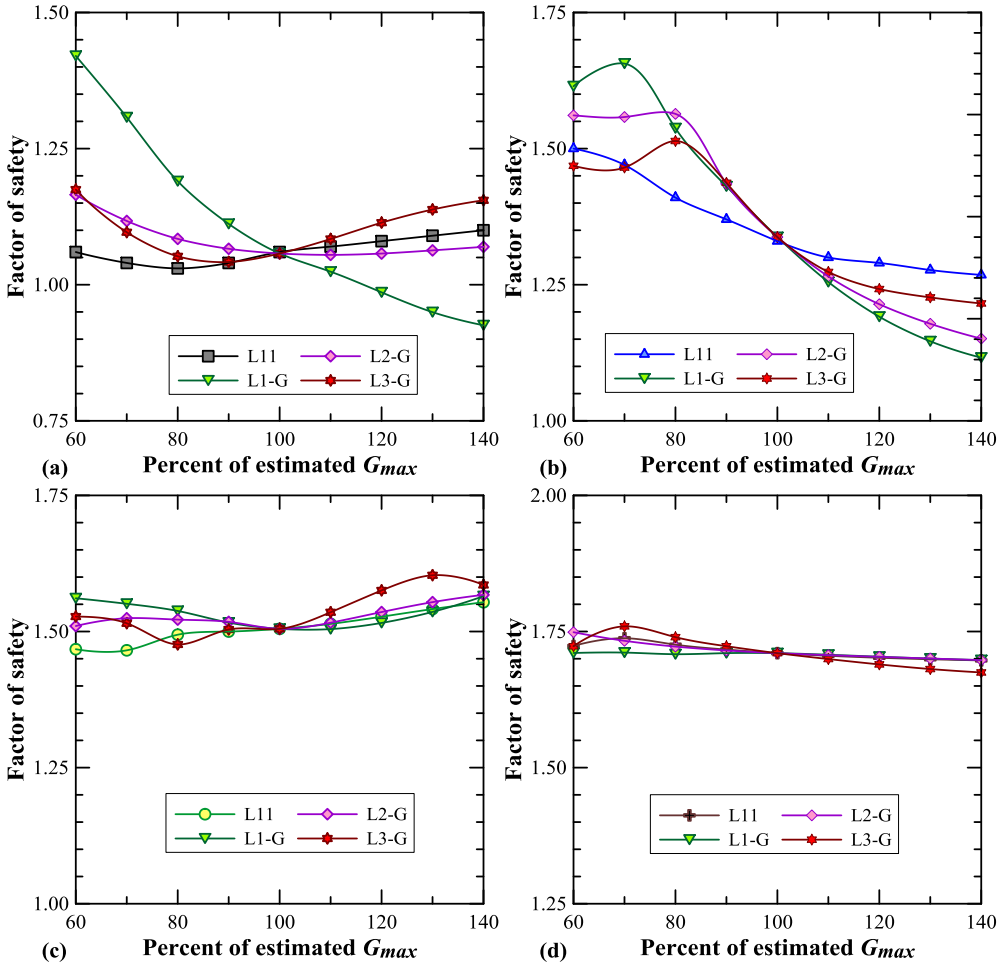

Figure 7-6: Variation of minimum FOS due to Caldwell earthquake (a) Left slip surface (b) Right slip surface; and Pawnee earthquake (c) Left slip surface (d) Right slip surface

The impact of inaccurate estimation of G_{max} values on seismic slope stability analysis was significant for the near resonance conditions (in the case of Caldwell EQ), despite having a low PGA of 0.05g. The effect was not prominent for Pawnee EQ since the acceleration induced in the structure by the seismic loading was small in magnitude. However, the effect is expected to be pronounced if an earthquake excitation of higher PGA is used for the analysis. Although the peak acceleration

was used as a measure of the seismic response of the structure, the FOS of a particular slip surface is not entirely dependent on the peak crest acceleration; rather it depends on the distribution of the forces induced by the earthquake on the slip surface under consideration.

Two different types of distribution of earthquake induced forces on a given slip surface may have the same peak crest acceleration, but will evidently have different FOS values. The displacement (mode) shapes can provide some understanding of the influence of inaccurate estimation of G_{max} values on the seismic response. Hence a detailed and case-specific study is required to understand the seismic response of the structure for the different combination of G_{max} values. A sensitivity analysis, as demonstrated in this study, should be performed for seismic slope stability assessment of critical structures, to incorporate the effect of probable incorrect estimation of G_{max} values. A similar study including the effect of reservoir water on the upstream side of the embankment structure is required to understand the changes in the sensitivity analysis results due to the presence of water.

7.4 Summary

This study shows that the variation in G_{max} values has a significant effect on the natural frequency of the structure, the peak crest acceleration and the factor of safety of the slopes when subjected to earthquake loading, especially for variation

in G_{max} values of lower layers of the structure. The effect of variation in G_{max} values was more pronounced when the variation occurred for a group of layers rather than that of a single layer. Moreover, previous studies have shown that the uncertainty in estimated G_{max} values increases with depth. This implies that an error in determining G_{max} values of a group of layers, especially for deeper layers of the structure, may have a significant effect on seismic response and slope stability analysis results. A sensitivity analysis, as demonstrated in this study, can provide useful information about the consequences of possible error in estimating the G_{max} values by a particular method, such as different in-situ tests, laboratory tests or using correlation equations.

Similar observations were made for a sensitivity analysis performed by varying the modulus values of along the shell of the dam, assuming that the shear wave velocity profile obtained from an in-situ test accurately estimated the material properties along the core of the dam. Such study would enable an engineer to gauge the impact of performing a seismic response and stability analysis using assumed modulus values for the shell of the dam, in absence of tests conducted along the slopes of the dam (Chakraborty et al. 2017b). The need for such an analysis along with the methodology and salient findings are provided in Appendix C.

Chapter 8: Conclusions and Scope for Future Studies

8.1 Summary

Earthen dams and levees are crucially important structures, whose stability and serviceability is of paramount importance to engineers. These structures are usually stable under normal working conditions but may become unstable in the event of earthquakes. Dams located in earthquake-prone areas are specifically designed to withstand the earthquake-induced forces. However, such design considerations were not considered in the 1930s, while designing and constructing the Eagle Mountain Dam, a hydraulic-fill dam in north Texas. Texas was not considered a seismically active zone, even a couple of decades ago. However, due to the increase in the number of earthquakes in Texas and surrounding states, the USGS has declared Texas to be a seismic hazard zone, with a 1% chance of experiencing an earthquake having PGA of 0.3g and above, in one year. This necessitates evaluating the performance of the EM dam under probable seismic events and determining the critical sections of the dam.

Hydraulic-fill dams around the world have a poor history of withstanding earthquake events, primarily due to liquefaction-induced damages in the sand layers of the dam and foundation. Owing to the method of construction, a significant extent of material variability exists along the body of the EM dam. Hence analyzing a typical section with representative material properties assigned

to different zones of the dam may not be able to portray the actual condition existing in the field. Moreover, unlike seismically active zones, real earthquake time-history data of past earthquakes were not available to evaluate the performance of the dam under probable future seismic events. Hence the purpose of this research work was to develop a comprehensive framework to perform a seismic response and stability analysis of hydraulic-fill dams, located in newly-declared induced-seismicity zones, incorporating the effect of material variability.

Extensive in-situ and laboratory test results were interpolated using geostatistics-based kriging analysis, to develop 3D models of the dam, depicting the variation of different material properties. These models were used to assign the material properties of the dam sections for different types of stability analyses. In the absence of the real earthquake time-history data, recorded at the dam site, a natural frequency based approach was implemented to study the response of the dam under different seismic events. Several earthquake time-history data, covering a wide range of predominant frequencies and peak accelerations, were selected to study the stability of the dam under probable seismic events. In addition to identifying the critical sections of the dam, the scenarios under which the stability of the dam may be most affected were determined.

8.2 Conclusions

Based on the observation made during this research study, the following conclusions can be drawn on various aspects involved while performing a seismic response and stability analysis:

- Small strain shear modulus (G_{max}) is an important parameter which governs the response of an earthen dam during seismic events. The G_{max} values can be determined by various methods such as laboratory tests on undisturbed samples, in-situ field tests and using correlation equations. Non-destructive testing techniques such as SASW test is often used to obtain the subsurface shear wave velocity profile to estimate the G_{max} values. Extensive laboratory and field testing performed as a part of this research work showed that the current SASW testing technique, using a hand-held hammer as an impact source, does not guarantee an acceptable test result with coherence greater than 0.95. Hence several trials are necessary to obtain satisfactory test results. The quality of the data was observed to improve drastically on using a constant impact energy source instead of using a hand-held hammer, which does not have any control over the impact energy. Stacking data of tests conducted with constant impact energy resulted in improved signal-to-noise ratio since waves of identical frequency contents were excited for each of the strikes. The coherence was

observed to be significantly improved over a wide range of frequencies, resulting in similar dispersion curves for a particular receiver spacing and created better overlap of the dispersion curves while generating the global dispersion curve. The use of a constant impact energy was hence found to be efficient and subsequently improve the quality and repeatability of the SASW field test.

- The natural frequency of an earthen dam is an essential parameter for seismic response analysis. The current methods for estimating the natural frequency cannot predict the degradation of natural frequency at large strain levels, experienced by the dam embankment materials, due to earthquake excitations. A thoroughly validated, novel method was developed as a part of this study which can be used to predict the strain-dependent natural frequency of an earthen embankment structure. The method involved subjecting the embankment structure under consideration to a synthesized wave, generated by superimposition of sinusoidal waves of a wide range of frequencies. The frequencies close to the natural frequency of the structure were excited due to resonance, and a fast Fourier transform of the recorded crest acceleration provided a measure of these frequencies. The first natural frequency of the dam subjected to a wide range of earthquake time-history data followed the same trend as that predicted by the developed method, validating the applicability of the

proposed method. The first natural frequency was found to remain constant at low strain levels, signifying linear elastic behaviour of the geomaterials. However, with an increase in the intensity of earthquake excitation, the first natural frequency was observed to degrade following a linear trend when plotted on a semi-logarithmic curve, with the root mean square (RMS) strain at the crest of the dam plotted in the logarithmic scale. The RMS strain at the middle of the crest of the dam was found to be a suitable surrogate measure of the disturbance level experienced by the dam during seismic events. This method was capable of incorporating the effect of non-linear material behaviour on the natural frequency of the dam at different strain levels.

- The natural frequency of the EM dam was found to decrease from 3.2 Hz at station 5 to 1.8 Hz at station 39. The variation in the construction method along the dam was the reason behind this observed behaviour. Station 5 was built by wetting and rolling the soil as compared to the hydraulic-fill portion of the dam (stations 14.5 to 39). The wetted and rolled zone of the dam had a higher shear wave velocity, as compared to the hydraulic-fill zone, probably due to a better control on the compaction of the soil layers, which was not possible in case of the hydraulic-fill method. Nonetheless, the strain-dependent variation of the first natural frequency was found to follow similar trends for all the sections of the dam. The slope of the linear

segment of the degradation curve was however found to depend on the material properties of the individual sections.

- The strength parameters obtained from the three-dimensional visualization models created using kriging analysis was able to capture the variation in different strength properties along the length of the hydraulic-fill dam. Assigning the respective material properties in the stability analysis is expected to give accurate results when compared to the traditional method of assigning representative material properties at different zones of the dam. The static stability analysis suggested that the dam is stable under normal working conditions. Pseudo-static analysis revealed that the hydraulic-fill segment of the dam, especially zone C_1 might be critical during seismic events. Low values of estimated undrained shear strength in the clay core of the dam were found to be the reason for low yield coefficient of sections belonging to zone C_1. A total stress analysis with additional consolidated undrained triaxial test results may provide a better understanding on the stability of slopes during earthquake events, since the use of undrained shear strength parameters makes the shear strength of soil independent of the overburden pressure.
- A reliability-based pseudo-static analysis, performed to incorporate the effect of uncertainty associated with the estimation of shear strength parameters, suggested that zone C_1 falls in the hazardous zone, for a

pseudo-static coefficient of 0.1g (roughly equivalent to an earthquake with PGA of 0.3g). Although the term "probability of failure" is used to assess the performance of the structure in case of a reliability based analysis, it should be noted that "failure" does not signify "catastrophic failure of the dam". "Probability of failure" in this study has been used as a measure of chances of the FOS of the slip surface to fall below 1, when the actual shear strength parameters existing in field is lower than that estimated and used in the analysis. The probability of failure was observed to drastically increase with an increase in horizontal seismic coefficient. Moreover, the reliability index was found to decrease, following a perfectly linear trend, with an increase in horizontal seismic coefficient. The reliability-based pseudo-static analysis was found to provide an index of the performance the dam under probable seismic events and can thus be used as an efficient tool to incorporate the effect of uncertainty associated with estimating the strength parameters.

- Besides pseudo-static analysis, Newmark deformation analysis was performed to evaluate the serviceability of the dam during earthquakes. Results suggest that the critical slip surfaces of the dam should not incur a permanent deformation exceeding 1 ft (0.3 m), for any earthquakes with a PGA of 0.3g, provided that there is no significant strength loss associated

with liquefaction. The EM dam satisfied the serviceability criteria recommended by USACE.

- The EM Dam is expected to be stable under earthquake excitations with PGA of 0.02g, corresponding to the deterministic seismic hazard analysis results. However, dynamic stability analysis, with the estimated increase in pore water pressure in the sand layers, showed chances of liquefaction of upstream sand shell and portions of the foundation sand layers, under some hypothetical earthquake scenarios. The effect was pronounced for earthquakes with PGA greater than 0.09 g and during seismic events when the predominant frequency of the earthquakes was close to the natural frequency of the EM dam. Under such near-resonance condition, the amplification of vibration was sufficient to cause liquefaction of upstream sand layers for earthquakes having PGA of 0.04g. This demonstrated the need of a natural frequency based approach for the dynamic analysis of a dam located in a newly-declared seismic hazard zone. A wide range of earthquakes, having various peak accelerations, and with predominant frequencies close to the natural frequency of the structure should be selected for the dynamic analysis and used as base excitations. Additional undrained cyclic triaxial test result on undisturbed sand samples would have enabled accurate estimation of excess pore water pressure and facilitated better assessment of the chances of cyclic liquefaction. The flow

liquefaction analysis based on the state parameter of the foundation sand layers suggested that the foundation sand layers are not expected to experience flow failures.

- All the analyses results were based on the G_{max} values estimated using the in-situ field tests conducted along the crest of the dam. However, the literature suggests chances of significant variability in the modulus values, based on the estimation methodology adopted (various in-situ tests, laboratory tests, and correlation equations). A sensitivity analysis by systematically varying the G_{max} values of different layers of the dam embankment was found to provide important insights on the impact of incorrect estimation of shear modulus, on seismic response and stability analysis. Results suggest that the effect of an inaccurate estimate of modulus values of the deeper thick layers of the embankment, close to the foundation, significantly affected the natural frequency and response of the structure. A sensitivity analysis is thus suggested to be performed for a critical project to have an understanding of the implications of incorrect estimation of the subsurface material properties.

8.3 Scope for future studies

The following are some of the areas which may be explored to advance the research work performed during this study:

- The ‘sum of sines’ method needs to be extended to three-dimensional models of a dam to better understand the variation of strain-dependent natural frequency of earthen structures. The study performed on two-dimensional plane strain models of the dam implicitly assumes the entire dam to be made up of the same material properties, as that present in the 2D model under consideration. However, such an assumption will seldom be correct and hence the behavior of a particular segment of the dam will depend on the stiffness and material properties of the adjacent sections. Such behavior may be thoroughly captured in a 3D analysis.
- In this study, the ‘sum of sines’ method was implemented using equivalent linear method of analysis, to capture the non-linear behavior of the geomaterial. Although the equivalent linear method gives acceptable results, it is in reality, a decoupled method of analysis. Hence the changes in material properties and effect of increase in pore water pressure, during the seismic shaking, cannot be accounted for in the equivalent method. Hence, the ‘sum of sines’ method needs to be extended using the fully coupled non-linear method of analysis to predict the strain-dependent variation in natural frequency.

- The reliability analysis was coupled with the pseudo-static analysis to determine the variation of probability of failure and reliability index with the pseudo-static coefficient. Since Monte Carlo simulations were used to perform the reliability analysis, it was computationally intensive and hence impossible to perform the same analysis for the dynamic stability analysis. Such an analysis would require to perform 35,000 simulations for each time step of the earthquake loading, for the entire duration of earthquake. Hence some simple method is required to study the variation in reliability index during earthquake shaking. Such an analysis would provide a better understanding of the performance of dam during earthquake events.
- The serviceability condition of the dam was checked using the Newmark deformation analysis. However, such an analysis is valid where there is no chance of liquefaction and excessive stress loss associated with earthquake shaking. Hence a deformation analysis is required to incorporate the effect of increase in pore water pressure and estimate the deformation incurred during different earthquake events. Extensive laboratory tests on undisturbed samples collected from the sand layers of the dam will be required to calibrate suitable constitutive models and perform the analysis.

References

Abdel-Ghaffar, A. M., and Koh, A.-S. (1981). "Longitudinal vibration of non-homogeneous earth dams." *Earthquake Engineering & Structural Dynamics*, 9(3), 279–305.

Abdel-Ghaffar, A. M., and Scott, R. F. (1979a). "Shear Moduli and Damping Factors of Earth Dam." *Journal of the Geotechnical Engineering Division*, 105(12), 1405–1426.

Abdel-Ghaffar, A. M., and Scott, R. F. (1979b). "Analysis of earth dam response to earthquakes." *Journal of Geotechnical Engineering Division*, 105(12), 1379–1404.

Abdel-Ghaffar, A. M., and Scott, R. F. (1981). "Vibration tests of full-scale earth dam." *International Journal of Rock Mechanics and Mining Sciences & Geomechanics Abstracts*, 18(4), 74.

Abdel-Ghaffar, A. M., Scott, R. F., and Craig, M. J. (1980). *Full-scale experimental investigation of a modern earth dam, Report number EERL-80-02*. California.

Abouseeda, H., and Dakoulas, P. (1998). "Non-linear dynamic earth dam-foundation interaction using a BE-FE method." *Earthquake Engineering & Structural Dynamics*, 27(9), 917–936.

Abramson, L. W., Lee, T. S., Sharma, S., and Boyce, G. M. (2001). *Slope Stability and Stabilization Methods*.

Addo, K. O., Kokanl, M. J., Woelierl, D. J., Beaten, N. F., and O'Brien, J. (1993). "A Case History of Dynamic Compaction Evaluation by the SASW Method." *7th Annual Vancouver Geotechnical Society Symposium*, Vancouver, 1–15.

Addo, K. O., and Robertson, P. K. (1992). "Shear-wave velocity measurement of soils using Rayleigh waves." *Canadian Geotechnical Journal*, 29(4), 558–568.

Ahmed, S. M. (2016). "Enhancing the CPT correlation with the small strain shear stiffness of sands." *Ain Shams Engineering Journal*, 1–10.

Akin, M. K., Kramer, S. L., and Topal, T. (2011). "Empirical correlations of shear wave velocity (Vs) and penetration resistance (SPT-N) for different soils in an earthquake-prone area (Erbaa-Turkey)." *Engineering Geology*, 119(1-2), 1–17.

De Alba, P., Chan, C. K., and Seed, H. B. (1976). *Determination of soil liquefaction characteristics by large-scale laboratory tests*. Shannon & Wilson.

Al-Hunaidi, M. O. (1992). "Difficulties with phase spectrum unwrapping in spectral analysis of surface waves nondestructive testing of pavements." *Canadian Geotechnical Journal*, 29(3), 506–511.

Al-Hunaidi, M. O. (1993). "Insights on the SASW nondestructive testing method." *Canadian Journal of Civil Engineering*, 20(6), 940–950.

Ambraseys, N. (1960a). "On the seismic behaviour of earth dams." *Proceedings of the 2nd World Conference on Earthquake Engineering*, 331–358.

Ambraseys, N. (1960b). "On the shear response of a two-dimensional truncated wedge subjected to an arbitrary disturbance." *Bulletin of the Seismological Society of America*, 50(1), 45–56.

Amorosi, A., Elia, G., Chan, A. C. H., and Kavvadas, M. (2008). "Fully coupled dynamic analysis of a real earth dam overlaying a stiff natural clayey deposit using an advanced constitutive model." *Proc. 12th Int. Conf. of IACMAG, Goa*, 2750–2757.

Anderson, D. G., Espana, C., and Mclamore, V. R. (1978). "Estimating in situ shear moduli at competent sites." *Proceedings of the ASCE Geotechnical Engineering Division Specialty Conference*, Pasadena, California, 181–197.

Aouad, M. F., Stokoe II, K. H., and Roesset, J. M. (1993). *Evaluation of Flexible Pavements and Subgrades using The Spectral-Analysis-of-Surface-Waves (SASW) Method, Report No. FHWA/TX-95+ 1175-7F*.

Ashmawy, A. K., Salgado, R., Guha, S., and Drnevich, V. P. (1995). "Soil damping and its use in dynamic analyses." University of Missouri--Rolla.

Asten, M., and Boore, D. (2005). "Comparison of Shear-velocity Profiles of Unconsolidated Sediments Near the Coyote Borehole (CCOC) Measured with Fourteen Invasive and Non-invasive Methods Editorial." *Journal of Environmental & Engineering Geophysics*, 10(2), 85–85.

Aydingun, O., and Adalier, K. (2003). "Numerical analysis of seismically induced liquefaction in earth embankment foundations. Part I. Benchmark model." *Canadian Geotechnical Journal*, 40(4), 753–765.

Ayothiraman, R., Raghu Kanth, S. T. G., and Sreelatha, S. (2012). "Evaluation of liquefaction potential of Guwahati: Gateway city to Northeastern India." *Natural Hazards*, 63(2), 449–460.

Babu, G. L. S., and Srivastava, A. (2010). "Reliability Analysis of Earth Dams." *Journal of Geotechnical and Geoenvironmental Engineering*, 136(7), 995–998.

Babu, G. L. S., Srivastava, A., and Sahana, V. (2007). "Analysis of stability of earthen dams in kachchh region, Gujarat, India." *Engineering Geology*, 94(3-4), 123–136.

Babu, G. L. S., Srivastava, A., and Sivapulliah, P. V. (2011). "Reliability analysis of strength of cement treated soils." *Georisk: Assessment and Management of Risk for Engineered Systems and Geohazards*, 5(3-4), 157–162.

Baecher, G. B., and Christian, J. T. (2005). *Reliability and statistics in geotechnical engineering*. John Wiley & Sons.

Baker, R. (2003). "A Second Look at Taylor's Stability Chart." *Journal of Geotechnical and Geoenvironmental Engineering*, 129(12), 1102–1108.

Baker, R., Shukha, R., Operstein, V., and Frydman, S. (2006). "Stability charts for pseudo-static slope stability analysis." *Soil Dynamics and Earthquake Engineering*, 26(9), 813–823.

Banerjee, A. (2017). "Response of Unsaturated Soils Under Monotonic and Dynamic Loading over Moderate Suction States." Doctoral Dissertation, The University of Texas at Arlington, Arlington, Texas.

Banerjee, A., Patil, U. D., Puppala, A. J., and Hoyos, L. R. (2018a). "Evaluation of Liquefaction Resistance in Silty Sand via Suction Controlled Cyclic Triaxial Tests." *PanAm Unsaturated Soils 2017*, American Society of Civil Engineers, Reston, VA, 543–552.

Banerjee, A., and Puppala, A. J. (2015). "Influence of Rate of Shearing on Strength Characteristics of Saturated and Unsaturated Silty Soil." *Proc. Indian Geotechnical Conference-2015*, Pune, India.

Banerjee, A., Puppala, A. J., Patil, U. D., Hoyos, L. R., and Bhaskar, P. (2018b). "A Simplified Approach to Determine the Response of Unsaturated Soils Using Multistage Triaxial Test." *IFCEE 2018*, American Society of Civil Engineers, Reston, VA, 332–342.

Beaty, M., and Byrne, P. M. (1998). "An Effective Stress Model for Pedicting Liquefaction Behaviour of Sand." *Geotechnical Earthquake Engineering and Soil Dynamics III*, 766–777.

Bishop, A. W., and Morgenstern, N. (1960). "Stability Coefficients for Earth Slopes." *Géotechnique*, 10(4), 129–153.

Boulanger, R. W., and Montgomery, J. (2016). “Nonlinear deformation analyses of an embankment dam on a spatially variable liquefiable deposit.” *Soil Dynamics and Earthquake Engineering*, 91, 222–233.

Boulanger, R. W., and Ziotopoulou, K. (2015). *PM4SAND (Version 3): A Sand Plasticity Model for Earthquake Engineering Applications*.

Brown, L. T., Boore, D. M., and Stokoe, K. H. (2000). “Comparison of shear-wave velocity profiles from SASW and downhole seismic tests at a strong-motion site.” *Proceedings of the 12th World Conference on Earthquake Engineering, Auckland, New Zealand*.

Bungenstab, F. C., and Bicalho, K. V. (2016). “Settlement predictions of footings on sands using probabilistic analysis.” *Journal of Rock Mechanics and Geotechnical Engineering*, 8(2), 198–203.

Bybordiani, M., and Arıcı, Y. (2017). “The use of 3D modeling for the prediction of the seismic demands on the gravity dams.” *Earthquake Engineering & Structural Dynamics*, 46(11), 1769–1789.

Caballero, S., Acharya, R., Banerjee, A., Bheemasetti, T. V., Puppala, A., and Patil, U. (2016). “Sustainable Slope Stabilization Using Biopolymer-Reinforced Soil.” *Geo-Chicago 2016*, American Society of Civil Engineers, Reston, VA, 116–126.

Caballero, S. R. (2017). “A COMPREHENSIVE RESILIENCE FRAMEWORK FOR THE SEISMIC EVALUATION OF HYDRAULIC FILL DAMS IN NORTH TEXAS.” The University of Texas at Arlington.

Caballero, S. R., Bheemasetti, T. V., Puppala, A. J., Verreault, L., and Koterba, D. (2017). “Three-Dimensional Visualization Model of the Eagle Mountain Dam Using Cone Penetration Test Data Based on Geostatistics.” *Geotechnical Frontiers 2017*, American Society of Civil Engineers, Reston, VA, 623–630.

Cai, Z., and Bathurst, R. J. (1996). “Deterministic sliding block methods for estimating seismic displacements of earth structures.” *Soil Dynamics and Earthquake Engineering*, 15(4), 255–268.

Cantieni, R. (2001). “Assessing a dam’s structural properties using forced vibration testing.” *Proc. IABSE International Conference on Safety, Risk and Reliability-Trends in Engineering, Malta*.

Cascone, E., and Rampello, S. (2003). “Decoupled seismic analysis of an earth dam.” *Soil Dynamics and Earthquake Engineering*, 23(5), 349–365.

Castro, G., Poulos, S. J., and Leathers, F. D. (1985). "Re-Examination of Slide of Lower San Fernando Dam." *Journal of Geotechnical Engineering*, 111(9), 1093–1107.

Castro, G., Seed, R. B., Keller, T. O., and Seed, H. B. (1992). "Steady State Strength Analysis of Lower San Fernando Dam Slide." *Journal of Geotechnical Engineering*, 118(3), 406–427.

Castro, R. R., Mucciarelli, M., Pacor, F., Federici, P., and Zaninetti, A. (1998). "Determination of the characteristic frequency of two dams located in the region of Calabria, Italy." *Bulletin of the Seismological Society of America*, 88(2), 503–511.

Cetin, K. O., Isik, N. S., Batmaz, S., and Karabiber, S. (2005). "A comparative study on the actual and estimated seismic response of Kiralkizi Dam in Turkey." *Journal of Earthquake Engineering*, 9(4), 445–460.

CGS. (2008). "Guidelines for evaluating and mitigating seismic hazards in California." *Calif. Geol. Surv. Spec. Publ. 117A*.

Chakraborty, S., Banerjee, A., Das, J. T., Mosadegh, L., and Puppala, A. J. (2018). "Impact of Variation of Small Strain Shear Modulus on Seismic Slope Stability Analysis of a Levee: A Sensitivity Analysis." *IFCEE 2018*, American Society of Civil Engineers, Reston, VA, 302–313.

Chakraborty, S., Bheemasetti, T. V., and Puppala, A. J. (2019a). "Effect of Constant Energy Source on Coherence Function in Spectral Analysis of Surface Waves (SASW) Testing." 59–65.

Chakraborty, S., Bheemasetti, T. V., Puppala, A. J., and Nazarian, S. (2017a). "A rational approach to select the number of field tests required to determine subgrade properties." *International Journal of Pavement Engineering*, 1–9.

Chakraborty, S., Bheemasetti, T. V., Puppala, A. J., and Verreault, L. (2019b). "Use of Constant Energy Source in SASW Test and Its Influence on Seismic Response Analysis." *Geotechnical Testing Journal*, 41(6), 20170220.

Chakraborty, S., Das, J. T., Banerjee, A., and Puppala, A. J. (2017b). "Effect of Erroneous Estimation of Small Strain Shear Moduli on Seismic Response of an Earth Dam." *Indian Geotechnical Conference*, Guwahati, India.

Chaney, R., Demars, K., Brignoli, E., Gotti, M., and Stokoe, K. (1996). "Measurement of Shear Waves in Laboratory Specimens by Means of Piezoelectric Transducers." *Geotechnical Testing Journal*, 19(4), 384–397.

Chang, Y., and Huang, T. (2005). "Slope stability analysis using strength

reduction technique." *Journal of the Chinese Institute of Engineers*, 28(2), 231–240.

Charatpangoon, B., Kiyono, J., Furukawa, A., and Hansapinyo, C. (2014). "Dynamic analysis of earth dam damaged by the 2011 Off the Pacific Coast of Tohoku Earthquake." *Soil Dynamics and Earthquake Engineering*, Elsevier, 64, 50–62.

Chatterjee, K., and Choudhury, D. (2014). "Seismic Analysis of Soil Slopes Using FLAC2D and Modified Newmark Approach." *Geo-Congress 2014 Technical Papers*, American Society of Civil Engineers, Reston, VA, 1196–1205.

Chen, L., Yuan, X., Cao, Z., Hou, L., Sun, R., Dong, L., Wang, W., Meng, F., and Chen, H. (2009). "Liquefaction macrophenomena in the great Wenchuan earthquake." *Earthquake Engineering and Engineering Vibration*, 8(2), 219–229.

Cheng, Y. M., Lansivaara, T., and Wei, W. B. (2007). "Two-dimensional slope stability analysis by limit equilibrium and strength reduction methods." *Computers and Geotechnics*, 34(3), 137–150.

Chillarige, A. V, Morgenstern, N. R., Robertson, P. K., and Christian, H. A. (1997). "Seabed instability due to flow liquefaction in the Fraser River delta." *Canadian Geotechnical Journal*, 34(4), 520–533.

Chopra, A. K. (1967). "Earthquake Response of Earth Dams." *Journal of the Soil Mechanics and Foundations Division*, 93(2), 65–81.

Chopra, A. K., and Chakrabarti, P. (1973). "The Koyna earthquake and the damage to Koyna dam." *Bulletin of the Seismological Society of America*, The Seismological Society of America, 63(2), 381–397.

Choudhury, D., Basu, S., and Bray, J. D. (2007). "Behaviour of Slopes under Static and Seismic Conditions by Limit Equilibrium Method." *Embankments, Dams, and Slopes*, American Society of Civil Engineers, Reston, VA, 1–10.

Chowdhury, R., Flentje, P., and Bhattacharya, G. (2009). *Geotechnical slope analysis*. Crc Press.

Chowdhury, R. N., and Xu, D. W. (1995). "Geotechnical system reliability of slopes." *Reliability Engineering & System Safety*, 47(3), 141–151.

Christian, J. T. (2004). "Geotechnical Engineering Reliability: How Well Do We Know What We Are Doing?" *Journal of Geotechnical and Geoenvironmental Engineering*, 130(10), 985–1003.

Christian, J. T. (2013). “Issues of Reliability in Stability of Slopes.” *Geo-Congress 2013*, American Society of Civil Engineers, Reston, VA, 2246–2261.

Christian, J. T., Ladd, C. C., and Baecher, G. B. (1994). “Reliability Applied to Slope Stability Analysis.” *Journal of Geotechnical Engineering*, 120(12), 2180–2207.

Christian, J. T., and Urzúa, A. (2017). “Anomalies in Pseudostatic Seismic Stability Analysis.” *Journal of Geotechnical and Geoenvironmental Engineering*, 143(5), 06017001.

Clough, R. W., and Chopra, A. K. (1966). “Earthquake stress analysis in earth dams.” *Journal of the Engineering Mechanics Division*, 92(2), 197–212.

Council, N. R. (1983). *Safety of Existing Dams*. National Academies Press, Washington, D.C.

Crespellani, T., Madiai, C., and Vannucchi, G. (1998). “Earthquake destructiveness potential factor and slope stability.” *Géotechnique*, 48(3), 411–419.

Dakoulas, P., and Gazetas, G. (1985). “A class of inhomogeneous shear models for seismic response of dams and embankments.” *International Journal of Soil Dynamics and Earthquake Engineering*, 4(4), 166–182.

Dash, H. K., and Sitharam, T. G. (2009). “Undrained Cyclic Pore Pressure Response of Sand–Silt Mixtures: Effect of Nonplastic Fines and Other Parameters.” *Geotechnical and Geological Engineering*, 27(4), 501–517.

Dawson, E., Motamed, F., Nesarajah, S., and Roth, W. (2000). “Geotechnical Stability Analysis by Strength Reduction.” *Slope Stability 2000*, American Society of Civil Engineers, Reston, VA, 99–113.

Dobry, R., and Alvarez, L. (1967). “Seismic failures of Chilean tailings dams.” *Journal of Soil Mechanics & Foundations Div*.

Duncan, J. M. (1996). “State of the Art: Limit Equilibrium and Finite-Element Analysis of Slopes.” *Journal of Geotechnical Engineering*, 122(7), 577–596.

Duncan, J. M. (2000). “Factors of Safety and Reliability in Geotechnical Engineering.” *Journal of Geotechnical and Geoenvironmental Engineering*, 126(4), 307–316.

Duncan, J. M., Wright, S. G., and Brandon, T. L. (2014). *Soil Strength and Slope Stability*. Wiley.

Elia, G., Amorosi, A., Chan, A. H. C., and Kavvadas, M. J. (2011). "Fully coupled dynamic analysis of an earth dam." *Géotechnique*, 61(7), 549–563.

Fan, K., Fredlund, D. G., and Wilson, G. W. (1986). "An interslice force function for limit equilibrium slope stability analysis." *Canadian Geotechnical Journal*, 23(3), 287–296.

Fell, R., MacGregor, P., Stapledon, D., and Bell, G. (2005). *Geotechnical engineering of dams*. CRC press.

FEMA. (2005). *Federal Guidelines for Dam Safety: Earthquake Analyses and Design of Dams, Federal Emergency Management Agency (FEMA), Washington DC*.

FEMA. (2017). "Information Needs for Dam Safety." <https://www.fema.gov/information-needs-dam-safety> (Mar. 31, 2018).

FEMA. (2018). "Benefits of Dams." <https://www.fema.gov/benefits-dams> (May 15, 2018).

Fenton, G. A., and Griffiths, D. V. (2010). "Reliability-Based Geotechnical Engineering." *GeoFlorida 2010*, American Society of Civil Engineers, Reston, VA, 14–52.

Finno, R. J., Harris, W. W., Mooney, M. A., and Viggiani, G. (1996). "Strain Localization and Undrained Steady State of Sand." *Journal of Geotechnical Engineering*, 122(6), 462–473.

Foster, M., Fell, R., and Spannagle, M. (2000). "The statistics of embankment dam failures and accidents." *Canadian Geotechnical Journal*, 37(5), 1000–1024.

Fredlund, D. G., and Krahn, J. (1977). "Comparison of slope stability methods of analysis." *Canadian Geotechnical Journal*, 14(3), 429–439.

Fredlund, D. G., Krahn, J., and Pufahl, D. E. (1981). "The relationship between limit equilibrium slope stability methods." *Proceedings of the International Conference on Soil Mechanics and Foundation Engineering*, 409–416.

Garevski, M., Zugic, Z., and Sesov, V. (2013). "Advanced seismic slope stability analysis." *Landslides*, 10(6), 729–736.

Gasparini, D. A., and Sun, W. J. (1982). "Random Vibration Analysis of Finite Element Models of Earth Dams." *Proceedings of the Conference on Soil Dynamics and Earthquake Engineering*, Southampton, 635–649.

Gauron, O., Boivin, Y., Ambroise, S., Saidou Sanda, A., Bernier, C., Paultre, P.,

Proulx, J., Roberge, M., and Roth, S.-N. (2018). “Forced-Vibration Tests and Numerical Modeling of the Daniel-Johnson Multiple-Arch Dam.” *Journal of Performance of Constructed Facilities*, 32(2), 04017137.

Gazetas, G. (1981). “A new dynamic model for earth dams evaluated through case histories.” *Soils and Foundations*, 21(1), 67–78.

Gazetas, G. (1987). “Seismic response of earth dams: some recent developments.” *Soil Dynamics and Earthquake Engineering*, 6(1), 2–47.

Gazetas, G., and Uddin, N. (1994). “Permanent Deformation on Preexisting Sliding Surfaces in Dams.” *Journal of Geotechnical Engineering*, 120(11), 2041–2061.

Griffiths, D. V., Huang, J., and Fenton, G. A. (2010). “Comparison of Slope Reliability Methods of Analysis.” *GeoFlorida 2010*, American Society of Civil Engineers, Reston, VA, 1952–1961.

Griffiths, D. V., and Lane, P. A. (1999). “Slope stability analysis by finite elements.” *Géotechnique*, 49(3), 387–403.

Gu, W. H., Morgenstern, N. R., and Robertson, P. K. (1993). “Progressive Failure of Lower San Fernando Dam.” *Journal of Geotechnical Engineering*, 119(2), 333–349.

Hack, R., Alkema, D., Kruse, G. A. M., Leenders, N., and Luzi, L. (2007). “Influence of earthquakes on the stability of slopes.” *Engineering Geology*, 91(1), 4–15.

Hall, J. F. (2006). “Problems encountered from the use (or misuse) of Rayleigh damping.” *Earthquake Engineering & Structural Dynamics*, 35(5), 525–545.

Hasofer, A. M., and Lind, N. C. (1974). “Exact and invariant second-moment code format.” *Journal of the Engineering Mechanics division*, ASCE, 100(1), 111–121.

Hatanaka, M. (1955). “Fundamental Considerations on the Earthquake Resistant Properties of the Earth Dam. Part I On the Vibration of Earth Dam.” *Bulletins - Disaster Prevention Research Institute, Kyoto University*, 11, 1–36.

Heinz, R. A. (1976). “Hydraulic Fill Dams/Earthquake Stability.” *Civil Engineering—ASCE*, ASCE, 46(5), 55–60.

Heisey, J. S., Stokoe, K. H., Hudson, W. R., and Meyer, A. H. (1982). *Determination of in situ shear wave velocities from spectral analysis of*

surface waves, Report No. FHWA/TX-82/34+256-2.

Hiltunen, D. R., and Woods, R. D. (1988). "SASW and crosshole test results compared." *Earthquake Engineering and Soil Dynamics II -Recent Advances in Ground-Motion Evaluation, ASCE*, 279–289.

Holtz, R. D., and Kovacs, W. D. (1981). *An introduction to geotechnical engineering*. Pearson; 2 edition.

Hryciw, R. D. (1990). "Small Strain Shear Modulus of Soil by Dilatometer." *Journal of Geotechnical Engineering*, 116(11), 1700–1716.

Idriss, I. M. (1973). *QUAD-4 A computer program for evaluating the seismic response of soil structures by variable damping finite element procedures EERC 73-16 Report*.

Idriss, I. M., and Boulanger, R. W. (2008). *Soil liquefaction during earthquakes. Monograph MNO-12, Earthquake Engineering Research Institute, Oakland, CA*.

Ike, C. C. O. (2008). "Classical Analysis of The Shear Vibration Characteristics of an Embankment Dam." *Nigerian Journal of Technology*, 27(1), 9–14.

Ishibashi, I., and Zhang, X. (1993). "Unified dynamic shear moduli and damping ratios of sand and clay." *Soils and Foundations*, 33(1), 182–191.

Ishihara, K. (1984). "Post-earthquake failure of a tailings dam due to liquefaction of pond deposit." *First International Conference on Case Histories in Geotechnical Engineering*, University of Missouri--Rolla, 1129–1143.

Ishihara, K. (1996). "Soil behaviour in earthquake geotechnics." Clarendon Press Oxford.

Ishizaki, H., and Hatakeyama, N. (1962). "Considerations on the Vibrational Behaviors of Earth Dams." *Bulletins - Disaster Prevention Research Institute, Kyoto University*, 52, 1–23.

Jafari, M. K., and Davoodi, M. (2006). "Dynamic characteristics evaluation of Masjed Soleiman Dam using in situ dynamic tests." *Canadian Geotechnical Journal*, 43(10), 997–1014.

Jansen, R. B. (2012). *Advanced dam engineering for design, construction, and rehabilitation*. Springer Science & Business Media.

Jibson, R. W. (2011). "Methods for assessing the stability of slopes during earthquakes—A retrospective." *Engineering Geology*, Elsevier B.V., 122(1-2), 43–50.

Joh, S. H. (1996). “Advances in the data interpretation technique for spectral-analysis-of-surface-waves (SASW) measurements.” *Doctoral Dissertation*, The University of Texas at Austin.

Kallioglou, P., Tika, T., and Pitilakis, K. (2008). “Shear Modulus and Damping Ratio of Cohesive Soils.” *Journal of Earthquake Engineering*, 12(6), 879–913.

Kayen, R., Moss, R. E. S., Thompson, E. M., Seed, R. B., Cetin, K. O., Kiureghian, A. Der, Tanaka, Y., and Tokimatsu, K. (2013). “Shear-Wave Velocity–Based Probabilistic and Deterministic Assessment of Seismic Soil Liquefaction Potential.” *Journal of Geotechnical and Geoenvironmental Engineering*, 139(3), 407–419.

Keightley, W. O. (1966). “Vibrational characteristics of an earth dam.” *Bull. Seismol. Soc. Am.*, 56(6), 1207–1226.

Krahn, J. (2003). “The 2001 R.M. Hardy Lecture: The limits of limit equilibrium analyses.” *Canadian Geotechnical Journal*, 40(3), 643–660.

Krahn, J. (2004a). *Dynamic modeling with QUAKE/W: an engineering methodology*. GEO-SLOPE.

Krahn, J. (2004b). “Stability modeling with SLOPE/W: An engineering methodology.” *GEOSLOPE/W International Ltd. Calgary, Alberta, Canada*.

Krahn, J. (2007). “Limit equilibrium, strength summation and strength reduction methods for assessing slope stability.” *Rock Mechanics: Meeting Society’s Challenges and Demands*, 311–318.

Kramer, S. L. (1996). *Geotechnical earthquake engineering*. (W. J. Hall, ed.), Prentice-Hall Civil Engineering and Engineering Mechanics Series, Upper Saddle River, NJ.

Kramer, S. L., and Smith, M. W. (1997). “Modified Newmark Model for Seismic Displacements of Compliant Slopes.” *Journal of Geotechnical and Geoenvironmental Engineering*, 123(7), 635–644.

Kuhlemeyer, R. L., and Lysmer, J. (1973). “Finite Element Method Accuracy for Wave Propagation Problems.” *Journal of the Soil Mechanics and Foundations Division*, ASCE, 99(5), 421–427.

Kulhawy, F. H., and Mayne, P. H. (1990). *Manual on estimating soil properties for foundation design, Report EL-6800 Electric Power Research Institute, EPRI*.

Kumar, J., and Hazra, S. (2014). “Effect of Input Source Energy on SASW Evaluation of Cement Concrete Pavement.” *Journal of Materials in Civil Engineering*, 26(6), 1–7.

Kumar, J., and Rakaraddi, P. G. (2013). “Effect of Source Energy for SASW Testing on Geological Sites.” *Geotechnical and Geological Engineering*, 31(1), 47–66.

Küpper, A. M. A. G. (1991). “Design of hydraulic fill.” University of Alerta.

Lam, L., and Fredlund, D. G. (1993). “A general limit equilibrium model for three-dimensional slope stability analysis.” *Canadian Geotechnical Journal*, 30(6), 905–919.

Laouafa, F., and Darve, F. (2002). “Modelling of slope failure by a material instability mechanism.” *Computers and Geotechnics*, 29(4), 301–325.

Law, K. T., and Lumb, P. (1978). “A limit equilibrium analysis of progressive failure in the stability of slopes.” *Canadian Geotechnical Journal*, 15(1), 113–122.

Lee, K. L., and Albaisa, A. (1974). “Earthquake Induced Settlements in Saturated Sands.” *Journal of the Geotechnical Engineering Division*, ASCE, 100(4), 387–406.

Lentini, V., and Castelli, F. (2017). “Resonant column and torsional shear tests for the evaluation of the shear modulus and damping ratio of soil.” 190003.

Leonards, G. (1982). “Investigation of failures.” *Journal of Geotechnical and Geoenvironmental Engineering*, 108(GT2), 187–246.

Leshchinsky, D. (2001). “Design Dilemma: Use peak or residual strength of soil.” *Geotextiles and Geomembranes*, 19(2), 111–125.

Liang, R. Y., Nusier, O. K., and Malkawi, a. H. (1999). “A reliability based approach for evaluating the slope stability of embankment dams.” *Engineering Geology*, 54, 271–285.

Lin, J.-S., and Whitman, R. V. (1983). “Decoupling approximation to the evaluation of earthquake-induced plastic slip in earth dams.” *Earthquake Engineering & Structural Dynamics*, 11(5), 667–678.

Liu, S. Y., Shao, L. T., and Li, H. J. (2015). “Slope stability analysis using the limit equilibrium method and two finite element methods.” *Computers and Geotechnics*, 63, 291–298.

MacGregor, P., Fell, R., Stapledon, D., Bell, G., and Foster, M. (2014).

Geotechnical engineering of dams. CRC press.

Makdisi, F. I., and Seed, H. B. (1978). "Simplified Procedure for Estimating Dam and Embankment Earthquake-Induced Deformations." *Journal of the Geotechnical Engineering Division*, 104(7), 849–867.

Malkawi, A. I., Hassan, W. F., and Abdulla, F. A. (2000). "Uncertainty and reliability analysis applied to slope stability." *Structural Safety*, 22(2), 161–187.

Mancuso, C., and Vinale, F. (1993). "Use of SASW in earth dam investigation." *Geotechnical Engineering of Hard Soils-soft Rocks: Proceedings of an International Symposium Under the Auspices of the International Society for Soil Mechanics and Foundation Engineering (ISSMFE), the International Association of Engineering Geology (IAEG*, 1291–1298.

Mansour, M. F. (2016). "A numerical study on permanent seismic deformation of dry sand slopes." *International Journal of Geotechnical Engineering*, 10(2), 99–106.

Marcuson III, W. F., Hynes, M. E., and Franklin, A. G. (1992). "Seismic Stability and Permanent Deformation Analyses: the Last Twenty Five Years." *ASCE, Stability and Performance of Slopes and Embankments II*.

Marcuson, W. F. (1978). "Definition of terms related to liquefaction." *Journal of the Geotechnical engineering division*, ASCE, 104(9), 1197–1200.

Marcuson, W. F., Hynes, M. E., and Franklin, A. G. (1990). "Evaluation and Use of Residual Strength in Seismic Safety Analysis of Embankments." *Earthquake Spectra*, 6(3), 529–572.

Marosi, K. T., and Hiltunen, D. R. (2004). "Characterization of Spectral Analysis of Surface Waves Shear Wave Velocity Measurement Uncertainty." *Journal of Geotechnical and Geoenvironmental Engineering*, 130(10), 1034–1041.

Martin, G. R., Finn, W. D. L., and Seed, H. B. (1975). "Fundementals of liquefaction under cyclic loading." *Journal of Geotechnical and Geoenvironmental Engineering*, 101(ASCE# 11231 Proceeding).

Matsui, T., and San, K.-C. (1992). "Finite element slope stability analysis by shear strength reduction technique." *Soils and foundations*, THE JAPANESE GEOTECHNICAL SOCIETY, 32(1), 59–70.

Mayne, P. W., and Rix, G. J. (1995). "Correlations between Shear Wave Velocity and Cone Tip Resistance in Natural Clays." *Soils and Foundations*, 35(2), 107–110.

Meehan, C. L., and Vahedifard, F. (2013). “Evaluation of simplified methods for predicting earthquake-induced slope displacements in earth dams and embankments.” *Engineering Geology*, 152(1), 180–193.

Mejia, L. H., and Dawson, E. M. (2006). “Earthquake deconvolution for FLAC.” *4th International FLAC Symposium on Numerical Modeling in Geomechanics*, 4–10.

Mejia, L. H., and Seed, H. B. (1983). “Comparison of 2D and 3D Dynamic Analyses of Earth Dams.” *Journal of Geotechnical Engineering*, 109(11), 1383–1398.

Mejia, L. H., Seed, H. B., and Lysmer, J. (1982). “Dynamic analysis of earth dams in three dimensions.” *Journal of the Geotechnical Engineering Division*, ASCE, 108(12), 1586–1604.

Mejia, L. H., Sun, J. I., and Leung, K. K. (2005). “Seismic upgrade of hydraulic fill dam by buttressing.” *Soil Dynamics and Earthquake Engineering*, 25(7-10), 571–579.

Melent’ev, V. A. (1980). “Development of hydraulic-fill dam construction in the Soviet Union.” *Power Technology and Engineering (formerly Hydrotechnical Construction)*, Springer, 14(12), 1268–1271.

Melo, C., and Sharma, S. (2004). “Seismic coefficients for pseudostatic slope analysis.” *13 th World Conference on Earthquake Engineering, Vancouver, Canada*.

Miller, G. F., and Pursey, H. (1955). “On the Partition of Energy between Elastic Waves in a Semi-Infinite Solid.” *Proceedings of the Royal Society A: Mathematical, Physical and Engineering Sciences*, 233(1192), 55–69.

Mogami, T., and Kubu, K. (1953). “The behaviour of soil during vibration.” *Proc. of 3rd Int. Conf. on SMFE*, 1152–1155.

Mononobe, N., Takata, A., and Matumura, M. (1936). “Seismic stability of the earth dam.” *Proceeding of the 2nd Congress on Large Dams*, Washington , DC, 435–442.

Montgomery, J., Boulanger, R. W., Armstrong, R. J., and Malvick, E. J. (2014). “Anisotropic Undrained Shear Strength Parameters for Nonlinear Deformation Analyses of Embankment Dams.” *Geo-Congress 2014 Technical Papers*, American Society of Civil Engineers, Reston, VA, 1294–1306.

Morgenstern, N. R., and Küpper, A. A. G. (1988). “Hydraulic fill structures-a

perspective." *Hydraulic Fill Structures*, 1–31.

Morgenstern, N. R., and Price, V. E. (1965). "The Analysis of the Stability of General Slip Surfaces." *Géotechnique*, 15(1), 79–93.

Moss, R. E. S. (2008). "Quantifying Measurement Uncertainty of Thirty-Meter Shear-Wave Velocity." *Bulletin of the Seismological Society of America*, 98(3), 1399–1411.

Mukherjee, M., and Prashant, A. (2009). "Evaluation of SASW test configurations and associated data uncertainties in generating site specific dispersion curves." *Soils and Foundations*, 49(5), 699–709.

Nazarian, S., and Stokoe II, K. H. (1983). *Evaluation of Moduli and Thicknesses of Pavement Systems by Spectral-Analysis-of-Surface-Waves Method, Report No. FHWA/TX-83/26+256-4*.

Nazarian, S., and Stokoe, K. H. (1985). *In situ determination of elastic moduli of pavement systems by spectral analysis of surface waves method (practical aspects), Report No. FHWA/TX-86/l3+368-lF 2*.

Newmark, N. M. (1965). "Effects of Earthquakes on Dams and Embankments." *Géotechnique*, 15(2), 139–160.

Nian, T. K., Chen, G. Q., Wan, S. S., and Luan, M. T. (2011). "Non-convergence Criterion on Slope Stability FE Analysis by Strength Reduction Method." *Journal of Convergence Information Technology*, 6(5), 78–88.

Okamoto, S. (1984). "Introduction to Earthquake Engineering." University of Tokyo Press, 474–477.

Okamoto, S., Hakuno, M., Kato, K., and Kawakami, F. (1969). "On the dynamical behavior of an earth dam during earthquakes." *Proceedings of the 4th World Conference on Earthquake Engineering*, Santiago, Chile, 443–457.

Parish, Y., Sadek, M., and Shahrour, I. (2009). "Review Article: Numerical analysis of the seismic behaviour of earth dam." *Natural Hazards and Earth System Science*, 9(2), 451–458.

Park, D. (2016). "Seismic Evaluation of Existing Earth-Cored Fill Dams based on Pseudostatic and FE-Newmark Approaches." *Journal of Korean Society of Hazard Mitigation*, 16(4), 215–225.

Patil, U. D., Banerjee, A., Puppala, A. J., and Hoyos, L. R. (2018). "Shear Strength Prediction of Compacted Silty Sand at Peak/Critical State Failure

over Wider Suction Range." *PanAm Unsaturated Soils 2017*, American Society of Civil Engineers, Reston, VA, 340–349.

Pelecanos, L. (2013). "Seismic Response and Analysis of Earth Dams." Imperial College London.

Pelecanos, L., Kontoe, S., and Zdravković, L. (2015). "A case study on the seismic performance of earth dams." *Géotechnique*, 65(11), 923–935.

Petersen, M. D., Mueller, C. S., Moschetti, M. P., Hoover, S. M., Shumway, A. M., McNamara, D. E., Williams, R. A., Llenos, A. L., Ellsworth, W. L., Michael, A. J., and others. (2017). "2017 one-year seismic-hazard forecast for the Central and Eastern United States from induced and natural earthquakes." *Seismological Research Letters*, Seismological Society of America, 88(3), 772–783.

Petrovski, J., Paskalov, T., and Jurukovski, D. (1974). "Dynamic full-scale test of an earthfill dam." *Géotechnique*, 24(2), 193–206.

Phoon, K.-K., and Kulhawy, F. H. (1999). "Evaluation of geotechnical property variability." *Canadian Geotechnical Journal*, 36(4), 625–639.

Piao, R. (Park), Rippe, A. H., Myers, B., and Lane, K. W. (2006). "Earth Dam Liquefaction and Deformation Analysis Using Numerical Modeling." *GeoCongress 2006*, American Society of Civil Engineers, Reston, VA, 1–6.

Pinyol, N. M., Alonso, E. E., and Olivella, S. (2008). "Rapid drawdown in slopes and embankments." *Water Resources Research*, 44(5).

Polito, C. P., Green, R. A., and Lee, J. (2008). "Pore Pressure Generation Models for Sands and Silty Soils Subjected to Cyclic Loading." *Journal of Geotechnical and Geoenvironmental Engineering*, 134(10), 1490–1500.

Popescu, R., Prevost, J. H., and Deodatis, G. (1997). "Effects of spatial variability on soil liquefaction: some design recommendations." *Géotechnique*, 47(5), 1019–1036.

Prevost, J. H., Abdel-Ghaffar, A. M., and Lacy, S. J. (1985). "Nonlinear Dynamic Analyses of an Earth Dam." *Journal of Geotechnical Engineering*, 111(7), 882–897.

Puppala, A. J., Kadam, R., Madhyannapu, R. S., and Hoyos, L. R. (2006). "Small-Strain Shear Moduli of Chemically Stabilized Sulfate-Bearing Cohesive Soils." *Journal of Geotechnical and Geoenvironmental Engineering*, 132(3), 322–336.

Raptakis, D., and Makra, K. (2015). “Multiple estimates of soil structure at a vertical strong motion array: Understanding uncertainties from different shear wave velocity profiles.” *Engineering Geology*, 192, 1–18.

Rathje, E. M., and Bray, J. D. (2000). “Nonlinear Coupled Seismic Sliding Analysis of Earth Structures.” *Journal of Geotechnical and Geoenvironmental Engineering*, 126(11), 1002–1014.

Richart, F. E., Hall, J. R., and Woods, R. D. (1970). “Vibrations of soils and foundations.”

Rix, G. J. (1990). “Experimental study of factors affecting the spectral-analysis-of-surface-waves method.” The University of Texas at Austin.

Robertson, P. K., and Cabal, K. L. (2015). *Guide to cone penetration testing for geotechnical engineering*. Gregg Drilling and Testing Inc.

Robertson, P. K., Campanella, R. G., Gillespie, D., and Greig, J. (1986a). “Use of Piezometer Cone Data.” *Use of In Situ Tests in Geotechnical Engineering, Specialty Publication, SM 92*, 1263–1280.

Robertson, P. K., Campanella, R. G., Gillespie, D., and Rice, A. (1986b). “Seismic Cpt to Measure in Situ Shear Wave Velocity.” *Journal of Geotechnical Engineering*, 112(8), 791–803.

Robertson, P. K., Sasitharan, S., Cunning, J. C., and Sego, D. C. (1995). “Shear-Wave Velocity to Evaluate In-Situ State of Ottawa Sand.” *Journal of Geotechnical Engineering*, 121(3), 262–273.

Roesler, S. K. (1979). “Anisotropic shear modulus due to stress anisotropy.” *Journal of the Geotechnical Engineering Division*, ASCE, 105(7), 871–880.

Rollins, K. M., Evans, M. D., Diehl, N. B., and III, W. D. D. (1998). “Shear Modulus and Damping Relationships for Gravels.” *Journal of Geotechnical and Geoenvironmental Engineering*, 124(5), 396–405.

Rosenblueth, E. (1975). “Point estimates for probability moments.” *Proceedings of the National Academy of Sciences*, 72(10), 3812–3814.

Sanchez-Salinero, I., Roesset, J. M., Stokoe, K. H., and Kenneth, H. (1986). *Analytical studies of body wave propagation and attenuation*.

Sayyedsadr, M., and Drnevich, V. (1989). “SASWOPR: A Program to Operate on Spectral Analysis of Surface Wave Data.” *Nondestructive Testing of Pavements and Backcalculation of Moduli*, ASTM International, 100 Barr Harbor Drive, PO Box C700, West Conshohocken, PA 19428-2959, 670–

682.

Seed, H. B. (1979). “Considerations in the earthquake-resistant design of earth and rockfill dams.” *Géotechnique*, 29(3), 215–263.

Seed, H. B. (1981). “Earthquake-Resistant Design of Earth Dams.” *Proceedings: First International Conference on Recent Advances in Geotechnical Earthquake Engineering and Soil Dynamics, April 26 - May 3, 1981, St. Louis, Missouri*, 1157–1173.

Seed, H. B., De Alba, P. A., and Makdisi, F. I. (1978). “Performance of Earth Dams during Earthquakes.” *Journal of the Geotechnical Engineering Division*, 104(7), 967–994.

Seed, H. B., and Idriss, I. M. (1970). *Soil moduli and damping factors for dynamic response analyses. Report No. EERC 70-10, Earthquake Engineering Resource Center, University of California, Berkley, California.*

Seed, H. B., Idriss, I. M., Lee, K. L., and Makdisi, F. I. (1975a). “Dynamic analysis of the slide in the Lower San Fernando Dam during the earthquake of February 9, 1971.” *Journal of Geotechnical and Geoenvironmental Engineering*, 101(ASCE# 11541 Proceeding), 889–911.

Seed, H. B., Lee, K. L., Idriss, I. M., and Makdisi, F. I. (1975b). “The slides in the San Fernando Dams during the earthquake of February 9, 1971.” *Journal of Geotechnical and Geoenvironmental Engineering*, 101(ASCE# 11449 Proceeding).

Seed, H. B., and Martin, G. R. (1966). “The seismic coefficient in earth dam design.” *Journal of Soil Mechanics & Foundations Div*, 92(Proc. Paper 4824).

Seed, H. B., Wong, R. T., Idriss, I. M., and Tokimatsu, K. (1986). “Moduli and Damping Factors for Dynamic Analyses of Cohesionless Soils.” *Journal of Geotechnical Engineering*, 112(11), 1016–1032.

Shafikhani, A. (2018). “A NEW APPROACH FOR PERFORMANCE EVALUATION OF BRIDGE INFRASTRUCTURE USING TERRESTRIAL LIDAR AND ADVANCED MATHEMATICAL MODELING.” University of Texas at Arlington.

Shafikhani, A., Bheemasetti, T. V., and Puppala, A. J. (2017). “Effect of Seasonal Changes on a Hybrid Soil–Geofoam Embankment System.” *International Journal of Geosynthetics and Ground Engineering*, 3(4), 39.

Shafikhani, A., Bheemasetti, T. V., Puppala, A. J., and Banerjee, A. (2018).

"Analysis and Interpretation of Inclinometer and Pressure Cell Data on a Soil-Geofoam Embankment." *Proceedings of GeoShanghai 2018 International Conference: Multi-physics Processes in Soil Mechanics and Advances in Geotechnical Testing*, Springer Singapore, Singapore, 410–418.

Sheu, J.-C. (1987). "Applications and limitations of the spectral-analysis-of-surface-waves method." The University of Texas at Austin.

Shukha, R., and Baker, R. (2008). "Design implications of the vertical pseudo-static coefficient in slope analysis." *Computers and Geotechnics*, 35(1), 86–96.

Siegel, T. C. (2013). "Liquefaction Mitigation Synthesis Report." *DFI Journal - The Journal of the Deep Foundations Institute*, 7(1), 13–31.

Song, Z., and Su, C. (2017). "Computation of Rayleigh Damping Coefficients for the Seismic Analysis of a Hydro-Powerhouse." *Shock and Vibration*, 2017, 1–11.

Spencer, E. (1967). "A Method of analysis of the Stability of Embankments Assuming Parallel Inter-Slice Forces." *Géotechnique*, 17(1), 11–26.

Steward, T., Sivakugan, N., Shukla, S. K., and Das, B. M. (2011). "Taylor's Slope Stability Charts Revisited." *International Journal of Geomechanics*, 11(4), 348–352.

Stokoe, K. H., Lee, S. H. H., and Knox, D. P. (1985). "Shear moduli measurements under true triaxial stresses." *Advances in the art of testing soils under cyclic conditions*, 166–185.

Stokoe, K. H., Rix, G. J., and Nazarian, S. (1991). "In situ seismic testing with surface waves." *International Journal of Rock Mechanics and Mining Sciences & Geomechanics Abstracts*, 28(2-3), A91.

Suits, L. D., Sheahan, T. C., Rosenblad, B. L., and Bertel, J. D. (2008). "Potential Phase Unwrapping Errors Associated with SASW Measurements at Soft-Over-Stiff Sites." *Geotechnical Testing Journal*, 31(5), 101411.

Suits, L., Sheahan, T., Leong, E., Yeo, S., and Rahardjo, H. (2005). "Measuring Shear Wave Velocity Using Bender Elements." *Geotechnical Testing Journal*, 28(5), 12196.

Taylor, D. W. (1937). *Stability of earth slopes*. Wright & Potter print.

Teachavorasinskun, S., Kato, H., Shibuya, S., Horii, N., and Tatsuoka, F. (1991). "Stiffness and damping of sands in torsion shear." University of Missouri--

Rolla.

Terzaghi, K. (1950). *Mechanism of Landslides, Geological Society of America*. Harvard University, Department of Engineering.

Tezcan, S. O., Bhatia, S. K., and Fiegle, S. (2001). "Seismic Stability and Rehabilitation Analysis of a Hydraulic Fill Dam." University of Missouri--Rolla.

Thevanayagam, S. (1998). "Effect of Fines and Confining Stress on Undrained Shear Strength of Silty Sands." *Journal of Geotechnical and Geoenvironmental Engineering*, 124(6), 479–491.

Thorel, L., Murillo, C., Garnier, J., and Caicedo, B. (2006). "Characterization of centrifuge model using SASW techniques." *Physical Modelling in Geotechnics*, Taylor & Francis, 223–228.

Tortajada, C. (2015). "Dams: An Essential Component of Development." *Journal of Hydrologic Engineering*, 20(1), A4014005.

Trifunac, M. D. (1972). "Comparisons between ambient and forced vibration experiments." *Earthquake Engineering & Structural Dynamics*, 1(2), 133–150.

Troncoso, J. H. (1988). "Evaluation of seismic behavior of hydraulic fill structures." *Conference on Hydraulic Fill Structures, (ASCE Geotechnical Special Publication No 21)*, Fort Collins, 475–491.

TRWD. (2016). "TRWD History." <http://www.trwd.com/about-trwd/history/> (May 18, 2018).

Tsiatas, G., and Gazetas, G. (1982). "Plane-strain and shear-beam free vibration of earth dams." *International Journal of Soil Dynamics and Earthquake Engineering*, 1(4), 150–160.

USACE. (1997). *Engineering and design: Introduction to probability and reliability methods for use in geotechnical engineering*.

USACE. (1998). "Risk-based analysis in geotechnical engineering for support of planning studies." *Engineer Technical Letter*, (1110-2), 556.

USACE. (2003). *Slope Stability Engineer Manual EM 1110-2-1902*.

USACE. (2010). "USACE Earthquake Research & Implementation Activities." <https://www.nehrp.gov/pdf/ACEHRNov2010_USACE.pdf>.

USBR. (2011). "Chapter 4 : Static Stability Analysis (Design Standards No. 13:

Embankment Dams).” *Design Standards No. 13. Embankment Dams.*, 4(13).

USGS. (2016). “Induced Earthquakes.” <https://earthquake.usgs.gov/research/induced/hazards.php> (May 12, 2018).

USSD. (2007). *Strength of Materials for Embankment Dams, United States Society on Dams*. *Society*.

Valenzuela, L. (2015). “Tailings Dams and Hydraulic Fills The 2015 Casagrande Lecture.” *Geotechnical Synergy in Buenos Aires 2015: Invited Lectures of the 15th Pan-American Conference on Soil Mechanics and Geotechnical Engineering and the 8th South American Congress on Rock Mechanics, 15--18 November 2015, Buenos Aires, Argentina*, 5.

Valenzuela, L. (2016). “Design, construction, operation and the effect of fines content and permeability on the seismic performance of tailings sand dams in Chile.” *Obras y proyectos*, (19), 6–22.

Vick, S. G. (1996). “Hydraulic tailings.” *Landslides: investigation and mitigation. Edited by AK Turner, RL Schuster, and LR Schuster. Transportation Research Board, Special Report*, 247, 577–584.

Vijayasri, T., Raychowdhury, P., and Patra, N. R. (2017). “Seismic Response Analysis of Renusagar Pond Ash Embankment in Northern India.” *International Journal of Geomechanics*, 17(6), 04016141.

Vucetic, M., and Dobry, R. (1991). “Effect of Soil Plasticity on Cyclic Response.” *Journal of Geotechnical Engineering*, 117(1), 89–107.

Wang, Y., and Kulhawy, F. H. (2008). “Reliability Index for Serviceability Limit State of Building Foundations.” *Journal of Geotechnical and Geoenvironmental Engineering*, 134(11), 1587–1594.

Wiltshire, R. L. (2002). “100 Years of embankment dam design and construction in the US Bureau of Reclamation.” *Just Add Water: Reclamation Projects and Development Fantasies in the Upper Basin of the Colorado River*, 67.

Wolff, T. (1996). “Probabilistic slope stability in Theory and Practice.” *Uncertainty in the Geologic Environment*, 419–433.

Wood, J. H. (1973). *Earthquake-induced soil pressures on structures. California Institute of Technology*.

Woodward, P. K., and Griffiths, D. V. (1993). “Three-dimensional finite element analyses of the natural frequencies of non-homogeneous earth dams.” *International Journal of Rock Mechanics and Mining Sciences &*

Geomechanics Abstracts, 30(3), A199.

Woodward, P. K., and Griffiths, D. V. (1996). "Influence of viscous damping in the dynamic analysis of an earth dam using simple constitutive models." *Computers and Geotechnics*, 19(3), 245–263.

Wright, S. G., Kulhawy, F. G., and Duncan, J. M. (1973). "Accuracy of equilibrium slope stability analysis." *Journal of Soil Mechanics & Foundations Div*, 99(Proc Paper 10097).

Wu, B. (2015). "A correction of the half-power bandwidth method for estimating damping." *Archive of Applied Mechanics*, 85(2), 315–320.

Xenaki, V. C., and Athanasopoulos, G. A. (2003). "Liquefaction resistance of sand–silt mixtures: an experimental investigation of the effect of fines." *Soil Dynamics and Earthquake Engineering*, 23(3), 1–12.

Xia, Z.-F., Ye, G.-L., Wang, J.-H., Ye, B., and Zhang, F. (2010). "Fully coupled numerical analysis of repeated shake-consolidation process of earth embankment on liquefiable foundation." *Soil Dynamics and Earthquake Engineering*, 30(11), 1309–1318.

Xiao, W., He, Y., and Zhang, Y. (2008). "Simplified analytical solution for free vibration characteristics of Hardfill dam." *Frontiers of Architecture and Civil Engineering in China*, 2(3), 219–225.

Xiong, M., and Huang, Y. (2017). "Stochastic seismic response and dynamic reliability analysis of slopes: A review." *Soil Dynamics and Earthquake Engineering*, Elsevier Ltd, 100(February), 458–464.

Yan, L., and Byrne, P. M. (1991). "Stress State and Stress Ratio Effects in downhole and crosshole in shear wave velocities on sand, Proceedings: 2 nd International Conference onRecent Advances in Geotechnical Earthquake Engineering and Soil Dynamics, St." *Louis, Missouri*, 1, 299–306.

Yang, J., Jin, F., Wang, J.-T., and Kou, L.-H. (2017). "System identification and modal analysis of an arch dam based on earthquake response records." *Soil Dynamics and Earthquake Engineering*, 92, 109–121.

Yegian, M. K., Marciano, E. A., and Ghahraman, V. G. (1991). "Seismic risk analysis for earth dams." *Journal of Geotechnical Engineering*, 117(1), 18–34.

Yiagos, A. N., and Prevost, J. H. (1991). "Two-phase elasto-plastic seismic response of earth dams: theory." *Soil Dynamics and Earthquake Engineering*, 10(7), 357–370.

Yingren, Z., and Shangyi, Z. (2004). “Application of strength reduction FEM in soil and rock slope.” *Chinese Journal of Rock Mechanics and Engineering*, 19, 37.

Youn, J.-U., Choo, Y.-W., and Kim, D.-S. (2008). “Measurement of small-strain shear modulus G max of dry and saturated sands by bender element, resonant column, and torsional shear tests.” *Canadian Geotechnical Journal*, 45(10), 1426–1438.

Yu, H. S., Salgado, R., Sloan, S. W., and Kim, J. M. (1998). “Limit Analysis versus Limit Equilibrium for Slope Stability.” *Journal of Geotechnical and Geoenvironmental Engineering*, 124(1), 1–11.

Zhenyu, W., Jiankang, C., Yanling, L., and Liang, P. (2015). “An algorithm in generalized coordinate system and its application to reliability analysis of seismic slope stability of high rockfill dams.” *Engineering Geology*, 188, 88–96.

Zhu, S., and Zhou, J. (2010). “Study on Seismic-spectrum Characteristics for 300m-grade Earth-Rockfill Dam.” *2010 Asia-Pacific Power and Energy Engineering Conference*, IEEE, 1–4.

Biographical Information

Sayantan Chakraborty was born on April 30, 1991 in Kolkata, West Bengal, India. He graduated from Bengal Engineering and Science University, Shibpur (now known as Indian Institute of Engineering Science and Technology) in May 2013 with a Bachelor's degree in Civil Engineering. He completed his Master's degree in Civil Engineering, with specialization in Transportation Engineering from the Indian Institute of Technology Kanpur, in July 2015. For his Master's thesis he studied the impact of moisture intrusion on durability of lime stabilized subgrades, under the supervision of Dr. Syam Nair.

In August 2015, he joined the doctoral program at the University of Texas at Arlington, under the supervision of Dr. Anand J. Puppala. He developed a seismic response and slope stability analysis framework for evaluating the stability of hydraulic fill dam. His doctoral research is presented in this dissertation. He successfully defended his doctoral dissertation on July 17, 2018.

Appendix A

This appendix contains the permissions obtained from the publishers of different journals, to reuse contents of the different articles, which were published or have been accepted for publication, as a part of this research work.

Permission to use the contents of manuscript ID ASTM GTJ-2017-0220.R1, titled "**Use of Constant Energy Source in SASW Test and Its Influence on Seismic Response Analysis**" which has been accepted for publication in ASTM Geotechnical Testing Journal.

DOI of the full article: 10.1520/GTJ20170220

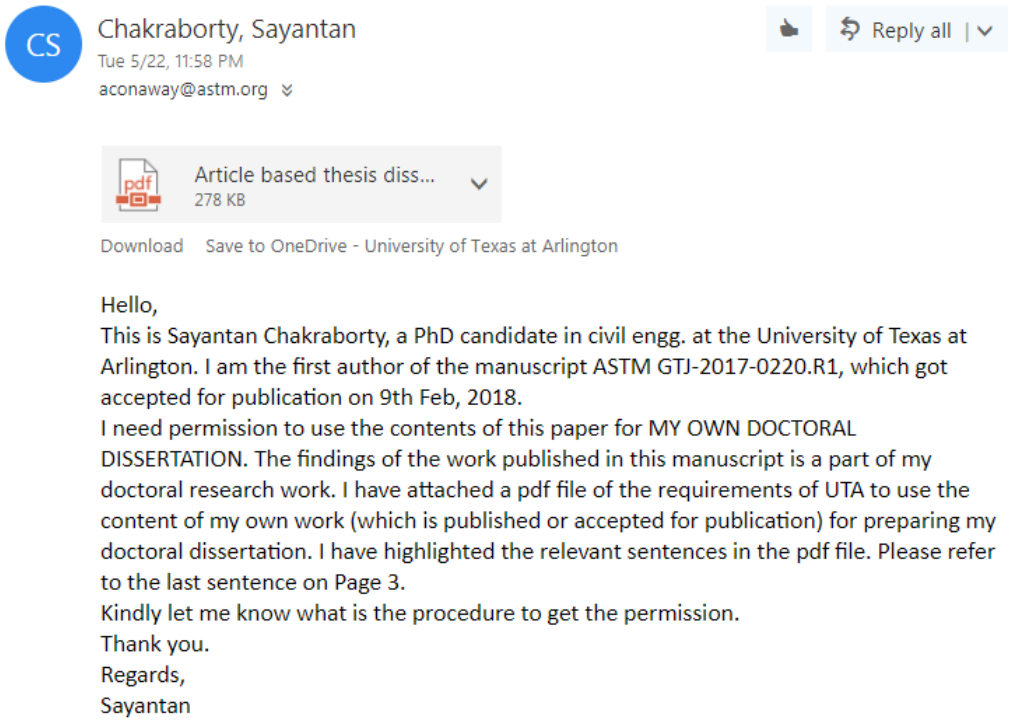

CS

Chakraborty, Sayantan

Tue 5/22, 11:58 PM

aconaway@astm.org

Reply all

Article based thesis diss...
278 KB

Download Save to OneDrive - University of Texas at Arlington

Hello,
This is Sayantan Chakraborty, a PhD candidate in civil engg. at the University of Texas at Arlington. I am the first author of the manuscript ASTM GTJ-2017-0220.R1, which got accepted for publication on 9th Feb, 2018.
I need permission to use the contents of this paper for MY OWN DOCTORAL DISSERTATION. The findings of the work published in this manuscript is a part of my doctoral research work. I have attached a pdf file of the requirements of UTA to use the content of my own work (which is published or accepted for publication) for preparing my doctoral dissertation. I have highlighted the relevant sentences in the pdf file. Please refer to the last sentence on Page 3.
Kindly let me know what is the procedure to get the permission.
Thank you.
Regards,
Sayantan

CA

Conaway, Alyssa <aconaway@astm.org>

Wed 5/23, 6:56 PM

Chakraborty, Sayantan

Reply all

Dear Sayantan,

Thank you for the information. I have sent everything to our Permissions Manager, Kathe Hooper. She or I will get back to you after we review.

Best,
~Alyssa

Alyssa Conaway
Publishing Specialist

ASTM INTERNATIONAL
Helping our world work better
---
100 Barr Harbor Drive
PO Box C700
West Conshohocken, PA 19428

HK

Hooper, Kathe <khooper@astm.org>

Thu 5/24, 10:35 PM

Article based thesis diss...
278 KB

Download Save to OneDrive - University of Texas at Arlington

Dear Sayantan,

This is in response to your email to Alyssa.

As the Author, ASTM permits you the right to include your paper in full or in part in a thesis or dissertation provided that this is not to be published commercially, and that your paper is first published by ASTM. Your paper, GTJ-2017-0220.R1, will publish in our November 2018 issue.

Please let me know if you have additional questions.

Kind regards,
Kathe

Kathe Hooper
Manager, Rights and Permissions

Permission to use the contents of manuscript ID 0019_0029_000294, titled "**Impact of Variation of Small Strain Shear Modulus on Seismic Slope Stability Analysis of a Levee: A Sensitivity Analysis**", which has been published in IFCEE 2018: Developments in Earth Retention, Support Systems, and Tunneling, ASCE Geotechnical Special Publication 297

DOI of the full article: 10.1061/9780784481608.029

From: Chakraborty, Sayantan <sayantan.chakraborty@mavs.uta.edu>
Sent: Tuesday, May 22, 2018 3:06 PM
To: PERMISSIONS <permissions@asce.org>
Subject: Requesting permission of re-use of Paper id_0019_0029_000294 (accepted for publication as ASCE GSP for IFCEE 2018)

Hello,

I am Sayantan Chakraborty, PhD candidate in Civil Engg. at the University of Texas at Arlington. I need to re-use the entire content of Paper id_0019_0029_000294, titled "Impact of variation of small strain shear modulus on seismic slope stability analysis of a levee: A sensitivity analysis" for MY OWN DOCTORAL DISSERTATION. I am the primary (first) author of this paper, which was based on the findings of a part of my PhD research work, and I need to include it in my article-based dissertation. I would like to request permission for its re-use, although the GSP paper has not be published online yet. Please let me know if anything else needs to be done on my part.

Thank you.

Regards,

Sayantan

Requesting permission of re-use of Paper id_0019_0029_000294 (accepted for publication as ASCE GSP for IFCEE 2018)

P PERMISSIONS <permissions@asce.org> Reply all
Today, 1:11 AM
Chakraborty, Sayantan

Dear Sayantan,
Thank you for your inquiry. As an original author of an ASCE journal article or proceedings paper, you are permitted to reuse your own content (including figures and tables) for another ASCE or non-ASCE publication, provided it does not account for more than 25% of the new work.

A full credit line must be added to the material being reprinted. For reuse in non-ASCE publications, add the words "With permission from ASCE" to your source citation. For Intranet posting, add the following additional notice: "This material may be downloaded for personal use only. Any other use requires prior permission of the American Society of Civil Engineers. This material may be found at [URL/link of abstract in the ASCE Library or Civil Engineering Database]."

Each license is unique, covering only the terms and conditions specified in it. Even if you have obtained a license for certain ASCE copyrighted content, you will need to obtain another license if you plan to reuse that content outside the terms of the existing license. For example: If you already have a license to reuse a figure in a journal, you still need a new license to use the same figure in a magazine. You need separate license for each edition.

For more information on how an author may reuse their own material, please view: http://ascelibrary.org/page/informationforasceauthorsreusingyourownmaterial

Sincerely,

Leslie Connelly
Senior Marketing Coordinator
American Society of Civil Engineers
1801 Alexander Bell Drive
Reston, VA 20191

PERMISSIONS@asce.org

703-295-6169
Internet: www.asce.org/pubs | www.ascelibrary.org | http://ascelibrary.org/page/rightsrequests

Permission to use the contents of the article titled "**A rational approach to select the number of field tests required to determine subgrade properties"**, which has been published in International Journal of Pavement Engineering.

DOI of the full article: 10.1080/10298436.2017.1394095

Our Ref: JB/GPAV/P18/1015

09 August 2018

Dear Sayantan Chakraborty,

Material requested: 'A rational approach to select the number of field tests required to determine subgrade properties' by Sayantan Chakraborty, Tejo V. Bheemasetti, Anand J. Puppala & Soheil Nazarian *International Journal of Pavement Engineering* (2017).

Thank you for your correspondence requesting permission to reproduce the above mentioned material from our Journal in your printed thesis and to be posted in the university's repository - University of Texas at Arlington.

We will be pleased to grant permission on the sole condition that you acknowledge the original source of publication and insert a reference to the article on the Journals website: http://www.tandfonline.com

This is the authors accepted manuscript of an article published as the version of record in International Journal of Pavement Engineering © Taylor & Francis https://doi.org/10.1080/10298436.2017.1394095

This permission does not cover any third party copyrighted work which may appear in the material requested.

Please note that this license does not allow you to post our content on any third party websites or repositories.

Thank you for your interest in our Journal.

Yours sincerely

Jo Bateman – Permissions Administrator, Journals

Taylor & Francis Group
3 Park Square, Milton Park, Abingdon, Oxon, OX14 4RN, UK.
Tel: +44 (0)20 7017 7617
Fax: +44 (0)20 7017 6336
Web: www.tandfonline.com
e-mail: joanne.bateman@tandf.co.uk

Appendix B

This appendix contains the article titled “A rational approach to select the number of field tests required to determine subgrade properties”, which has been published in International Journal of Pavement Engineering.

International Journal of Pavement Engineering

ISSN: 1029-8436 (Print) 1477-268X (Online) Journal homepage: http://www.tandfonline.com/loi/gpav20

A rational approach to select the number of field tests required to determine subgrade properties

Sayantan Chakraborty, Tejo V. Bheemasetti, Anand J. Puppala & Soheil Nazarian

To cite this article: Sayantan Chakraborty, Tejo V. Bheemasetti, Anand J. Puppala & Soheil Nazarian (2017): A rational approach to select the number of field tests required to determine subgrade properties, International Journal of Pavement Engineering, DOI: 10.1080/10298436.2017.1394095

To link to this article: http://dx.doi.org/10.1080/10298436.2017.1394095

INTERNATIONAL JOURNAL OF PAVEMENT ENGINEERING, 2017
https://doi.org/10.1080/10298436.2017.1394095

Taylor & Francis
Taylor & Francis Group

A rational approach to select the number of field tests required to determine subgrade properties

Sayantan Chakraborty[a], Tejo V. Bheemasetti[a], Anand J. Puppala[a] and Soheil Nazarian[b]

[a]Department of Civil Engineering, The University of Texas, Arlington, TX, USA; [b]Department of Civil Engineering, The University of Texas, El Paso, TX, USA

ABSTRACT

This paper presents a rational approach to answer the questions of how many field tests need to be performed at a test site to determine its subgrade strength properties, and what inferences can be drawn from limited number of field tests. MATLAB simulations were performed to generate various data sets that corresponded to site variability, with the coefficient of variation (CoV) ranging from 10 to 80%. Studies were performed based on coefficient of variation (CoV) and regression analysis. This study provides two important charts for evaluating subgrade properties at test sites: (1) to determine the number of field tests to be performed, after which there would not be any significant change in the inferences drawn from the test results; (2) inferences pertaining to subgrade soil property of a field test site, based on a limited number of tests. In order to demonstrate the applicability of the charts developed through this research, light weight deflectometer (LWD) spot tests that were performed at a test site, were considered. The results were used to draw inferences about the modulus of the subgrade material and the possible variability of the test site, in addition to the maximum number of tests that might be performed.

ARTICLE HISTORY
Received 10 November 2016
Accepted 10 October 2017

KEYWORDS
Field tests; material variability; subgrade property; Coefficient of Variation (CoV); regression analysis

1. Introduction

Field testing plays a dominant role in determining the in situ properties of pavement layers. Over the years, several developments and innovations to accurately represent the in situ condition of the material properties have taken place in the field of material testing (Heisey *et al.* 1982, Nazarian *et al.* 1993, Siekmeier *et al.* 2000, Puppala 2013). In transportation geotechnics, the design and analysis parameters are obtained either from laboratory tests on soil samples or from in situ field tests. The results obtained from these tests varies significantly due to the heterogeneity of the subgrade soils (Vanmarcke 1977, Phoon and Kulhawy 1999, Baecher and Christian 2005). In the last decade, researchers have extensively used reliability-based design methodology to incorporate the spatial variability of the material properties in design and analysis (Christian and Baecher 2011, Phoon and Ching 2012, Juang *et al.* 2013, 2014, Bheemasetti 2015, Puppala *et al.* 2016). Despite an increase in these studies that accounts for different measurement errors and uncertainties associated with testing and materials, very little effort has been made to develop generalised guidelines to aid practitioners and researchers with the field testing (Lumb 1971, Orchant *et al.* 1988, Spry *et al.* 1988, Filippas *et al.* 1988, Phoon *et al.* 1995, Phoon and Kulhawy 1996, Jaska *et al.* 1997, Zou *et al.* 2016). Current standards and specifications for testing and the sampling rate in the field vary among different state agencies. Table 1 presents a compilation of standards and specifications developed for five different state agencies. It should be noted that the specifications for each state agency provided in Table 1 are only a representative portion of the entire specification. Based on the specific application and material, the sampling and testing frequencies are different for all of the state agency specifications.

Despite these specifications, whether a test is accepted or rejected can vary greatly due to the heterogeneity of the subsoil conditions and the criteria established by the owner/contractor of the project. While sampling and collecting data for such inhomogeneous conditions, it is important to consider the coefficient of variation (CoV) besides the mean value obtained from the series of tests performed. The coefficient of variation, which is a measure of variability, is mathematically defined as the ratio of the sample standard deviation to the sample mean. Several researchers have studied the coefficient of variation of various subgrade soil properties obtained from field and laboratory measurements (Haldar and Tang 1979, Asaoka 1982, Reyna and Chameau 1991, Kulhawy *et al.* 1991). A higher scatter among the collected data would result in a higher coefficient of variation and hence would signify higher variability. Such a test site may require more tests than a less heterogeneous site.

While conducting in situ tests to determine a given engineering property, it is important to determine the number of tests required to satisfy the design criteria. Performing more tests is generally thought to provide a more representative result, but increasing the number of tests also often increases the project time and associated costs. Hence, engineers have to

CONTACT Anand J. Puppala anand@uta.edu

Table 1. Specifications for field testing and sampling rate.

Agency	Specifications	Reference manual
Texas DOT (TxDOT)	Untreated base courses: 1 minimum test result per 2294 cubic metres per lift for in-place density Treated subgrade and base courses: 1 minimum test result per 2294 cubic metres per lift for in-place density	TxDOT: guide schedule of sampling & testing
North Dakota DOT (NDDOT)	1 test result per 4180 square metres rural or 1255 square metres urban of concrete pavement for fine and coarse aggregates 1 test result per 4180 square metres rural or 1255 square metres urban of concrete pavement for materials finer than No. 200 sieve	Section 500: rigid pavement
Arizona DOT (ADOT)	Proctor Density and Optimum Moisture: one per soil type, and as needed Compaction and Gradation: one per 457 metres or change in material	Section 203: materials quality assurance programme
Colorado DOT (CDOT)	1 test per 1530 cubic metres or fraction thereof of testable material as described in CDOT standard specifications Density: 1 per 382 cubic metres when within 30.5 m of bridge approach	Section 203: materials quality assurance programme
Virginia DOT (VDOT)	1 test per 6.5 roadway kilometres, or fraction thereof, consisting of the average of 5 readings. Minimum of 5 readings per project, unless total quantity of individual material is less than 5,00,000 kg per project	Section 206: methods and frequencies of sampling

optimise between cost and an accepted variability (coefficient of variation) of the collected data. A site having high variability demands more tests to capture the entire spectrum of possibilities, whereas a site with uniform properties can be assessed with fewer tests. In this research study, an attempt was made to mathematically determine the maximum number of tests to be performed, beyond which further testing would not convey any extra information. In addition, charts were developed to assist in evaluating the material property of a test site based on sample test results. The following sections present the details and analysis.

2. Database

This section presents the database used in this analysis for mathematically determining the number of tests required to gather information about specific characteristics of a site, accepting a given degree of variability. The random number generator function was used to generate the datasets required for performing the analysis. The coefficient of variation was varied from 0.1 (10%) to 0.8 (80%), with an increment of 0.1 (10%) to account for different degrees of variabilities in material properties and site conditions. 500 data points were generated for each coefficient of variation value, representing 20 test sections at a given site, with 25 test samples for each section. Figure 1 represents the data points generated for performing the analysis. The data generated was further used for performing the analysis, as presented in the following sections.

3. Analysis and results

3.1. Maximum number of samples to be tested

This section presents the analysis performed to determine the maximum number of samples to be tested, beyond which no significant change in the test results can be observed. In other words, performing additional tests will not significantly change the inferences drawn about the site properties. Several parameters, as well as the database presented in the earlier section, were utilized to perform the analysis. The terminology of the statistical parameters and the corresponding analogy to pavement studies are provided below.

Spot tests	Pavement tests for determining modulus, density and/or moisture content
N	Number of samples; represents number of spot tests
n_{cond}	Number of tests conducted; represents number of spot tests conducted
n_{req}	Number of required tests; represents number of spot tests required
s	Number of test sections; number of pavement sections considered
CoV	Coefficient of Variation; a measure of variability involved in the results of spot tests
Sample data-set	Spot test values at a section
Population	All spot test values possible at a field test site

Using the above notations, the solution to the objective of this section can be expressed mathematically as:

$$[\text{Result of}(n+1)^{\text{th}}\text{test} - \text{Result of}(n)^{\text{th}}] \approx 0 \quad (1)$$

The 'Result' in equation 1 refers to the difference between the maximum and minimum values of sample CoV for a respective number of tests. When the result of 'n' samples tested and 'n + 1' samples tested are equal, it represents a limiting value for the number of field tests required beyond which there is no significant change in the inference drawn from the test results. In order to understand the influence of the additional number of tests on CoV values, an analysis was performed for the generated database for 0.1 and 0.4 population CoV, as depicted in Figure 2. Sample datasets were created from the population database by varying 'n' from 2 to 25 for all of the tests sections. For instance, a sample data-set with 'n' equal to 2 represents 2 test values. CoV values for all of the sample datasets were calculated for all 20 test sections, and were plotted against the number of tests.

From Figure 2 plots, it can be observed that the calculated sample CoV followed a funnel-shaped zone as the number of tests increased. The CoV band was found to be thick with fewer samples, signifying higher deviation from the population CoV. For example, if two tests are performed at a test site having a certain mean value of a given property, either of the following two extreme possible outcomes may occur: (a) The results may be very close, depicting a low sample standard deviation and hence,

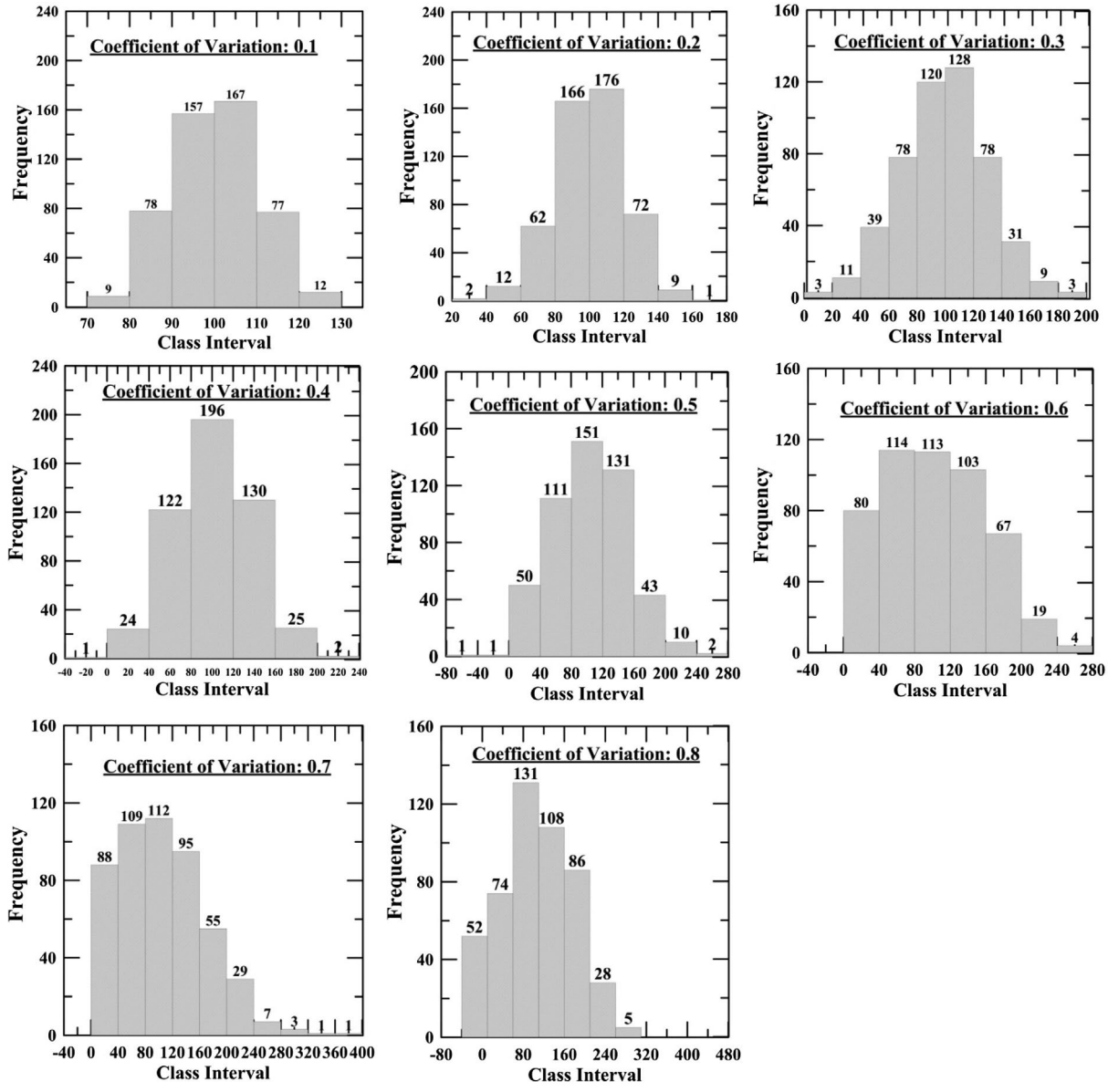

Figure 1. Graphical representation of database.

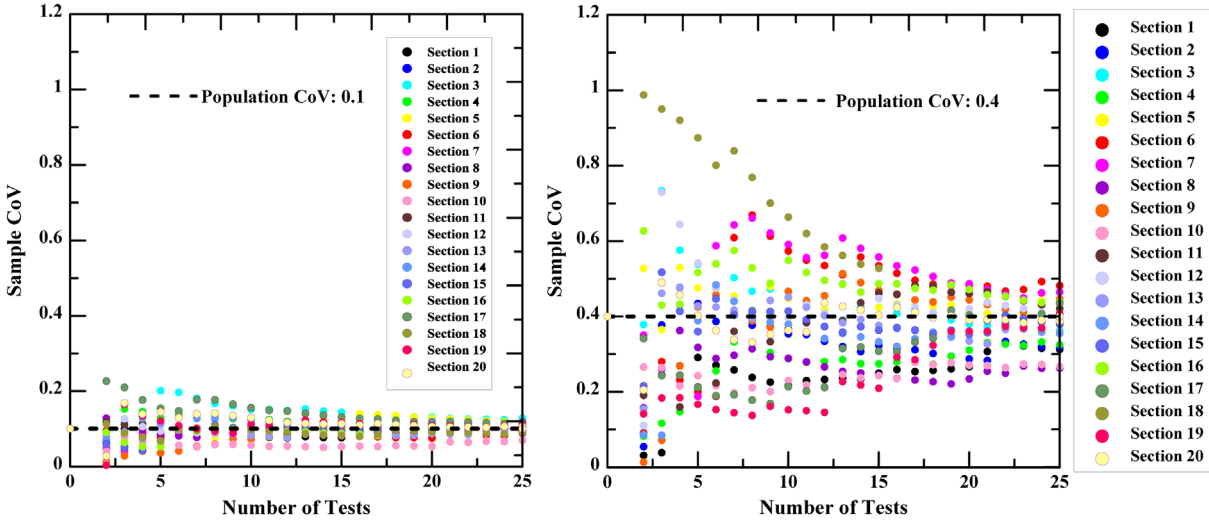

Figure 2. CoV calculated for '*n*' tests for a population CoV of 0.1 and 0.4.

low sample CoV value, or (b) The test results may be significantly different, depicting a high sample CoV value. These two cases would signify the extreme limits of the funnel-shaped zones for 'n' = 2, as shown in Figure 2. Similar observations were identified when more tests were performed. With an increase in the number of samples being tested, there is a decrease in variation in the calculated sample CoV. Figure 2 also shows that there was a band of constant thickness (spread in calculated CoV) beyond a certain 'n' number of samples tested from the 20 sections. This highlights the fact that beyond a certain number of tests, the sample CoV approached a constant value. Hence the maximum number of tests conducted should correspond to that particular 'n_{max}' value, beyond which the variation in calculated CoV becomes constant.

In order to determine the maximum number of tests (n_{max}), the framework presented in equation 1 was used. Sample data-sets were created for all of the test sections by varying 'n' from 2 to 25. For instance, a data-set for 'n' equal to 2 is comprised of 20 CoV values corresponding to 20 test sections. The difference between maximum and minimum CoV was determined for 'n' tests (with 'n' varying from 2 to 25). Then, the difference between the difference of maximum and minimum CoV for 'n' and '$n + 1$' tests was determined. A difference close to 0, implies that despite increasing the number of tests, there is no significant reduction in the spread of the sample CoV. For each population CoV (varying from 0.1 to 0.8), such plots were generated for 40 repetitions. The number 'n' was determined from those 40 plots, beyond which the difference remained almost 0. An averaged 'n' value was calculated from the 40 repetitions for a given population CoV, representing the 'n_{max}' (maximum number of tests to be conducted) for the population CoV. Figure 3 shows the representative charts for determining maximum 'n' value for CoV of 0.1 and 0.4 for 1 of the 40 repetitions.

From Figure 3, it can be inferred that the difference between the difference of maximum and minimum CoV for 'n' and '$n + 1$' tests approached close to 'zero' after a certain number of tests. The corresponding 'n' value from the plot was determined, and an averaged 'n' value (for 40 repetitions), representing the 'n_{max}', was obtained for each of the 8 population CoVs (0.1 to 0.8). The 'n_{max}' value was plotted against the population CoV, as shown in Figure 4. It can be inferred from Figure 4 that with an increase in the CoV values, the 'n_{max}' values also increased, signifying the need for conducting more tests for a heterogeneous site with high variability. The dashed lines represent a 95% confidence interval for the data-set used. It should be noted that the plot provided in Figure 4 does not represent an absolute number of tests to be performed for a specific CoV. The flowchart provided in Figure 5 provides the stepwise procedure for using the plot developed in Figure 4.

3.2. Inferences about material property at a test site based on limited testing

This section presents the analysis performed to interpret the test site conditions based on the sample CoV determined from limited number of test results. The analysis described in the previous section provided an approach to determine the number of field tests beyond which no significant change occurs in the test results. However, in a few projects, where there are constraints associated with time and project costs, performing the maximum number of field tests may not be possible. In such instances, it is important to deduce information about the test site based on constrained field investigations. The errors associated with interpreting the CoV of a test site can be explained mathematically by formulating a hypothesis, as shown below.

Null Hypothesis (H_0): Sample CoV represents actual CoV of the test site

Alternative Hypothesis (H_1): Sample CoV defers from actual CoV of the test site

The null hypothesis shown above states that the CoV value determined, based on sample tests, represents the CoV at a test site, whereas the alternative hypothesis states that the sample CoV is *not* representative of the actual test site. The alternative hypothesis requires a larger number of tests and aids in interpreting the actual CoV of a test site; however, when there are

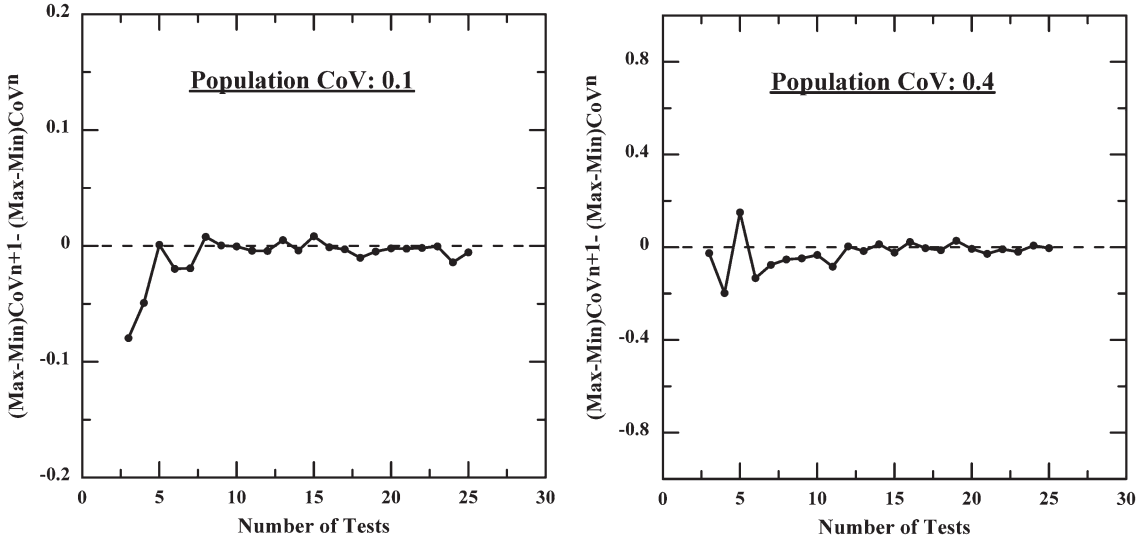

Figure 3. Spread of sample CoV with number of tests.

constraints on the budget and project time, decisions are made based on available results. Four types of decisions are presented in Table 2.

From Table 2, it can be inferred that the decisions made will be accurate if the sample CoV reflects the field test site or if the null hypothesis is rejected when the sample CoV defers from the actual field CoV. In other cases, the conclusions drawn could lead to two types of errors, such as Type I and Type II. A Type I error is an inaccurate conclusion made by rejecting the null hypothesis even if it was true. A Type II error is an inaccurate conclusion made by failing to reject the null hypothesis when it is false. Hence, it is essential to develop an approach which can estimate the population CoV of a test site. This section presents an attempt to develop an inferential chart for assessing the population CoV values with respect to sample CoV.

The database presented in the earlier sections was used for the analysis. The sample CoV was calculated for each section by considering only two tests per section. Later, the new CoV was calculated by including each new sample tested, up to a maximum of 25 samples. It was observed that the variations in the calculated sample CoV for '*n*' tests per section was higher with a smaller number of samples, whereas the variations decreased when more samples were tested. In order for the analysis not be biased, the maximum and minimum calculated CoV obtained for each '*n*' was averaged for 40 repetitions. This process was performed for all of the population CoVs varying from 0.1 to 0.8. Figure 6 presents the sample CoV variation obtained by averaging the obtained maximum and minimum CoV for 40 repetitions for a population CoV of 0.1 and 0.4.

From Figure 6, it can be inferred that both the maximum and minimum CoV tend to approach a constant bandwidth after a certain number of samples. While performing the analysis, it was observed that the calculated sample CoV's were less than or greater than the population CoVs, despite coming from a population of a given CoV. However, the calculated sample CoV was found to lie within a certain range, depending on the number of samples being tested. The range was found to be broad when the population CoV was large, which represents a site with high variability, whereas the range was small with more uniform subgrade soil properties for a low population CoV. The variation in the maximum calculated CoV was observed to approach a constant value with an increase in the number of samples tested for all the CoV's. Figure 7 presents a chart from which inferences about sample CoVs can be drawn with respect to population CoV and the number of samples tested.

It should be noted that if the sample CoV is smaller than the population CoV, accepting such hypothesis does not affect the overall the pavement performance. However, if the sample CoV is larger than the population CoV, the wrong conclusions drawn from such test results would result in a Type II error, which affects the pavement performance. Hence, the plots provided in Figure 7 represent only the variation of maximum CoV (averaged for 40 repetitions) against '*n*'. Figure 8 presents the flowchart that can be used to understand how to determine

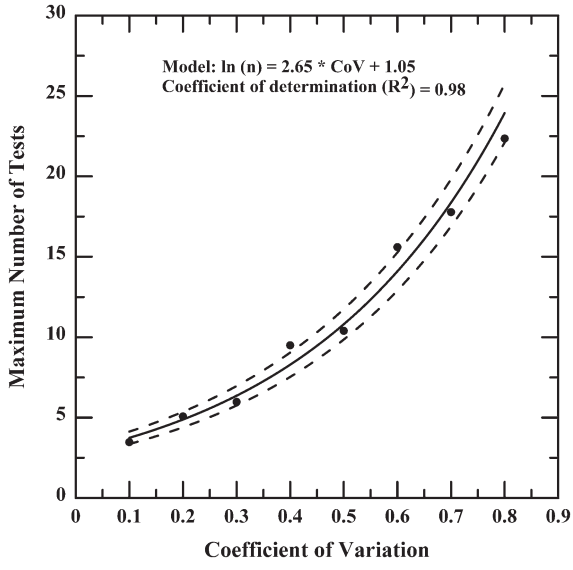

Figure 4. Variation in maximum number of tests required for a given population CoV.

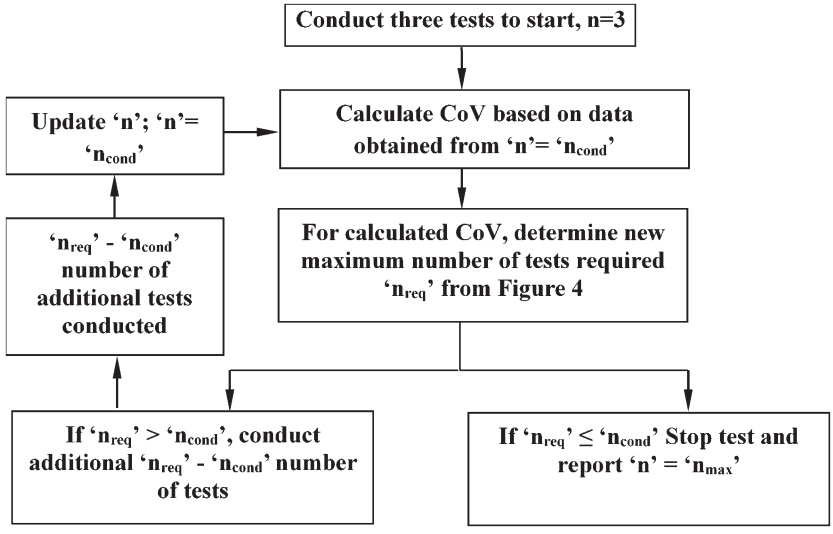

Figure 5. Flowchart showing the process of using Figure 4.

the population CoV based on sample CoV from the chart in Figure 7.

4. Application of developed framework

This section presents the details and analysis of applying the developed flow charts at a test site located along SH 267 near Dublin, Texas. Several spot tests were performed at this site in order to develop correlations between the compaction metre values and the spot test results (Siddagangaiah *et al.* 2014). Since this paper focuses on spot tests results, the compaction metre values, which are continuous in nature, were not considered. The spot test results consist of modulus values from Light Weight Deflectomer (LWD), moisture content values from Nuclear Gauge Density (NDG), and results from Portable Seismic Property Analyzer (PSPA). Table 3 presents a summary of the spot test results and sample CoV values for the test site near Dublin, Texas.

From the test results presented in Table 3, it can be observed that 12 tests were performed for each type of spot test. The coefficient of variation in the test results varied from 0.13 (13%) to 0.4 (40%). Figure 7 was used to determine the variability in the subgrade material for the complete test site. Figure 9 presents the analysis performed on the spot test results. The sample CoV calculated for the LWD (CoV = 0.4), NDG (CoV = 0.13) and PSPA (CoV = 0.2) tests were plotted on Figure 7 (marked by star mark) with respect to 12 number of tests (shown in Figure 9). It can be observed that the LWD test result lies above the maximum possible CoV line for population CoV of 0.2 and that for NDG and PSPA tests fall above the maximum possible CoV line for population CoV of 0.1.

Hence, from Figure 9, it can be inferred that the CoV for LWD test results for the entire field (i.e. population CoV) will be greater than or equal to 0.2 (20%) based on 12 test samples, whereas the population CoV for the site based on the spot test results from NDG and PSPA are greater than or equal to 0.1 (10%). It should be noted that the inferences drawn from the test results depict the test site variability based on 12 field tests. The inference drawn about the population CoV, for a given parameter of interest (e.g. subgrade modulus calculated from LWD tests) is thus dependent on the information obtained for a certain number of tests conducted. Figure 5 was applied to determine the maximum number of field tests to be performed at the site. The LWD modulus values, obtained on the subgrade as presented below, were used for performing the analysis.

LWD Modulus (in MPa): {28.26, 41.37, 44.13, 47.57, 53.78, 55.16, 57.92, 68.26, 82.74, 89.63, 47.57, 75.84}

From the test results, it can be inferred that the LWD modulus varied from 28.26 to 89.63 MPa. According to Figure 5, the first step is to conduct 3 tests (i.e. $n = 3$). Suppose three random tests provided subgrade modulus result corresponding to test numbers 1, 2 and 12. The sample CoV for this three test results (28.26, 41.37 and 75.84 MPa) is 0.5. The variability in the test result is obvious from the high deviation in the modulus value obtained from three spot tests. Based on Figure 4, it can be inferred that ten tests are required for sample CoV of 0.50 CoV value. Since, $n_{required}$ (=10) > $n_{conducted}$ (=3), seven additional tests are needed to meet the requirement of ten tests. Suppose, 7 addition tests are conducted (Tests 3 through 9) and the following subgrade modulus is obtained : 44.13, 47.57, 53.78, 55.16. 57.92, 68.26 and 82.74 MPa. The new CoV value for the ten test results (including the 3 initial tests) is 0.30. The corresponding $n_{required}$ value for the sample CoV of 0.3 is 6 (Figure 4). Since, the $n_{conducted}$ (=10) > $n_{required}$ (=6), the total 'n' values can be recorded as the n_{max} values, which is equal to 10. It should be noted that the

Table 2. Types of decisions in hypothesis testing (Montgomery *et al.* 2009).

Decision	H_0 is true	H_0 is false
Fail to reject H_0	No error	Type II error
Reject H_0	Type I error	No error

Table 3. Spot test results at SH 267 test site.

Spot tests	Number of tests	Sample CoV (%)
LWD	12	40
PSPA	12	20
NDG	12	13

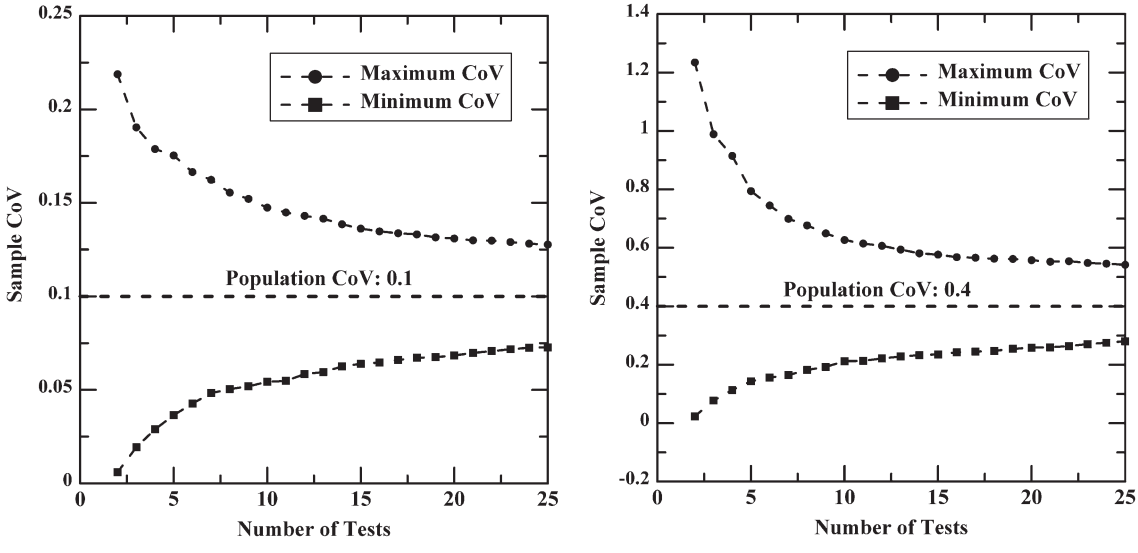

Figure 6. Variation of sample CoV with number of tests.

maximum number of test results is dependent on the available test data. The available test data is the only source of information about the site condition and the inference about the site is drawn based on the available information from the limited number of test results. If the test results are widely different (i.e. high sample CoV), more number of tests will be required to infer about the site conditions and vice versa. For instance, the maximum number of tests would be only five if the LWD results from Tests 1, 2 and 3 are considered. For the SH 267 test site, 12 tests were conducted. Therefore, it can be concluded that the test results obtained from the 12 tests represented the entire field test site and it is expected that conducting more number of tests will not provide further information about the variability of the site (since $12 > n_{max} = 10$).

The specifications for field testing and sampling rate recommended by different department of transportations (Table 1) does not incorporate the effect of soil variability, which inherently exists in the field. The recommendations does not differentiate between a homogeneous and a heterogeneous site, since the number of tests to be conducted depends on unit length, area or volume of the site. The charts developed through this study tries to provide a rational approach to select the number of field tests required to determine subgrade properties. Figures 4 and 5 can be used to determine the maximum number of tests that may be performed, beyond which there might not be significant improvement in the inferences drawn about the site variability. These are the maximum number of tests which may be performed when time and cost are not constraints. However, in most projects, limited number of tests (lesser than n_{max}) are generally performed. Figures 7–9 may be used in such circumstances to infer about the site variability based on limited number of testing.

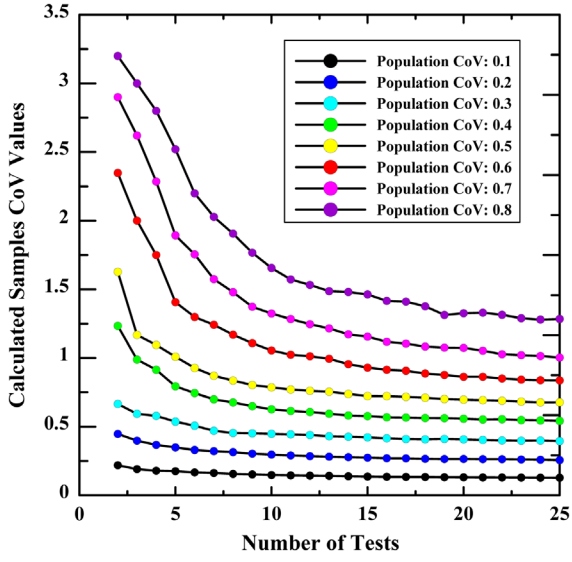

Figure 7. Inferential chart on population CoV based on sample CoV.

5. Summary and conclusions

The main objective of this research study was to develop an approach to determine the maximum number of field tests that could be performed, beyond which there would be no significant change in the test results, and to discover what information about a test site could be inferred, based on the limited number of test results. The analysis was performed on a database that was generated for CoV values varying from 0.1 to 0.8. Through this analysis, some important findings were obtained which can be beneficial to both researchers and practitioners.

It was observed that the calculated sample CoV followed a funnel-shaped zone and reached a constant bandwidth with an increase in the number of samples tested. The middle of the constant thickness region represented the population CoV, and the CoV band was thicker when fewer samples were tested, signifying higher deviation from the population CoV. This conclusion implies that with a smaller number of field tests conducted on a pavement layer, the standard deviation will be high; and with an increase in number of tests, the variation will be reduced to the inherent variability present in the material properties.

A plot was developed in this study to determine the maximum number of field tests (n_{max}), based on calculated sample CoV values. This chart will act as guideline when the specifications for the acceptability criteria of a material property have been established before the start of the project. In order to use this chart, the testing will start with at least three tests at random locations. Based on the CoV obtained from the tests, the

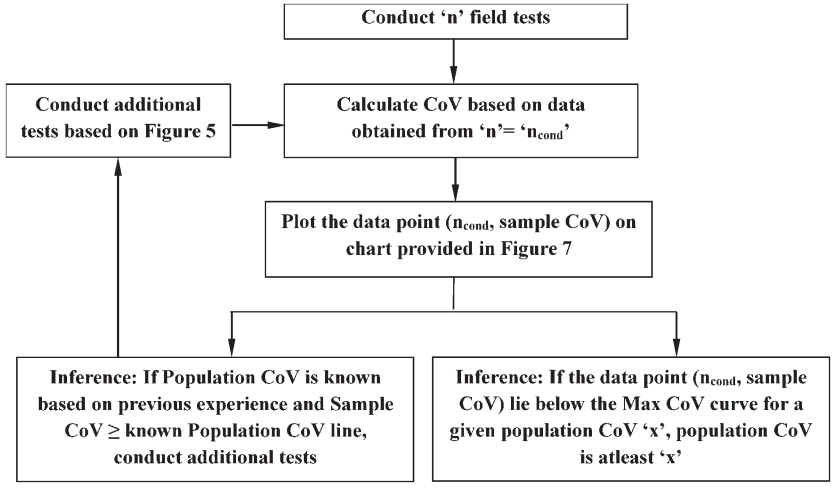

Figure 8. Flowchart showing the process for making inferences about population CoV.

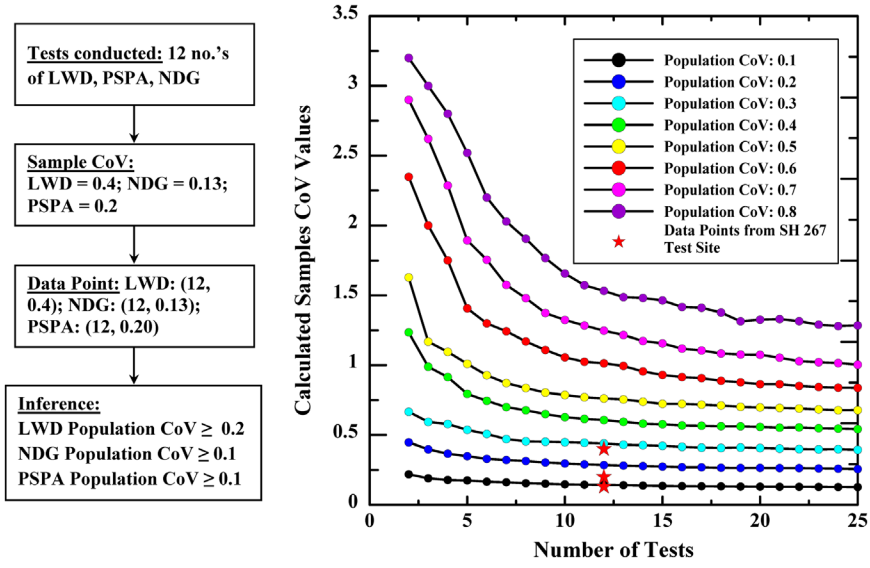

Figure 9. Determination of variability at SH 267 test site.

chart will guide how many more tests should be performed in order to conclude the material property with the established specifications. A flow chart was also provided, along with the 'n_{max}' and CoV plot.

A series of plots was developed for the population CoV, sample CoV, and number of tests. These plots will act as a guideline for gaining information about a test site. Often, field investigations are limited to a few spot tests, and a conservative average value or a minimum value is reported. However, the average value or minimum value are biased, which can lead to two types of inaccurate conclusions. The Type II error can affect the performance of the pavement. Hence, the charts developed through this research study provide an estimate of the variability of a field test site, based on limited testing. The charts provided here are based on an assumption that the field test results have different degrees of variability.

Disclosure statement

No potential conflict of interest was reported by the authors.

ORCID

Sayantan Chakraborty http://orcid.org/0000-0002-6809-5953

References

Asaoka, A., 1982. Spatial variability of the undrained strength of clays. *Journal of the Geotechnical Engineering Division*, 108(5), 743–756. doi: 10.1016/0148-9062(82)91398-5

Baecher, G.B. and Christian, J.T., 2005. *Reliability and statistics in geotechnical engineering*. Wiley.

Bheemasetti, T.V., 2015. Spatial variability models and prediction analysis of soil properties using geostatistics.

Christian, J.T. and Baecher, G.B., 2011. Unresolved problems in geotechnical risk and reliability. In *Geo-Risk 2011: Risk Assessment and Management*, 50–63. doi: 10.1061/41183(418)3

Filippas, O.B., Kulhawy, F.H., and Grigoriu, M.D., 1988. *Reliability-based foundation design for transmission line structures: uncertainties in soil property measurement*. Report EL-5507 (3).

Haldar, A. and Tang, W.H., 1979. Probabilistic evaluation of liquefaction potential. *Journal of the Geotechnical Engineering Division*, 105(2), 145–163.

Heisey, J.S., Stokoe, I.I., and Meyer, A.H., 1982. Moduli of pavement systems from spectral analysis of surface waves. *Transportation research record*, 852.

Jaksa, M.B., Brooker, P.I., and Kaggwa, W.S., 1997. Inaccuracies associated with estimating random measurement errors. *Journal of Geotechnical and Geoenvironmental Engineering*, 123 (5), 393–401. doi:10.1061/(asce)1090-0241(1997)123:5(393).

Juang, C.H., *et al*, 2013. Robust geotechnical design of drilled shafts in sand: new design perspective. *Journal of Geotechnical and Geoenvironmental Engineering*, 139 (12), 2007–2019. doi:10.1061/(asce)gt.1943-5606.0000956.

Juang, C.H., *et al.*, 2014. Robust geotechnical design of braced excavations in clays. *Structural Safety*, 49, 37–44. doi:10.1016/j.strusafe.2013.05.003.

Kulhawy, F.H., Roth, M.J.S., and Grigoriu, M.D., 1991, June. *Some statistical evaluations of geotechnical properties*. In Proceedings on ICASP6, 6th International Conference on Applied Statistics and Probability for Civil Engineering. Mexico, 705–712.

Lumb, P., 1971. *Precision and accuracy of soil tests*. In Proceedings, 1st international conference on applications of statistics and probability in soil and structural engineering, Hong Kong, 329–345.

Montgomery, D.C., Runger, G.C., and Hubele, N.F., 2009. *Engineering statistics*. John Wiley & Sons, Hoboken, New Jersey.

Nazarian, S., Baker, M.R., and Crain, K., 1993. *Development and testing of a seismic pavement analyzer* (No. SHRP-H-375).

Orchant, C.J., Kulhawy, F.H., and Trautmann, C.H., 1988. *Reliability-based foundation design for transmission line structures: Volume 2, Critical evaluation of in situ test methods: final report* (No. EPRI-EL-5507-Vol. 2). Electric Power Research Inst., Palo Alto, CA; Cornell Univ., Ithaca, NY. Geotechnial Engineering Group.

Phoon, K.K. and Ching, J., 2012. Beyond coefficient of variation for statistical characterization of geotechnical parameters. *Keynote lecture of Geotechnical and Geophysical Site Characterization*, 4, 113–130.

Phoon, K.K. and Kulhawy, F.H., 1996. On quantifying inherent soil variability. Uncertainty in the geologic environment (GSP58). New York, NY: ASCE, 326–340.

Phoon, K.K. and Kulhawy, F.H., 1999. Characterization of geotechnical variability. *Canadian Geotechnical Journal*, 36 (4), 612–624. doi:10.1139/cgj-36-4-612.

Phoon, K.K., Kulhawy, F.H., and Grigoriu, M.D., 1995. *Reliability-based design of foundation for transmission line structure* (Report TR-105000). Palo Alto: Electric Power Research Institute.

Puppala, A., 2013. *An innovative hybrid sensor for rapid assessment of sulfate-induced heaving in stabilized soils*. NCHRP-IDEA Program Project Final Report.

Puppala, A. J., Bheemasetti, T. V., Zou, H., Yu, X., Pedarla, A., & Cai, G., 2016. Spatial variability analysis of soil properties using geostatistics.

In *Handbook of Research on Advanced Computational Techniques for Simulation-Based Engineering*, 195–226. IGI Global, Hershey, Pennsylvania. doi:10.4018/978-1-4666-9479-8.ch008.

Reyna, F. and Chameau, J.L., 1991. Dilatometer based liquefaction potential of sites in the Imperial Valley.

Siddagangaiah, A.K, *et al*., 2014. *Improvement of base and soil construction quality by using intelligent compaction technology*. TxDOT-FHWA Project Report.

Siekmeier, J.A., Young, D., and Beberg, D., 2000. Comparison of the dynamic cone penetrometer with other tests during subgrade and granular base characterization in Minnesota. In *Nondestructive testing of pavements and backcalculation of moduli: third volume*. ASTM International, West Conshohocken, PA, 175–188. doi:10.1520/STP14767S.

Spry, M.J., Kulhawy, F.H., and Grigoriu, M.D., 1988. *Reliability-based foundation design for transmission line structures: Geotechnical site characterization strategy*. Report EL-5507(1).

Vanmarcke, E.H., 1977. Probabilistic modeling of soil profiles. *Journal of the geotechnical engineering division*, 103 (11), 1227–1246. doi:10.1016/0148-9062(78)90012-8.

Zou, H., *et al.*, 2016. Assessment of measurement errors of piezocone penetration test in soft clay. *Geotechnical Testing Journal*, 39 (5), 721–741. doi:10.1520/GTJ20150074.

Appendix C

This appendix contains the article titled “Effect of Erroneous Estimation of Small Strain Shear Moduli on Seismic Response of an Earth Dam”, which has been presented at the Indian Geotechnical Conference, 2017, Guwahati, India.

Effect of Erroneous Estimation of Small Strain Shear Moduli on Seismic Response of an Earth Dam

Sayantan Chakraborty
Jasaswee T. Das
Aritra Banerjee
Anand J. Puppala
Department of Civil Engineering, The University of Texas at Arlington, Texas-76019, USA
E-mail: sayantan.chakraborty@mavs.uta.edu; jasaswee.das@mavs.uta.edu, aritra@uta.edu, anand@uta.edu

ABSTRACT: The small strain shear modulus (G_{max}) of an earthen dam affects its natural frequency; thereby influencing its response to seismic excitation. Generally, G_{max} is estimated by in-situ tests such as SCPT or SASW, which provide the shear modulus along the core of the dam. However, simplified assumptions are made regarding the variation of G_{max} along the shell of the dam. This paper illustrates the implication of assuming the dam as horizontally layered structure with the shell of each layer being assigned the same G_{max} value as that of the core. The G_{max} values of the shell of two-30 m high dams were systematically varied with respect to the initially assumed G_{max} value without varying the properties of the core of dam. The effect of underestimation and overestimation of G_{max} of the shell was studied for different layers of the dam to understand the implication of the erroneous estimations at the surface, middle, and deeper layers of the dam. Results suggest that the effect of erroneous estimation of the dam shell properties on seismic response was significant. Moreover, the variation in G_{max} values of the deeper layers was found to considerably affect the response of the structure as compared to that of near surface layers.

Keywords: *small strain shear modulus; seismic response; earth dam; dynamic characterization; sensitivity analysis*

1. Introduction

Dams and levees are critical engineered structures which play a vital role in flood control, water storage, irrigation, electricity generation and recreational purposes, and contribute toward the advancement of a nation (FEMA, 2015). These structures which are otherwise stable under normal field conditions may be susceptible to slope failures under earthquake loading conditions. The impact of a catastrophic failure of these structures directly affects the public life and economy of the nation. Thus, seismic response analysis and slope stability studies are important for new projects, and for safety evaluation of existing dams and levees. Although, use of finite element or finite difference based software have enabled engineers to perform seismic slope stability analysis with ease, nevertheless, the validity of the analysis depends on the accuracy involved in the estimation of the material properties from in-situ tests, which are used as inputs to the software.

Small strain shear modulus (G_{max}) is an important input parameter used in seismic response analysis (Dakoulas and Gazetas 1985; Gazetas 1987). The natural frequency of the dam, and propagation of the earthquake excitation (via shear waves) from the base of the dam to the crest is dependent on the shear modulus of the structure (Kramer 1996). In practice, G_{max} is usually obtained by conducting in-situ tests such as SCPT, SASW or through laboratory tests such as resonant column or bender element tests (Stokoe et al. 1991). The difficulty in obtaining undisturbed samples required for laboratory tests makes SASW and SCPT favorable alternatives for determination of G_{max}. However, the aforementioned tests are mostly conducted on the crest of the dam; hence simplified assumptions have to be made regarding the G_{max} of the shell of the dam. The dam is often idealized to consist of horizontal layers, and the material is assigned with the G_{max} values obtained from in-situ tests conducted on the dam crest (Pelecanos 2013). In some cases, the shell of the dam is considered to have uniform G_{max} properties (Onder Cetin et al. 2005; Parish et al. 2009), whereas some analyses assume G_{max} to increase as a function of effective mean stress (Tsiatas and Gazetas 1982).

The purpose of this research was to study the influence of inaccurate estimation of G_{max} of the shell of an earthen dam on its seismic response. Since the response of an earth structure subjected to earthquake excitation depends on the shear wave velocity (and hence on G_{max}), it is expected that the error in estimation of G_{max} in the shell of the dam will affect the response of the structure. A dam with assumed geometry and material properties was used to study the effect of error in estimating the properties of dam shell on the peak acceleration value and frequency content of the crest acceleration of the dam subjected to earthquake acceleration time-history data. The properties of the dam shell were systematically varied with respect to the initially assumed material properties without varying the properties of core of the dam. The G_{max} profile of the dam core was assumed to have been accurately estimated from in-situ testing. The effect of underestimation and overestimation of the G_{max} of the shell was studied for different layers of the dam to understand the implication of the erroneous estimation at the surface, middle and deeper layers of the dam.

2. Methodology

This section presents the approach adopted to study the effect of erroneous estimation of G_{max} properties of the dam shell. Two hypothetical earthen dams, one with a side slope of 1.5H:1V, and the other having a side slope of 3H:1V were considered for the study. These geometries represent the extreme values of slopes encountered in the field (Chopra 1967). Each dam was idealized as a three-layered structure, and the layers were assigned G_{max} values which are representative of shear moduli obtained from existing literature (Chopra 1967; Clough and Chopra 1966; Onder Cetin et al. 2005). The small strain shear modulus profile of the dam core was assumed to be determined accurately from in-situ tests and was hence kept constant, while systematically varying the shear moduli along the shell of the dam. The geometry of both the dams, and the variation of G_{max} along the dam core is shown in Figs. 1 and 2.

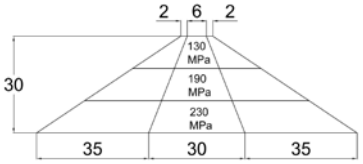

Fig. 1 Geometry of dam with side slope 1.5H:1V

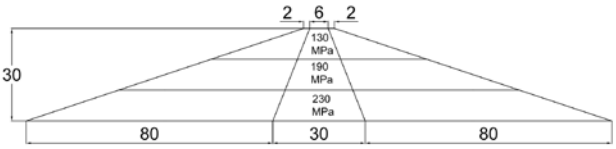

Fig. 2 Geometry of dam with side slope 3H:1V

Note: All dimensions in Figs. 1 and 2 are in meters.

The height of both the earthen structures was 30 meters, and they were assigned a uniform density, Poisson's ratio and damping ratio of 20 kN/m^3, 0.33 and 0.02, respectively. Two types of variation in shear moduli were implemented in this study – Type I and Type II, which are described in the subsequent section, and the corresponding G_{max} values are shown in Table 1 and 2. Both the embankment structures were subjected to seismic excitations corresponding to an earthquake time history data recorded at Caldwell, Kansas, USA when an M4.7 earthquake struck Oklahoma on November 19, 2015. The earthquake data was scaled to a peak acceleration of 0.05g. The acceleration time history data and the frequency content of the earthquake is shown in Figs. 3 and 4. A plane strain, linear elastic, finite element-based analysis was performed to study the response of the structure to earthquake excitations. A low PHA was used to induce low strain levels during the shaking analysis, where G_{max} values can be used (linear elastic). Contrarily, a high PHA would require non-linear analysis, which uses modulus degradation curve to obtain the G values at different strain levels. However, the purpose of this study was to comprehend the effect of erroneous estimation of G_{max} values and hence a PHA of 0.05g was used. The peak acceleration recorded at the crest of the dam was compared for different G_{max} profile combinations, and the predominant frequency of the crest acceleration was obtained by performing a Fast Fourier Transform (FFT).

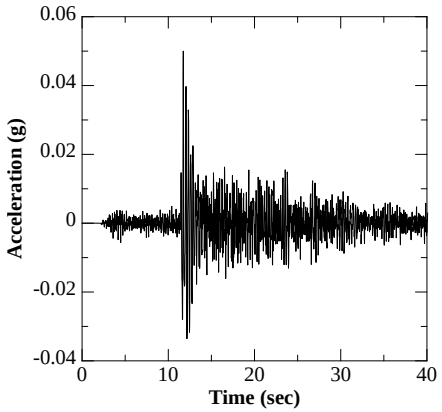

Fig. 3 Acceleration time-history data of earthquake used in the study

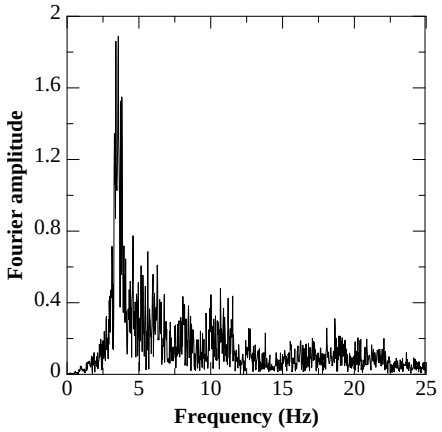

Fig. 4 Frequency content of the earthquake

2.1 Type I variation

A sensitivity analysis was performed by maintaining a constant G_{max} value for each layer of the dam core, while the G_{max} values for each layer along the shell of the dam were simultaneously varied from 70% to 130% of the G_{max} value of the corresponding dam core layer, in intervals of 10%.

Table-1 G_{max} combinations used for Type-I variation

Layer	% of core	L1	L2	L3
Core G_{max} (MPa)	100	130	190	230
Shell G_{max} (MPa)	70	91	133	161
	80	104	152	184
	90	117	171	207
	100	130	190	230
	110	143	209	253
	120	156	228	276
	130	169	247	299

Note. L1=top layer; L2=middle layer; L3=bottom layer.

It may be noted that, the case in which the shell is assigned 100% core G_{max}, corresponds to a horizontally-layered structure with the same G_{max} assigned to the core and shell of the dam for each layer. This analysis would facilitate understanding the effect of idealizing the earthen dam to consist of horizontal layers, with G_{max} values solely

varying along different layers. The study was expected to capture the effect of discrepancy between the simplistic assumption of moduli properties of the dam shell, i.e. a homogeneous G_{max} profile for the core and shell of a particular layer, and a sensitivity analysis-based approach, i.e. a weaker shell (70% to 90% of core G_{max}) or a stiffer shell (110% to 130% of the core G_{max}) as compared to the dam core.

2.2 Type II variation

In this case, the G_{max} along the core of the dam was kept unaltered while the G_{max} along the shell was varied for each layer, one at a time. In other words, two layers were assigned uniform G_{max} values identical to that of the core of the respective layers, whereas the G_{max} for the shell portion of the remaining layer was varied from 70% to 130% (increment of 10%, similar to previous case) of the core G_{max} of the corresponding layer. This procedure was subsequently repeated for all the layers to understand the relative importance of accurately estimating the shear modulus of the shell along the height of the dam.

Table-2 G_{max} combinations used for Type-II variation

Case	% of core	L1	L2	L3
Type II L1	70	**91**	190	230
	80	**104**	190	230
	90	**117**	190	230
	100	**130**	190	230
	110	**143**	190	230
	120	**156**	190	230
	130	**169**	190	230
Type II L2	70	130	**133**	230
	80	130	**152**	230
	90	130	**171**	230
	100	130	**190**	230
	110	130	**209**	230
	120	130	**228**	230
	130	130	**247**	230
Type II L3	70	130	190	**161**
	80	130	190	**184**
	90	130	190	**207**
	100	130	190	**230**
	110	130	190	**253**
	120	130	190	**276**
	130	130	190	**299**

Note: Only the layer whose shell G_{max} is varied is marked in bold.
L1=top layer; L2=middle layer; L3=bottom layer.

3. Results and Discussion

This section presents variations in the seismic response of the earth dams to earthquake excitations upon systematically altering the G_{max} values of the dam shell. The peak crest acceleration was used as a measure of the seismic response of the structure in conjunction with the predominant frequency of the crest acceleration which provides a measure of the natural frequency of the structure. Figures 5 and 6 illustrates the peak crest acceleration recorded for the different combinations of shell G_{max} and provides insight on the importance of accurate estimation of shear moduli profile within the dam. The analyses for Type I variation show a significant difference in the peak crest acceleration (for both the dams) when the shell is less stiff as compared to the core (G_{max} of shell < G_{max} of core) but is erroneously assigned the G_{max} properties of the core (G_{max} of shell = G_{max} of core). The peak crest acceleration shows a rapid decline with decreasing stiffness of the dam shell.

However, for the dam with side slope of 1.5:1 (Fig. 5), an increase in the shell stiffness (G_{max} of shell > G_{max} of core) did not cause significant change in the peak crest acceleration. Special attention should be focused on the trend of peak crest acceleration for Type I variation on dam with side slope of 3:1,when the shell is stiffer than the core. As illustrated in Fig. 6, the peak crest acceleration in this case, shows a substantial increase when the G_{max} of the shell is 10% more than the G_{max} of the core (G_{max} of shell = 110% G_{max} of core). The rationale behind this behavior could be explained by examining the frequency content of the crest acceleration. The predominant frequency of the crest acceleration was found to vary from 2.93Hz to 3.56 Hz as the stiffness of the shell varied from 70% of core G_{max} to 130% of core G_{max}. It was observed that for G_{max} of shell = 110% of core G_{max}, resonance occurred at 3.39 Hz, when the natural frequency of the structure was identical to the predominant frequency of the earthquake excitation. The resulting amplification effect is manifested in the higher peak crest acceleration values. Therefore, it could be reasonably concluded that the variation in shear modulus of the shell alters the natural frequency of the dam, which affects the peak crest acceleration/seismic response of the structure.

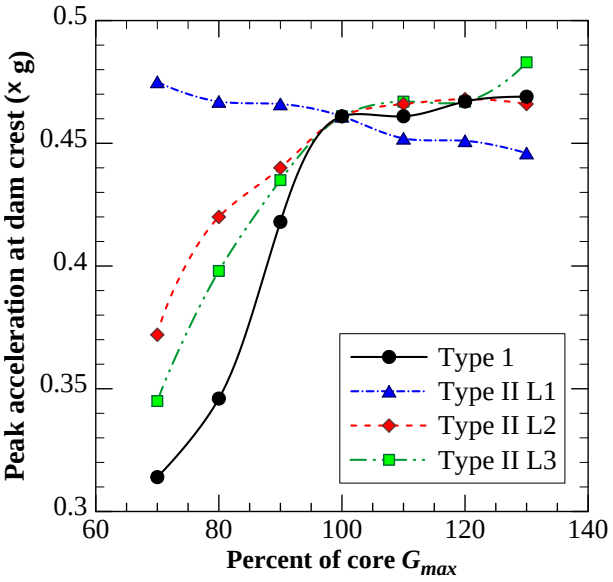

Fig. 5 Peak crest acceleration for different G_{max} combination used dam with 1.5H:1V side slope

Different combinations of shear moduli for the crest and the shell lead to variation in the natural frequency of the structure. The combinations which cause the natural frequency of the structure to be close to the fundamental frequency of the input earthquake excitation, would affect resonance. Thus, similar error in estimation of shear modulus of the shell of the dam may not result in similar variation in seismic response of two different dams, as

highlighted in the comparison of the peak crest acceleration values for the dams with side slope of 1.5:1 and 3:1.

This research also offers insight into the relative importance of the horizontal layers in the analysis. The study lends credence to the fact that, irrespective of the dam geometry, an erroneous estimation of the shear moduli of the top layer(s) (1st layer in this case) may not have a considerable effect on the seismic response of the structure. However, as evidenced from Figure 5 and 6, an inaccurate assessment of the G_{max} values of deeper layers (L2 and L3 layer in this case) would significantly influence the peak crest acceleration of the structure.

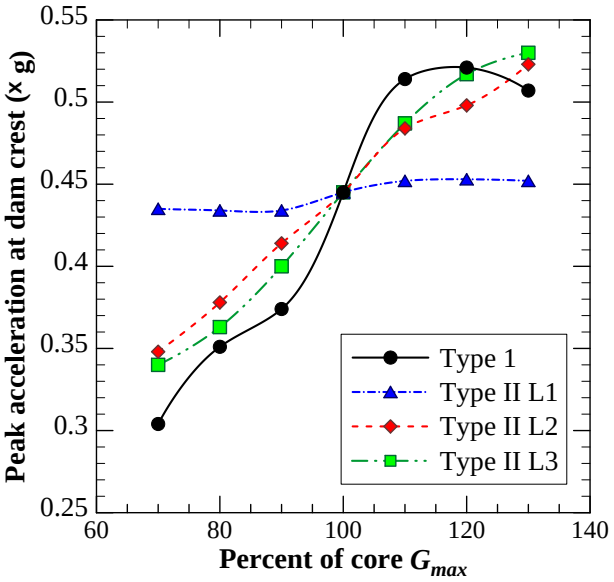

Fig. 6 Peak crest acceleration for different G_{max} combination used dam with 3H:1V side slope

4. Conclusion

Small strain shear modulus is an important parameter for seismic response analysis of an earthen dam. In-situ tests like SCPT or SASW provide information about the variation of G_{max} of the core of the dam, since the tests are performed along the crest of the dam. Due to the difficulty in performing such tests along the slope of the structure, simplified assumptions are generally made regarding the G_{max} of the shell. This study provides an insight on the possible error in seismic response analysis of an earthen structure when the earthen dam is approximated as a layered structure, where the shell of the dam is assigned the same G_{max} as that of the core.

Based on the findings of this study, it could be concluded that the G_{max} of the shell affects the natural frequency of the structure and hence influences the response of the structure to seismic excitation. The effect was found to be significant when the predominant frequency of the earthquake excitation was similar to the natural frequency of the structure. If the actual G_{max} combination of the shell and crest results in a close match between the natural frequency of the structure and the predominant frequency of the earthquake, approximating layered structure with G_{max} profile obtained from in-situ test may underestimate the seismic response of the structure. However, if the layered structure approximation leads to near resonance condition for a particular seismic excitation, the seismic response may be overestimated, since the actual G_{max} combination existing in field might result in a natural frequency different from that estimated from the layered structure.

Hence for critical projects, it might be necessary to conduct laboratory tests on samples collected from the shell of the dam. Based on the observations of this study, samples for laboratory tests should preferably be collected from deeper layers of the dam. The effect of erroneous estimation of G_{max} value near the top of the dam was found to be insignificant. A sensitivity analysis should be performed to have an understanding of the implication of making simplified approximation about the G_{max} value along the shell of the dam.

5. References

Banerjee, A. (2017). Response of Unsaturated Soils Under Monotonic and Dynamic Loading over Moderate Suction States. Doctoral Dissertation, The Univeristy of Texas at Arlington, Texas

Chopra, A. K. (1967). Earthquake Response of Earth Dams. *Journal of the Soil Mechanics and Foundations Division*, 93(2), pp. 65–81.

Clough, R. W., and Chopra, A. K. (1966). Earthquake stress analysis in earth dams. *Journal of the Engineering Mechanics Division*, 92(2), pp. 197–212.

Dakoulas, P., and Gazetas, G. (1985). A class of inhomogeneous shear models for seismic response of dams and embankments. *International Journal of Soil Dynamics and Earthquake Engineering*, 4(4), pp. 166–182.

Federal Emergency Management Agency (FEMA) (2015). *Evaluation and monitoring of seepage and internal erosion*, P-1032.

Gazetas, G. (1987). Seismic response of earth dams: some recent developments. *Soil Dynamics and Earthquake Engineering*, 6(1), pp. 2–47.

Kramer, S. L. (1996). *Geotechnical earthquake engineering*. (W. J. Hall, ed.), Prentice-Hall Civil Engineering and Engineering Mechanics Series, Upper Saddle River, NJ.

Onder Cetin, K., Isik, N. S., Batmaz, S., and Karabiber, S. (2005). A comparative study on the actual and estimated seismic response of Kiralkizi Dam in Turkey. *Journal of Earthquake Engineering*, 9(4), pp. 445–460.

Parish, Y., Sadek, M., and Shahrour, I. (2009). Review Article: Numerical analysis of the seismic behaviour of earth dam. *Natural Hazards and Earth System Science*, 9(2), pp. 451–458.

Pelecanos, L. (2013). Seismic Response and Analysis of Earth Dams. Doctoral Dissertation. Imperial College London, London, U.K.

Stokoe, K. H., Rix, G. J., and Nazarian, S. (1991). In situ seismic testing with surface waves. *International Journal of Rock Mechanics and Mining Sciences & Geomechanics Abstracts*, 28(2-3).

Tsiatas, G., and Gazetas, G. (1982). Plane-strain and shear-beam free vibration of earth dams. *International Journal of Soil Dynamics and Earthquake Engineering*, 1(4), pp. 150–160.